CENOZOIC STRATIGRAPHY, STRUCTURE, AND EPITHERMAL MINERALIZATION OF NORTH-CENTRAL BLACK RANGE, NEW MEXICO IN THE REGIONAL GEOLOGIC FRAMEWORK OF SOUTH-CENTRAL NEW MEXICO

by

Richard W. Harrison

Submitted in Partial Fulfillment of the
Requirement for the Degree of Ph.D. in Geoscience

New Mexico Institute of Mining and Technology
Socorro, New Mexico

Preface

This dissertation was written as a series of articles, each dealing with different aspects of Cenozoic geology of the Chloride mining district (north-central Black Range) and south-central New Mexico. Some of these articles have been published prior to completion of this volume. These articles are:

Harrison, R.W., 1986, General geology of Chloride mining district, Sierra and Catron Counties, New Mexico: New Mexico Geological Society, Guidebook 37, p. 265-272.

Harrison, R.W., 1988a, Primary structural control of epithermal mineralized shoots in southeastern Chloride mining district, New Mexico: New Mexico Geology, v. 10, p. 80-81.

Harrison, R.W., 1988b, A regional study of precious metal mineralization: Chloride mining district, New Mexico; in Torma, A.E., and Gundiler, I.H., (eds.), Precious and Rare Metal Technologies: Elsevier Science Publishers B.V., Amsterdam, p. 51-67.

Harrison, R.W., 1989, Exotic blocks within the Tertiary Rubio Peak Formation in the north-central Black Range, New Mexico: Occurrence, insights into

post-emplacement tectonic activity, economic implications, and emplacement hypothesis: New Mexico Geological Society, Guidebook 40, p. 99-106.

Chapter 1 of this volume is an introduction to this dissertation, largely taken from Harrison (1986). Chapters 2, 3, & 4 contained within this volume are to be submitted to the New Mexico Bureau of Mines and Mineral Resources for publication as a Bulletin under multiple authorship. All of the Plates contained within this volume, except for Plates 5 & 7, will be included in the Bulletin submittal. Plates 5 & 7 will be submitted to the New Mexico Bureau of Mines & Mineral Resources for publication as a geologic map and cross section at a later date. The copies of these two plates contained within this volume are dated status reports to be updated in the future.

Abstract

The Chloride mining district has been an area of intermittent precious- and base-metal mining activity for the past one hundred years. Metal values in excess of $20,000,000 have been produced from epithermal vein deposits that occur within the district. Tertiary volcanic and volcaniclastic rocks of the Mogollon-Datil volcanic field host the epithermal vein deposits. The oldest Tertiary unit in the Chloride mining district is the Rubio Peak Formation. Rubio Peak Formation overlies Paleozoic rocks with angular unconformity and is divisible into a lower, sediment-dominated sequence overlain by a volcanic-dominated sequence. Very large exotic blocks of Paleozoic rocks occur as gravity-slide deposits within the lower Rubio Peak Formation. Overlying the Rubio Peak Formation are tuff of Victoria Tank, tuff of Rocque Ramos Canyon, Kneeling Nun Tuff, sandstone of Monument Park, Caballo Blanco Tuff, tuff of Koko Well, basaltic andesite of Poverty Creek, and a complex sequence of rhyolitic volcanic and volcaniclastic rocks. Sediments of the Santa Fe Group, with minor interbedded lava flows, cap the Cenozoic volcanic stratigraphic section. Geochemical data shows a pattern in Eocene volcanism from mafic to silicic rock types, followed by a volcanic quiescence of approximately five million years, succeeded by a brief, but voluminous, late Oligocene volcanic cycle from mafic to silicic rock types.

Dextral strike-slip faulting along north-northeast trends is the oldest Cenozoic deformation, cutting only Rubio Peak Formation and older rocks. Epithermal vein deposits occupy high-angle, normal faults that formed during late Oligocene as part of initial development of the Rio Grande rift. Unmineralized, high-angle normal faults along north, northwest, north-northeast to northeast and east trends cut the entire stratigraphic section and in part reactivated older structures.

Epithermal vein deposits consist of quartz, calcite, (fluorite, barite) gangue material with sulfide mineralization occurring in structurally controlled mineral shoots. Sulfide mineralization occurred in two stages in the southern portion of the district; an older stage of Pb, Zn, Cu, (Ag, Au) mineralization, followed by a second stage of Cu, Ag, Zn, Pb, (Au) mineralization. Second stage mineralization is extremely rich in copper, silver, and zinc. A single stage of Ag, Au, (Cu) mineralization occurred in the northern part of the district. Vein mineralization is spatially and temporally related to emplacement of late Oligocene rhyolite intrusives.

Table of Contents

List of Figures for Chapters 2, 3, 4

List of Tables for Chapters 2, 3, & 4

List of Plates

CHAPTER 1. INTRODUCTION

The Chloride mining district (previously Apache, Phillipsburg, and Black Range districts) is located along the eastern flank of north-central Black Range, Sierra County, New Mexico (Fig.1). Precious- and base-metal epithermal mineralization occurs within fissure-filling vein systems hosted by volcanic and volcaniclastic rocks of the mid-Tertiary Mogollon-Datil volcanic field. The mining district lies almost exclusively within the Gila National Forest, bordering upon the Gila Wilderness Area. Terrain is rugged and, although NM-59 traverses the northern part of the district, access is limited to four-wheel drive and foot travel through much of the remainder of the mining district.

Approximate production from the district for the period 1880-1932 is estimated at $1,000,000 in gold and silver (minor copper, lead, and zinc) (Harley 1934). During the period 1932-1982, only small amounts of direct shipping ore were produced from the district, with no available production estimates. In 1982-1985, St. Cloud, U.S. Treasury, Great Republic, and Minnehaha mines produced just over two million ounces of silver, nine thousand ounces of gold, and three thousand tons of copper, in addition to several thousand tons each of lead and zinc. The bulk of this production was from the St. Cloud and U.S. Treasury mines. Since 1986, the Midnight mine has produced approximately three hundred thousand ounces of silver and

Figure 1. Location map of Chloride mining district.

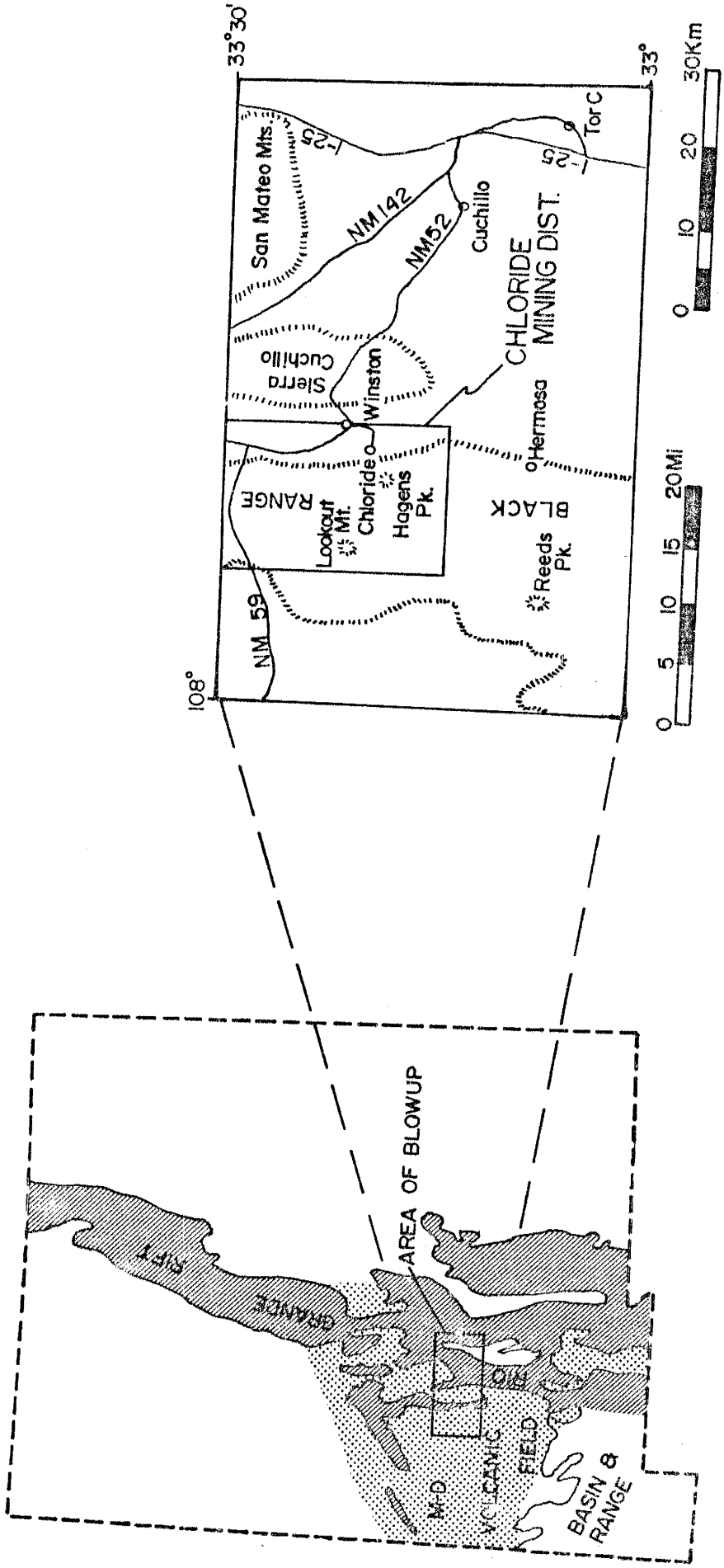
33°30'
33°
108°
San Mateo Mts.
NM142
NM52
NM 59
Cuchillo
Tor C
CHLORIDE MINING DIST.
Sierra Cuchillo
Winston
Hermosa
Chloride
Hagens Pk.
Lookout Mt.
Reeds Pk.
RANGE
BLACK
30Km
20
10
0
20Mi
15
10
5
0
AREA OF BLOWUP
RIFT
GRANITE
RIO
VOLCANIC
FIELD
BASIN & RANGE

five hundred tons of copper, and the Great Republic and Minnehaha mines have produced a couple hundred thousand tons of high-silica smelter flux.

Previous Investigations

Silliman (1882) visited the mining district during its boom days of the 1880's and early 90's. He was impressed by the greater than 13 km length of the Great Master Lode and its high-grade black streaks that assayed 50-60 oz/ton gold and over 200 oz/ton silver.

Gordon (Lindgren et al., 1910) later visited the region and briefly described the history, geology, and mineral deposits. He described the general stratigraphy and structure of the district and included a sketch map showing unsurveyed claim locations in relation to major drainages and prominent landmarks. The two vein systems recognized by Gordon are Au, Ag, (Cu) mineralization along north-south trends and Ag, Cu mineralization along east-west trends.

The most extensive report on geology and past mining activity to date for the Chloride mining district was published by Harley (1934). He presented geologic descriptions of many mines in the district that are presently inaccessible. He also re-emphasized the north-south and east-west vein systems recognized by Gordon in Lindgren et al. (1910).

The preliminary geologic map of the Winston quadrangle by

Maxwell & Heyl (1976) shows epithermal-vein systems in the southwestern portion of the district as well as some of the major allochthonous Paleozoic limestone blocks of the region. They interpreted these exotic blocks to be either of Magdalena Group or of San Andres Limestone and to have been emplaced by gravity-sliding mechanisms. Maxwell & Heyl (1980) described the mineralization and structure of deposits in the Hermosa, Chloride, and Phillipsburg mining areas, the latter two of which are incorporated into the Chloride mining district in this report. They also recognized two vein categories in the Chloride (Phillipsburg) area: (1) an older series of northwest-trending en echelon fault zones with fissure veins containing Cu, Pb, Zn, Ag, Au mineralization; and (2) north-northeast-trending veins with quartz, calcite, and fluorite mineralization "cut by thin dark-gray to black reticulate seams containing Au, Ag and minor Cu."

Larsen (1975), Winston (1975), Woodard (1982), Abitz (1984), Neal (1985) and Behr (1988) completed M.S. theses on geology and geochemistry of volcanic rocks in and around the Chloride district. Freeman & Harrison (1984) briefly described the regional geology and some of the recent mining activity within the district. Neal and Larson (1986) address mineral and fluid geochemistry of the Hoosier vein system.

Epithermal Vein Deposits

Epithermal mineral deposits in the Chloride mining district occur as open-space, fissure-filling veins with or without disseminated mineralization in adjacent wallrocks. Vein deposits consist dominantly of quartz and calcite (minor fluorite, barite) gangue material, with varying amounts of sulfide and native-metal mineralization occurring in distinct, structurally controlled shoots. Rocks of the Rubio Peak Formation are primary hosts for vein deposits, with a few occurences in tuff of Rocque Ramos Canyon and Kneeling Nun Tuff. Basaltic andesite of Poverty Creek occurs in the hanging wall of one northern vein, but its emplacement there is believed to be post-mineralization.

Quartz occurs as multiple pulses of coarse-grained to vuggy to cryptocrystalline and as milky white, clear, or amethystine varieties. Calcite, fluorite, and barite mineralization always occur as latest-stage vein filling. Quartz and adularia mineralization occur concurrently with sulfide and gold mineralization.

Districtwide sulfide mineralogy is varied in both vertical and lateral dimensions. In a vertical direction, both upper precious-metal and lower base-metal horizons described by Buchanan (1981) for epithermal systems are recognized in individual deposits of the Chloride mining district. Most of the Au mineralization occurs in the upper precious-metal horizon of individual deposits. Regional

lateral-zonation patterns are also recognized for both base and precious metals, portions of which were noted by Lindgren et al. (1910), Harley (1934), and Maxwell & Heyl (1980). A district-wide study of precious-metal mineralization is presented by Harrison (1989c).

Southern Chloride district

Cu-Ag mineralization in the southern part of the district is localized within a circular belt, 3-8 km in radius, centered on the Chloride Creek dome (Fig. 2). Veins radiate away from this dome along west, north, and northwest trends. Mineralogy in this Cu-Ag stage consists of bornite, chalcocite, argentite, minor chalcopyrite, and native silver along Silver Monument and New Era vein systems west of the Chloride Creek dome; bornite, chalcocite, and argentite along Dreadnaught and Black Hawk vein systems north of Chloride Creek dome; and bornite, digenite, chalcocite, covellite, and betehkenite along St. Cloud-U.S. Treasury, Hoosier, Colossal, and Midnight (Pye Lode) vein systems southwest of Chloride Creek dome. Ag in this stage is largely contained by primary Cu minerals as lattice substitutions. For similar mineralization at Butte, Montana, Brimhall et al. (1984) indicate possible Ag contents in chalcocite-digenite up to 926 ppm, bornite up to 1,075 ppm (0.1 wt%) and covellite up to 10,000 ppm (1 wt%).

An older stage of Pb, Zn Cu (Ag) mineralization occurs in

Figure 2. Major vein systems of the Chloride mining district.

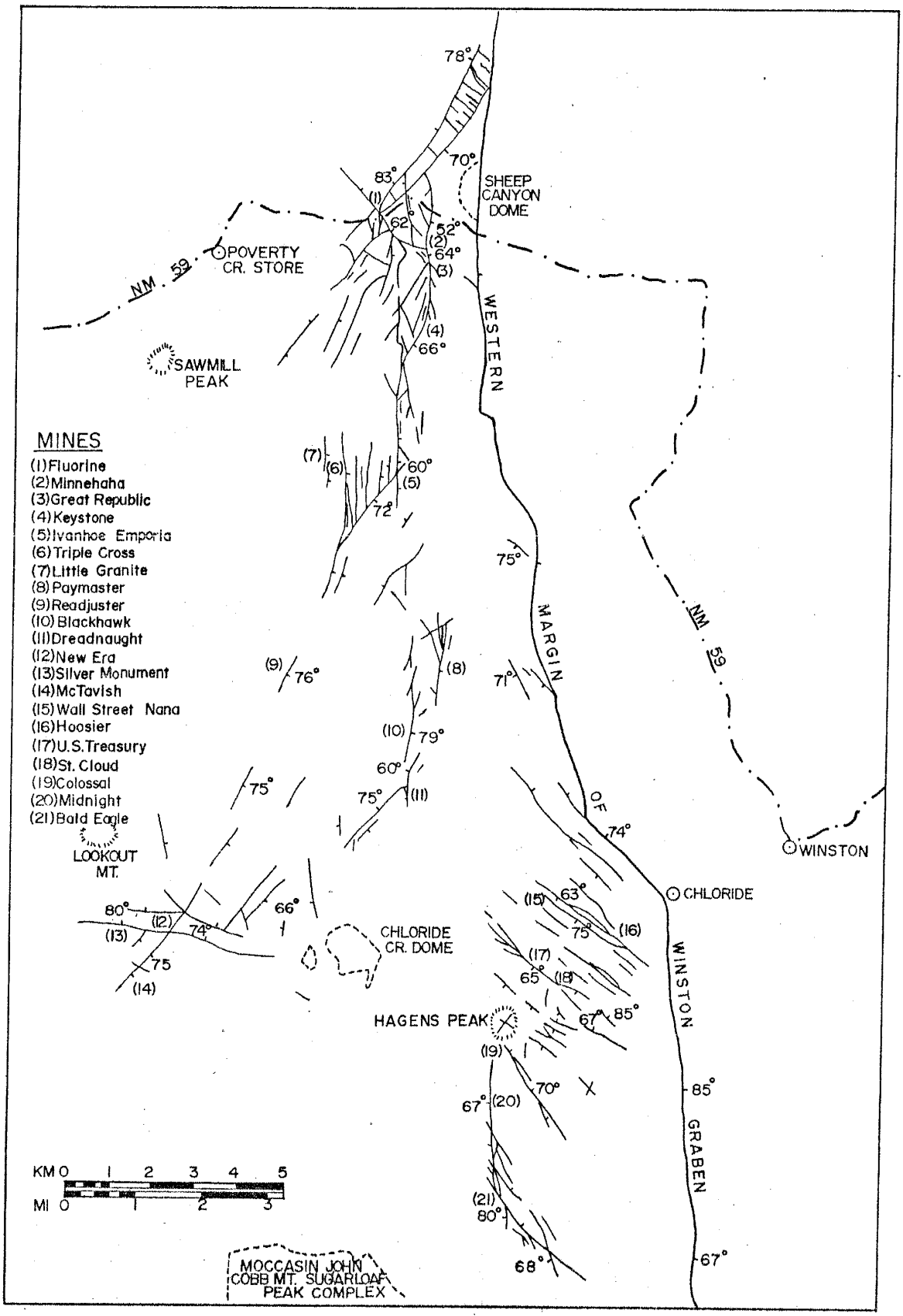
MINES
(1) Fluorine
(2) Minnehaha
(3) Great Republic
(4) Keystone
(5) Ivanhoe Emporia
(6) Triple Cross
(7) Little Granite
(8) Paymaster
(9) Readjuster
(10) Blackhawk
(11) Dreadnaught
(12) New Era
(13) Silver Monument
(14) McTavish
(15) Wall Street Nana
(16) Hoosier
(17) U.S. Treasury
(18) St. Cloud
(19) Colossal
(20) Midnight
(21) Bald Eagle
NM. 59
POVERTY CR. STORE
SAWMILL PEAK
SHEEP CANYON DOME
WESTERN
MARGIN
OF
WINSTON GRABEN
CHLORIDE
WINSTON
CHLORIDE CR. DOME
HAGENS PEAK
LOOKOUT MT.
MOCCASIN JOHN
COBB MT. SUGARLOAF
PEAK COMPLEX
KM 0 1 2 3 4 5
MI 0 1 2 3

vein systems in the southeastern portion of the Chloride district. Mineralogy in this first-stage mineralization consists of galena, sphalerite, and chalcopyrite (polybasite, pyrargyrite, pyrite). This stage is much poorer in precious-metal content than the second-stage mineralization, except in shallow areas where secondary processes greatly increase tenor, such as at the Bald Eagle mine.

The first and second mineralization stages overlap each other in portions of the Hoosier, St. Cloud-U.S. Treasury, Colossal, and Midnight-Bald Eagle (Pye Lode) vein systems. A mineral paragenesis typical of these vein systems is given in Fig. 3. Whether the two stages are genetically related, or represent two distinct, unrelated mineralizing pulses is unresolved. Vein textures in the St. Cloud-U.S. Treasury system clearly show a temporal difference in the two stages of mineralization, and K-Ar ages indicate as much as 2.5 my difference. Stage 1 mineralization at the Bald Eagle mine yielded a date of 28.9 $\pm$ 1.1 my, while stage 2 mineralization at the Silver Monument, Hoosier, and St. Cloud mines yielded dates of 26.3 $\pm$ 1.1 my, 26.9 $\pm$ 2.0 my, and 26.5 $\pm$ 1.1 my, respectively (M. Bauman, unpubl. report for FRM Minerals, 1984). There exists a great similarity between stage 1 mineralization in the Chloride district and sulfide mineralization in the Palomas (Hermosa) mining distrist 8-11 km to the south. Palomas mineralization is described by Jicha (1954), Jahns (1957), and Shepard (1984).

It seems quite possible that Chloride district stage 1 mineralization and Palomas mineralization are representatives of a distinct hydrothermal event associated with the Moccasin John flow-dome complexes located midway between the two mining districts.

Of all the complexities in Chloride district mineralization, the most obvious and extreme variation is in the amount of lead and zinc sulfide occurrences. These metals are present in large quantities in the southeastern part of the district and virtually absent throughout the remainder of the district. Cu, Ag. (Au) mineralization is ubiquitous to the entire district in some form.

A possible explanation for Pb, Zn variation is offered by Shikazono (1985), who studied Neogene vein-type deposits in Japan and noted Cu-Pb-Zn-rich mineralization in association with organic-bearing sedimentary rocks. Au, Ag mineralization, on the other hand, was found by Shikazono (1985) to occur dominantly in association with only volcanic rocks.

These ideas are consistent with observations for the area of high Pb, Zn mineralization on the Chloride district. Paleozoic sedimentary rocks are interpreted from geophysical data as existing beneath a relatively shallow volcanic cover in this area when compared to the rest of the district (Ericksen et al., 1970). This interpretation is supported by detailed geologic mapping of the Winston quadrangle (Harrison, 1989b; Plate 1).

Figure 3. Mineral paragenesis for epithermal vein systems in southeastern portion of Chloride mining district.

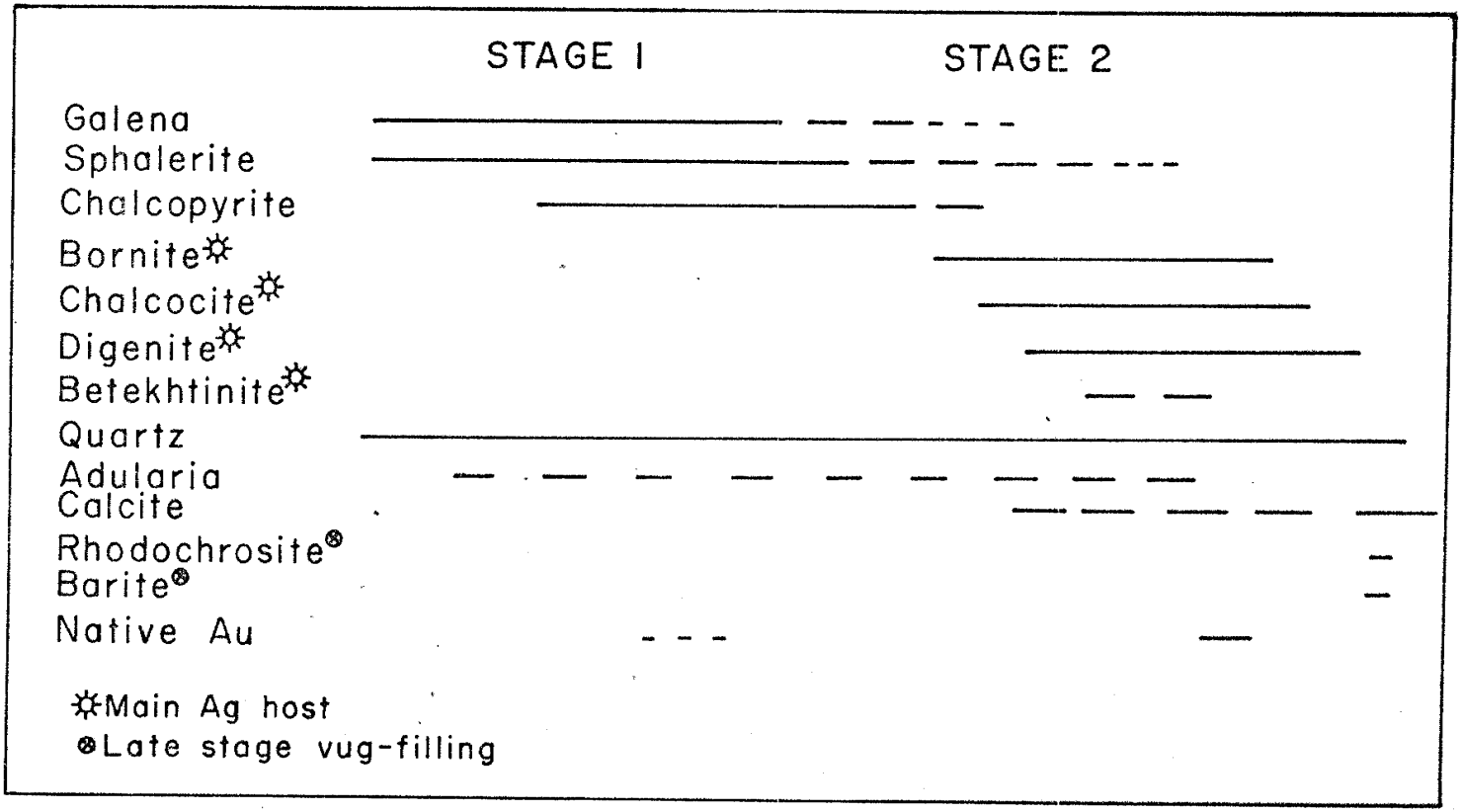
STAGE 1
STAGE 2
Galena
Sphalerite
Chalcopyrite
Bornite☼
Chalcocite☼
Digenite☼
Betekhtinite☼
Quartz
Adularia
Calcite
Rhodochrosite⊗
Barite⊗
Native Au
☼Main Ag host
⊗Late stage vug-filling

Northern Chloride district

Epithermal vein systems in the northern part of the district exist along dominantly north trends with lesser northeast and northwest trends. The longest continuous vein system in the district, the Great Master Lode, occurs in this area, winding along north and northeast trends for more than 11 km. Vein adularia at the Minnehaha mine, on the Great Master Lode, yielded a K-Ar age of 26.2 ± 1.2 my, nearly identical to dates for stage 2 mineralization in the southern half of the district (M. Bauman, unpubl. report for FRM Minerals, 1984).

Northern gangue mineralogy differs slightly from that in southern vein systems in that a moderate amount of fluorite and barite occur in the north and are virtually absent in the south. Sulfides in northern vein systems occur primarily as dark, very fine-grained bands, pods, and streaks. Mineralogy is principally acanthite, tetrahedrite, and pyrite with lesser bornite, chalcopyrite, and native Au occurrences. A rhyolite flow-dome complex located in Sheep Canyon is possibly a control for northern epithermal mineralization, as the Chloride Creek dome appears to be for southern mineralization.

References

Abitz, R.J., 1984, Volcanic geology and geochemistry of the northeastern Black Range Primative Area and vincinity, Sierra County, New Mexico (unpublished M.S. thesis): University of New Mexico, Albuquerque, 121 p.

Behr, C., 1988, Geochemical analyses of ore fluids from the St. Cloud-U.S. Treasury vein system, Chloride mining district, New Mexico (unpublished M.S. thesis): New Mexico Institute of Mining and Technology, Socorro, 125 p.

Brimhall, G.H., Jr., Cunningham, A.B., and Stoffregen, R., 1984, Zoning in precious metal distribution within base metal sulfides: a new lithologic approach using generalized inverse methods: Economic Geology, v. 79, p. 209-226.

Buchanan, L.J., 1981, Precious metal deposits associated with volcanic environments in the southwest: Arizona Geological Society Digest, v. 14, p. 237-262.

Ericksen, G.E., Wedon, H., Jr., Eaton, G.P., and Leland, G.R., 1970, Mineral resources of the Black Range Primitive Area, Grant, Sierra, and Catron Counties, New Mexico: U.S. Geological Survey, Bulletin 1319-E, 162 p.

Freeman, P.S., and Harrison, R.W., 1984, Geology and development of the St. Cloud silver deposit, Sierra County, New Mexico: Arizona Geological Society Digest, v. 15, p. 2310233.

Harley, G.T., 1934, The geology and ore deposits of Sierra County, New Mexico: New Mexico Bureau of Mines and Mineral Resources, Bulletin 10, 220 p.

Jahns, R.H., 1957, The Pelican area, Palomas (Hermosa) district, Sierra County, New Mexico: New Mexico Bureau of Mines and Mineral Resources, Bulletin 55, 5 p.

Jicha, H.L., Jr., 1954, Paragenesis of the Palomas (Hermosa) district, southwestern New Mexico: New Mexico Bureau of Mines and Mineral Resources, Circular 27, 20 p.

Larsen, M.E., 1975, Geology and ore deposits of the Silver Monument and New Era mines, Sierra County, New Mexico (unpublished M.S. thesis): University of Texas at El Paso, 54 p.

Lindgren, W., Graton, L.C., and Gordan, C.H., 1910, The ore deposits of New Mexico: U.S. Geological Survey, Professional Paper 68, p. 260-266.

Maxwell, C.H., and Heyl, A.V., 1976, Preliminary geologic map of the Winston quadrangle, Sierra County, New Mexico: U.S. Geological Survey, Open-file Report 76-858, 1 sheet.

Maxwell, C.H., and Heyl, A.V., 1980, Mineralization and structure of the Hermosa, Chloride, Philipsburg areas, New Mexico: Global Tectonics and Metallogeny, v. 1, no. 2, p. 129-133.

Neal, W.S., and Larson, P.B., 1986, Mineral and fluid geochemistry of the Hoosier vein, Chloride mining district, New Mexico (abstract): Geological Society of America, Abstracts with Programs, v. 18, no. 6, p. 703.

Shepard, M.D., 1984, Geology and ore deposits of the Hermosa mining district, Sierra County, New Mexico (unpublished M.S. thesis): University of Texas at El Paso, 215 p.

Shikazono, N., 1985, Gangue minerals from Neogene vein-type deposits and an estimate of their CO2 fugacity: Economic Geology, v. 80, p. 754-768.

Silliman, B. Jr., 1882, The mineral regions of southern New Mexico: American Institute of Mining Engineering, Transactions, v. 10, p. 440-443.

Winston, M.E., 1975, Geology of the Silver Monument area, Sierra County, New Mexico (unpublished M.S. thesis): University of Texas at El Paso, 65 p.

Woodard, T.W., 1982, Geology of the Lookout Mountain area, Black Range, Sierra County, New Mexico (unpublished M.S. thesis): University of New Mexico, Albuquerque, 95 p.

Cenozoic Stratigraphy, Geochemistry, Structure, and Geologic History of North-central Black Range, New Mexico in the Vicinity of Chloride Mining District and Taylor Creek Tin District.

R.W. Harrison, T.L. Eggleston,
W.C. McIntosh, and C.E. Chapin

CHAPTER 2. CENOZOIC STRATIGRAPHY AND GEOCHEMISTRY

Introduction

Cenozoic stratigraphy of north-central Black Range, New Mexico, in vicinity of Chloride mining district and Taylor Creek tin district consists predominantly of volcanic and volcaniclastic units that are part of Mogollon-Datil volcanic field. Geographically, this area lies near the center of the volcanic field. A map showing location of Chloride mining district and Taylor Creek tin district in north-central Black Range is presented in Figure 1a. Many of the units occurring in north-central Black Range are recognized regionally and are correlative to units found in southern Black Range (Seager et al., 1982), Sierra Cuchillo (Osburn et al., 1986; Jahns et al., 1978;), and Black Range composite of Elston and others (1975). Some of the ignimbrite sheets used by McIntosh (1989) to develop a stratigraphic framework for entire Mogollon-Datil volcanic field are found in north-central Black Range. As expected of volcanic terrane, some units present in vicinity of Chloride mining district and Taylor Creek tin district appear to be unique to this area. A composite stratigraphic section for Cenozoic rocks of north-central Black Range and regional stratigraphic correlations are shown in Figure 1b.

Total thickness of Cenozoic section in north-central Black Range is in excess of 3500 m. Numerous intermediate to silicic flow-dome complexes and dikes occur in the

Figure 1a. Location map showing Chloride mining district and Taylor Creek tin district in north-central Black Range.

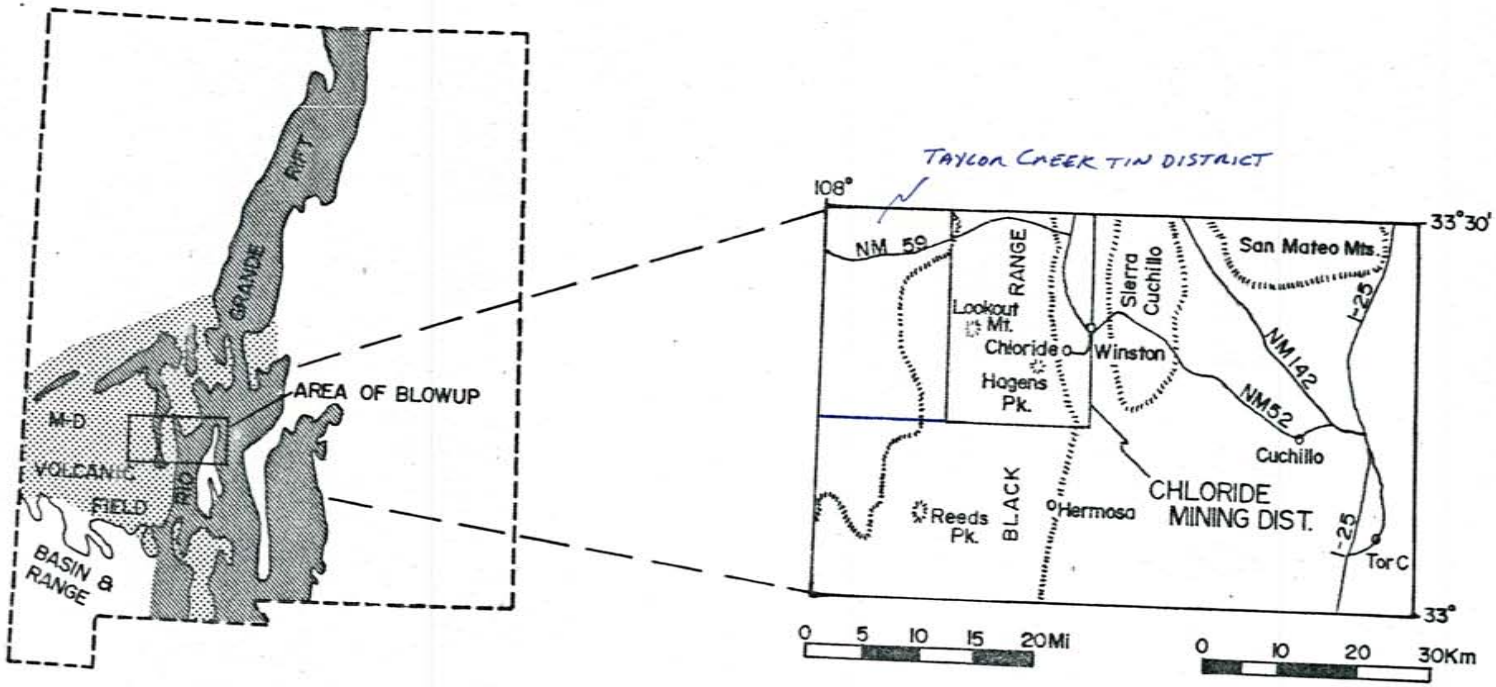
RIO GRANDE RIFT
AREA OF BLOWUP
M-D
VOLCANIC
FIELD
BASIN & RANGE
TAYLOR CREEK TIN DISTRICT
108°
33°30'
33°
NM 59
BLACK RANGE
Lookout Mt.
Chloride
Hagens Pk.
Winston
Sierra Cuchillo
San Mateo Mts.
I-25
NM 142
NM52
Cuchillo
Reeds Pk.
Hermosa
CHLORIDE MINING DIST.
Tor C
0 5 10 15 20Mi
0 10 20 30Km

Figure 1b. Stratigraphic correlation chart for Cenozoic volcanic and volcaniclastic rocks of south-central New Mexico. Sections representing the Chloride-Winston area and the Taylor Creek area make up composite of north-central Black Range.

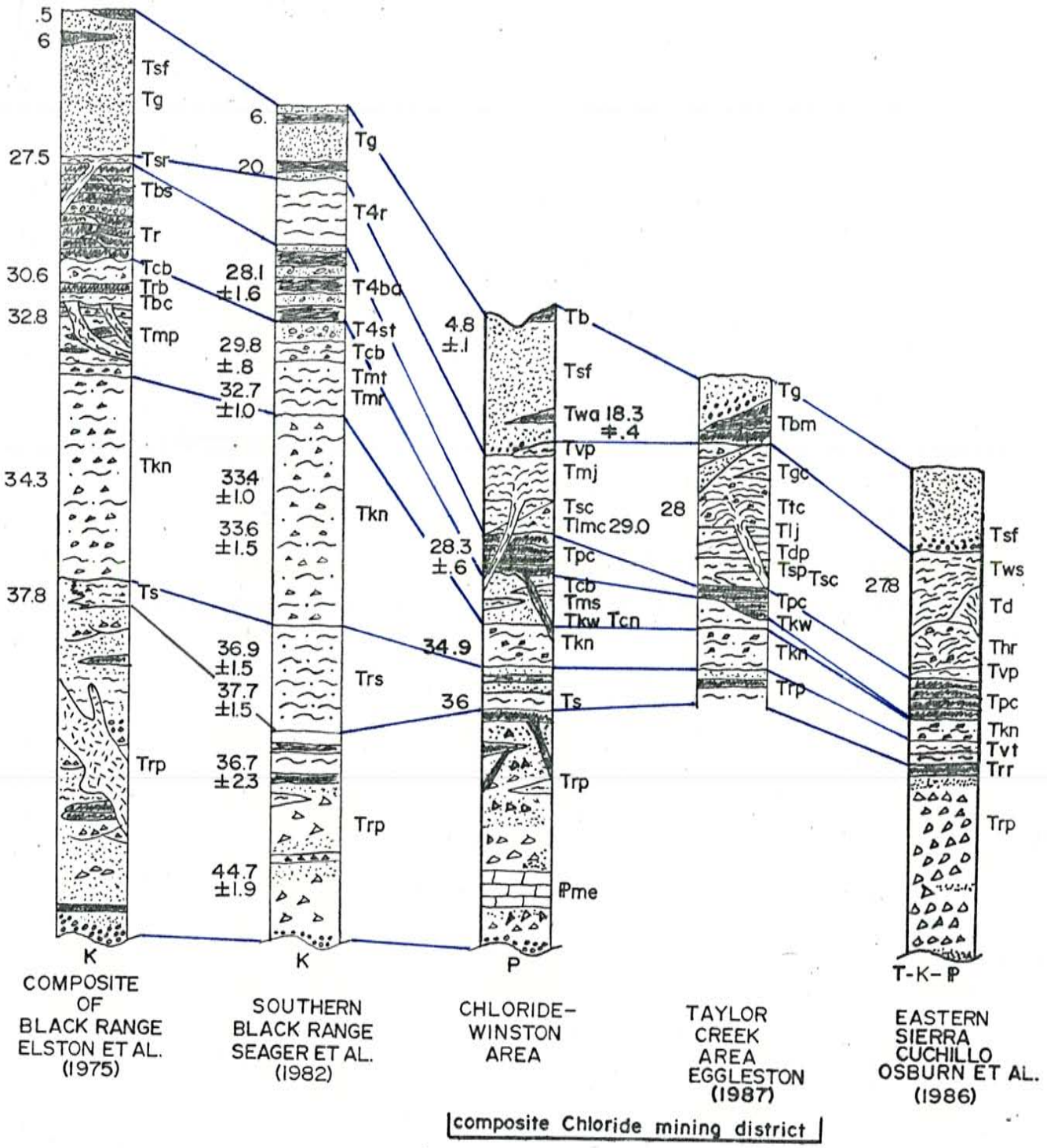

composite Chloride mining district

Figure 16.
Explanation:

Composite of Black Range (Elston et al., 1975); Tsf-Tg- Santa Fe Group & Gila Group; Tsr- Swartz Rhyolite; Tbs- Bear Springs Basalt; Tr- Razorback Formation; Tcb- Caballo Blanco Rhyolite; Trb- Rustler Basalt; Tbc- Box Canyon Tuff; Tmp- Mimbres Peak Formation; Tkn- Kneeling Nun Tuff; Ts- Sugarlump Tuff; Trp- Rubio Peak Formation;

Southern Black Range (Seager et al., 1982); Tg- Gila Group; T4r- younger rhyolite; T4ba- basaltic andesite flows; T4st- undifferentiated tuffs and sedimentary rocks; Tcb- Caballo Blanco Rhyolite Tuff; Tmt- tuffs of Mimbres Peak Formation; Tmr- rhyolites of Mimbres Peak Formation; Tkn- Kneeling Nun Tuff; Trs- Sugarlump Formation; Trp- Rubio Peak Formation;

Chloride-Winston area (this report); Tsf- Santa Fe Group; Tb- basalt of Table Top Mt.; Twa- Winston andesite, Bearwallow Mountain Formation; Tvp- Vicks Peak Tuff; Tmj- Moccasin John Rhyolite; Tsc- tuff of Stiver Canyon; Tlmc- tuff of Little Mineral Creek; Tpc- basaltic andesite of Poverty Creek; Tcb- Caballo Blanco Tuff; Tms- sandstone of Monument Park; Tkw- tuff of Koko Well; Tcn Cuchillo Negro Complex; Tkn- Kneeling Nun Tuff; Tdc- tuff of Rocque Ramos Canyon; Ts- tuff of Victoria Tank; Trp- Rubio Peak Formation.

Taylor Creek area (Eggleston, 1987; this report); Tg- Gila Group; Tbm- Bearwallow Mountain Formation; Tgc- tuff of Garcia Camp; Ttc- Taylor Creek Rhyolite; Tlj- La Jencia

Tuff; Tdp- Dolan Peak Rhyolite; Tsp- tuff of Stiver Canyon; Tsp- Sawmill Peak Rhyolite; Tpc- basaltic andesite of Poverty Creek; Tkw- tuff of Koko Well; Tkn- Kneeling Nun Tuff; Trp- Rubio Peak Formation.

Eastern Sierra Cuchillo (modified slightly from Osburn et al., 1986); Tsf- Santa Fe Group; Tws- Willow Springs Rhyolite; Td- unnamed dacite flows; Thr- rhyolite of HOK Ranch; Tvp- Vicks Peak Tuff; Tpc- basaltic andesite of Poverty Creek; Tkn- Kneeling Nun Tuff; Tvt- tuff of Victorio Tank; Trr- tuff of Roque Ramos Canyon; Trp- Rubio Peak Formation.

section and have contributed to its aggregation. In general, the Cenozoic stratigraphic section of north-central Black Range can be divided into four volcanic-sedimentary groups: 1) Eocene volcaniclastic and volcanic rocks of intermediate composition; 2) Eocene-Oligocene ash-flow tuffs and minor volcaniclastic material of silicic composition; 3) Oligocene flows and flow-dome complexes of basaltic andesite to high-silica rhyolite compositions; and 4) late Oligocene-Neogene volcaniclastic deposits (Santa Fe Group-Gila Group) with minor intercalated mafic to intermediate volcanic rocks. Detrital fragments of pre-Cenozoic rocks are found only within about 350 m of the base of Cenozoic section, and in Pliocene-Quaternary deposits of Santa Fe Group.

Cenozoic magmatic activity in north-central Black Range has been episodic, punctuated with periods of quiescence. Magmatically active periods can be divided into four approximate time intervals: 43-35 Ma, 29.1-28.1 Ma, 25-18 Ma, and 4-5 Ma. The oldest time interval is represented by a continuum from intermediate volcanism of Rubio Peak Formation through eruption of Kneeling Nun Tuff. The relatively brief period from 29.1-28.1 Ma saw widespread and voluminous eruption of basaltic andesite of Poverty Creek and many rhyolite to high-silica rhyolite flow-dome complexes and related pyroclastic rocks. The 25-18 Ma interval contains widespread mafic to intermediate volcanism from isolated stratovolcances and flow domes that are

collectively referred to as Bearwallow Mountain Formation. The youngest volcanic time interval is represented by minor basaltic eruptions.

Cenozoic basal unconformity

Deposition of Cenozoic rocks in south-central New Mexico occurred upon an irregular, regional unconformity that exposed various Mesozoic and Paleozoic formations. This unconformity is diachronous and largely related to uplift during early stages of Laramide orogeny. In the Cutter Sag – Jornada del Muerto basins northeast of Truth or Consequences, the McRae Formation (Cretaceous-Tertiary) of Kelley and Silver (1952) and Bushnell (1953, 1955) lies unconformably upon Cretaceous Mesa Verde Group. Farther south in southern Jornada del Muerto, the Love Ranch Formation (late Paleocene ?-Eocene) of Kottlowski and others (1956) lies unconformably upon basal McRae Formation (Seager et al., 1986); in southern Caballo Mountains, Love Ranch Formation unconformably overlies rocks of Permian to Precambrian age (Seager et al., 1986).

Intermediate volcanic and volcaniclastic rocks of Rubio Peak Formation and correlative Palm Park and Red Rock Ranch Formations (late Eocene) unconformably overlie rocks of Early Tertiary through Precambrian age, except for in the Love Ranch basin where rocks of the Palm Park Formation conformably overlie the Eocene Love Ranch Formation (Seager et al., 1986). Figure 2 is a regional map of southwestern New Mexico showing a simplified paleo-outcrop pattern for rocks underlying Rubio Peak Formation and correlative units.

In north-central Black Range, exposures of Cenozoic

Figure 2. Regional map of southwestern New Mexico showing simplified paleo-outcrop pattern of rocks underlying late Eocene formations: Rubio Peak Formation, Palm Park Formation, Red Rock Ranch Formation, and Dog Springs Member of lower Datil Group. Box indicates approximate position of north-central Black Range. Light-green colored areas= Tertiary or Cretaceous rocks are immediately below Rubio Peak Formation or equivalent; dark-green areas=Permian rocks below Rubio Peak Formation; blue areas=Pennsylvanian through Precambrian rocks immediately beneath Rubio Peak Formation.

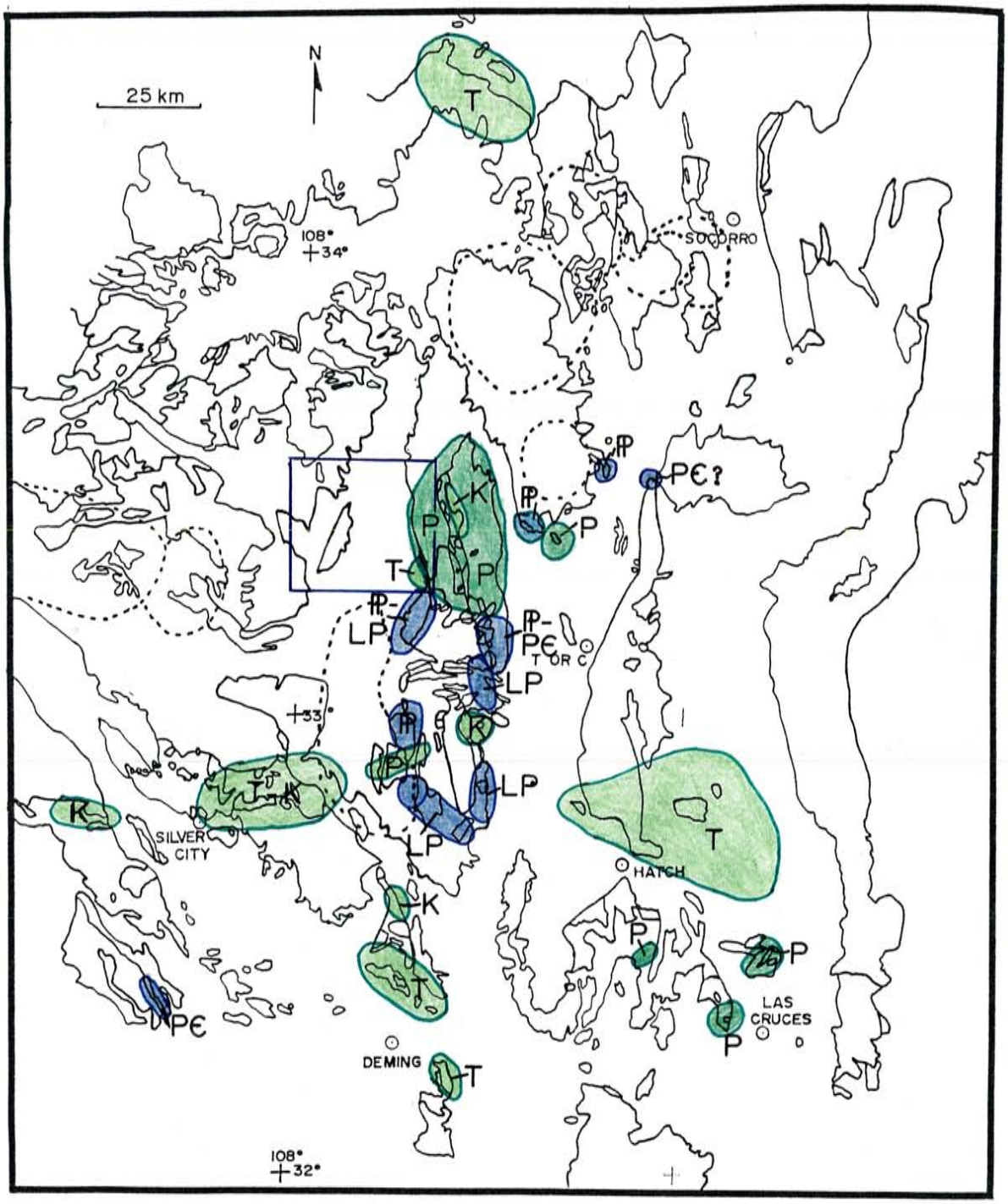
25 km
N
108°
+34°
SOCORRO
T
K
P
T
LP
PP-PC
T OR C
LP
+33°
LP
LP
T
K
SILVER CITY
HATCH
T
K
P
P
P
LAS CRUCES
PC
DEMING
T
108°
+32°
PC?
PP
P

basal unconformity are restricted to southeastern Chloride mining district in southeastern quarter of Winston quadrange (Plate 1). There, rocks of the Rubio Peak Formation rest with angular unconformity upon red-bed sandstone, siltstone, and shale of the Permian Abo Formation, and locally upon thin, discontinuous outcrops of conglomerate beds that have been included within the Rubio Peak Formation in this report, but as discussed later, are probably correlative to Lobo and Love Ranch Formations. Both narrow and relatively deep (> 40 m) and broad (> 1 km wide) paleovalleys have been cut into Abo Formation and filled with rocks of Rubio Peak Formation.

What Paleozoic units underlie most of north-central Black Range is a matter of conjecture. There are no outcrops of pre-Cenozoic rocks for more than 75 km to the west of Abo exposures described above (Dane and Bachman, 1965), except for a very small occurrence of Pennsylvanian limestone described by Aldrich (1976). Towards the south, in southern Black Range, rocks of the Rubio Peak Formation lie upon progressively older Paleozoic units. Eastward, in Sierra Cuchillo, debris-flow breccias of the Rubio Peak Formation lie upon Upper Permian San Andres Formation and locally upon remnants of Upper Cretaceous strata (Jahns et al., 1978).

Rubio Peak Formation

The oldest Cenozoic unit in north-central Black Range is Rubio Peak Formation of Jicha (1954). This unit crops out extensively throughout Chloride mining district, but has no exposures in Taylor Creek area. As used by Jicha (1954), Elston (1957), and Elston et al. (1975), the Rubio Peak Formation consists of Early Tertiary volcanic and volcaniclastic rocks of intermediate composition (andesite-latite) that occur beneath Kneeling Nun Tuff. Upper portions of Rubio Peak Formation interfinger with a sequence of ash-flow tuffs referred to as Sugarlump Tuff by Jicha (1954), Jones et al. (1967), and Elston (1976); and as Sugarlump Formation by Seager et al. (1982).

Rubio Peak Formation is correlative to Palm Park Formation of Kelley and Silver (1952), and Seager et al. (1971) in southern Caballo Mountains-Las Cruces area; Red Rock Ranch Formation of Farkas (1969), and Deal and Rhodes (1976) in southern San Mateo Mountains; and Dogs Springs Member of lower Datil Group of Osburn and Chapin (1983), and Cather (1986) in Datil-Gallinas Mountains. Rubio Peak Formation is equivalent to latite-andesite sequence of Jahns et al. (1978), andesite-latite of Montoya Butte of Maldonado (1974), and pyroclastic latite and andesite-latite flows of Hilland (1969) in Sierra Cuchillo. The Macho Andesite of Jicha (1954) is also included as part of Rubio Peak Formation by Seager et al. (1982).

As indicated by Elston (1976) and Seager et al. (1987), the Orejon Andesite of Dunham (1935) and Glover (1975) in the Organ Mountains is equivalent to Palm Park Formation; the unnamed epiclastic rocks and pyroxene-hornblende andesite of Ratte et al. (1969) in Blue Range Primitive Area is also probably correlative to Rubio Peak Formation, as is lower andesite unit of Stearns (1962) (Elston, 1976). In extreme southern New Mexico, probable correlative rocks occur in Tres Hermanas Mountains, Cedar Mountain Range, and in Pyramid Mountains (Clemons and Mack, 1988).

When all of the above formations are grouped together, it becomes apparent that volcanic and volcaniclastic rocks of Eocene age and intermediate composition (generally typified by phenocrysts of plagioclase and hornblende, ± pyroxene and biotite) are ubiquitous for all of southwestern New Mexico. Figure 3 shows the known distribution of Rubio Peak Formation, Palm Park Formation, Red Rock Ranch Formation, and Dog Springs Member of lower Datil Group in southwestern New Mexico. Red areas on this figure show locations of known or suspected vents. It is important to note that boundaries on Figure 3 are rather arbitrarily drawn, based on present-day knowledge and exposures. Similar rocks certainly exist farther south in Mexico, and probably occur buried in the center of Mogollon-Datil volcanic field.

Figure 3. Known distribution of Eocene volcanic and volcaniclastic rocks of intermediate composition in southwestern New Mexico; includes Rubio Peak Formation, Palm Park Formation, Red Rock Ranch Formation, and Dog Springs Member of lower Datil Group. Intrusives are shown in red. See text for descriptions and discussion.

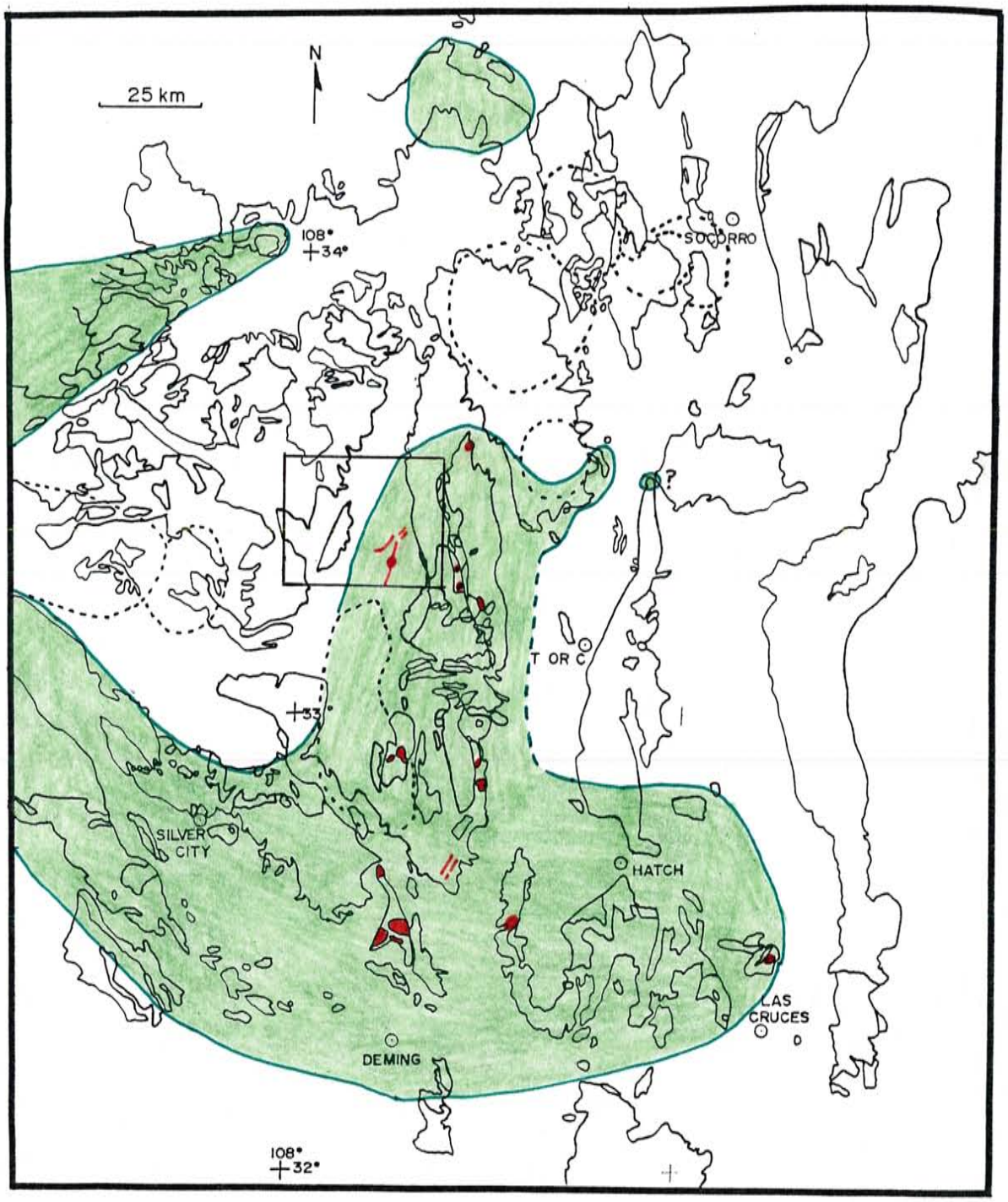
25 km
N
108°
+34°
SOCORRO
T OR C
+33°
SILVER CITY
HATCH
LAS CRUCES
DEMING
108°
+32°

Age dates and constraints

Age dates and other constraints indicate that Rubio Peak Formation and correlative rocks were deposited over a period of several million years, generally in the range of 45-37 Ma. Reported K/Ar radiometric ages for intrusive and extrusive rocks of Rubio Peak Formation are 44.7 ± 1.9 Ma, 38.0 ± 1.5 Ma, 37.6 ± 2.0 Ma, 36.7 ± 2.3 Ma (Seager et al., 1982); 36.7 ± 1.4 Ma (Loring and Loring, 1980); 37.3 ± 2.3 Ma (Marvin and Cole, 1978). A lithic dacite tuff interbedded with Macho Andesite has yielded a K/Ar age of 40.7 ± 1.4 Ma (Loring and Loring, 1980). Seager and Clemons (1975) report K/Ar ages of 43-40 Ma for Palm Park Formation; Seager et al. (1982) report ages of 51, 43, and 42 Ma. Osburn and Chapin (1983) report an average for two samples from Dog Springs Member of lower Datil Group of 39.1 Ma (K/Ar).

Minimum age constraints for the Rubio Peak Formation are provided from 40Ar/39Ar dating of sanidine from overlying Cueva Tuff-36.2 Ma, Bell Top 3 Tuff-35.7 Ma, Farr Ranch Tuff-35.6 Ma, and Kneeling Nun Tuff-34.9 Ma by McIntosh (1989). A similar minimum age constraint of ~36 Ma is given by Lucas (1986) from paleontologic evidence for the age of arkosic sediments (sandstone of Cliff Canyon) that directly overlie Rubio Peak Formation in the Chloride mining district. Sandstone of Cliff Canyon is stratigraphically equivalent to the Placitas Canyon lakebeds in southern San

Mateo Mountains described by Farkas (1969), Axelrod (1975), and Axelrod and Bailey (1976); a unit that is overlain by a basaltic andesite flow (Uvas Canyon andesite of Farkas, 1969) dated at 35.1 ± 1.8 Ma by Cather (1986).

An upper age limit for the Rubio Peak Formation is poorly constrained, and as indicated in the section on basal unconformity appears to be diachronous. Double S Peaks stock in sec. 35, T. 12 S., R. 7 W., dated by K/Ar at 39.2 ± 0.9 Ma, intrudes debris-flow deposits of the Rubio Peak Formation. In southern Salado Mountains (sec. 12, T. 14 S., R. 7 W.), rocks of the Rubio Peak Formation overlie a 43.7 ± 1.7 Ma (K/Ar) andesite dike (LaMarre, 1975; Seager and Mayer, 1988). Rocks of the Rubio Peak Formation unconformably overlie the Willow Springs-Cuchillo laccolith in Sierra Cuchillo (sec. 22, T. 11 S., R. 8 W.) dated at 50.1 ± 2.6 Ma (Chapin et al., 1975), and also unconformably overlie the 57-60 Ma copper porphyry intrusives in the Santa Rita area (Elston, 1976).

Intrusive sites of Rubio Peak age

Intrusive sites of Rubio Peak age appear to be numerous and widespread throughout southern New Mexico, but are poorly documented with few radiometric dates. A granodiorite porphyry stock in Cooke's Range has been dated by K/Ar at 38.8 ± 1.4 Ma by Loring and Loring (1980) and has the size and appearance of a major volcanic center. Many

smaller, yet similar, porphyry sills and semiconcordant masses were mapped by Seager et al. (1982) in the southern Black Range and Animas Mountains, and were interpreted as representing intrusive phases of Rubio Peak Formation. Additional intrusive bodies with similar characteristics and mineralogy, although undated, are found in the Tres Hermanas and Victorio Mountains, and along Fluorite Ridge in southern Cooke's Range (Griswold, 1961).

An andesite porphyry intrusive at southeastern end of San Diego Mountain yielded a K/Ar age of 42.2 ± 1.6 Ma; a plagioclase separate from a stock (?) of hornblende andesite (Cleofas andesite) in Dona Ana Mountains yielded a K/Ar age of 35.9 ± 1.6 Ma (Clemons, 1979). Approximately one dozen small stocks and dikes related to a major vent area of hornblende-biotite latite porphyry occur in the Good Sight Mountains; these intrusives have yielded K/Ar ages of 38.1 ± 2.0 Ma and 37.6 ± 2.0 Ma (Clemons, 1979).

As mentioned earlier, the Double S Peaks monzonite stock in southern Sierra Cuchillo has been dated at 39.2 ± 0.9 Ma. This stock possesses a characteristic common to several Rubio Peak-age intrusives, in that it is intrusive into basal Rubio Peak volcaniclastic deposits. [The Rubio Peak intrusives in the Good Sight Mountains show this relationship (Clemons, 1978; 1979)]. Also in southern Sierra Cuchillo, numerous intrusive bodies (dikes, sills, plugs, stocks, and laccoliths of both aphanitic latite-andesite and porphyritic monzonite) are correlative

with the Rubio Peak Formation on the basis of similar relative ages and composition (McMillan, 1979). Although undated, these intrusives are clearly of Rubio Peak age since they intrude into the middle of Rubio Peak section (Jahns et al., 1978). In northern Sierra Cuchillo, several dikes and one small plug intrude only Rubio Peak equivalent section (Maldonado, 1974), and are interpreted to represent an intrusive phase of the Rubio Peak Formation.

In the Chloride mining district, many Rubio Peak dikes and small plugs are mapped, especially in southern portions of the district (see Plates 1 & 2). Both porphyritic (plagioclase, hornblende, minor pyroxene) and aphanitic varieties are recognized in this area. These intrusives crosscut only volcaniclastic sediments of lower Rubio Peak Formation, and based on similar mineralogy and composition are interpreted as feeders for the extensive lava flows found in upper Rubio Peak Formation. Although these intrusives are undated, some age constraint is provided by 26-29 Ma epithermal quartz veins that offset these dikes. It is also important to note that hornblende-bearing volcanic rocks do not occur in the stratigraphic section above Rubio Peak Formation in the Chloride mining district.

Description of the Rubio Peak Formation in Chloride district

Rocks of the Rubio Peak Formation are widely exposed in the Chloride mining district. These rocks are the primary host of epithermal base- and precious-metal deposits that define the district. Extensive outcrops of Rubio Peak Formation are found through the center of Winston quadrangle (Plate 1), in the southeastern quarter of Lookout Mountain quadrangle (Plate 2), and in a 2 to 3 km-wide strip that runs along the eastern side of Sawmill Peak quadrangle (Plate 3) and the western side of adjoining Iron Mountain quadrangle (Plate 4).

Total thickness of the Rubio Peak Formation in the Chloride mining district varies from approximately 800 to 1000 m. Districtwide, the Rubio Peak Formation is divisible into a lower section of dominantly volcaniclastic deposits overlain by an upper section of dominantly intermediate lava flows and lesser volcaniclastic deposits.

Lower Rubio Peak

Basal conglomerate unit

Deposits of poorly sorted, clast-supported, boulder to cobble conglomerate with minor sandstone intervals locally occur at the base of the Rubio Peak Formation in

southeastern Chloride mining district (Trpc unit on Plate 1). These deposits contain rounded to well-rounded clasts of Permian Abo Formation, holocrystalline monzonitic rocks (some with pyrite disseminations), various intermediate volcanic rocks, and Paleozoic limestone (Fig. 4). Volumetrically, monzonite clasts are more abundant than Abo clasts which are are in turn, much more abundant than volcanic and limestone clasts. Clasts range in size from small pebbles to more than 1 m in diameter. In stratigraphic position and lithology of clasts, these rocks are similar to the Starvation Draw Member of Rubio Peak Formation described by Seager et al. (1982) in Cooke's Range, a unit that is generally correlative to Love Ranch Formation. The primary difference between the basal conglomerate unit of the Rubio Peak Formation in north-central Black Range and the Starvation Draw Member in Cooke's Range is the absence of Precambrian clasts in the former, a reflection of source-area terranes.

Exposures of the basal conglomerate unit are restricted to the southeastern edge of Chloride mining district in the Winston quadrangle, adjacent to the Winston graben. This unit has a maximum thickness of approximately 100 m along Monument Creek in secs. 16 & 17, T. 12 S., R. 8 W. and thins northward to about 15 m along the southside of South Fork of Cuchillo Negro Creek.

In the Monument Creek area, conglomerate deposits appear to grade upward into matrix-supported debris-flow deposits

Figure 4. Photograph of basal conglomerate member of Rubio Peak Formation, light-colored rocks are holocrystalline and monzonitic, reddish rocks are from Abo Formation. South Fork of Cuchillo Negro, extreme southern end of sec. 31, T. 11 S., R. 9 W.

over an interval of a few meters. Elsewhere however, indications are that erosion locally removed the basal conglomerate deposits prior to deposition of overlying debris-flow deposits. Both to north and south of conglomerate outcrops in the Monument Creek - South Fork of Cuchillo Negro Creek area, debris-flow deposits rest directly upon rocks of the Abo Formation, and locally fill steep paleo-valleys cut 20-30 m into the Abo Formation. In the Chloride Creek area, two small outcrops of the basal conglomerate unit are preserved in the footwall of a small thrust fault associated with Eocene wrench faulting. At these locations, rocks of the Abo Formation have been thrust over conglomerate deposits, and are directly overlain by debris-flow deposits.

Additional relationships consistent with the idea that an erosional surface partially removed basal conglomerate deposits are found in exposures along South Fork of Cuchillo Negro Creek (primarily in sections 5 & 6, T. 12 S., R. 8 W.). There, a northerly striking paleovalley is revealed, approximately one km wide, floored by rocks of the Abo Formation, and filled with rocks of the Rubio Peak Formation. Both flanks of the paleovalley dip steeply, 25-33 degrees, towards its axis. Approximately 15 m of the basal conglomerate unit is found on the eastern flank of this paleovalley, but conglomerate deposits are totally absent on the western flank, where matrix-supported, debris-flow deposits rest directly upon Abo Formation.

Small, cobble-size Abo and Paleozoic limestone clasts occur sparsely in these debris-flow deposits for a few meters above the Abo contact on western flank, but monzonite clasts are absent. Implications are that either the basal conglomerate unit was partially removed from the paleovalley prior to deposition of debris flows, or that the conglomerate deposits never completely filled the paleovalley. Figure 5 schematically shows all relationships observed between Abo Formation, basal conglomerate unit of Rubio Peak Formation, and debris-flow deposits of lower Rubio Peak Formation in southeastern Chloride mining district.

From pebble imbrications, Cather (1986) determined an overall east-to-west transport direction for the basal conglomerate unit in the area of Miranda Homestead (sec. 9, T. 12 S., R. 8 W.), between South Fork of Cuchillo Negro Creek and Monument Creek. Similar transport directions have been obtained for this report from outcrops in South Fork of Cuchillo Negro and Monument Creeks.

Figure 5. Schematic cross-section showing various relations observed between lower Cenozoic unconformity, basal conglomerate unit of Rubio Peak Formation (Trpc), and debris-flow deposits (Trp) in lower Rubio Peak Formation. Not to scale.

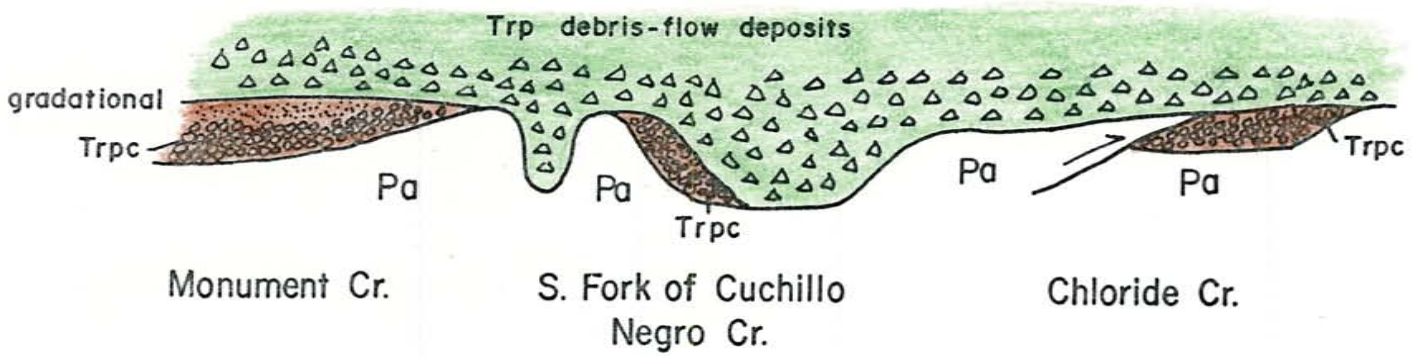
Trp debris-flow deposits
gradational
Trpc
Pa
Pa
Trpc
Pa
Pa
Trpc
Monument Cr.
S. Fork of Cuchillo Negro Cr.
Chloride Cr.

tuff of Miranda Homestead

Intertongued with the basal conglomerate unit is a strongly altered, moderately welded, lithic-rich, moderately crystal-rich ash-flow tuff. This tuff contains 10-15 % phenocrysts of white- and flesh-colored feldspars, quartz, and biotite. The name of this tuff is derived from exposures on Miranda Homestead in sections 9 & 16, T. 12 S., R. 8 W., where it has its maximum thickness of approximately 20 m. Laterally, tuff of Miranda Homestead grades into a water-laid tuff (Maxwell and Heyl, 1976). There is no known source area for this extremely minor unit.

debris-flow deposits

Debris-flow deposits volumetrically dominate the lower Rubio Peak Formation in the Chloride mining district. In northern half of the district, lower Rubio Peak Formation is totally comprised of debris-flow deposits. Approximately 300 m north of N.M. Highway 59 in the middle of sec. 34, T. 9 S., R. 9 W., an exploration core hole penetrated approximately 200 m of uninterrupted heterolithic, matrix-supported debris-flow deposits (unpub. drill report, St. Cloud Mining Co., with permission). In southern half of the Chloride mining district, debris-flow deposits interfinger with sandstone deposits and intermediate lava flows described in subsequent sections (see Fig. 6, sections

Figure 6. Stratigraphic sections derived from drill-hole intercepts for Rubio Peak Formation in southern Chloride mining district (from unpublished drill logs of First Miss Gold, Inc. and St. Cloud Mining Company, with permission).

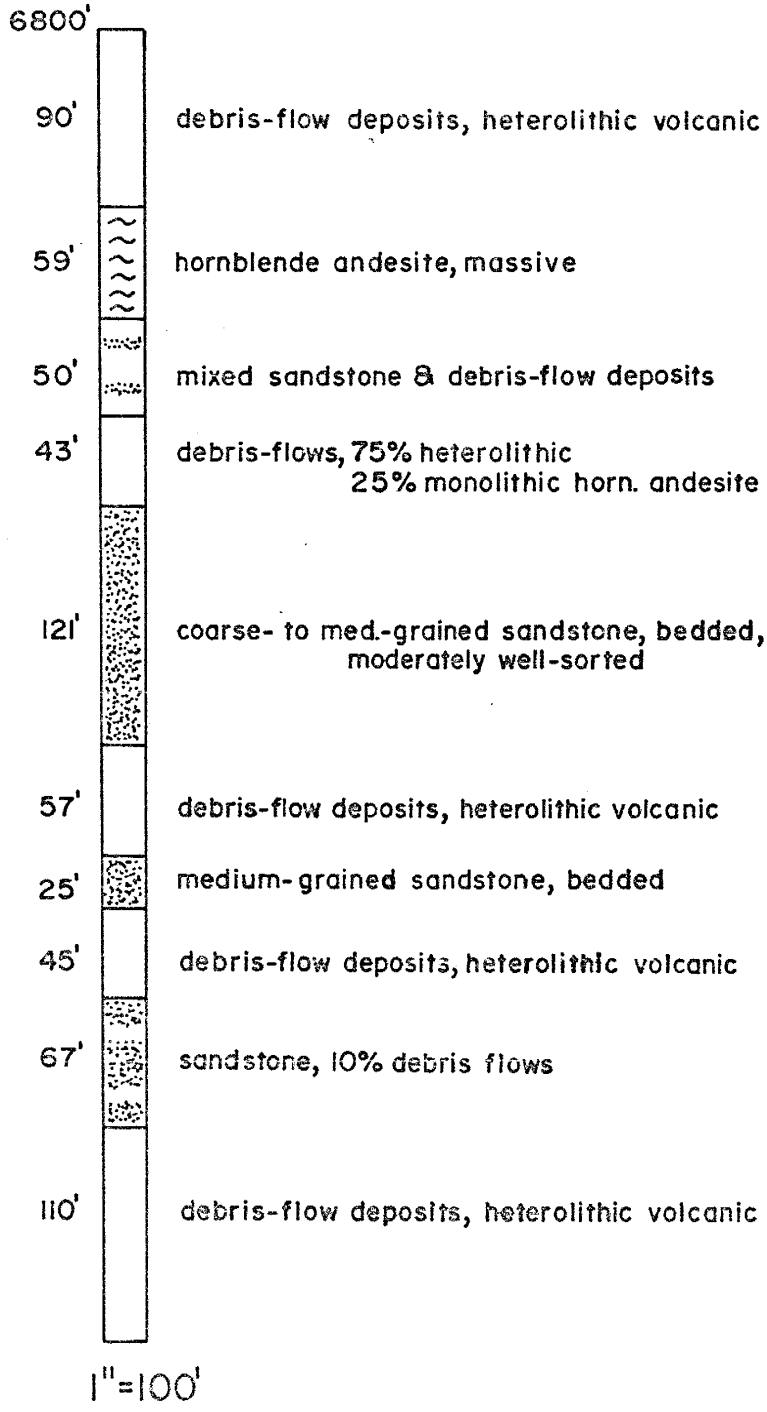

Section A. Rubio Peak Formation, south of Way Up Mt.
approx. 33°16'40"N, 107°43'02"W

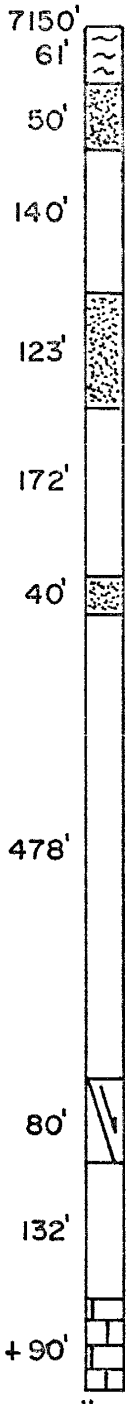

andesite lava, hornblende & plagioclase

coarse-grained sandstone, poorly sorted

debris-flow deposits, heterolithic volcanic

sandstone, poorly sorted, non-bedded

debris-flow deposits, heterolithic volcanic

sandstone, poorly sorted, massive

debris-flow deposits, heterolithic volcanic

normal fault zone (HW ↓ FW)

debris-flow deposits, heterolithic volcanic

limestone & shale, exotic gravity slide block?

Section B. Rubio Peak Formation near U.S. Treasury mine
approx. 33°19'35"N, 107°43'10" W

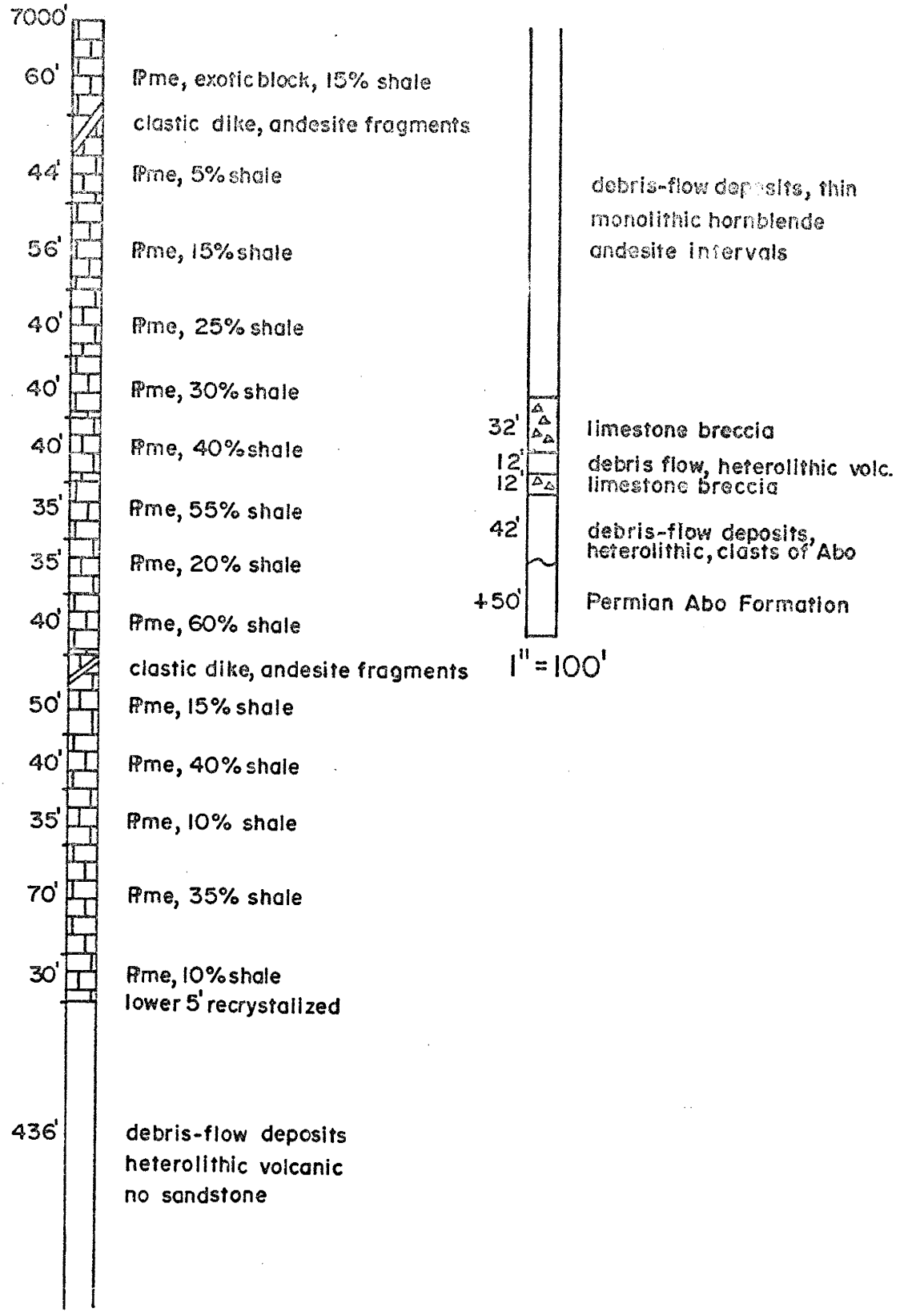

Section C. Rubio Peak Formation near Hoosier mine
center of sec. 19, T. 11 S., R. 8W.

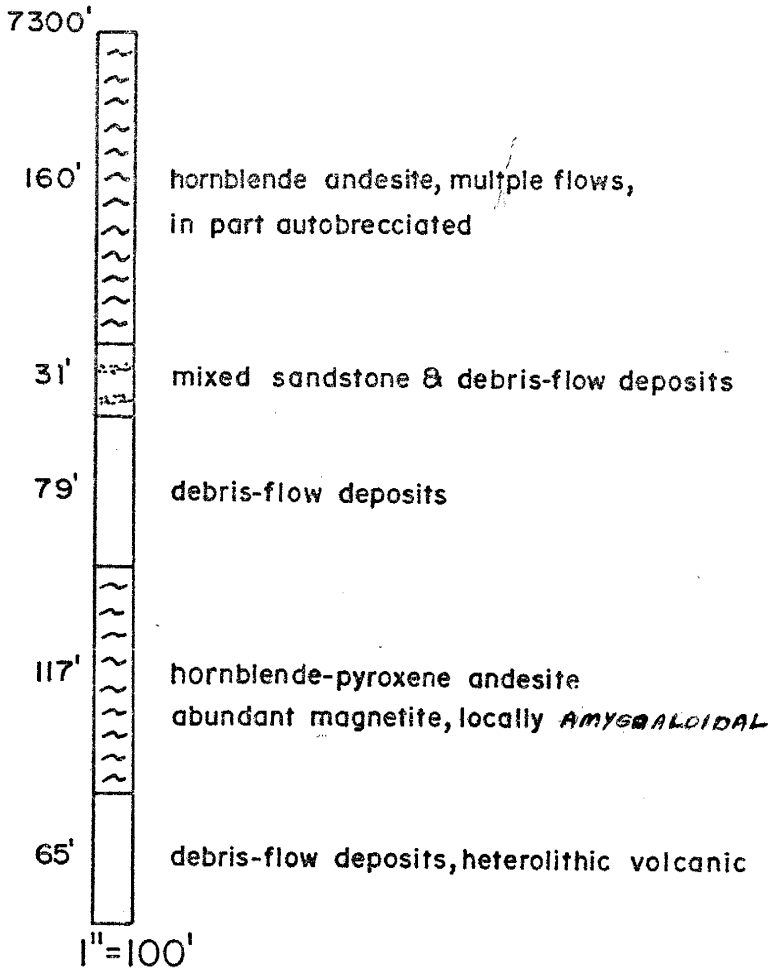

Section D. Rubio Peak Formation between Chloride and S. Fork Cuchillo Negro Creeks, western Chloride mining dist.
approx. 33° 19' 42" N, 107° 46' 40" W

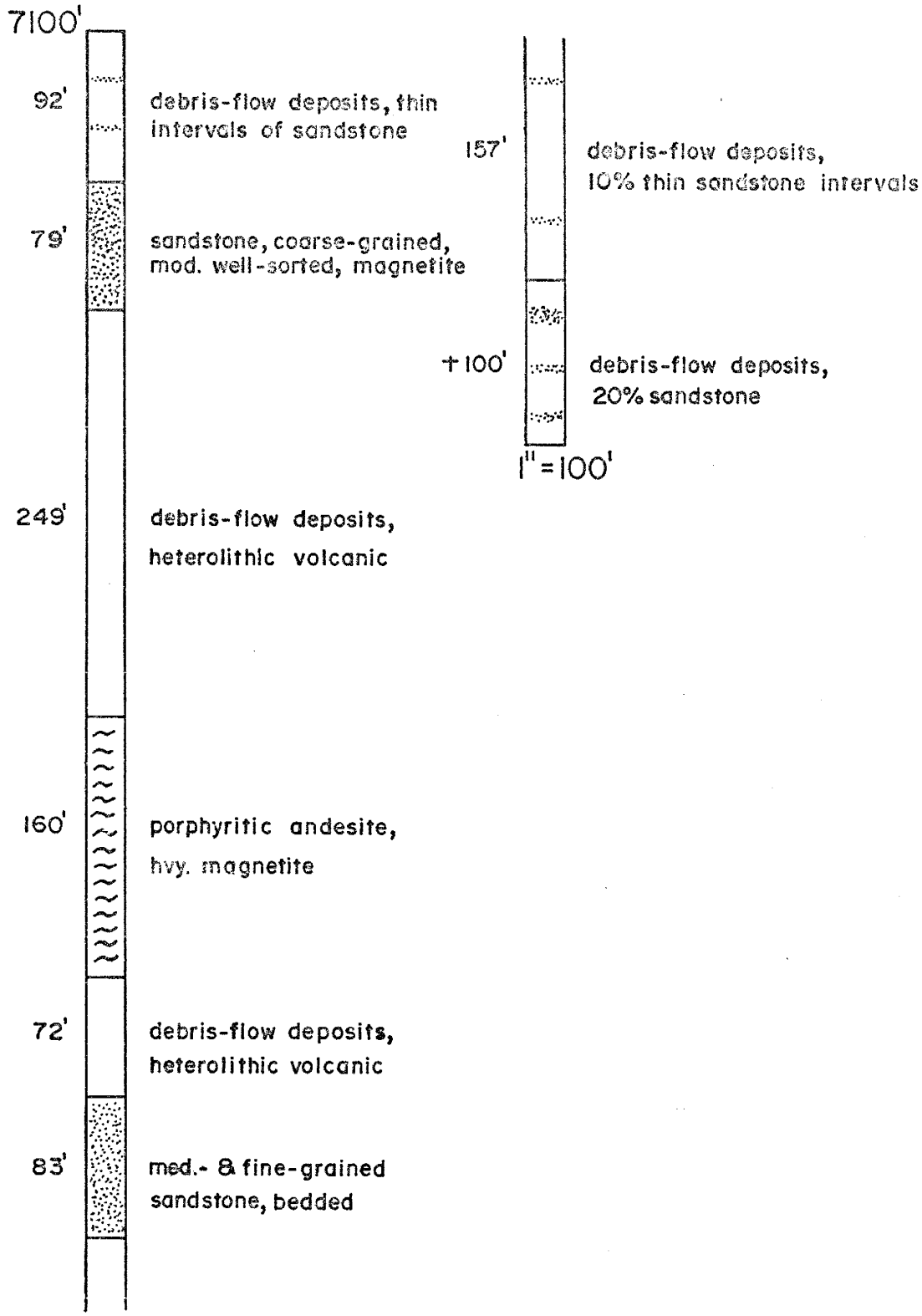

Section E. Rubio Peak Formation, Chloride Cr. about 7700' east of Silver Mon. mine, 33°20'11"N, 107°46'48"W

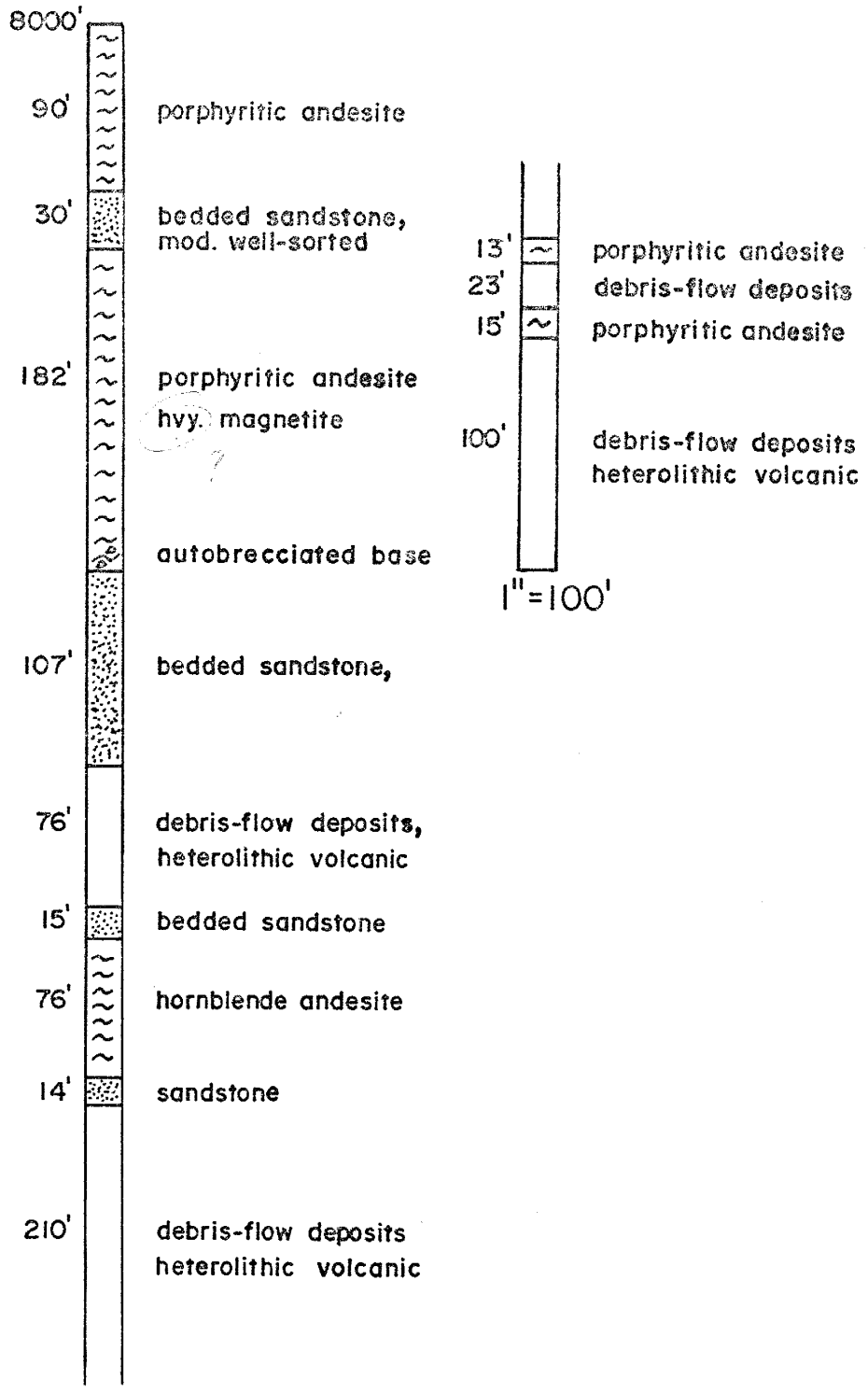

Section F. Rubio Peak Formation about 2000' east of Silver Monument discovery shaft, 33°20'N, 107°48'05"W

A thru F).

Debris-flow deposits in the Chloride mining district are massive, poorly to non-bedded, and matrix-supported (Fig. 7a). They most commonly contain subangular to subrounded, heterolithic clasts of aphanitic and porphyritic, intermediate volcanic rocks; locally, monolithic intervals of hornblende andesite are found; and persistently throughout the southeastern quarter of the district, a 15-20 m thick horizon of limestone breccia occurs approximately 10-30 m above the base of debris-flow deposits (see Fig. 6, section C). Size of clasts in debris-flow deposits range from lapilli to pebbles and small cobbles, to large boulders a meter or more in diameter. Very rarely, clasts that are themselves consolidated breccias are found. Extreme variations in clast sizes are noted both laterally and vertically over short distances. Matrix of debris-flow deposits consists of fragmental detritus, generally 0.5 to 0.2 mm in size. There is a paucity of clay-sized material. Matrix material occasionally fills fractures in clasts.

Individual flows are difficult to discern in the massive debris-flow accumulations occurring in Chloride mining district. At most locations, individual debris flows have consolidated into massive, monotonous deposits several hundred meters thick (Fig. 7b). The only indications of multiple flows are occasional thin fluvial intervals (probably from reworking of debris-flow material), and the interfingering relationships of debris-flow deposits with

Figure 7. a) Photograph of matrix-supported, heterolithic debris-flow deposits in southern Chloride mining district.

b) Photograph of pinnacles eroded in massive debris-flow deposits of lower Rubio Peak Formation along South Fork of Cuchillo Negro Creek, southeastern Chloride mining district.

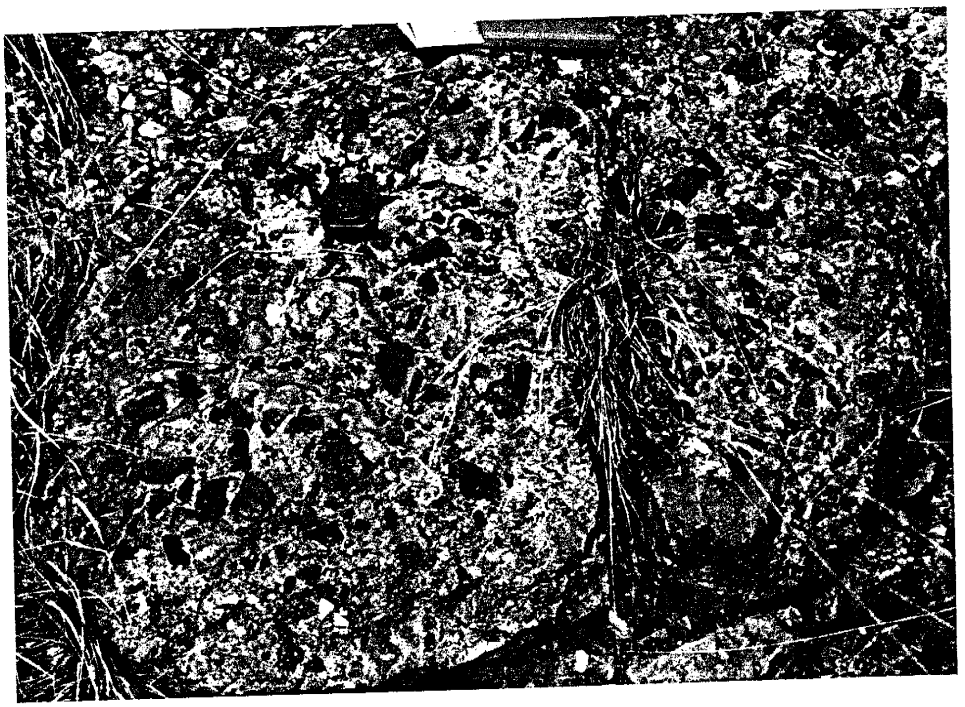

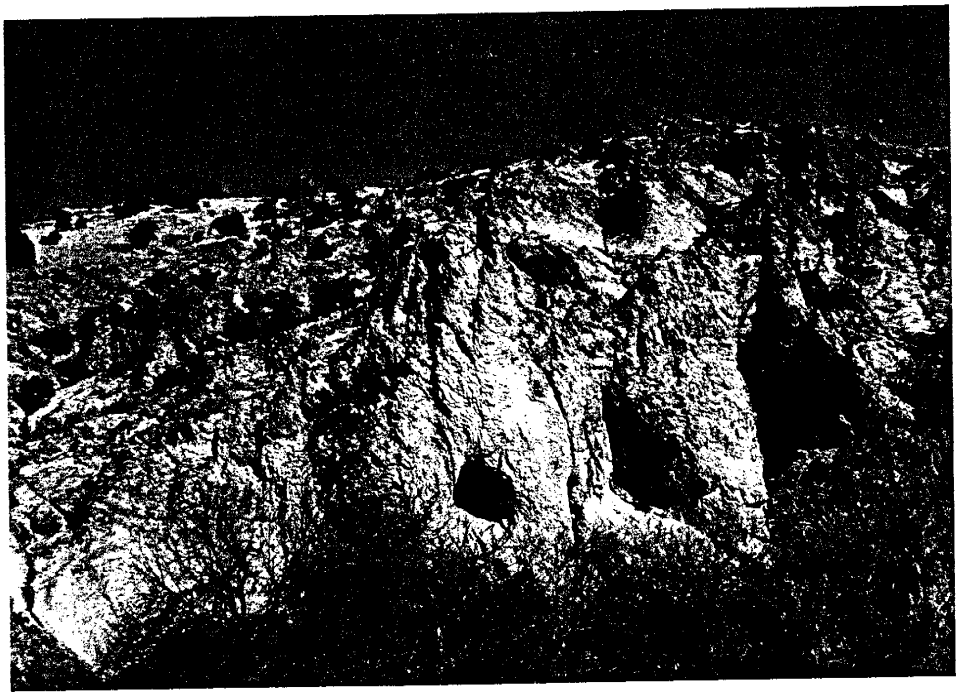

sandstone and lava-flow deposits.

Petrographically, matrix of debris-flow deposits consists of chaotic microporphyritic-microgranular (0.2 to 0.5 mm) material that is usually moderately to strongly altered to calcite, epidote, and chlorite-smectite. Altered plagioclase, hornblende, augite (?), and minor quartz microphenocrysts exist in matrix. Euhedral to subhedral magnetite grains, partially altered to hematite, are abundant in matrix, often making up 20-40 % of its volume. Aggregates of sphene are also common.

Debris-flow deposits in Chloride mining district show all of the characteristics ascribed to their classification by Smith (1986). These characteristics include en masse mode of deposition, lack of stratification, variable grading (none, reverse, reverse-to-normal, coarse-tail normal), matrix support, variable long-axis orientation, and minor to no imbrication. These last two characteristics make flow direction determinations tentative to impossible. Attempts to make such determinations for debris-flow deposits in Chloride mining district have produced chaotic, meaningless results.

Characteristics of flows responsible for debris-flow deposits include: laminar flow in basal boundary layer at time of deposition, perhaps turbulent on very steep slopes; support of clasts is provided by matrix strength (dependent upon abundance and type), grain dispersive pressure, and buoyancy provided by matrix (Smith, 1986). The ability of

debris flows to transport extremely large clasts is attested to by deposits in the Chloride mining district, where blocks several meters in diameter are commonly found. Relatively steep slopes (-.10 to -.15%) are required to develop debris flows; once initiated, debris flows can travel in excess of 80 km (Smith, 1988).

sandstone deposits

In southern half of the Chloride mining district, sandstone deposits occur interfingered with both debris-flow deposits and andesitic lava flows (Fig. 6, sections A,B,D,E,&F). Best exposures of these sandstone deposits are in southwestern quarter of the Winston quadrangle (Plate 1) and the southeastern quarter of Lookout Mountain quadrangle (Plate 2). Sandstone deposits in lower Rubio Peak Formation are virtually absent from the northern half of Chloride mining district.

In outcrop, three gradational varieties of sandstone deposits are recognized in the southern half of Chloride mining district. The first variety is found in close proximity to debris-flow deposits and is very massive, poorly bedded, poorly to non-sorted, and lacks cross-stratification and other fluvial sedimentary features (Fig. 8a & 8b). Petrographically, this sandstone variety consists of detrital grains (.1 to .5 mm) of predominantly plagioclase, with abundant lithic fragments, and less abundant altered ferromagnesian minerals cemented by interstitial microcrystalline material that is extensively altered to chlorite-smectite and calcite. Quartz occurs as rare individual grains. Sphene and magnetite make up 2 to 4 % of rock volume. Very fine-grained matrix material (<.1 mm) is volumetrically minor, making up only about 5 % of rock. Major element analysis for one sample of this

sandstone is given in Table 1. This first variety of sandstone closely fits descriptions of hyperconcentrated-flow deposits provided by Smith (1986; 1987; 1988), and Scott (1988).

Figure 8. a) Photograph of massive, crudely bedded sandstone in lower Rubio Peak Formation, Byers Run, southern Chloride mining district.

b) Closeup photograph of above, showing massive non-sorted nature of sandstone interpreted to have been deposited from hyperconcentrated flow.

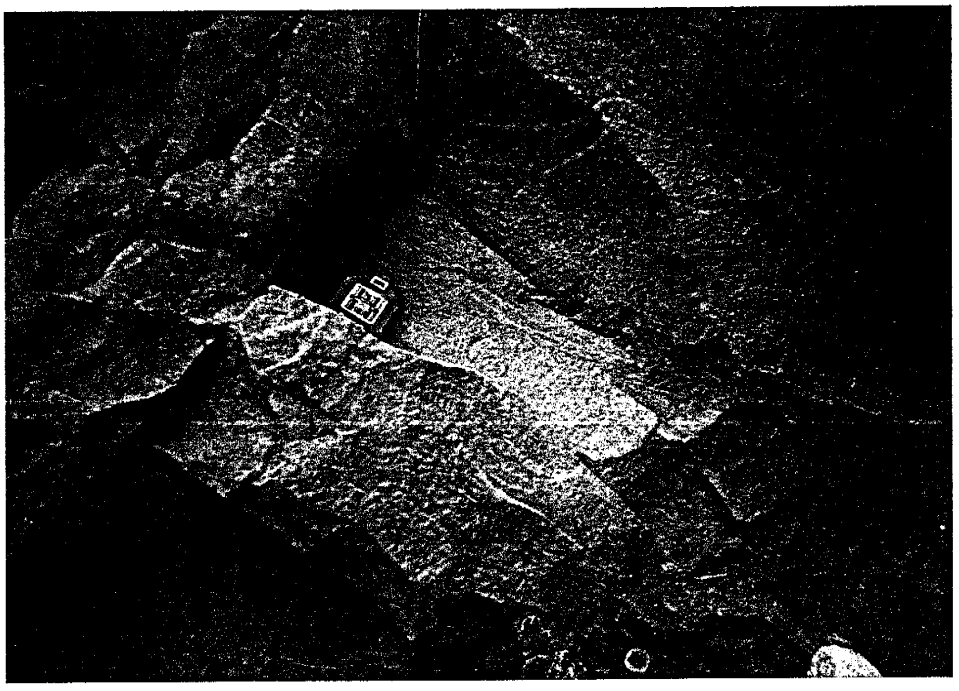

Table 1. Major-element analysis for sandstone in the lower Rubio Peak Formation; collected about 400 m north of U.S. Treasury mine (unsurveyed); slightly altered.

SiO2	59.15
Al2O3	16.04
Fe2O3	6.39
MgO	3.97
CaO	6.49
Na2O	4.06
K2O	1.86
Ti2O	1.01
P2O5	0.41
MnO	0.08
LOI	2.40
Total	101.85

Deposits of the second sandstone variety are very similar to the first variety, but tend to show some characteristics of slighty more-dilute flows. These sandstone deposits show some broad planar crossbedding, are poorly to moderately sorted, and overall are crudely stratified with numerous horizontal, thin (10 cm or less) beds (Fig. 9). Locally, this variety is well-stratified with intercalated siltstone horizons. Thin, discontinuous pebble-rich and pumice-rich intervals are occasionally found intercalated with these sandstone deposits. Cut-and-scour features, and other indicators of channelized, turbulent flow are lacking in these deposits. Interpretation is that deposition of these deposits was primarily from hyperconcentrated sheet flows.

A third variety of Rubio Peak sandstone occurs primarily in the southwestern quarter of Chloride mining district and shows characteristics of normal streamflow deposition. Typically, this sandstone variety consists of fine-grained, moderately well-sorted, well-stratified, cross-bedded deposits, with minor interbedded conglomerate and siltstone deposits. Petrographically, this variety of sandstone consists of broken grains of plagioclase (An 30-40), pyroxene, hornblende, opaques, andesite lithics, and minor quartz, all 2 mm or less in diameter, set in a matrix of altered ash. Matrix material commonly makes up 20-40 % of these sandstone deposits. Conglomerate intervals are composed of rounded, heterolithic volcanic clasts of

Figure 9. Photograph of sandstone deposit similar to that shown in Fig. 8, but showing development of thin horizontal beds, moderate sorting, and occasional crossbedding.

intermediate composition.

Distribution of the three varieties of Rubio Peak sandstone deposits described above displays an overall sequential progression southwestward and up section, away from major accumulations of debris-flow deposits. This progression is very similar to downstream patterns attributed to transition from debris flows to hyperconcentrated streamflow to normal streamflow observed in volcaniclastic terranes elsewhere by Pierson and Scott (1985), Scott (1988), and Smith (1986; 1987; 1988). In the Chloride mining district, this transition is the only flow-direction indicator available for the volcaniclastic deposits of lower Rubio Peak Formation, suggesting a transport from northeast toward southwest.

Exotic limestone blocks

Exotic blocks of Pennsylvanian limestone, as much as 170 m thick and several square kilometers in outcrop, rest upon and are overlain by both debris-flow and sandstone deposits of lower Rubio Peak Formation. Figure 10 is a photograph of a large exotic block overlying Tertiary volcaniclastic deposits in southern Chloride mining district. Occurrences of exotic blocks are found in a district-long belt from extreme southern to northern ends of Chloride mining district (see Plates 1, 2, 4, 5, and Harrison, 1988). Exploration drilling in northern third of sec. 25, T. 9 S., R. 8 W. (just north of Plate 3) penetrated approximately 160 m of Madera Limestone (J. Peace, 1984, personal communication) that is believed to be a buried exotic block. However, the base of limestone was not reached by drilling. Exposures of the Permian Abo Formation in Hermosa mining district (approximately 9 km south of southernmost Chloride mining district) were interpreted by Shepard (1984) as exotic blocks similar to those found in Chloride district.

Emplacement of exotic blocks in Chloride mining district was interpreted as the product of gravity slide mechanisms by Maxwell and Heyl (1976); an interpretation that is supported by this report. The lower contacts of the exotic limestone blocks are typically sharp; however, locally they are brecciated and contain gouge and cataclastic material. Clastic dikes and thin clastic sills frequently intrude

Figure 10. Photograph of large exotic block of Pennsylvanian ~~Hadera~~ limestone overlying Tertiary volcaniclastic deposits of lower Rubio Peak Formation, near St. Cloud mine in southern Chloride mining district.

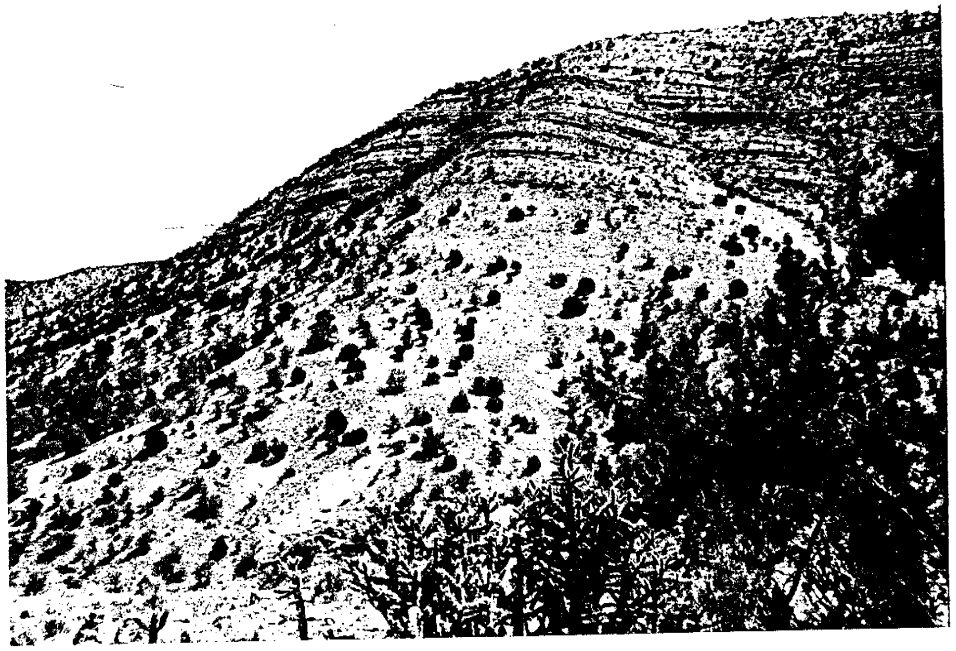

upward into the exotic blocks (Fig. 11), some as much as 100 m. Wood fragments commonly are found in sandstone deposits immediately beneath large exotic blocks. Figure 6, section C depicts a stratigraphic section from the top of an exotic block down through lower Rubio Peak Formation in vicinity of Hoosier mine, southern Chloride mining district. More detailed descriptions of exotic blocks, along with an emplacement hypothesis, and economic implications, are presented in Harrison (1988).

Figure 11. a) Photograph of clastic dike (center) intruded into an exotic limestone block, about 100 m north of old St. Cloud mine.

b) Closeup photograph of clastic dike.

lithic-rich ash-flow tuff

Interbedded within volcaniclastic deposits of the lower Rubio Peak Formation in southern Chloride mining district is a poorly welded, lithic-rich, crystal-poor, ash-flow tuff. This tuff contains 5-10 % phenocrysts of plagioclase, sanidine (?), and biotite, and commonly displays blue-green alteration (celadonite) of pumice. Outcrops of this tuff are spotty and limited to Chloride Creek-Mineral Creek area (especially secs. 7, 18, and 19, T. 11 S., R. 8 W.); for this reason it was not mapped separately on Plate 1. Maximum thickness of this tuff is approximately 30 m. It most commonly occurs interbedded with debris-flow deposits.

upper Rubio Peak Formation

In the Chloride mining district, rocks of upper Rubio Peak Formation consist dominantly of intermediate lava flows. Three basic textures of lava flows are recognized: porphyritic, coarsely porphyritic (turkey-track), and aphanitic. In the southern half of the district, lava flows are intercalated with debris-flow and sandstone deposits of lower Rubio Peak Formation (see Fig. 6, sections A, D, E, & F). In the northern half of the district, intermediate lava deposits occur as multiple flows of all three textural types that are in part interfingered with ash-flow tuff and rhyolite lava deposits, and all overlie debris-flow deposits

of lower Rubio Peak Formation. Figure 12 is a composite stratigraphic section of upper Rubio Peak Formation in the northern Chloride mining district, showing relationships between intermediate lava-flow deposits, rhyolitic lava and ash-flow tuffs, and volcaniclastic deposits of the lower Rubio Peak Formation.

In outcrop, lava flows generally exhibit massive cores with autobrecciated tops and bases. Source areas were local flow-dome complexes and dikes that occur at many localities distributed throughout the Chloride mining district. Cross-cutting relationships and great thicknesses indicate that a major intrusive center for upper Rubio Peak intermediate lavas exists in the Bald Eagle region of southeastern Chloride mining district (Plate 1). Large masses of both aphanitic and porphyritic, hornblende andesites intrude sandstone and debris-flow deposits in this area, and several dikes radiate away from this center. Approximately 1 mile east of the Bald Eagle area, in secs. 17, 18, 19, & 20, T. 12 S., R. 8 W., a half dozen, small (100-200 m), roughly circular plugs of hornblende andesite intrude sandstone and debris-flow deposits. These intrusives display a distinctive north-northeast alignment that is interpreted to represent a structural control on emplacement. Another possible Rubio Peak intrusive site occurs along Mineral Creek in the center of sec. 13, T. 11 S., R. 8 W., where several hundred meters of porphyritic andesite exist. However, cross-cutting relationships, if

Figure 12. Composite stratigraphic section for upper Rubio Peak Formation in the northern Chloride mining district. This section was developed through detailed mapping of the area, primarily in Sawmill Peak and Iron Mountain quadrangles (Plates 3 & 4). Nowhere is a complete section exposed.

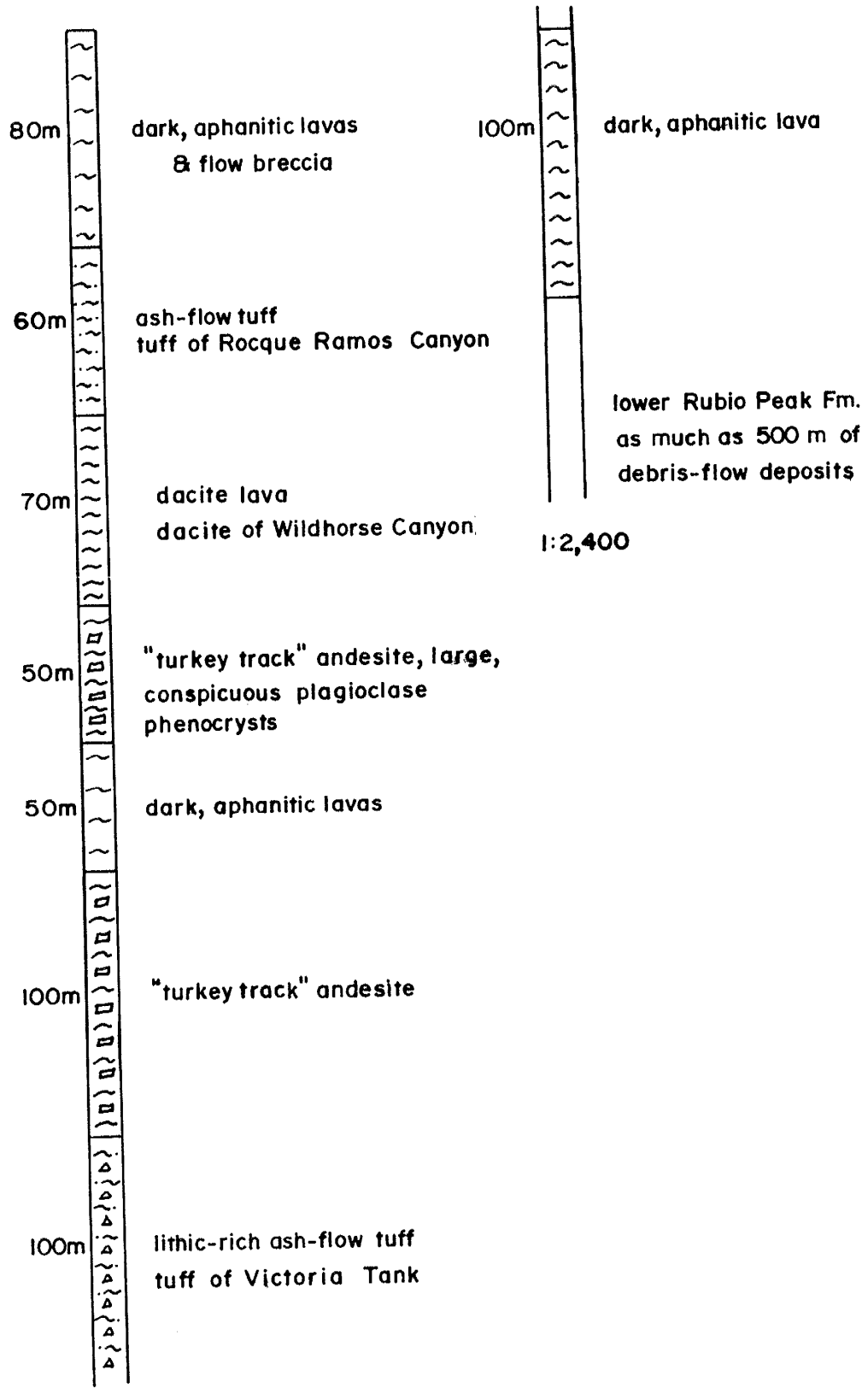
80m
dark, aphanitic lavas
& flow breccia
60m
ash-flow tuff
tuff of Rocque Ramos Canyon
70m
dacite lava
dacite of Wildhorse Canyon
50m
"turkey track" andesite, large,
conspicuous plagioclase
phenocrysts
50m
dark, aphanitic lavas
100m
"turkey track" andesite
100m
lithic-rich ash-flow tuff
tuff of Victoria Tank
100m
dark, aphanitic lava
lower Rubio Peak Fm.
as much as 500 m of
debris-flow deposits
1:2,400

present, are not exposed in this area. Another possible intrusive center is located about 300 m west of the Silver Monument mine (Plate 2), where several hundred meters of porphyritic andesite occur with well-developed vertical flow banding and no visible bottom. However, true cross-cutting relationships are not exposed at this location either.

All intermediate lavas in upper Rubio Peak Formation contain varying amounts of plagioclase (An 30-50), pyroxene, and hornblende, either as phenocrysts or microphenocrysts. Amounts of pyroxene and hornblende vary considerably for individual flows. Some flows contain only hornblende, some contain dominantly pyroxene, and others contain mixed proportions of both. Augite appears to be by far the dominant pyroxene mineral. Relict phenocrysts of olivine, completely altered to fibrous serpentine, occur sparsely in some Rubio Peak flow rocks. Aggregates of sphene are common to all intermediate lavas. Euhedral to subhedral grains and aggregates of magnetite are ubiquitous to all intermediate lavas, frequently in such quantities that these rocks are mildly to moderately magnetic. Very rarely, xenocrysts (?) of rounded quartz are found in Rubio Peak lavas, surrounded by reaction rims of fine-grained pyroxene and opaque minerals (magnetite ?). Groundmass of intermediate lavas display a pilotaxitic texture, with microlites of dominantly plagioclase (An 30-50), with subordinate mafic minerals. Amygdules occur in some lavas; they generally range in size from 0.2 to 2.0 mm, and typically are filled with

chlorite-epidote, quartz, and calcite.

Chemistry of igneous rocks in the Rubio Peak Formation

Several reports have produced major oxide analyses for igneous rocks of Rubio Peak Formation at various locations in southwestern New Mexico. This data plus additional analyses for rocks in Chloride mining district are tabulated in Table 2. Harker variation diagrams for Rubio Peak rocks are presented in Figure 13.

SiO2 contents for all Rubio Peak analyses range from 53.80 % to 62.43 %. K2O + Na2O contents range from 6.00 % to 10.94 %; however, the high value represents one anomalous sample from this report that possibly reflects alteration (K-metasomatism ?). Aside from this anomalous sample, total alkali contents range from 6.0 % to 8.08 %. Using a chemical classification for volcanic rocks based on total alkali verus silica content of Le Maitre (1984), rocks of Rubio Peak Formation occur in several classes, dominantly trachyandesite (latite), but also in andesite, and basaltic andesite (Fig. 13). Total alkali and K2O show positive correlation with silica content (Fig. 13). CaO, Fe2O3 (total Fe), MgO, and P2O5 show inverse correlation with silica. Other elements show weak to no correlation with silica.

Rocks of the Rubio Peak Formation straddle the line dividing alkali and subalkali fields of Irvine and Baragar (1971) (Fig. 13a). Samples from the Chloride mining district [those of this report and Abitz (1984, 1989)] fall

Table 2. Major-element analyses of igneous rocks in the Rubio Peak Formation.

	1	2	3	4	5	6	7	8
SiO2	54.33	54.36	55.69	61.49	55.61	57.64	57.30	58.43
Al2O3	16.88	16.81	16.89	15.99	16.30	17.01	16.16	17.91
Fe2O3	7.43	7.22	6.87	6.27	6.91	6.11	6.74	5.64
MgO	4.45	4.87	2.60	2.19	2.84	2.63	3.82	3.27
CaO	5.93	5.80	6.02	4.15	5.70	4.49	5.33	6.30
Na2O	4.33	4.26	3.50	4.65	4.20	3.43	3.35	3.61
K2O	2.55	2.53	3.79	3.29	2.95	4.40	3.64	2.25
TiO2	1.03	1.01	.98	.96	.91	1.15	1.13	.83
P2O5	.32	.32	.28	.25	.58	.33	.34	.29
MnO	.08	.07	.09	.07	.11	.07	.10	.06
LOI	2.41	2.30	2.80	1.35	4.76			
Total	99.74	99.54	99.50	100.60	100.87	97.26	97.37	98.59

	9	10	11	12	13	14	15	16
SiO2	54.80	56.20	61.28	62.43	59.37	61.88	58.39	60.77
Al2O3	17.45	17.50	16.58	16.50	16.17	16.46	17.22	16.97
Fe2O3	6.72	5.02	4.07	4.75	5.69	4.20	4.95	4.12
MgO	6.38	3.81	1.76	1.78	3.00	1.66	2.35	1.92
CaO	6.07	6.85	5.42	4.55	5.12	4.75	5.66	4.56
Na2O	3.95	3.73	4.10	4.10	3.46	4.05	4.34	3.70
K2O	2.05	2.07	3.47	2.87	2.81	4.00	2.85	3.68
TiO2	.88	.97	.51	.70	1.01	.45	1.05	1.43
P2O5	.35	.29	.25	.29	.36	.25	.31	.23
MnO	.08	.14	.06	.08	.07	.10	.08	.14
LOI		1.26	2.45	2.38	2.66	2.34	1.94	2.03
Total	98.73	100.31	99.95	100.43	99.72	100.17	99.86	100.25

	17	18
SiO2	53.80	59.43
Al2O3	17.45	17.91
Fe2O3	6.72	5.64
MgO	6.38	2.27
CaO	6.07	6.30
Na2O	3.95	3.61
K2O	2.05	2.25
TiO2	.88	.83
P2O5	.35	.29
MnO	.08	.06
Total	97.73	98.59

1) Trp lava, Chloride Cr., below Lyons Pk., this report

2) Trp lava, Chloride Cr., near Silver Monument, this report

3) Trp dike, Chloride Cr., ~ 2 mi E of Lyons Pk. this report

4) Trp lava, ~1000 ft North of U.S. Treasury mine, slightly altered, this report

5) Trp dike, Midnight mine, altered, this report

6) Trp lava, 33-10'-42"N, 107-47'-11"W, Abitz, 1989

7) Trp lava, 33-10'-47"N, 107-47'-16"W, Abitz, 1989

8) Trp lava, 33-06'-39"N, 107-45'-39"W, Abitz, 1989

9) Trp lava, 33-10'-25"N, 107-46'-79"W, Abitz, 1989

10) Trp lava, 33-35'-31"N, 107-43'-24"W, Fodor, 1975

11) Macho andesite, SE1/4SW1/4 sec.20, T.19S., R.7W., Jicha, 1954

12) Trp lava, SE1/4NE1/4 sec.36, T.18S., R.7W., Jicha, 1954

13) Trp lava, NW1/4NW1/4 sec.19, T.18S., R.7W., Jicha, 1954

14) Trp lava, NE1/4NE1/4 sec.17, T.9S., R.10W., Elston, 1957

15) Trp lava, SE1/4, sec.22, T.19S., R.10W., Fodor, 1975

16) Trp lava, NW1/4, sec.29, T.13S., R.13W., Fodor, 1975

17) Trp lava, 33-17'-42"N, 107-46'-42"W, Abitz, 1982

18) Trp lava, 33-16'-56"N, 107-47'-17"W, Abitz, 1982

Figure 13. Major-element variation diagrams for rocks of the Rubio Peak Formation, solid squares are for samples analyzed for this report from north-central Black Range; SiO2 vs K2O + Na2O rock classification from Le Maitre (1984).

Rubio Peak Formation
K2O+Na2O %
SiO2 %
basalt
basaltic andesite
andesite
dacite
latite
trachyandesite
alkali
subalkali
0
1
2
3
4
5
6
7
8
9
10
11
12
13
14
40
50
60
70
80

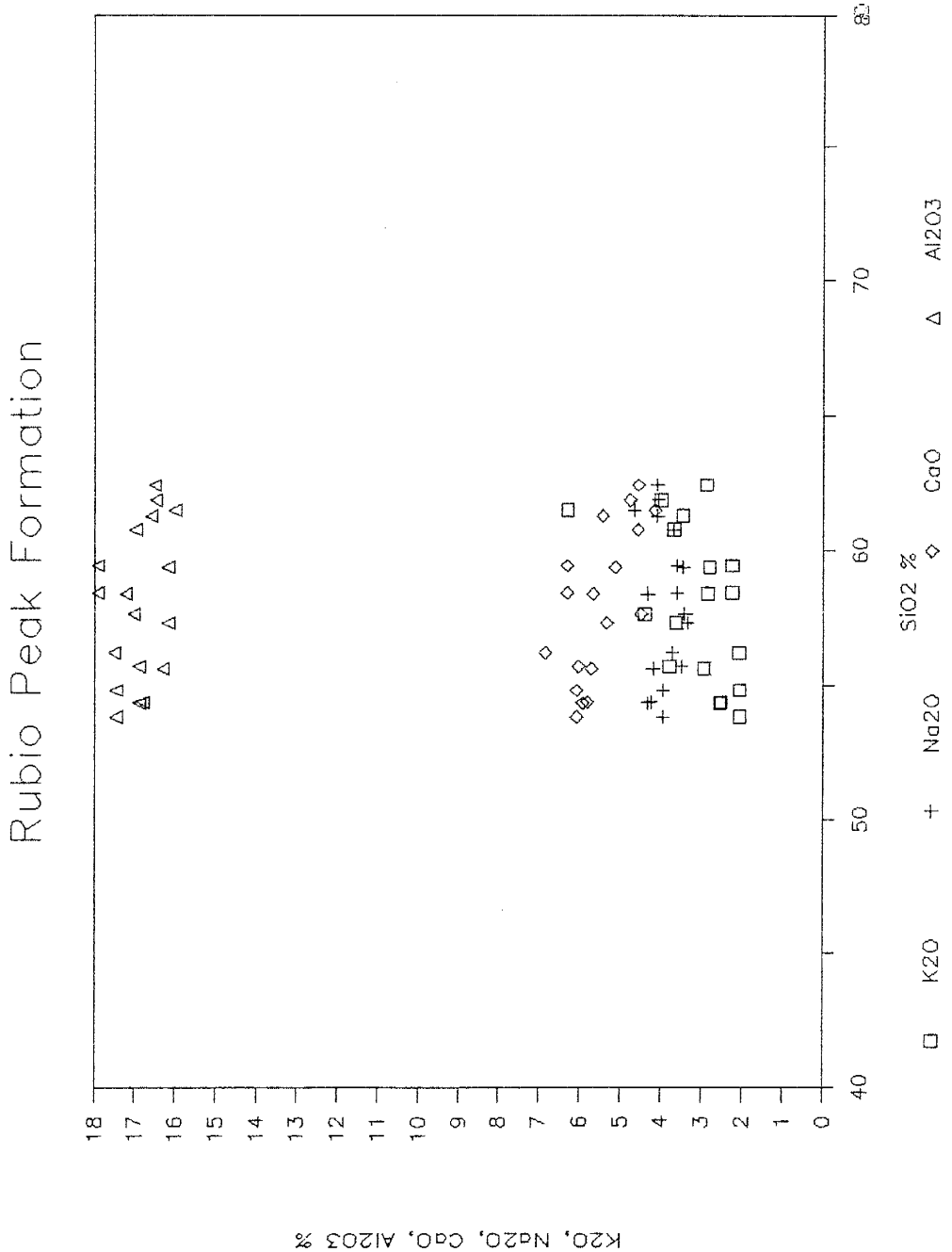
Rubio Peak Formation
K2O, Na2O, CaO, Al2O3 %
SiO2 %
K2O
Na2O
CaO
Al2O3

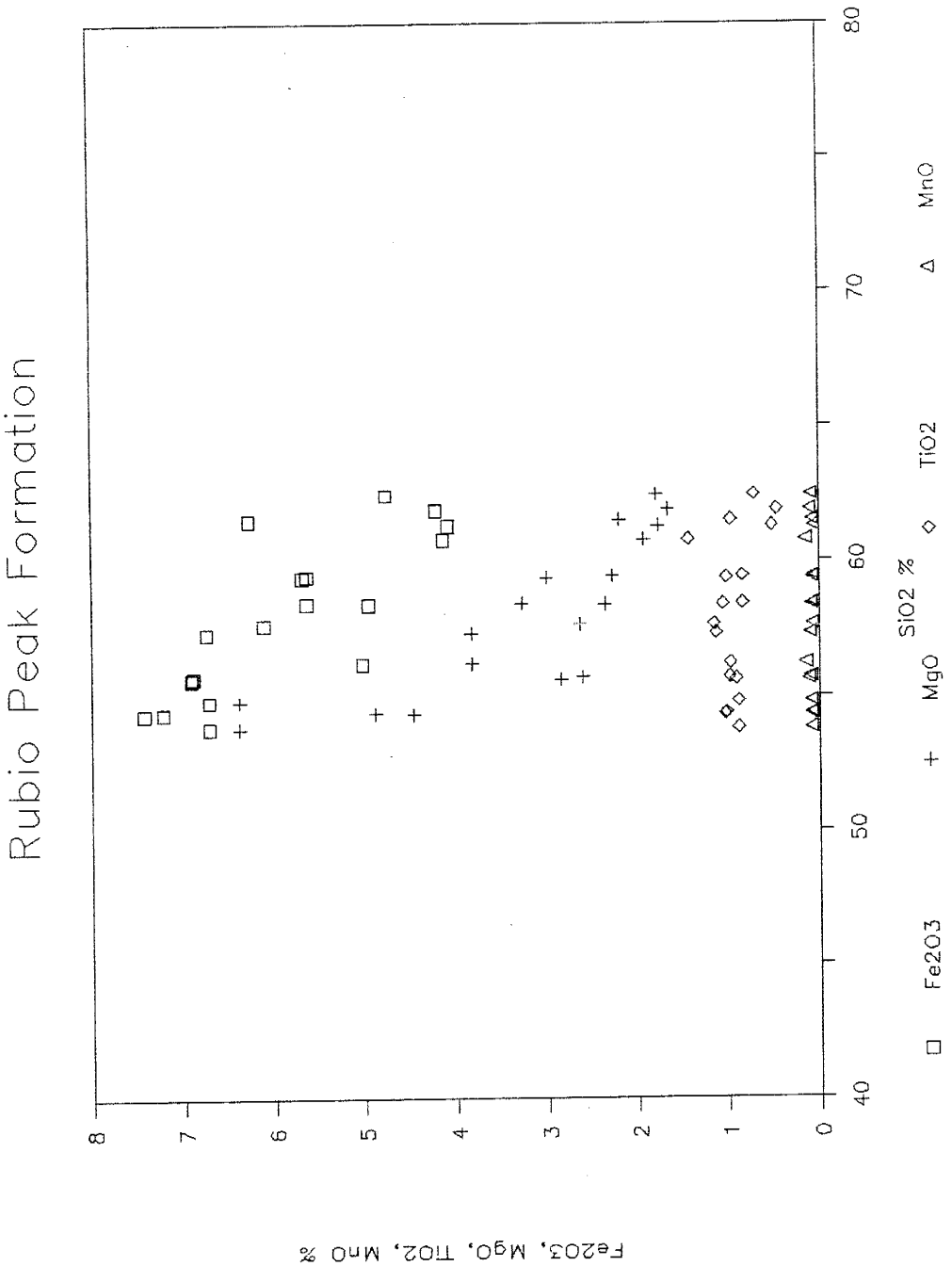
Rubio Peak Formation
Fe2O3, MgO, TiO2, MnO %
0
1
2
3
4
5
6
7
8
40
50
60
70
80
SiO2 %
□ Fe2O3
+ MgO
◇ TiO2
△ MnO

in alkali field or on dividing line.

More detailed chemical analyses of Rubio Peak rocks, including trace element, rare earth element, and strontium isotope analysis, are provided by Abitz (1989). One of his conclusions is that rocks of Rubio Peak Formation have volcanic arc affinities.

Alteration of the Rubio Peak Formation in Chloride mining district

Regionally, rocks of the Rubio Peak Formation in Chloride mining district show mild to pervasive propylitic alteration, presumedly by hydrothermal fluids responsible for epithermal mineralization found in the district, although alteration could be deuteric in part. Volcaniclastic rocks of the lower Rubio Peak Formation appear to have been most susceptible to alteration, Maxwell and Heyl (1976) mapped altered Rubio Peak rocks as their andesite (Tabt) map unit. Plate 6 shows a regional alteration pattern for Chloride mining district and environs.

Alteration assemblage consists dominantly of calcite after plagioclase, chlorite-smectite-epidote after ferromagnesium minerals and matrix material, plus or minus pyrite. Locally, there has been complete breakdown and replacement of all phenocrysts. Some granular magnetite could also be part of this alteration scheme. In addition

to mineral replacements, epidote occurs as fracture coatings, stains, aggregated clusters of crystals, and in veinlets with quartz. Adjacent to epithermal vein deposits, rocks of Rubio Peak Formation show varying degrees of silification and potassic alteration (k-spar, sericitic, and argillic).

units between the Rubio Peak Formation and Kneeling Nun Tuff

In the Chloride mining district and environs, three ash-flow tuffs, a dacite lava, and fine-grained volcaniclastic deposits occur in the stratigraphic interval below Kneeling Nun Tuff and above, or interfingered with, uppermost Rubio Peak Formation. Within this interval, deposits have complex interfingering relationships. Kneeling Nun Tuff overlies deposits of this stratigraphic interval with angular unconformity, more so in the southern half of district than in the northern half.

Two of the ash-flow tuffs (Victoria Tank and Rocque Ramos Canyon) appear to be regionally extensive and therefore serve as important stratigraphic controls. In the southern half of Chloride district, these two tuffs are intercalated with volcaniclastic deposits (sandstone of Cliff Canyon); in the northern half of Chloride district, these tuffs are intercalated with dacite of Wildhorse Canyon and andesitic lavas of upper Rubio Peak Formation. Previously, some these deposits have been included within the Rubio Peak Formation (Woodard, 1982; Harrison, 1988, 1989; Eggleston and Harrison, in review). But because of their more-silicic composition (see Table 3, Fig. 14), all of these units are separated from Rubio Peak Formation for this report. Table 4 outlines the relative stratigraphic relationships between units in this interval.

Table 3. Major-element analyses of volcanic rocks between the Rubio Peak Formation and Kneeling Nun Tuff.

	1	2	3	4	5	6	7
SiO2	67.11	70.21	68.29	66.83	67.66	69.73	74.08
Al2O3	15.09	14.31	14.32	15.88	16.15	15.70	13.22
Fe2O3	2.45	1.91	2.56	3.92	2.36	2.23	1.65
MgO	.35	.30	.39	1.19	.23	.33	.45
CaO	1.00	2.23	.52	2.33	1.16	.55	.64
Na2O	4.04	2.51	2.76	3.36	4.46	2.99	3.78
K2O	6.29	6.93	8.27	4.18	6.67	6.76	5.38
TiO2	.48	.37	.48	.64	.50	.50	.29
P2O5	.07	.06	.08	.31	.06	.07	.05
MnO	.05	.04	.04	.05	.02	.02	.02
LOI	1.48	2.34	1.98	.93	.83	.49	1.18
Total	98.41	101.21	99.69	99.62	100.10	99.37	100.74

1) Tuff of Stone House Ranch, center of sec. 11, T. 11 S., R. 8 W., this report.
2) Tuff of Victoria Tank, center of sec. 11, T. 11 S., R. 8 W., this report.
3) Tuff of Rocque Ramos Canyon, SW1/4 sec. 23, T. 11 S., R. 7 W., this report.
4) Dacite of Wildhorse Canyon, center of sec. 32, T. 9 S., R. 9 W., this report.
5) Tuff of Luna Park, 33-29'-53"N, 107-25'-21"W, southern San Mateo Mts., Bornhorst (1980).
6) Tuff of Rocque Ramos Canyon, sec. 26, T. 11 S., R. 7 W, 33-19'-31" N, 107-31'-59" W, Eggleston (1987).
7) Tuff of Victoria Tank, sec. 26, T. 11 S., R. 7 W., 33-19'-41" N, 107-32'-20" W, Eggleston (1987).

Figure 14. Variation diagrams for units in stratigraphic interval between the Rubio Peak Formation and Kneeling Nun Tuff, data from Table 3; Tsh- tuff of Stone House Ranch, Trr- tuff of Rocque Ramos Canyon, Tvt- tuff of Victoria Tank, Tlp- tuff of Luna Park, Twh- dacite of Wildhorse Canyon. Solid squares indicate samples analyzed for this report.

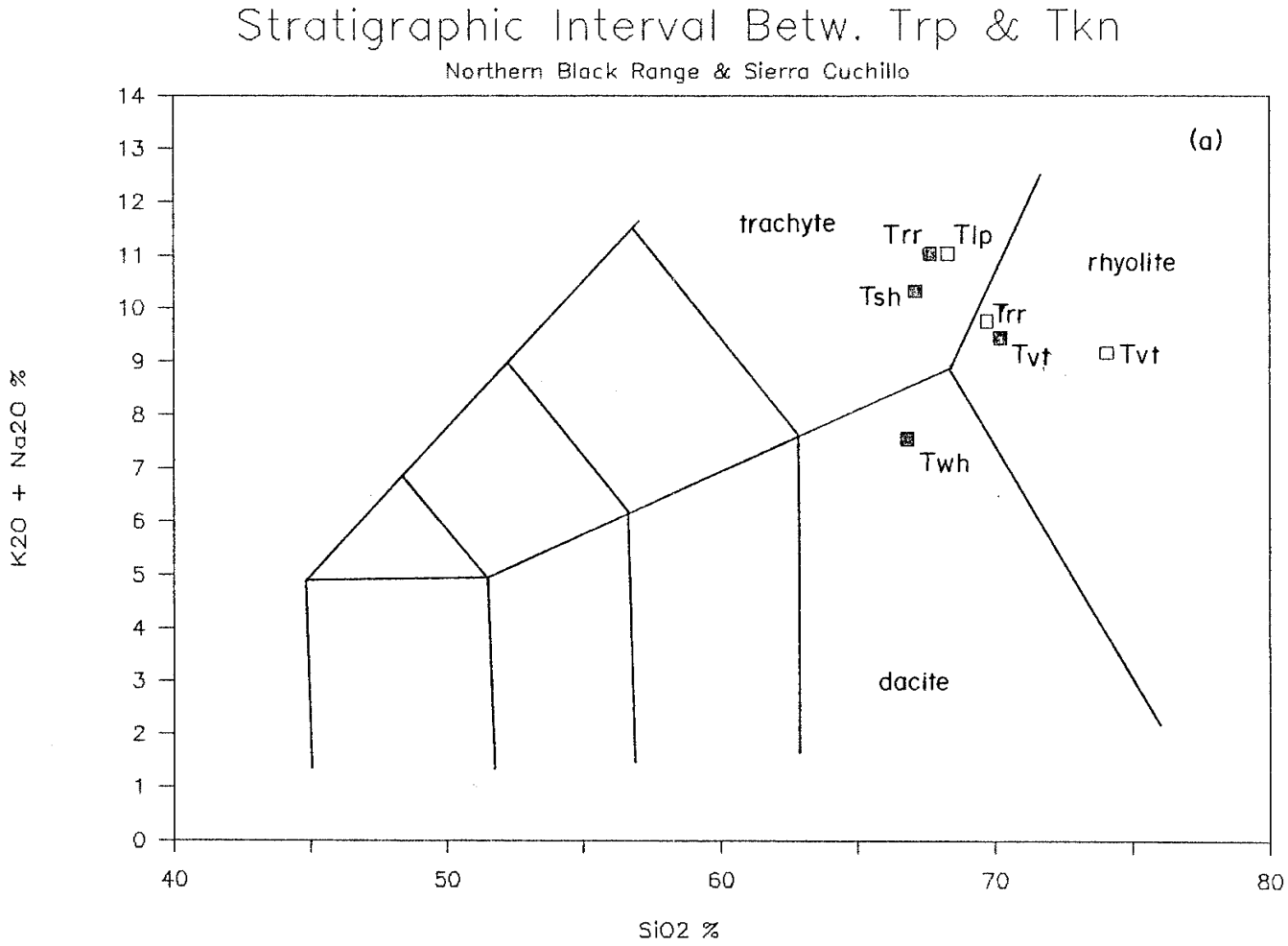
Stratigraphic Interval Betw. Trp & Tkn
Northern Black Range & Sierra Cuchillo
(a)
trachyte
rhyolite
dacite
Trr
Tlp
Tsh
Trr
Tvt
Tvt
Twh
K2O + Na2O %
SiO2 %
0
1
2
3
4
5
6
7
8
9
10
11
12
13
14
40
50
60
70
80

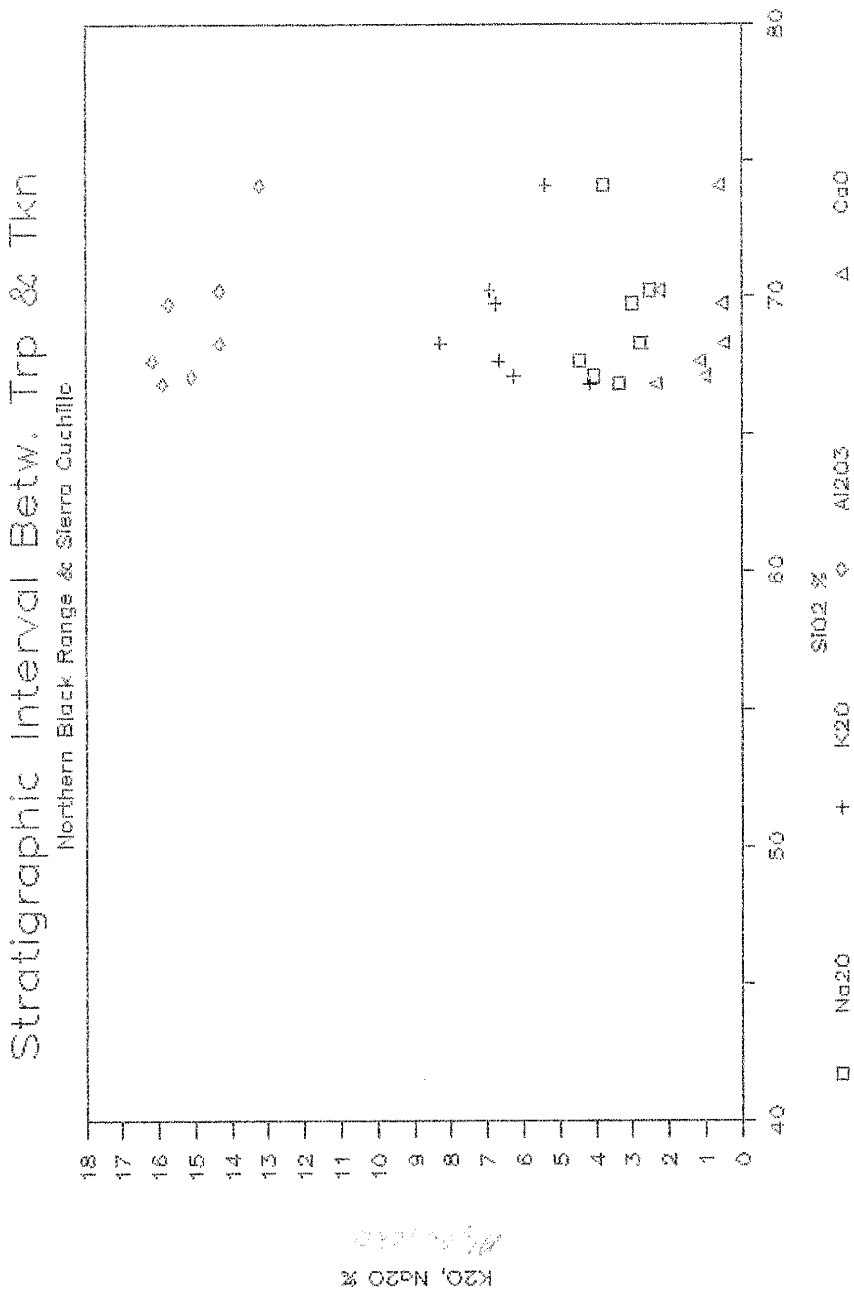
Stratigraphic Interval Betw. Trp & Tkn
Northern Black Range & Sierra Cuchillo
K2O, Na2O %
SiO2 %
Na2O
K2O
Al2O3
CaO
0
1
2
3
4
5
6
7
8
9
10
11
12
13
14
15
16
17
18
40
50
60
70
80

Table 4. Relative stratigraphic relationships between the units below Kneeling Nun Tuff and interfingered with upper Rubio Peak Formation.

southern Chloride district		northern Chloride district
Kneeling Nun Tuff		Kneeling Nun Tuff
sandstone of Cliff Canyon tuff of Stone House Ranch sandstone of Cliff Canyon		Rubio Peak aphanitic lava
tuff of Rocque Ramos Canyon	<->	tuff of Rocque Ramos Canyon
sandstone of Cliff Canyon		Rubio Peak lavas
tuff of Victoria Tank	<->	tuff of Victoria Tank
Rubio Peak lavas & sediments		Rubio Peak lavas

ash-flow tuffs

The three ash-flow tuffs interbedded in the upper Rubio Peak Formation below Kneeling Nun Tuff in the environs of Chloride mining district are (from oldest to youngest): tuff of Victoria Tank, tuff of Rocque Ramos Canyon, (tuff of Bear Creek of Eggleston and Harrison, in review), and tuff of Stone House Ranch. All three names are new and informal, although used under personal-communication citation by McIntosh (1989) for his regional correlations of ignimbrites. These three ash-flow tuffs are time-stratigraphic equivalents of the Sugarlump Tuff of Jicha (1954) and Jones et al. (1967), the Sugarlump Latite and Rhyolite of Elston (1957), and the Sugarlump Formation of Seager et al. (1982).

tuff of Stone House Ranch

The upper tuff in the above sequence is tuff of Stone House Ranch, named for exposures in center of sec. 11, T. 12 S., R. 8 W. in Winston quadrangle (Plate 1). This is the only known locality of this minor tuff, where it has a thickness of approximately 30 m. A generalized statigraphic section for this area is given in Figure 15. For mapping purposes, tuff of Stone House Ranch was combined with underlying tuff of Victoria Tank on Plate 1 (Tdc map unit).

Tuff of Stone House Ranch consists of two members. The

Figure 15. Stratigraphic section for the type locality of tuff of Stone House Ranch in center sec. 11, T. 12 S., R. 8 W. This is only known occurrence of this unit.

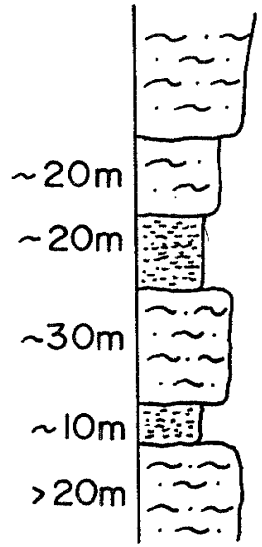

mod.-welded

Kneeling Nun Tuff
poorly welded base

~20m

~20m fine-grained volcaniclastic ROCKS
w/pumiceous air-fall beds

~30m tuff of Stone House Ranch

~10m fine-grained volcaniclastic ROCKS

>20m tuff of Rocque Ramos Canyon

upper member is buff-white in color, poorly welded, crystal poor, and contains about 5% phenocrysts of altered feldspar and traces of biotite. Small, dark (mafic?) pumice are conspicuous in this member. The lower member is reddish in color, moderately welded, pumice-rich, and moderately crystal-rich, with approximately 15% phenocrysts of plagioclase, sanidine, and minor biotite. The two members are welded together with a gradational contact.

Paleomagnetic data of McIntosh (1989) indicates that the tuff of Stone House Ranch is distinct from other known ignimbrites in Mogollon-Datil volcanic field. Given the close stratigraphic proximity of this unit to Kneeling Nun Tuff, similar major element chemistry of both tuffs, and the close geographic proximity to Emory cauldron (source of the Kneeling Nun Tuff), tuff of Stone House Ranch may be a precursor unit related to Kneeling Nun Tuff.

Major-element analysis of tuff of Stone House Ranch is presented in Table 3, along with analyses of other volcanic rocks from this stratigraphic interval. Chemically, tuff of Stone House Ranch is classified as a trachyte under scheme for volcanic rocks of Le Maitre (1984) (Fig. 14a). Variation diagram for SiO2 vs. K2O and Na2O is presented in Fig 14b; variation diagram for SiO2 vs. Al2O3, Fe2O3, and CaO is presented in Fig. 14c.

tuff of Rocque Ramos Canyon

The tuff of Rocque Ramos Canyon is named for exposures along that canyon in eastern Sierra Cuchillo, sec. 11, T. 11 S., R. 7 W. There, this tuff crops out in low rounded hills, stratigraphically overlying tuff of Victoria Tank and beneath Kneeling Nun Tuff.

Tuff of Rocque Ramos Canyon occurs extensively throughout most of the Chloride mining district, where it forms rounded cliffs and steep slopes. It reaches maximum thicknesses of approximately 70 m in the northern half of district and typically thins southward. It is absent in the extreme southern part of Chloride mining district, adjacent to Emory caldera (Plates 1 & 2). Presumedly, the tuff of Rocque Ramos Canyon was eroded away in this area during tumescence prior to eruption of Kneeling Nun Tuff. Fine-grained volcaniclastic sediments and non-welded tuff beds (sandstone of Cliff Canyon described in next section) commonly occur below (Fig. 16), and locally above (Fig. 17), tuff of Rocque Ramos Canyon in southern half of Chloride mining district.

In northern half of the district, tuff of Rocque Ramos Canyon is intercalated with aphanitic and porphyritic lavas of uppermost Rubio Peak Formation and dacite of Wildhorse Canyon (Fig. 12); all of which lie disconformably beneath Kneeling Nun Tuff. Based on 40Ar/39Ar ages of McIntosh (1989) for tuff of Rocque Ramos Canyon, this interfingering

Figure 16. Stratigraphic section on the north side of Chloride Creek, approximately 33-20'-10" N, 107-43'-40" W.

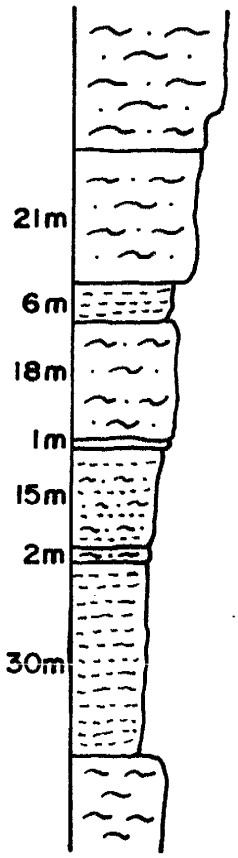

Kneeling Nun Tuff

poorly welded base
angular unconformity

tuff of Rocque Ramos Canyon

sandstone of Cliff Canyon
fine-grained, purple volcaniclastic

poorly to non-welded, crystal-poor ash-flow tuff
tuff of Victoria Tank
lithic-rich, crystal-rich non-welded tuff
interbedded f-g, purple volcaniclastics and non-welded, chalky tuff beds w/ 10-15% plagioclase & trace qtz
non-welded, pumice-rich tuff w/ plagioclase & biotite

fine-grained, bedded, purple volcaniclastics w/ several thin (10-15cm), white pumice beds near top

Rubio Peak andesite

Figure 17. Stratigraphic section on the south side of Dry Creek, east-center sec. 1, T. 11 S., R. 9 W.

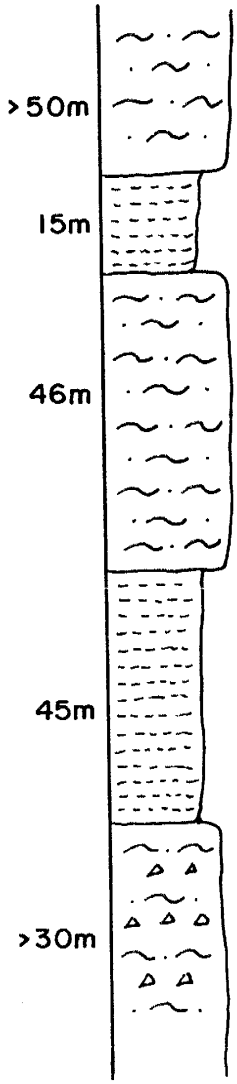

Kneeling Nun Tuff

sandstone of Cliff Canyon
fine-grained, purple volcaniclastic

10-15% white & pink plagioclase, minor biotite

tuff of Rocque Ramos Canyon
welding decreases upward

15-20% white plagioclase & biotite

sandstone of Cliff Canyon

tuff of Victoria Tank
poorly welded, crystal-poor, lithic-rich
ash-flow tuff

relationship found in northern Chloride mining district indicates that Rubio Peak intermediate volcanism persisted until 34.9 Ma, just prior to eruption of Kneeling Nun Tuff

Tuff of Rocque Ramos Canyon is a moderately to poorly welded, moderately crystal-rich, ash-flow tuff. Phenocrysts constitute 10-20% of the rock with subequal amounts of plagioclase and sanidine, and 1-2% biotite. Small (1.5-2.0 cm) devitrified pumice is common in this tuff. Locally, this tuff is silicified, and in places it contains a few tenths of one percent disseminations of iron-oxides after pyrite. Andesite lithic fragments, as much as 40 cm in diameter, are present but rare.

Petrographically, subhedral phenocrysts of plagioclase (An 28-34), sanidine, biotite, and rare quartz occur in a totally devitrified groundmass. Feldspars are generally 2-4 mm in size, biotite approximately 1.5 mm. Opaques, both magnetite and Fe-oxides after magnetite and pyrite, occur from 0.5 to 2.0 %.

Under the chemical classification scheme for volcanic rocks of Le Maitre (1984), tuff of Rocque Ramos Canyon is a trachyte to rhyolite rocktype (Fig. 14a). This unit is low in CaO, about 0.5 %, and has K2O + Na2O values of 9 to 10 %.

Tuff of Rocque Ramos Canyon is a new name for tuff of Bear Springs used by Eggleston and Harrison (in review) in Sawmill Peak area, northern Chloride mining district (Plate 3). Based on paleomagnetic data and 40Ar/39Ar age dating, McIntosh (1989) correlated tuff of Rocque Ramos Canyon with

Bell Top 4 tuff (Clemons and Seager, 1973; Clemons, 1975; 1976) found principally in Goodsight-Cedar Hills area. McIntosh (1989) reports a 40Ar/39Ar age of 34.93 Ma for tuff of Rocque Ramos Canyon near Double 9 Peak, immediately east of Chloride mining district, and 40Ar/39Ar ages of 35.01 and 34.94 Ma for Bell Top 4 tuff in Goodsight-Cedar Hills area. Similarities of whole rock geochemistry (Table 3 of this report and fig. 5 of Clemons, 1975) and phenocryst contents further substantiate correlation of tuff of Rocque Ramos Canyon with Bell Top 4 tuff. Correlation between these units and unnamed crystal tuff of Mayer (1987) and Seager and Mayer (1988) in Salado Mountains is tentative and needs further investigation. Tuff of Rocque Ramos Canyon is not present immediately north of this area, where Kneeling Nun Tuff rests directly upon tuff of Victoria Tank and debris-flow deposits of lower Rubio Peak Formation (Harrison, unpublished mapping along Palomas Creek in Williamsburg NW quadrangle). Correlations of tuff of Rocque Ramos Canyon with tuffs of Sugarlump Formation of Elston (1957) and Seager et al. (1982) in southern Black Range-Silver City area are also tentative and in need of further investigation.

From present-day knowledge, it appears that tuff of Rocque Ramos Canyon-Bell Top 4 tuff has an minimum aerial extent of approximately 3700 km2 (Fig. 18). Assuming an average thickness of about 30 m, this unit has a minumum volume of approximately 110 km3. These conservative

Figure 18. Approximate aerial distribution of the tuff of Rocque Ramos Canyon-Bell Top 4 tuff in south-central New Mexico, partially adapted from McIntosh (1989).

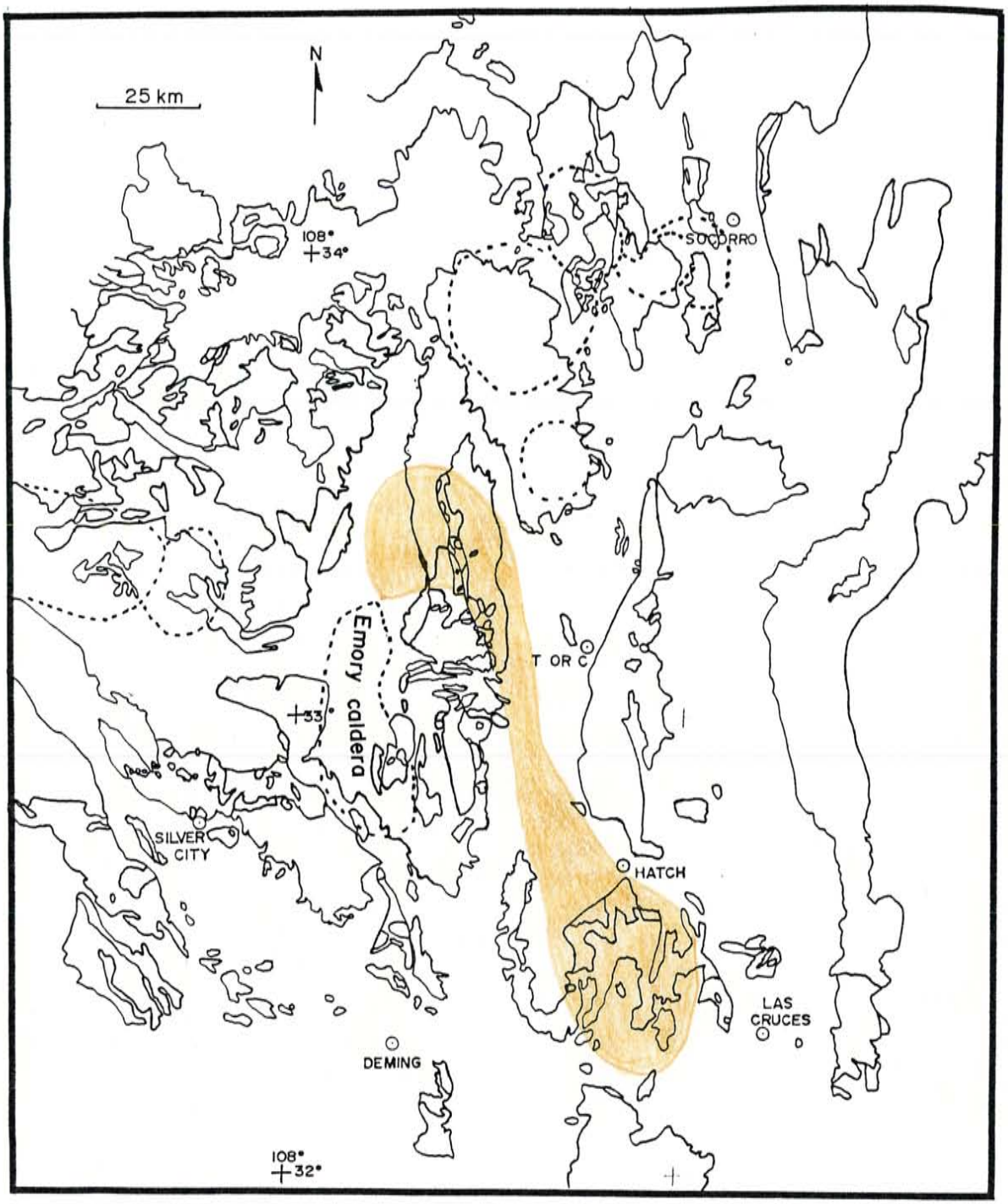
25 km
N
108°
+34°
SOCORRO
Emory caldera
T OR C
+33°
SILVER CITY
HATCH
LAS CRUCES
DEMING
108°
+32°

calculations would place this tuff unit in the magnitude 5 volume classification of Smith (1960), indicative of major subsidence or caldera-forming collapse in source area. However, there is no known source area or caldera fill for tuff of Rocque Ramos Canyon-Bell Top 4 tuff. Similar age and aerial distribution of this unit to Kneeling Nun Tuff lead McIntosh (1989) to suggest a common source area for these tuffs (i.e. Emory caldera). In contrast, Clemons (1975) has suggested a source area for the Bell Top 4 tuff in northern Cedar Hills area of Sierra de las Uvas, based on dense-welding and elongated-pumice characteristics found there. This matter remains unresolved.

Tuff of Victoria Tank

Tuff of Victoria Tank is named for exposures in sec. 3, T. 12 S., R. 7 W. and sec. 34, T. 11 S., R. 7 W., near Victoria Tank in eastern Sierra Cuchillo. There, this tuff is approximately 80 m thick, overlies a porphyritic andesite lava in upper Rubio Peak Formation, and occurs beneath tuff of Rocque Ramos Canyon. The distinctive characteristic of tuff of Victoria Tank is its high content of lithic fragments, typically constituting 20 to 40 % of rock volume.

In the Chloride mining district, tuff of Victoria Tank is restricted in outcrop to the northern half of the district, particularly, Sawmill Peak quadrangle (Trlt unit on Plate 3), where it is as much as 100 m thick. In this area, tuff of Victoria Tank crops out in low resistant hills, and is intercalated with andesitic lavas of upper Rubio Peak Formation (Fig. 12). Southernmost exposures of this unit in Chloride mining district occur along Chloride and Mineral Creeks, where it is intercalated with sedimentary deposits (sandstone of Cliff Canyon) (Figs. 16 & 17).

Tuff of Victoria Tank is a lithic-rich, pumice-rich, crystal-poor ash-flow tuff. Degrees of welding vary from moderate in Chloride mining district to dense in portions of the eastern Sierra Cuchillo. This unit contains 10 % or less phenocrysts of plagioclase, sanidine, and biotite. Subangular lithic fragments of red, aphanitic rhyolite (?)

and gray-black, aphanitic andesite make up 20 to 40 % of the rocks volume, and occur up to 6 cm in diameter. In eastern Sierra Cuchillo, well-lineated pumice (north-south elongation) ocuur in tuff of Victoria Tank (mile 26.4 of Osburn et al., 1986). Throughout eastern Sierra Cuchillo, a lithic-poor, basal vitrophyre is present for this tuff (unpublished mapping by R.W. Harrison) but is absent in Chloride mining district.

Microscopically, tuff of Victoria Tank consists of 8 to 10 % rounded plagioclase (An 25-30) and sanidine phenocrysts that are typically altered and range from 1 to 3 mm in size. Subhedral biotite makes up approximately 1 % of rock volume; angular quartz, opaque magnetite blebs, and subhedral hornblende occur in trace amounts. Subrounded lithic fragments make up 30 to 40 % of the rock, and exist down to .2 mm in diameter. Groundmass shows a vitroclastic texture of compressed pumice and glass shards, mostly devitrified.

Two major-element chemical analyses have been determined for tuff of Victoria Tank, one for this report and one by Eggleston (1987) (Table 3). Both samples are from eastern Sierra Cuchillo, and both analyses indicate that tuff of Victoria Tank is a rhyolite under classification scheme of Le Maitre (1984) (Fig. 14a).

Tuff of Victoria Tank is extensive throughout eastern Sierra Cuchillo, and is believed to be correlative to unnamed lithic tuff of Mayer (1987) and Seager and Mayer (1988) in Salado Mountain-Garcia Peaks area. Relationships

between tuff of Victoria Tank and Sugarlump Formation in southern Black Range (Seager et al., 1982) and Mimbres-Silver City area (Elston, 1957) are uncertain. Tuff of Victoria Tank is tentatively correlated with Sugarlump Tuff of Hedlund (1977) in Hillsboro and San Lorenzo quadrangles. This correlation is based on similar stratigraphic position, abundance of lithic fragments, and similar phenocryst contents.

Based on paleomagnetic data, McIntosh (1989) tentatively correlated tuff of Victoria Tank with both tuff of Luna Park, found in the southern San Mateo Mountains (Herman, 1988), and tuff of Farr Ranch, a unit that he dated by 40Ar/39Ar at 35.6 Ma, found extensively throughout northern portions of Mogollon-Datil volcanic field, and believed to have had a source in that area (McIntosh, 1989). However, lithologic considerations suggest that these correlations for tuff of Victoria Tank by McIntosh (1989) may be inaccurate. In particular, the lithic-rich nature of tuff of Victoria Tank is ubiquitous for all exposures in Black Range, Sierra Cuchillo, and Salado Mountains but tuffs of Farr Ranch and Luna Park are lithic-poor units. Also, phenocryst contents of Farr Ranch and Luna Park (15-25 %) are greater than that recognized for tuff of Victoria Tank. Furthermore, the lithic-rich and densely welded characteristics of Victoria Tank seem inconsistant with the idea that this unit represents a distal portion of an ignimbrite sheet whose source area is many tens of

kilometers away, in the northern portion of Mogollon-Datil volcanic field. Rather, it is the opinion of this author that tuff of Victoria Tank is a local unit, restricted to Sierra Cuchillo-Black Range area, and that it probably has a local source (possibly Emory caldera ?). Known aerial extent of lithic-rich tuff of Victoria Tank is shown in Figure 19. From this outcrop pattern and major-element geochemistry (Tables 3 & 5), it is at least conceivable that tuff of Victoria Tank represents a precursor unit that preceded eruption of Kneeling Nun Tuff.

Figure 19. Approximate aerial distribution of lithic-rich tuff of Victoria Tank in south-central New Mexico.

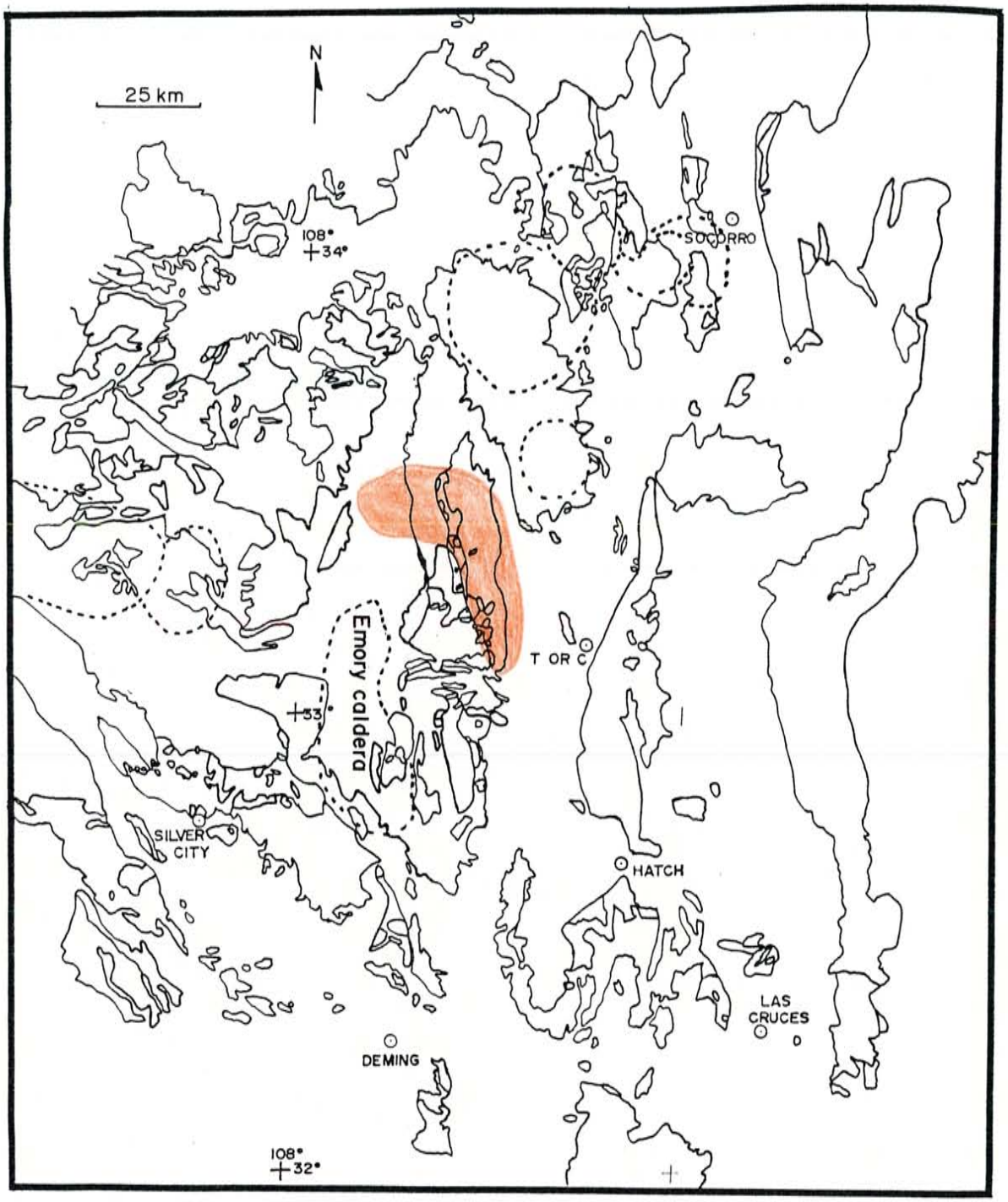
25 km
N
108°
34°
SOCORRO
Emory caldera
T OR C
33°
SILVER CITY
HATCH
LAS CRUCES
DEMING
108°
32°

dacite of Wildhorse Canyon

Dacite of Wildhorse Canyon is a minor lava flow found only in extreme northern part of the Chloride mining district, in secs. 28, 29, and 32, T. 9 S., R. 9 W., Sawmill Peak quadrangle (Twh map unit on Plate 3). It is named for exposures along Wildhorse Canyon. Maximum exposed thickness in this area is approximately 70 m, but some of these exposures may be intrusive vent areas. Stratigraphically, dacite of Wildhorse Canyon is below tuff of Rocque Ramos Canyon and overlies intermediate lavas of upper Rubio Peak Formation and tuff of Victoria Tank (Fig. 12). This unit was referred to as rhyolite of Wildhorse Canyon by Eggleston and Harrison (in review), prior to geochemical analysis. It is believed to be correlative to quartz latite lava (Tqli map unit) of Fodor (1976) in northern Black Range.

Dacite of Wildhorse Canyon contains 15 to 25 % large phenocrysts of plagioclase (2-3 cm) and 1 to 5 % phenocrysts of biotite. Plagioclase is commonly altered to chalky, white clays. Locally, carapace breccia is preserved on top of lava flows. One chemical analysis of this unit is presented in Table 3 (sample # 4). Dacite of Wildhorse Canyon contains slightly less silica, and distinctly less total alkalis than ash-flow tuffs that occur in the stratigraphic interval below Kneeling Nun Tuff (Fig. 14a).

sandstone of Cliff Canyon

The name sandstone of Cliff Canyon was proposed by Woodard (1982) for arkosic to quartzose volcaniclastic rocks that occur directly above Rubio Peak Formation and below Kneeling Nun Tuff. Type locality is along Cliff Canyon, near its confluence with Bear Creek in NW 1/4 sec. 34, T. 10 S., R. 9 W., Lookout Mountain quadrangle (Plate 2). There, sandstone of Cliff Canyon rests upon aphanitic and porphyritic andesite lavas of Rubio Peak Formation, and is directly beneath Kneeling Nun Tuff. Tuffs of Stone House Ranch, Rocque Ramos Canyon, and Victoria Tank occur intercalated with sandstone of Cliff Canyon in many areas (Figs. 15, 16, & 17).

Sandstone of Cliff Canyon is found extensively throughout the central portions of Chloride mining district, but is absent from extreme northern and southern portions of the district. This unit is poorly consolidated, and thus forms less resistant slopes. It has a maximum thickness of approximately 60 m.

This unit consists of purplish and white, fine-grained, well-sorted, thin- to medium-bedded sandstones and siltstones. In northern outcrops, basal conglomerate deposits are locally found that contain andesitic clasts derived from the Rubio Peak Formation. Sandstone deposits are typically white in color and consist of subrounded to rounded grains of quartz, sanidine, plagioclase, and minor

biotite. Siltstone deposits are typically purple to blue-gray in color and appear to be more andesitic in composition; however, no petrographic work has been done with these deposits. Thin, tuffaceous air-fall beds occur locally in upper portions of the sandstone of Cliff Canyon.

Lucas (1986) found mammal fossils within siltstone beds belonging to sandstone of Cliff Canyon at two localities along Turkey Creek in Chloride mining district: SW1/4SE1/4 sec. 24, T. 10 S., R. 9 W., and SW1/4SW1/4 sec. 14, T. 10 S., R. 9 W. He interpreted these fossils as indicative of an early Chadronian age (approximately 36 Ma). This age interpretation is consistent with radiometric dating, as his collection sites are stratigraphically below tuff of Rocque Ramos Canyon, dated by 40Ar/39Ar at 34.93 Ma (McIntosh, 1989).

Discussion of stratigraphic interval between Rubio Peak Formation and Kneeling Nun Tuff

The stratigraphic interval directly beneath Kneeling Nun Tuff and overlying (or interfingered with) Rubio Peak Formation throughout south-central New Mexico is extremely complex, and as indicated by McIntosh (1989), is one of the least understood stratigraphic intervals in the entire Mogollon-Datil volcanic field. Even the number of distinct ignimbrites occurring in this interval is not known, and regional correlations between ignimbrites are tentative at

best. And perhaps most enigmatic of all, there are no known source areas for any of the voluminous ash-flow tuffs in this interval, that even under very conservative estimates represent several hundreds of cubic kilometers of volcanic rock!

There are, however, some unifying features for this stratigraphic interval. First, this interval represents a distinct change in both volcanic rock type and style of eruption from the underlying Rubio Peak Formation. In effect, effusive, intermediate lavas of the Rubio Peak Formation give way to dominantly explosive, more-silicic volcanism. Second, all volcanic units in this interval have a paucity of quartz phenocrysts (the lowest, major volcanic unit in the stratigraphy of south-central New Mexico that contains significant amounts of quartz is Kneeling Nun Tuff). Third, ash-flow tuffs of this interval are most commonly intercalated with fine-grained volcaniclastic rocks, such as the sandstone of Cliff Canyon described above. Fourth, high-precision 40Ar/39Ar dating by McIntosh (1989) indicates that all the ash-flow tuff units in this interval were erupted over a relatively short time span of a few hundred thousand years, just prior to eruption of Kneeling Nun Tuff. And finally, distribution of ash-flow tuffs in this interval virtually surround Emory caldera (Fig. 20), source of Kneeling Nun Tuff (Elston et al., 1975).

Perhaps the simplest and most straightforward

Figure 20. Approximate aerial extent of ash-flow tuffs that occur directly beneath Kneeling Nun Tuff and above, or interfingered with, upper Rubio Peak Formation in south-central New Mexico.

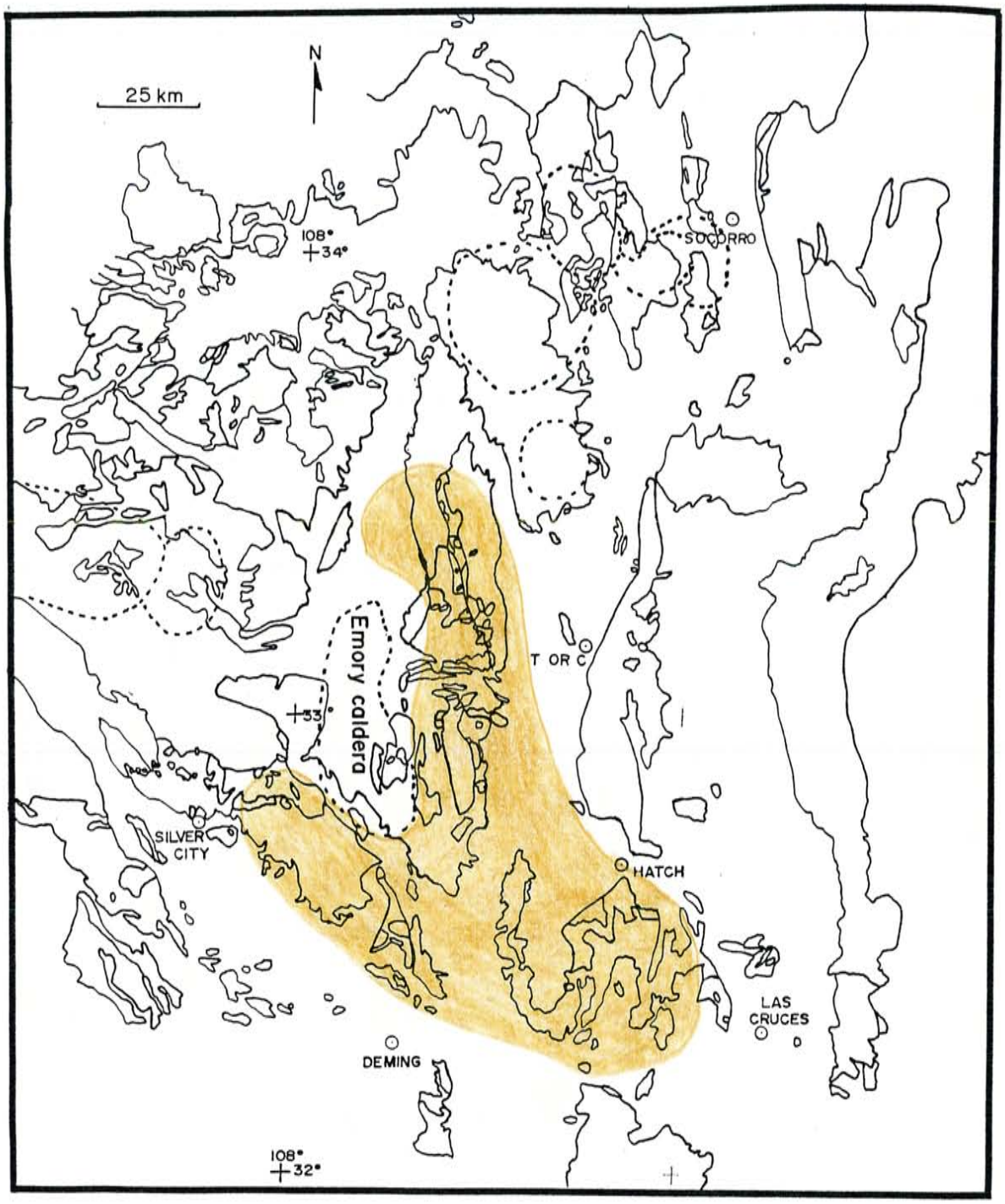
25 km
N
108°
34°
SOCORRO
Emory caldera
T OR C
33°
SILVER CITY
HATCH
LAS CRUCES
DEMING
108°
32°

interpretation for this stratigraphic interval is that, collectively, these rocks represent volcanic activity that preceded eruption of Kneeling Nun Tuff. And, source areas for ash-flow tuffs of this interval were from within Emory caldera. Much more detailed work (mapping, geochemical studies, and high-precision age dating) is needed to resolve complexities and problems of this stratigraphic interval.

Kneeling Nun Tuff

Kneeling Nun Tuff is found throughout north-central Black Range and is one of the most continuous units in south-central and south-western New Mexico. Figure 21 shows approximate regional distribution of Kneeling Nun Tuff in south-central and south-western New Mexico. Kneeling Nun Tuff is named after a rock pinnacle known as Kneeling Nun of Santa Rita that overlooks the Chino mine in sec. 35, T. 17 S., R. 12 W.

This unit was first described by Jicha (1954) and Kuellmer (1954) in the southern Black Range and was extended into the northern Black Range by Erickson et al. (1970). Kneeling Nun Tuff was misidentified as Hells Mesa Tuff in northern Chloride mining district by Coney (1976), a practice followed by Woodard (1982) in western Chloride mining district. In hand specimen and petrographically, Kneeling Nun Tuff and Hells Mesa Tuff are indistinguishable, but through stratigraphic relationships, age dating, and vertical zonations (Kneeling Nun Tuff is normally zoned, Hells Mesa Tuff is reversely zoned) these two units are separable.

The source area for Kneeling Nun Tuff is the Emory caldera (Elston et al., 1975; Abitz 1989), the northern margin of which is within 13 km (southwest) of the Chloride mining district. From the northern margin of Emory caldera, a nearly continuous outflow sheet of Kneeling Nun Tuff can

Figure 21. Approximate distribution of the Kneeling Nun Tuff in south-central and western New Mexico, largely adapted from McIntosh (1989).

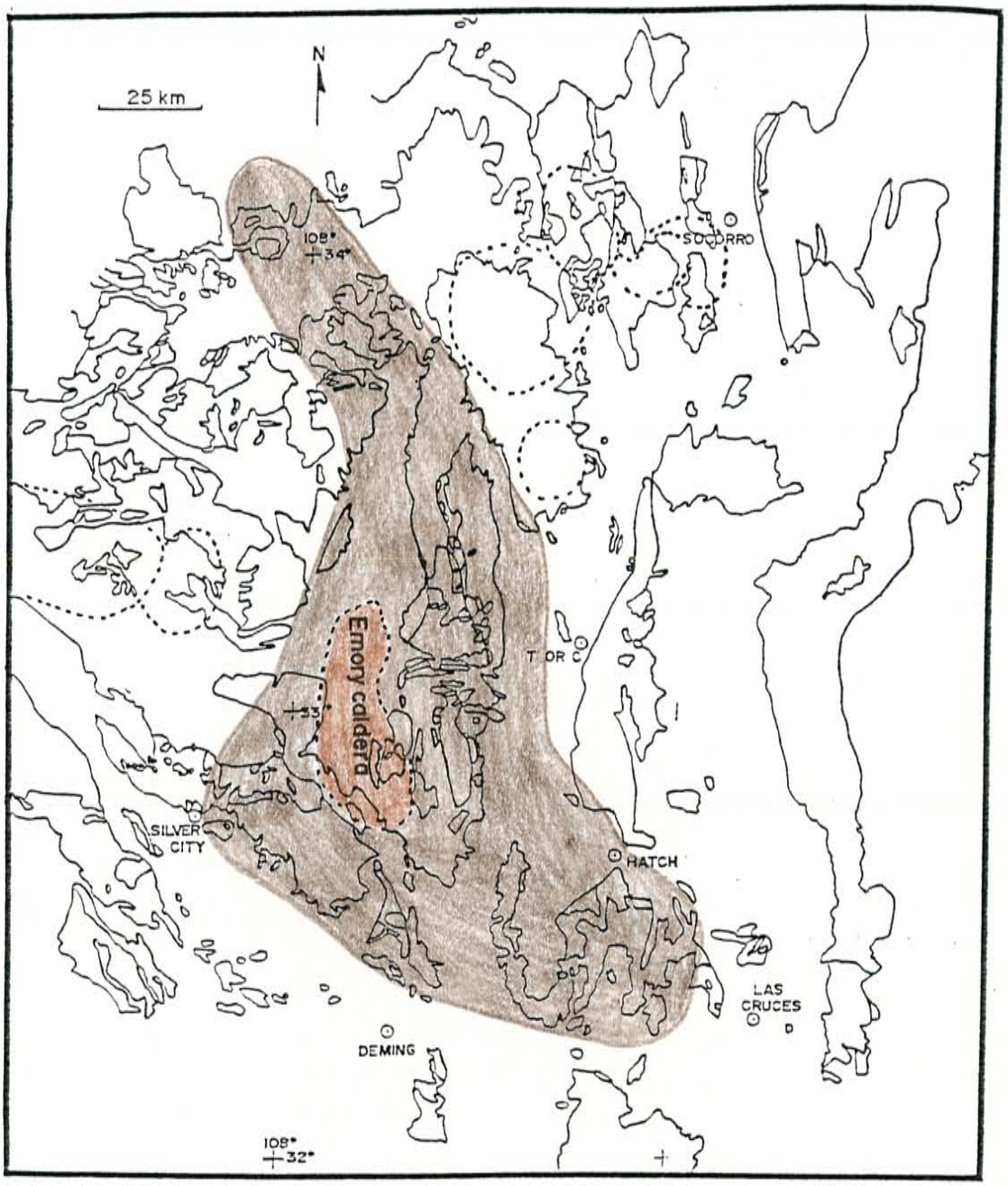
25 km
N
108°
34°
SOCORRO
Emory caldera
T OR C
33°
SILVER CITY
HATCH
LAS CRUCES
DEMING
108°
32°

be traced northward for over 32 km, thus forming an important stratigraphic marker horizon. Over this entire extent, Kneeling Nun Tuff maintains a thickness of 150 to 200 m, is a major cliff forming unit, and in many places caps high plateaus.

Adjacent to Emory caldera in the southern Chloride mining district, Kneeling Nun Tuff lies with angular unconformity upon rocks of lower Rubio Peak Formation. The angular unconformity at base of Kneeling Nun Tuff changes northward into a disconformity, where Kneeling Nun Tuff overlies rocks of the upper Rubio Peak Formation and the sandstone of Cliff Canyon. It is interpreted that these relationships are indicative of tumescence around Emory caldera prior to eruption of Kneeling Nun Tuff.

A radiometric K-Ar age of 34.2 $\pm$ 1.0 Ma (recalculated using new IUGS constants) was reported for the Kneeling Nun Tuff by McDowell (1971). McIntosh (1989) determined a slightly older age of 34.9 Ma using high-precision 40Ar/39Ar dating techniques.

In north-central Black Range, Kneeling Nun Tuff is a multiple-flow, compound-cooling unit of poorly to moderately welded, crystal-rich, ash-flow tuff. From 20 to 45% phenocrysts of quartz, sanidine, plagioclase, and biotite occur within the tuff; it is normally zoned from a very crystal-rich, quartz-rich, biotite-poor basal member to a moderately crystal-rich, quartz-poor, more biotite-rich upper member. Basal member is white and poorly welded,

upper member is generally tan and moderately welded.

Microscopically, the lower member is composed of 30 to 45 % phenocrysts of rounded and embayed quartz (20-25 %), sanidine (8-12 %), plagioclase (An 25-30; 5-10 %), biotite (0.5-1 %), with traces of hornblende (typically altered to opaques), and rare, small (0.5-1 mm) lithic fragments of andesite. Groundmass consists of partially devitrified pumice and shards with vitroclastic and common axiolitic textures. Microscopically, the upper member is composed of 15 to 25 % phenocrysts of quartz (5-10 %), sanidine (5-10 %), plagioclase (An 25-30, 5-10 %), and biotite (2-4 %), with common lithic fragments of andesite, as much as 5 cm in diameter. Slightly flatten pumice in upper member is more pronounced and as much as 3 cm in long dimension. A gradational increase in pumice content upward was noted by Woodard (1982) in upper member of this unit.

Major-element analyses for outflow facies Kneeling Nun Tuff found in the north-central Black Range and Sierra Cuchillo is presented in Table 5. Under the classification scheme of Le Maitre (1984), this unit is considered a rhyolite (Fig. 22a). Some chemical characteristics of outflow facies Kneeling Nun Tuff include K2O % greater than Na2O and total iron contents greater than CaO % (Fig. 22b).

An interesting zonation pattern between outflow-facies and intracaldera-fill Kneeling Nun Tuff is revealed through comparisons of variation diagrams. Figures 22c and 22d are variation diagrams developed from data on intracaldera

Table 5. Major-element analyses of the Kneeling Nun Tuff in north-central Black Range and Sierra Cuchillo, outflow facies.

	1	2	3	4	5	6	7	8
SiO2	69.22	70.38	70.97	69.69	69.83	70.02	75.13	70.41
Al2O3	15.19	14.66	14.18	14.23	15.03	14.47	14.05	14.38
Fe2O3	2.82	3.06	2.61	2.46	2.57	2.56	1.47	2.57
MgO	.68	.59	.61	1.38	.34	.73	.15	.67
CaO	1.72	1.54	1.30	1.33	1.47	.69	.69	1.53
Na2O	3.92	4.00	4.16	3.84	3.44	1.02	2.83	3.28
K2O	4.16	4.24	4.38	5.81	5.79	6.67	4.32	4.53
TiO2	.47	.48	.39	.42	.43	.44	.02	.04
P2O5	.14	.12	.11	.13	.16	.13	.06	.10
MnO	.05	.04	.04	.02	.02	.03	.01	.01
LOI	.94	1.03	1.21	1.41	.51	3.91	1.06	2.38
Total	99.31	100.72	99.96	100.72	99.59	100.67	99.80	99.93

1) Upper member of Kneeling Nun Tuff, Sec. 2, T. 12 S., R. 8 W., Winston graben, this report.
2) Upper member of Kneeling Nun Tuff, 33-19'-50" N, 107-44'-35" W, Chloride Creek Box, this report.
3) Lower member of Kneeling Nun Tuff, 33-20'-05" N, 107-46'-37" W, Lyons Peak, north of Chloride Creek, this report.
4) Upper member of Kneeling Nun Tuff, SW1/4 sec. 14, T. 11 S., R. 7 W., eastern Sierra Cuchillo, this report.
5) Upper member of Kneeling Nun Tuff, sec. 26, T. 11 S., R. 7 W., 33-19'-33" N, 107-31'-59" W, eastern Sierra Cuchillo, Eggleston, 1987.
6) Upper member of Kneeling Nun Tuff, sec. 26, T. 11 S., R. 7 W., 33-19'-35" N, 107-31'-47" W, eastern Sierra Cuchillo, Eggleston, 1987.
7) Upper member of Kneeling Nun Tuff, SE1/4SW1/4 sec. 21, T. 10 S., R. 9 W., plateau between Turkey and Little Bear Creek, western Chloride mining district, Woodard, 1982.
8) Upper member of Kneeling Nun Tuff, SW1/4SW1/4 sec. 27, T. 11 S., R. 9 W., South Fork of Cuchillo Negro Creek, southwestern Chloride mining district, Woodard, 1982.

Figure 22. Major-element variation diagrams for Kneeling Nun Tuff; a. SiO_2 vs. $K_2O + Na_2O$ for outflow facies in north-central Black Range and Sierra Cuchillo; b. SiO_2 vs. K_2O, Na_2O, CaO, Fe_2O_3, and Al_2O_3 for outflow facies; c. SiO_2 vs. $K_2O + Na_2O$ for caldera-fill facies d. SiO_2 vs. K_2O, Na_2O, CaO, Fe_2O_3, and Al_2O_3 for caldera-fill facies. Data for c & d from Abitz (1989). Solid squares represent samples analyzed for this report.

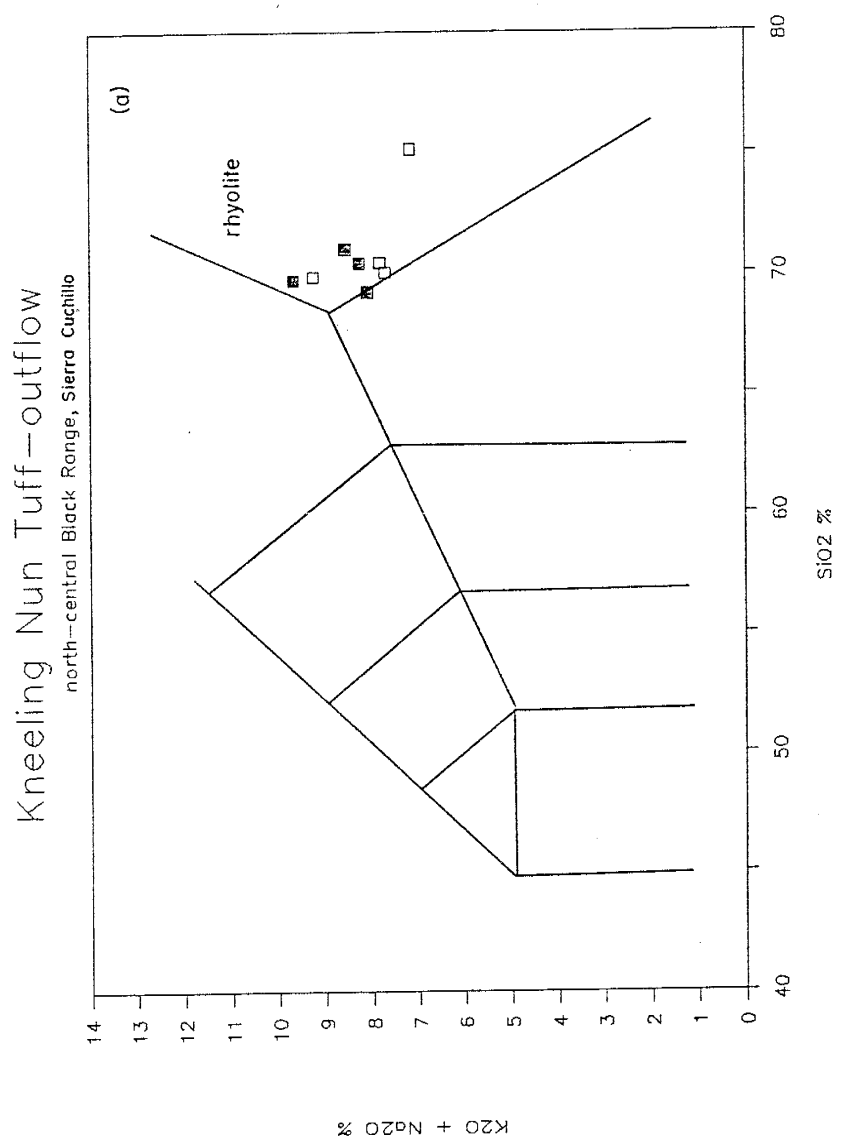
Kneeling Nun Tuff—outflow
north—central Black Range, Sierra Cuchillo
(a)
rhyolite
K2O + Na2O %
SiO2 %
0
1
2
3
4
5
6
7
8
9
10
11
12
13
14
40
50
60
70
80

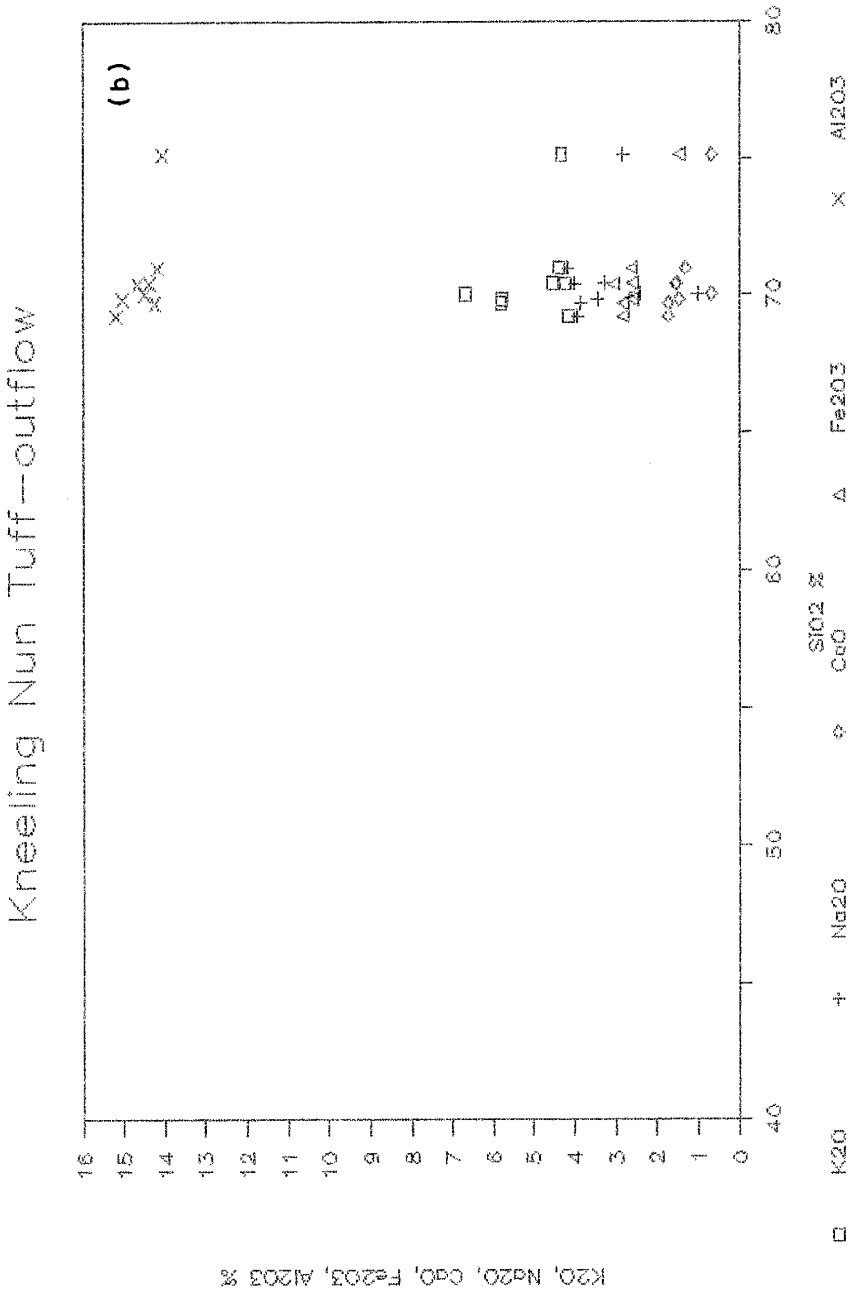
Kneeling Nun Tuff—outflow
(b)
K2O, Na2O, CaO, Fe2O3, Al2O3 %
SiO2 %
□ K2O
+ Na2O
◇ CaO
△ Fe2O3
× Al2O3
0
1
2
3
4
5
6
7
8
9
10
11
12
13
14
15
16
40
50
60
70
80

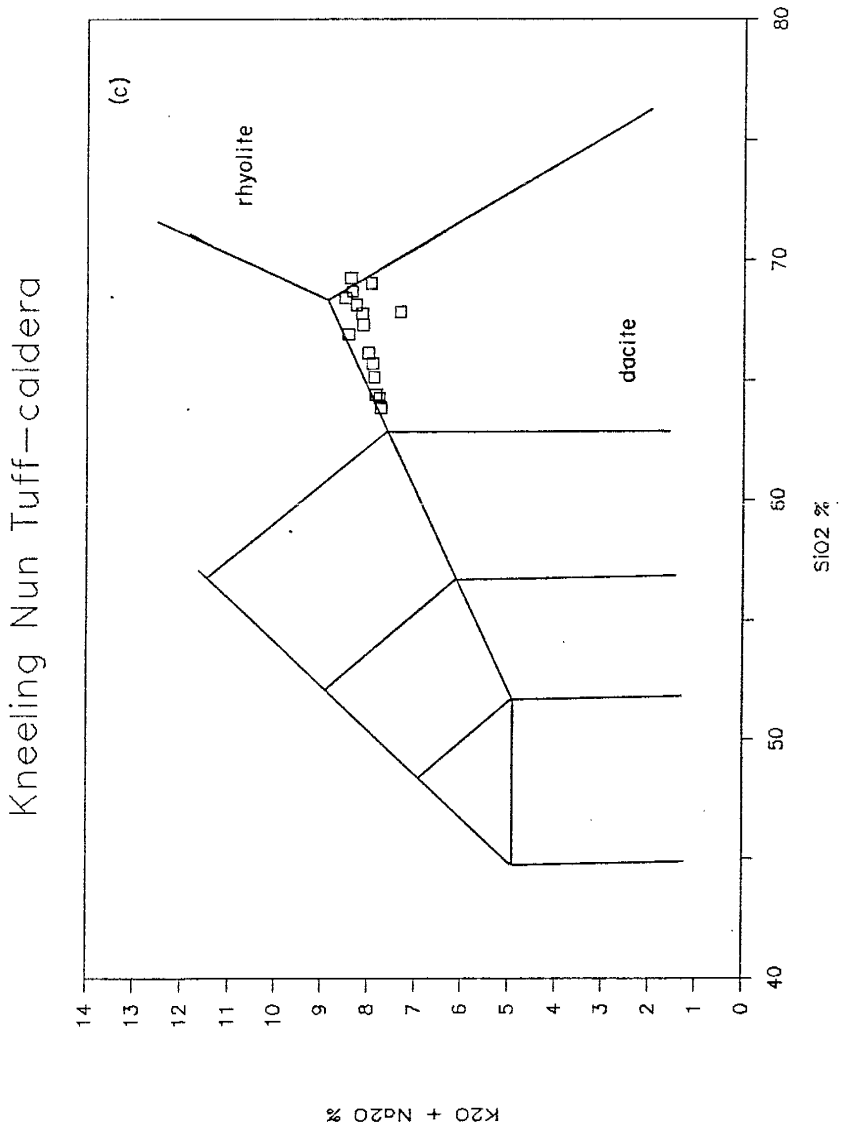
Kneeling Nun Tuff—caldera
(c)
rhyolite
dacite
K2O + Na2O %
SiO2 %
0
1
2
3
4
5
6
7
8
9
10
11
12
13
14
40
50
60
70
80

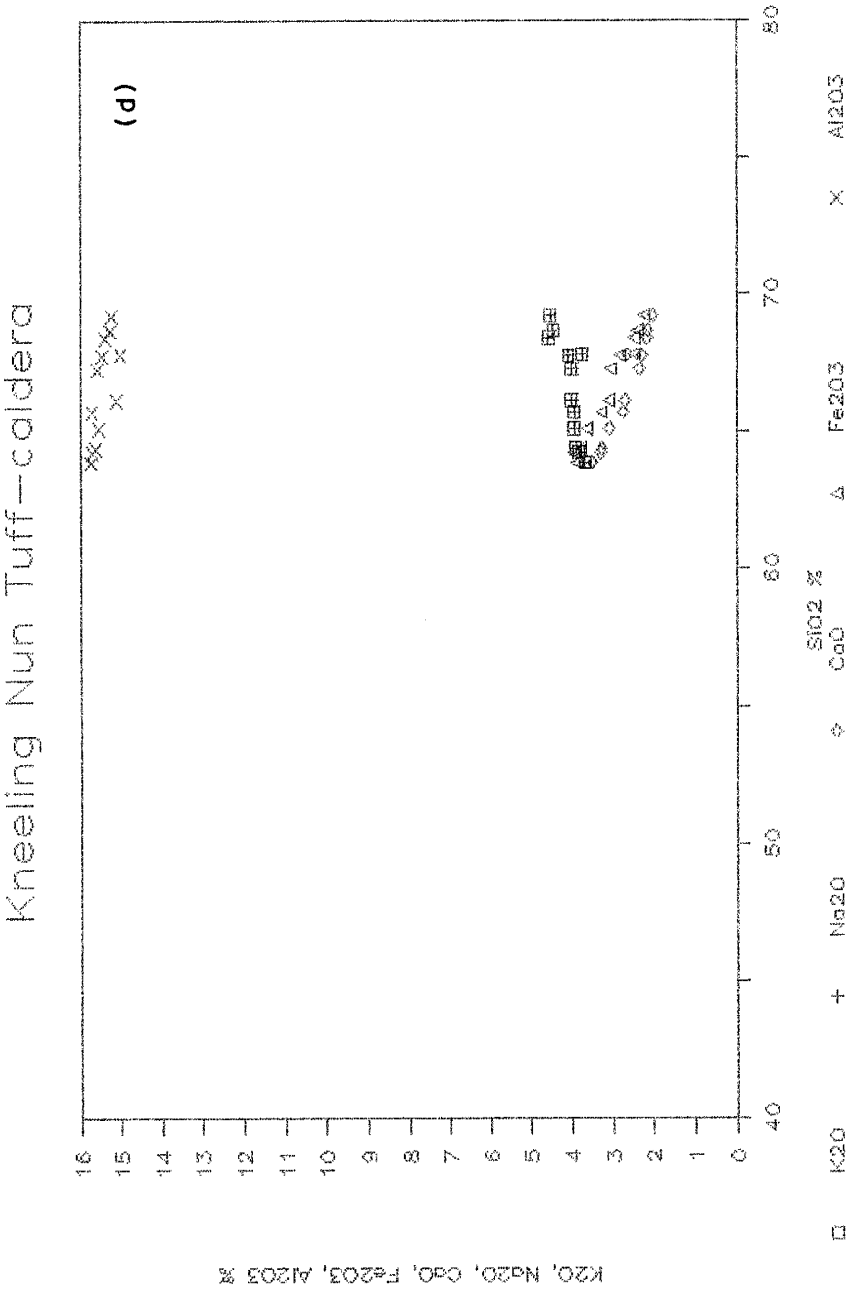
Kneeling Nun Tuff—caldera
(d)
K2O, Na2O, CaO, Fe2O3, Al2O3 %
SiO2 %
K2O
Na2O
CaO
Fe2O3
Al2O3

Kneeling Nun Tuff from Abitz (1989). Comparison of Figures 22a and 22c show that outflow-facies Kneeling Nun Tuff is slightly, but distinctively, more silicic than intracaldera-fill Kneeling Nun Tuff. Figure 22d reveals that K2O and Na2O occur in approximately equal amounts in intracaldera fill, whereas K2O is greater than Na2O in outflow facies (Fig. 22b). Figure 22d shows that CaO and total iron occur in subequal amounts in intracaldera-fill Kneeling Nun Tuff, in contrast to outflow facies (Fig. 22b); the main difference is a relative increase in CaO content in intracaldera rocks. The overall zonation pattern revealed through these comparisons is that intracaldera Kneeling Nun Tuff is slightly more mafic in major-element composition than outflow facies Kneeling Nun Tuff occurring in north-central Black Range and Sierra Cuchillo. This zonation is consistant with eruption of a normally zoned magma. Reference is given to Abitz (1989) for detailed study of intracaldera-fill Kneeling Nun Tuff.

Cuchillo Negro Complex

Cuchillo Negro complex is a new and informal name given to an intrusive-extrusive volcanic complex occurring on both sides of Cuchillo Negro Creek in secs. 13, 14, 22, & 23, T. 12 S., R. 8 W., Winston and Chise quadrangles. This area is the only known occurrence of this minor unit, but outcrops there provide excellent exposures of vent and near-vent rocks.

Exact stratigraphic position of Cuchillo Negro complex is not clear from field relationships. Intrusive member of this unit distinctly cross-cuts rocks of Rubio Peak Formation and tuff of Rocque Ramos Canyon, but relationships to younger rocks are not straightforward. A whole rock K-Ar age of 34.7 ± 0.8 Ma was determined for this unit, however, the error range is such that Cuchillo Negro complex could be either older or younger than Kneeling Nun Tuff. For mapping purposes on Plate 1 (Winston quadrangle), Cuchillo Negro complex was assumed to be younger than Kneeling Nun Tuff.

If rocks of Cuchillo Negro complex are slightly younger than Kneeling Nun Tuff, then they occupy a stratigraphic position similar to that of Mimbres Peak Formation described by Jicha (1954), Elston (1957), Elston et al. (1975), and Seager et al. (1982) in southern Black Range. Mimbres Peak Formation was interpreted as moat and ring-fracture deposits of Emory caldera by Elston et al. (1975). Rhyolite member of Cuchillo Negro complex strongly resembles rhyolitic lavas

of Mimbres Peak Formation.

Cuchillo Negro complex consists of three intrusive rock types, and three extrusive ash-flow tuffs with intercalated volcaniclastic sediments and one rhyolite lava flow. Figure 23 is a generalized cross-section through the complex, Figure 24 is a detailed stratigraphic section for extrusive members of Cuchillo Negro complex. Table 6 presents major-element analyses for most volcanic members of Cuchillo Negro complex; Figure 25 shows variation diagrams derived from Table 6.

Intrusive rock types found in the Cuchillo Negro complex are crystal-poor rhyolite, moderately crystal-rich basaltic andesite, and amygdule-rich trachyte. Rhyolite is flow-banded and contains 5-10 % phenocrysts of plagioclase and sanidine. Basaltic andesite member contains 20-25 % large (up to 5mm) phenocrysts of plagioclase and conspicuous apple-green pyroxene. This member also contains 2-3 % euhedral magnetite and is characteristically magnetic. Trachyte member cross cuts all other rock types and contains numerous, irregular-shaped amygdules as much as 10 mm in diameter, commonly lined with calcite, quartz, and unidentified zeolites. The basaltic andesite member also contains 10-15 % plagioclase phenocrysts. Foliations found within center of vent are generally steep and elongated in northwest-southeast direction. Dikes of amygdule-rich trachyte typically strike northeasterly, as does an arm of the main intrusive body occurring along the eastern margin.

Figure 23. Schematic cross-section through the Cuchillo Negro complex in secs. 13 & 14, T. 12 S., R. 8 W., showing relationships between the various members. Intrusive phases are known to cross-cut the tuff of Rocque Ramos Canyon; relationships with the Kneeling Nun Tuff are not clear from field exposures, but are inferred from relative age dates.

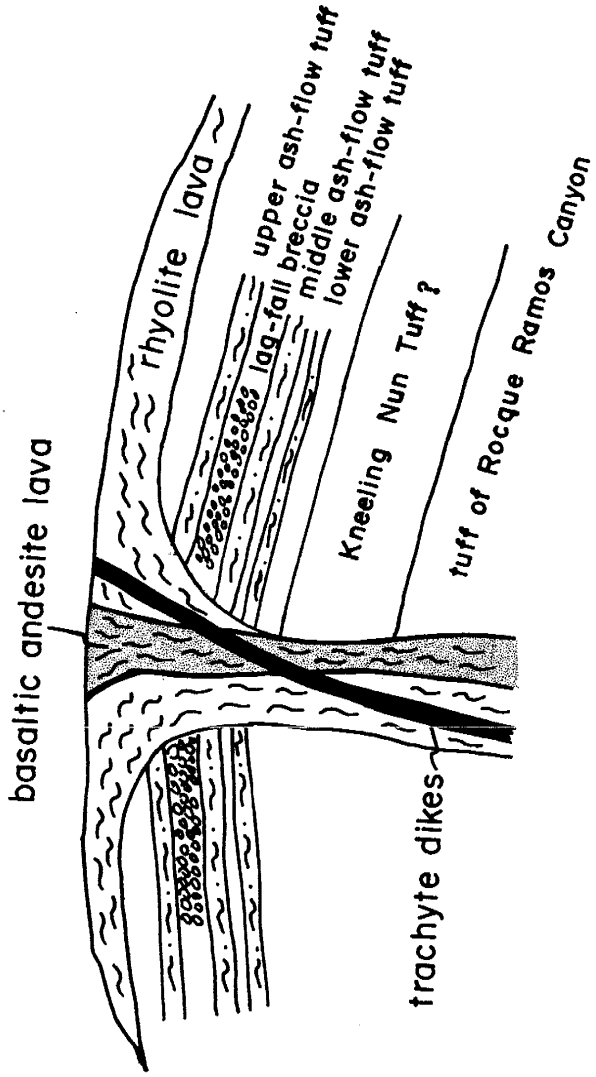
basaltic andesite lava
rhyolite lava
upper ash-flow tuff
lag-fall breccia
middle ash-flow tuff
lower ash-flow tuff
Kneeling Nun Tuff?
tuff of Rocque Ramos Canyon
trachyte dikes

Figure 24. Stratigraphic section through the extrusive members of Cuchillo Negro complex as exposed in the west bank of Cuchillo Negro Creek, sec. 13, T. 12 S., R. 8 W.

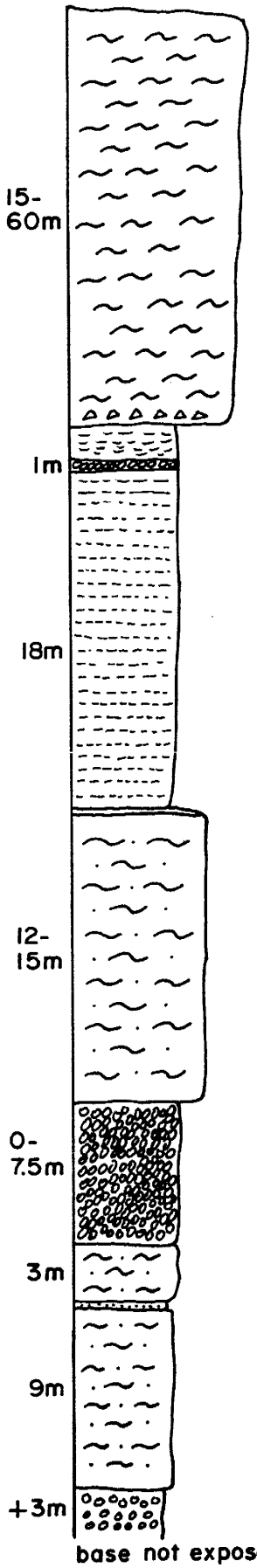

15-60m dense, flow-banded rhyolite lava
5% plagioclase & sanidine, trace biotite

brecciated base with red spherulites

1m boulder conglomerate

18m fine-grained mudstone-sandstone
thin, horizontal beds, pumice-rich intervals
5-8cm thick bed of coarse crystal near center

10-15cm, white, non-welded tuff, lithic-rich, pumice-rich

12-15m moderately welded, lithic-rich ash-flow tuff
3-4% biotite, 5-10% plagioclase

0-7.5m paleo-channel of lag-fall breccia
heterolithic pebbles & boulders, dominantly of Rubio Peak-like volcanic rocks with sparse Paleozoic & PC, non-sorted, poorly bedded, pumiceous matrix

3m white, non-welded tuff, 3% biotite, 3% feldspar
6-10cm sandstone, abundant lithics & biotite

9m non-welded, lithic-rich, pumice-rich, ash-flow tuff, 2% biotite 5% plagioclase, 5mm-3cm lithics of aphanitc, red-purple volcanic rocks

+3m coarse-grained volcaniclastic ROCKS

base not exposed

Table 6. Major-element analyses for rocks of the Cuchillo Negro Complex.

	1	2	3	4	5	6	7
SiO2	68.96	69.84	72.25	65.16	66.78	65.25	62.80
Al2O3	13.63	13.56	13.79	14.85	14.45	14.57	15.77
Fe2O3	3.16	3.13	3.27	3.30	2.02	2.89	6.17
MgO	1.24	1.06	.37	1.53	1.20	1.69	2.09
CaO	1.96	1.68	1.08	2.55	2.90	2.23	3.88
Na2O	2.77	2.69	3.15	2.15	1.94	1.77	4.06
K2O	5.67	5.65	5.73	5.61	3.89	4.64	3.87
TiO2	.56	.59	.60	.55	.34	.46	.96
P2O5	.10	.10	.11	.13	.04	.76	.25
MnO	.05	.05	.05	.05	.04	.04	.06
LOI	1.75	1.91	.92	4.52	4.72	4.29	1.03
Total	99.85	100.26	101.32	100.40	98.32	98.20	100.40

1) Flow-banded rhyolite member, this report.
2) Flow-banded rhyolite member, this report.
3) Flow-banded rhyolite member, this report.
4) Upper ash-flow tuff member, this report.
5) Middle ash-flow tuff member, this report.
6) Lower ash-flow tuff member, this report.
7) Amygdaloidal lava member, this report.

Figure 25. Major-element variation diagrams for rocks of the Cuchillo Negro complex, derived from Table 6; (a) SiO_2 vs. $K_2O + Na_2O$, (b) SiO_2 vs. K_2O, Na_2O, CaO, Fe_2O_3, and Al_2O_3.

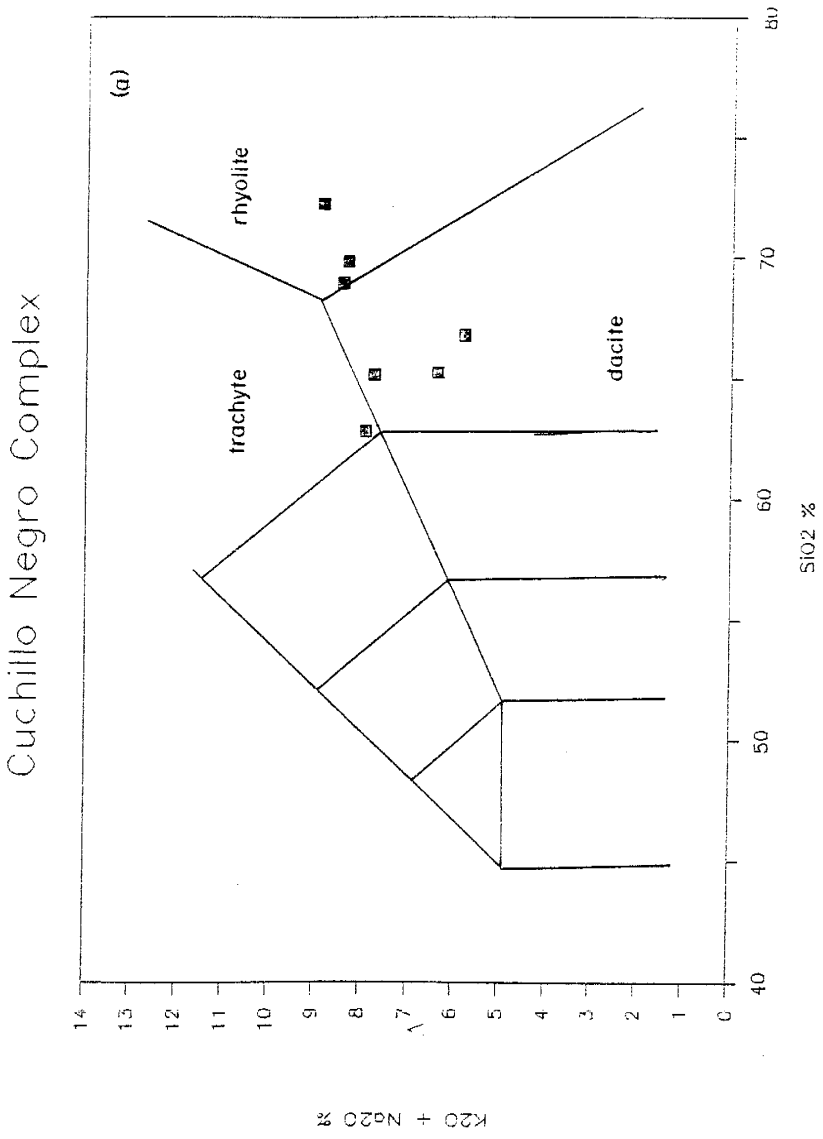
Cuchillo Negro Complex
(a)
rhyolite
trachyte
dacite
K2O + Na2O %
SiO2 %
40
50
60
70
0
1
2
3
4
5
6
7
8
9
10
11
12
13
14

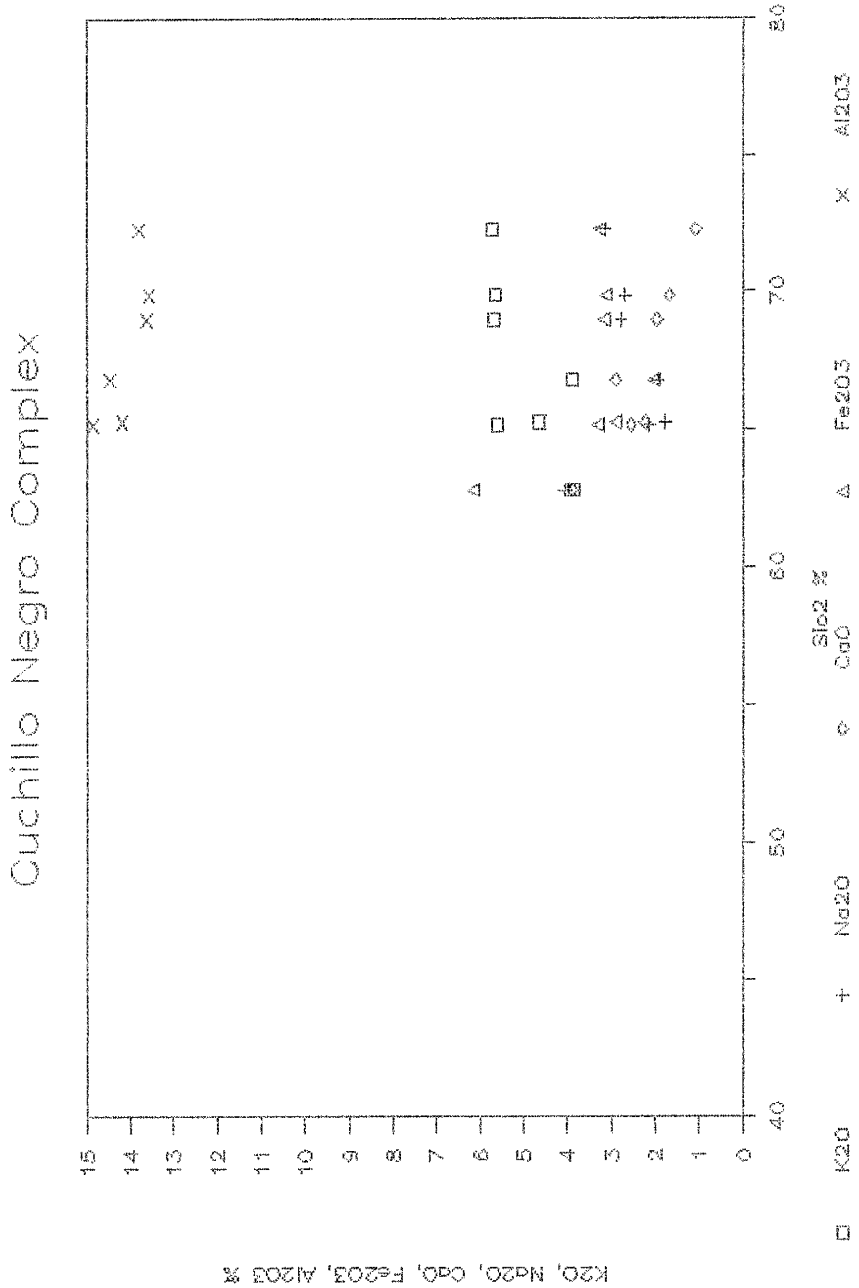
Cuchillo Negro Complex
K2O, Na2O, CaO, Fe2O3, Al2O3 %
0
1
2
3
4
5
6
7
8
9
10
11
12
13
14
15
40
50
60
70
80
SiO2 %
□ K2O
+ Na2O
◇ CaO
△ Fe2O3
× Al2O3

Extrusive members of the Cuchillo Negro complex consist of three dacite ash-flow tuffs that are intercalated with volcaniclastic sediments, and a flow-banded rhyolite lava identical to intrusive rhyolite. Lower ash-flow tuff is tan in color, non-welded, lithic-rich, pumice-rich, and crystal-poor. It contains about 2 % biotite and less than 5 % plagioclase phenocrysts. Lithic fragments are aphanitic, red-purple volcanic rocks, from 5 mm to 3 cm in diameter. Middle ash-flow tuff is white, non-welded, crystal-poor, and contains few lithic fragments. It contains approximately 3 % conspicuous green biotite and 2-3 % plagioclase. The upper ash-flow tuff is flesh-colored, slightly to moderately welded and lithic-rich. It contains 3-4 % biotite and 5-10 % plagioclase phenocrysts. Lithic fragments are similar to those found in lower tuff.

Volcaniclastic sediments occur intercalated between all three ash-flow tuffs. A thin (6-10 cm), horizontally bedded sandstone interval occurs between lower and middle tuffs, and contains abundant lithic fragments and biotite.

Between middle and upper tuffs is a paleo-channel of near-vent, lag-breccia that consists of chaotic, non-sorted, crudely stratified, heterolithic pebble and boulder detritus. Clasts are dominantly Rubio Peak-like volcanic rocks with sparse Paleozoic and Precambrian rock types. These lag-breccia deposits are basically clast supported, with pumiceous material as matrix. The initial interpretation of these deposits as lag breccias was made by

G.P.L. Walker during a field trip to the area in 1987. As such, these lag breccias represent co-ignimbrite deposits that form within a proximal deflation zone around a collapsing eruption column (Walker, 1985).

Overlying the upper ash-flow tuff is a relatively thick (~18 m) sequence of fine-grained sandstone and mudstone deposits. These deposits consist of thin, horizontal beds, many of which are pumice rich. A thin (5-8 cm) bed of coarse sandstone (crystals of plagioclase and biotite) occurs near the middle of this sequence, and a meter-thick bed of boulder conglomerate occurs near the top of the sequence. This sequence of volcaniclastic deposits perhaps represents moat fill, related to subsidence after eruption of ash-flow tuffs.

Capping the entire sequence described above is a flow-banded rhyolite lava, similar to intrusive, vent-filling rhyolite. This member contains approximately 5 % phenocrysts of plagioclase and sanidine, commonly altered chalky white. It is the thickest extrusive member (typically as much as 30 to 50 m) of the Cuchillo Negro complex and is commonly found capping hills and forming bluffs.

Early Oligocene hiatus in volcanism in south-central New Mexico

After eruption of Kneeling Nun Tuff (and post-caldera-collapse volcanic units, such as Cuchillo Negro complex, Mimbres Peak Formation), a major hiatus in local volcanic activity occurred throughout a large portion of south-central New Mexico which includes the eastern half of Chloride mining district. This hiatus is expressed in the stratigraphic record by an absence of volcanic and volcaniclastic rocks in the interval between Kneeling Nun Tuff (34.9 Ma) and basaltic andesite of Poverty Creek (~29 Ma) over an area in excess of 2700 square kilometers (Fig. 26). This area is roughly centered upon present-day Sierra Cuchillo-Animas uplift. The relatively continuous occurrence and thickness of Kneeling Nun Tuff, plus lack of paleo-valleys cut into Kneeling Nun Tuff, suggests that this area existed as a stable high plateau during the early Oligocene volcanic hiatus. Presumedly, subsurface drainage of this paleo-plateau was facilitated by abundance of joint fractures in Kneeling Nun Tuff. Even today, the base of the Kneeling Nun Tuff is a major location of springs throughout this area.

The early Oligocene volcanic hiatus in south-central New Mexico can be envisioned as marking the end of a chemical evolution of igneous rocks in this area. Figure 27 shows major-element variation diagrams (data from Tables 2, 3, 4,

5, & 6) for rocks believed to have had origins in south-central New Mexico, and in the stratigraphic interval from Rubio Peak Formation thru Cuchillo Negro complex. This includes all units interpreted as having been erupted from Emory caldera, i.e. Kneeling Nun Tuff, tuff of Stone House Ranch, tuff of Rocque Ramos Canyon, and tuff of Victoria Tank. The two most prominant trends revealed by these diagrams are pronounced increase in silica content and decrease in CaO content through this time period. K2O content shows a slight, but distinct, overall increase with time, as does total alkali content; Na2O content decreases slightly.

Figure 26. Approximate area of the early Oligocene plateau capped by Kneeling Nun Tuff. In this area, Kneeling Nun Tuff is directly overlain by the basaltic andesite of Poverty Creek or correlative rocks.

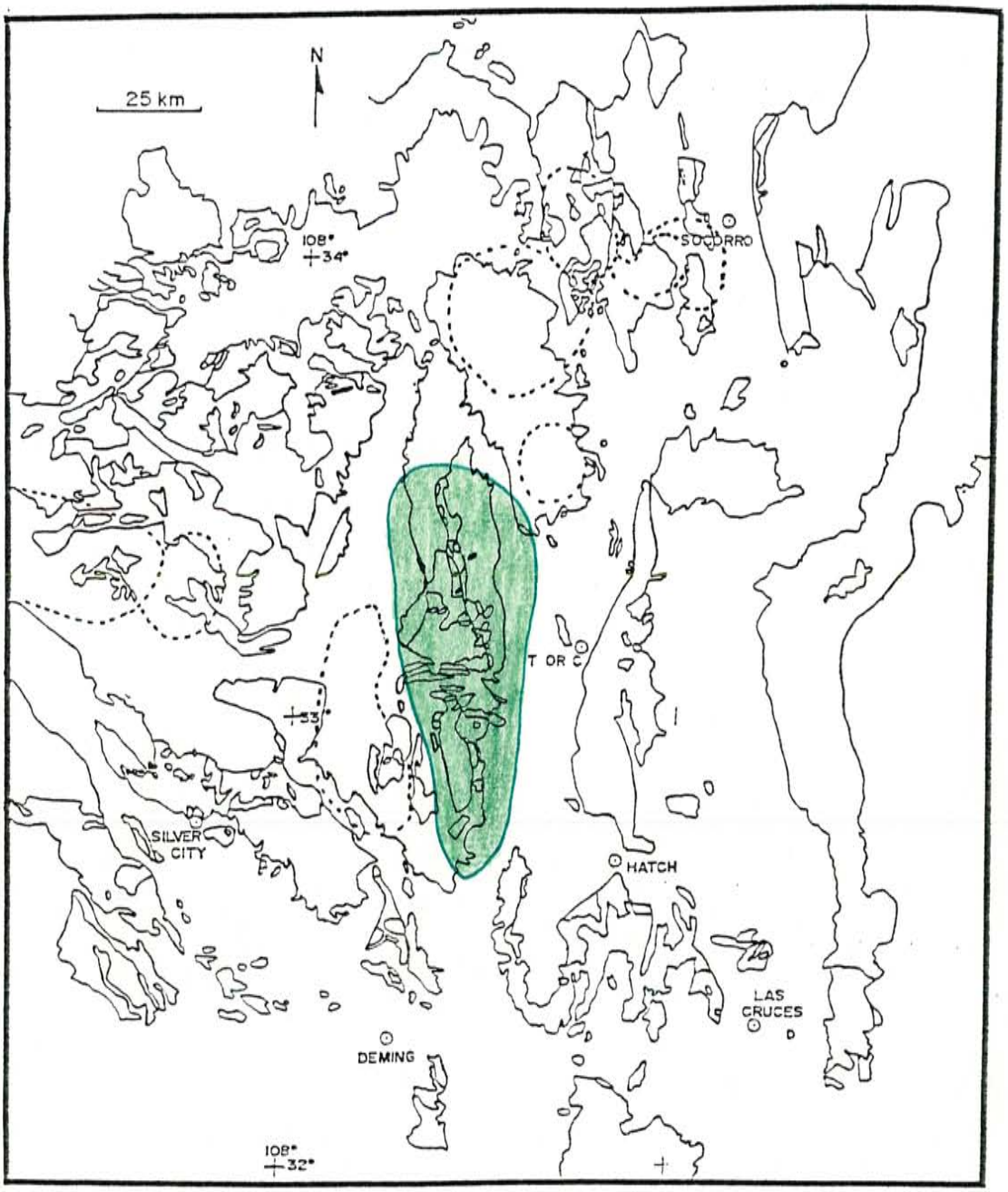
25 km
N
108°
34°
SOCORRO
T OR C
33°
SILVER CITY
HATCH
LAS CRUCES
DEMING
108°
32°

Figure 27. Major-element variation diagrams for volcanic rocks whose origin is believed to have been in the north-central Black Range, and in the stratigraphic interval from Rubio Peak Formation thru Cuchillo Negro Complex; data from Tables 2, 3, 5, & 6. (a) SiO2 vs. K2O + Na2O, (b) SiO2 vs. K2O, Na2O, CaO, Fe2O3.

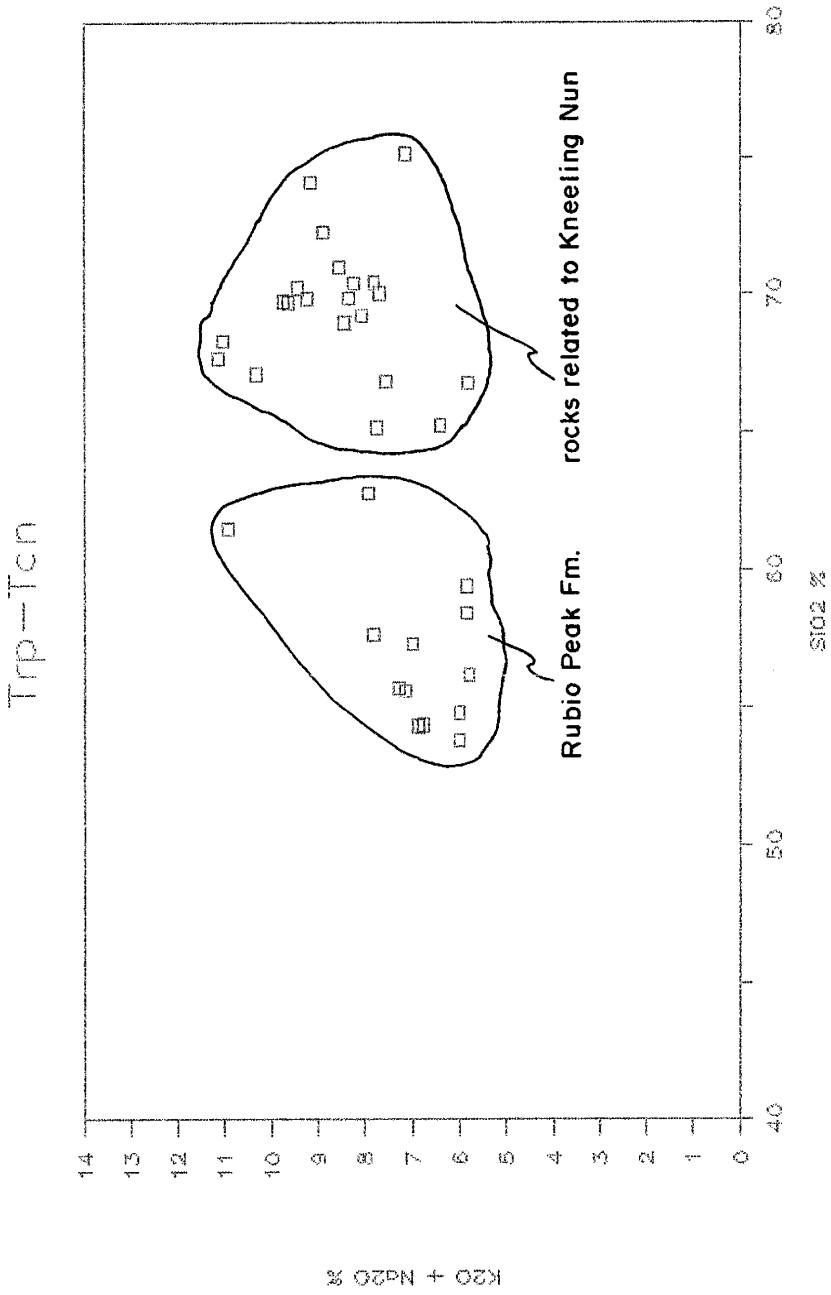
Trp—Tcn
rocks related to Kneeling Nun
Rubio Peak Fm.
K2O + Na2O %
SiO2 %
0
1
2
3
4
5
6
7
8
9
10
11
12
13
14
40
50
60
70
80

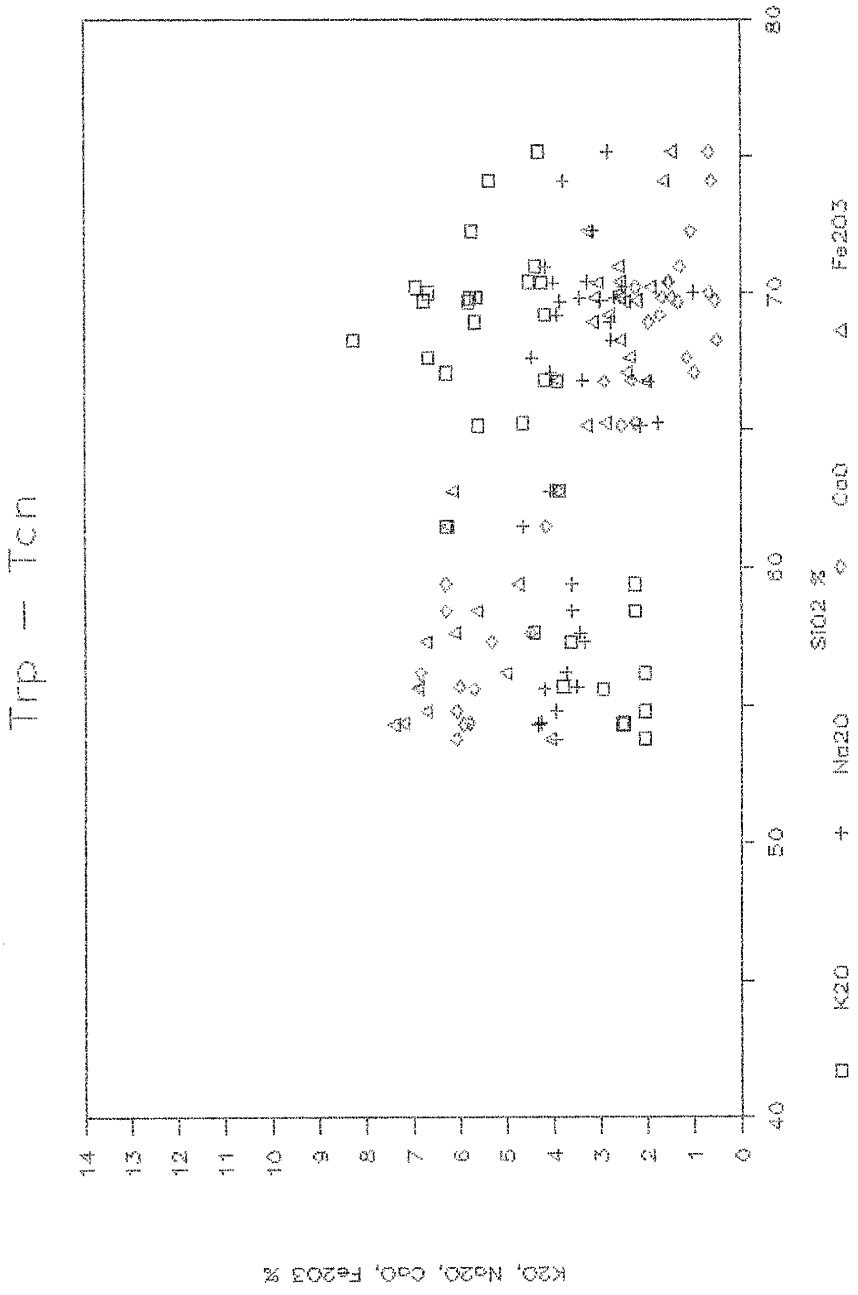
Trp — Tcn
K20, Na20, CaO, Fe2O3 %
SiO2 %
K20
Na20
CaO
Fe2O3

Stratigraphic interval between the Kneeling Nun Tuff and basaltic andesite of Poverty Creek: sandstone of Monument Park-Caballo Blanco Tuff-tuff of Koko Well

Along the Continental Divide in north-central Black Range, a sequence of intercalated volcaniclastic and volcanic rocks occur overlying Kneeling Nun Tuff and below basaltic andesite of Poverty Creek. Distinguishable units within this sequence include: sandstone of Monument Park, tuff of Koko Well, and Caballo Blanco Tuff. In relative positions, Caballo Blanco Tuff is stratigraphically above tuff of Koko Well, and always occurs interbedded within sandstone of Monument Park (Fig. 28); in some places, tuff of Koko Well lies directly upon Kneeling Nun Tuff, and in other places, it is separated by as much as 20 m of sandstone of Monument Park (Fig. 29); at most localities, tuff of Koko Well lies directly beneath basaltic andesite of Poverty Creek. Figure 30 is a schematic north-south cross-section showing relationships between units of this stratigraphic interval. All these units are relatively conformable in attitude with Kneeling Nun Tuff and appear to represent deposition in broad depressions along the margin of the paleo-plateau described in previous section. The upper contact with basaltic andesite of Poverty Creek is a low-amplitude angular unconformity.

Figure 28. Stratigraphic section between Kneeling Nun Tuff and basaltic andesite of Poverty Creek, near type locality of sandstone of Monument Park, 33-19'-36" N, 107-50'30" W.

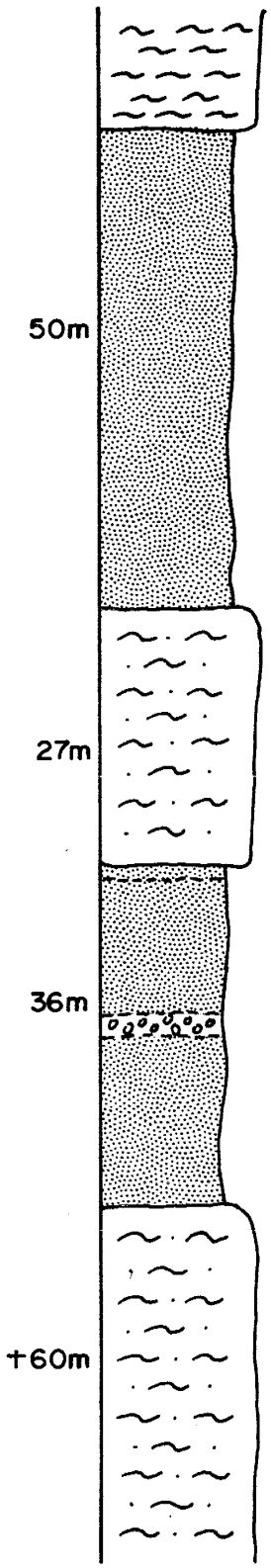

basaltic andesite of Poverty Creek

sandstone of Monument Park
fine- to medium-grained, feldspathic
1-2cm horizontal beds, sparse low-angle
cross beds

50m

Caballo Blanco Tuff
poorly welded, 15-20% phenocrysts of
euhedral quartz (>5mm), sanidine, plagioclase,
& brown biotite

27m

1m very quartz-rich sandstone

sandstone of Monument Park

36m

3-5m conglomerate, rounded pebbles & cobbles of
Kneeling Nun Tuff, minor Rubio Peak Form.

thinnly bedded, fine-to medium-grained
rounded & euhedral quartz, sanidine,
plagioclase, & biotite

+60m

Kneeling Nun Tuff

Figure 29. Stratigrapic section between the Kneeling Nun Tuff and basaltic andesite of Poverty Creek, south bank of Turkey Creek near Santana Place, center of sec. 19, T. 10 S., R. 9 W., Sawmill Peak quadrangle.

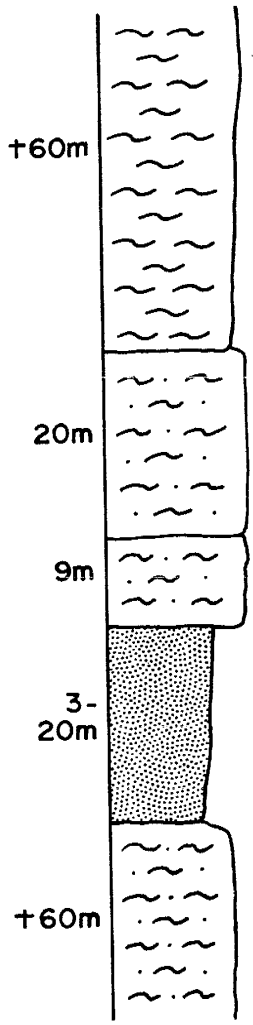

basaltic andesite of Poverty Creek
multiple flows of dark aphanitic lava

upper tuff of Koko Well
poorly welded, crystal-poor, pumice-rich

lower tuff of Koko Well
mod. to densely welded, mod. crystal-rich, 10% sanidine, plagioclase, biotite, & trace horblende

sandstone of Monument Park
well-sorted, fine-grained sandstone, rounded grains of quartz, sanidine, plagioclase, & biotite

Kneeling Nun Tuff

Figure 30. Schematic north-south cross-section for the stratigraphic interval between the Kneeling Nun Tuff and basaltic andesite of Poverty Creek, along the Continental Divide between Chloride mining district and Taylor Creek tin district. All units within this interval pinch out towards viewer (eastward), where the basaltic andesite of Poverty Creek rests directly upon Kneeling Nun Tuff.

S N

basaltic andesite of Poverty Creek

Kneeling Nun Tuff

← approximate distance of 20km →

Tcb-Caballo Blanco Tuff Tkw-tuffs of Koko Well

Tmps-sandstone of Monument Park

sandstone of Monument Park

The name sandstone of Monument Park was proposed by Woodard (1982) for volcaniclastic deposits that locally occur between Kneeling Nun Tuff and basaltic andesite of Poverty Creek. Type locality is southwest of Monument Park in SE1/4SE1/4 sec. 13, T. 11 S., R. 10 W. in Lookout Mountain quadrangle (Plate 2). This minor unit is limited in aerial extent to western half of Chloride mining district and east of Continental Divide. It pinches out rapidly both to north and south, but has a maximum thickness of approximately 200 m. In lithology, appearance, and stratigraphic position, this unit is identical to epiclastic rocks of North Seco Creek of Abitz (1989); a unit interpreted by him as moat deposits along eastern side of Emory caldera.

Sandstone of Monument Park consists of poorly indurated volcaniclastic sandstone, with minor purple siltstone beds, and local pebble-cobble conglomerate intervals. Sandstone beds are well-sorted, sparsely cross-bedded, and contain rounded to subrounded grains of quartz, sanidine, plagioclase, and minor biotite. Conglomerate intervals are dominated by clasts of Kneeling Nun Tuff with minor andesitic to basaltic andesite clasts. Woodard (1982) describes sandstones within this unit as microscopically consisting of approximately 17 % subrounded to rounded, equigranular quartz, 11 % sanidine, 20 % plagioclase

(An30-34), 1 % chlorite, 0.5 % opaque minerals, 50 % clay matrix, and with rare andesite and rhyolite fragments (up to 1.5 mm in diameter).

Caballo Blanco Tuff

In the southwestern quarter of Chloride mining district, Caballo Blanco Tuff of Elston (1957) is interbedded with sandstone of Monument Park (Fig. 20). This tuff has discontinuous outcrops in this area, with a maximum thickness of approximately 27 m. Outcrops of Caballo Blanco Tuff are more extensive and continuous immediately south of Chloride mining district, where it is found totally circling Emory caldera. Woodard (1982) referred to Caballo Blanco Tuff as Rhyolite Tuff Member of sandstone of Monument Park.

McIntosh (1989) gives an average 40Ar/39Ar age of 31.65 ± .06 for Caballo Blanco Tuff. This age indicates that the thin interval (~27 m) of sandstone of Monument Park occurring between Kneeling Nun Tuff and Caballo Blanco Tuff in western Chloride mining district represents approximately 3.2 million years of time.

Caballo Blanco Tuff in western Chloride mining district is a poorly to moderately welded, crystal-rich ash-flow tuff with 20-35 % phenocrysts of quartz, sanidine, plagioclase, and biotite. Quartz phenocrysts are both rounded and euhedral (doubly terminated), and as much as 5 mm in size. Minor amounts of red-colored, rhyolitic lithic fragments

occur in Caballo Blanco Tuff.

Tuffs of Koko Well

In the northern half of Chloride district, a thin interval of sandstone of Monument Park and two ash-flow tuffs, welded together, occur between Kneeling Nun Tuff and basaltic andesite of Poverty Creek (Fig. 29). An informal name of tuff of Koko Well was proposed by Eggleston (1987) for the ash-flow tuffs within this stratigraphic interval from exposures along NM-59 in SW1/4 sec. 6, R. 10 W., T. 10 S. at Koko Well. Tuffs of Koko Well crop out in a thin, five-mile-long strip, roughly centered on their type locality. Three, small outcrops of upper tuff of Koko Well occur in northernmost Winston quadrangle (Plate 1).

Upper tuff of Koko Well is a massive, poorly welded, crystal-poor, pumice-rich ash-flow tuff. This unit contains approximately 5 % sanidine, 0.5-1 % plagioclase, and trace amounts of quartz and biotite. Maximum thickness for upper tuff of Koko Well is approximately 60 m; relatively thick outcrops commonly contain shallow habitation caves. Based on lithologic and stratigraphic similarities, upper tuff of Koko Well has been informally considered to be correlative to Rock House Canyon Tuff, a unit occurring extensively throughout the northern portion of Mogollon-Datil volcanic field. Support for this correlation was provided by McIntosh (1989) from paleomagnetic data and 40Ar/39Ar

dating. A mean 40Ar/39Ar age of 34.4 Ma is given for Rock House Canyon Tuff by McIntosh (1989). The correlation of upper tuff of Koko Well with Rock House Canyon Tuff provides one of the few stratigraphic ties between the northern and southern portions of Mogollon-Datil volcanic field.

Lower tuff of Koko Well is a moderately to densely welded, moderately crystal-rich ash-flow tuff. This unit contains approximately 6 % sanidine, 2-3 % plagioclase, 1 % biotite, and trace amounts of hornblende and pyroxene. Chemically, it is an alkali-rich rhyolite (Eggleston, 1987). Maximum thickness of the lower tuff of Koko Well is approximately 15 m. This unit has no known correlative units elsewhere in Mogollon-Datil volcanic field. It is similar in stratigraphic position and phenocryst content to tuff of Lebya Well of Ratte et al. (1989), but paleomagnetic data of McIntosh (1989) oppose their correlation. Stratigraphic position (and bracketed age restraints of 34.4 to 34.9 Ma) for lower tuff of Koko Well is also similar to that of ash-flow tuffs belonging to Mimbres Peak Formation (and Cuchillo Negro Negro complex, discussed in previous section). It seems quite possible that lower tuff of Koko Well is related to these post-Emory caldera volcanic units, although its dense welding and lack of quartz phenocrysts are anomalous.

basaltic andesite of Poverty Creek

Elston et al. (1973) and Coney (1976) gave the name basaltic andesite of Poverty Creek to the sequence of dark, aphanitic lava flows exposed in SW1/4 sec. 6, T. 10 S., R. 10 W., in northern portion of north-central Black Range. There, these rocks overlie upper tuff of Koko Well and are beneath a complex series of rhyolite ash-flow tuffs and rhyolite lavas. Basaltic andesite of Poverty Creek at its type locality consists of multiple greenish to dark-gray flows, typically with autobrecciated tops and massive cores. Flows are commonly separated by thin (a few-meters thick), green and red, fine-grained volcaniclastic sediments that contain andesitic detritus. The base of the sequence consists of aphyric, aphanitic basaltic andesite lavas that grade upward into more silicic rock types which characteristically are somewhat more porphyritic, with as much as 10 % phenocrysts of plagioclase, pyroxene, and rare biotite. Sparse xenoliths of quartz are also found in basaltic andesite of Poverty Creek. Conglomerate beds with rounded to angular pebbles and cobbles of Poverty Creek-like volcanic rocks are common at the top of the sequence. At its type locality, this unit is approximately 200 m thick.

Microscopically, basal Poverty Creek rocks are comprised of 90-95 % plagioclase microlites, from 0.2-0.5 mm in size, in a pilotaxitic groundmass. Rare phenocrysts of plagioclase (An 40-45) and pyroxene are also found in basal

rocks. Microscopically, rocks from the upper sequence vary from aphanitic to slightly porphyritic. The upper rocks locally contain 75-90 % plagioclase microlites, with 3-10 % plagioclase (An 35-40) phenocrysts, and with lesser pyroxene and biotite, in a pilotaxitic groundmass.

Basaltic andesite of Poverty Creek is part of a regionally widespread interval containing very similar rocks that all occur at the same stratigraphic interval. Basaltic andesite of Poverty Creek has been extended throughout the Sierra Cuchillo (unpublished mapping by R.W. Harrison, T.L. Eggleston, and G.R. Osburn), where it is identical to the lower andesite unit of Jahns et al. (1978); basaltic andesite of Poverty Creek is also correlative to the unnamed basaltic andesite of Mayer (1987) and Seager and Mayer (1988) in Salado Mountains. Other units that are believed to be correlative to basaltic andesite of Poverty Creek include: Razorback Formation of Elston (1957) in southern Black Range, Mimbres Valley, and Cobre Mountains; Alum Mountain Formation of Elston (1968), Elston et al. (1968, 1970), Ratte et al. (1972) along the western flank of the Black Range and in the Pinos Altos Mountains and Alum Mountain-Copperas Mountain area; T4ba map unit of Seager et al. (1982) in southern Black Range; most of Mimbres River-McKnight Mountain andesite of Ericksen et al. (1970) in south-central New Mexico; Houston Andesite of Ferguson (1927) and Rhodes (1976) in Mogollon area. Many of the above correlation were made previously by Elston et al.

(1973).

When all of the above formations are considered together, it is clear that they define a major volcanic interval, certainly worthy of group status. Figure 31 shows the approximate distribution of basaltic andesite of Poverty Creek and correlative units in south-central and southwestern New Mexico. These rocks essentially blanketed a large portion of the southern Mogollon-Datil volcanic field, thus forming an important time-stratigraphic interval.

Radiometric ages for this stratigraphic interval are few in number, but are consistantly in the range of 28 to 30 Ma. A K-Ar age of 28.3 $\pm$ 0.6 Ma is given by Woodard (1982) for basaltic andesite of Poverty Creek in western Chloride mining district. A K-Ar age of 28.8 $\pm$ 0.6 Ma was determined for basaltic andesite of Poverty Creek in a vent area occurring in Winston graben (center of sec. 2, T. 12 S., R. 8 W.). A 28.1 $\pm$ 0.6 Ma radiometic age is given for the T4ba unit in the Hillsboro area of the southern Black Range by Seager et al. (1982, 1984). Three K-Ar ages of 29.0 $\pm$ 1.0, 29.6 $\pm$ 1.0, and 29.3 $\pm$ 1.0 Ma are given for Alum Mountain Formation by Ratte et al. (1972). Age constraints provided by high-precision 40Ar/39Ar dating by McIntosh (1989) indicate that Poverty Creek and correlative units are slightly older than 29 Ma, as Tuff of Little Mineral Creek (29.1 Ma), tuff of Mudhole (29.11 Ma), Davis Canyon Tuff (29.0 Ma), and La Jencia Tuff (28.9 Ma) all overlie these

Figure 31. Approximate distribution of the basaltic andesite of Poverty Creek and correlative units in south-central and southwestern New Mexico.

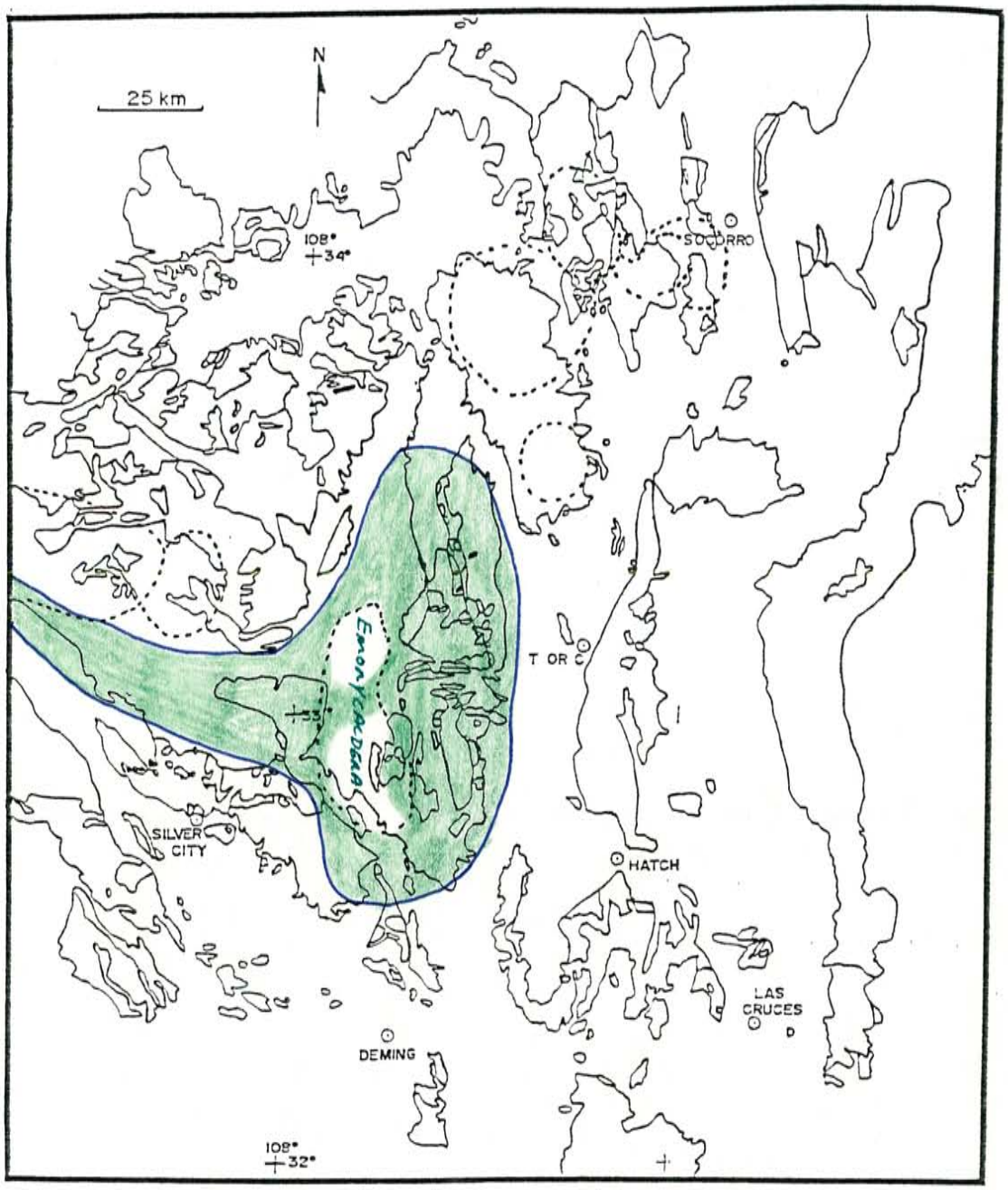
25 km
N
108°
34°
SOCORRO
T OR C
EMORY CALDERA
SILVER CITY
HATCH
LAS CRUCES
DEMING
108°
32°

rocks.

Numerous major-element chemical analyses have been determined for basaltic andesite of Poverty Creek and correlative units. Table 7 presents a tabulation of 33 analyses of these rocks from various contributors (first five for this report from north-central Black Range and eastern Sierra Cuchillo). These analyses indicate a relatively wide range in silica content, from ~53 to ~65 %. The few analyses that attempt to ascertain vertical zonation (Eggleston, 1987; and this report) suggest that there is an overall increase in silica content upward in the Poverty Creek section, coupled with a decrease in CaO content. A similar upsection zonation is noted in Alum Mountain Formation by Ratte et al. (1972, 1979), where youngest rocks obtain rhyolitic compositions.

Figure 32 shows variation diagrams for basaltic andesite of Poverty Creek and correlative units derived from Table 7. Under the chemical classification of Le Maitre (1984), the field name 'basaltic andesite' of Poverty Creek appears largely to be a misnomer, as rocks of this group have compositions not only of basaltic andesite, but also andesite, trachyandesite, and dacite (Fig. 32a). Poverty Creek and correlative units display a decrease in CaO, Fe2O3, MgO, and TiO2 contents and a slight increase in K2O content with increasing SiO2 content.

Although distinctly different in age, mineral content, and petrographic textures, rocks of basaltic andesite of

Table 7. Tabulation of major-element analyses for the basaltic andesite of Poverty Creek and correlative units. Strontium isotope analyses are also listed where available.

	1	2	3	4	5	6	7	8
SIO2	65.20	65.19	64.65	59.60	61.49	61.77	60.20	58.74
A1203	15.18	14.72	16.39	16.59	15.99	17.50	19.51	18.00
Fe203	4.32	4.15	4.74	6.55	6.27	5.63	4.90	6.79
MgO	2.34	2.54	1.03	3.24	2.19	.75	2.17	3.70
CaO	4.02	4.11	3.04	5.51	4.15	3.85	5.25	5.66
Na2O	3.96	3.63	3.97	3.75	4.65	4.30	3.51	3.91
K2O	3.06	2.44	3.83	2.20	3.23	3.09	2.25	1.95
TiO2	.64	.63	.79	1.15	.96	1.05	.73	.76
P2O5	.18	.18	.29	.38	.25	.53	.73	.33
MnO	.07	.01	.06	.06	.07	.01	.09	.09
LOI	1.02	1.82	1.75	1.38	1.35	CO2	.09	.05
SUM	99.99	100.05	99.40	100.61	100.60	100.30	99.34	99.98
87Sr/86Sr							0.7060	

1) POVERTY CREEK FORMATION, LAVA FROM MIDDLE OF SECTION ON CARRIZO PEAK, CENTER SEC. 2, T. 11 S., R. 7 W., THIS REPORT
2) POVERTY CREEK FORMATION, LAVA FROM UPPER SECTION ON CARRIZO PEAK, THIS REPORT
3) POVERTY CREEK FORMATION, LAVA FROM NORTHERN CHLORIDE MINING DISTRICT, SEC. 2, T. 10 S., R. 9 W., THIS REPORT
4) POVERTY CREEK FORMATION, INTRUSIVE FROM WINSTON GRABEN, NW1/4 SEC. 2, T. 12 S., R. 8 W., THIS REPORT
5) POVERTY CREEK FORMATION, LAVA FROM WINSTON GRABEN, SEC. 2, T. 12 S., R. 8 W., THIS REPORT
6) POVERTY CREEK FORMATION, FROM UPPER SECTION IN TAYLOR CREEK AREA; EGGLESTON, 1987
7) POVERTY CREEK FORMATION, LAVA IN SOUTHWESTERN CHLORIDE MINING DISTRICT; ABITZ, 1984
8) POVERTY CREEK FORMATION, LAVA FROM S. BLACK RANGE; ERICKSEN & OTHERS, 1970

	9	10	11	12	13	14	15	16
SiO2	58.21	57.29	61.63	59.00	57.87	58.80	58.98	60.95
Al2O3	16.98	18.28	15.18	15.00	17.50	15.20	16.60	17.65
Fe2O3	7.57	7.18	6.87	5.50	6.79	6.79	6.45	6.32
MgO	3.58	3.80	1.85	3.00	3.66	2.82	3.33	2.15
CaO	5.73	5.95	3.90	4.80	5.66	5.31	5.60	4.72
Na2O	3.68	3.59	3.90	4.39	3.20	3.86	3.56	3.80
K2O	1.94	2.05	4.31	2.56	2.69	3.09	2.73	2.98
TiO2	1.74	1.23	1.44	1.06	1.24	1.21	1.08	1.00
P2O5	.42	.43	.81	.40	.42	.45	.38	.37
MnO	.09	.10	.12	.03	.09	.08	.08	.06
CO2	.05	.08						
SUM	99.99	101.01	100.01	95.74	99.12	97.61	98.79	100.00
87Sr/86Sr					.7056	.7059	.7060	

9) POVERTY CREEK FORMATION, LAVA FROM S. BLACK RANGE; ERICKSEN & OTHERS, 1970
10) POVERTY CREEK FORMATION, LAVA FROM S. BLACK RANGE; ERICKSEN & OTHERS, 1970
11) POVERTY CREEK FORMATION, LAVA FROM S. BLACK RANGE; ERICKSEN & OTHERS, 1970, #262
12) POVERTY CREEK FORMATION, LAVA FROM N. BLACK RANGE; BORNHORST, 1980, #329
13) RAZORBACK FORMATION, LAVA FROM N. BLACK RANGE; BORNHORST, 1980, #308
14) RAZORBACK FORMATION, LAVA FROM N. BLACK RANGE; BORNHORST, 1980, #309
15) RAZORBACK FORMATION, LAVA FROM N. BLACK RANGE; BORNHORST, 1980, #310
16) McKNIGHT MT. FORMATION; LAVA FROM McKNIGHT MT., ERICKSEN & OTHERS, 1970, #498

	17	18	19	20	21	22	23	24
SiO2	59.02	63.66	53.96	56.93	52.23	52.31	54.63	54.77
Al2O3	17.21	17.31	16.86	16.55	16.34	16.36	17.43	16.85
Fe2O3	6.77	4.66	7.70	7.21	9.04	8.91	8.31	8.00
MgO	3.69	2.16	4.00	1.57	6.29	5.83	3.24	3.99
CaO	5.64	4.74	7.45	4.91	8.44	8.51	7.23	7.40
Na2O	3.69	3.81	4.11	4.07	3.50	3.56	4.63	3.93
K2O	2.56	2.58	1.99	2.79	1.32	1.33	2.00	1.94
TiO2	.98	.77	1.15	1.00	1.39	1.87	1.49	2.15
P2O5	.33	.24	.55	.51	.25	.26	.58	.58
MnO	.11	.08	.07	.14	.14	.13	.06	.08
LOI	2.15	3.94	1.39	1.87	1.49	2.15		
SUM	100.00	100.01	99.99	99.62	100.05	100.21	100.78	100.56

17) McKNIGHT MT. FORMATION; ERICKSEN & OTHERS, 1970, #488
18) McKNIGHT MT. FORMATION; ERICKSEN & OTHERS, 1970, #485
19) POVERTY CREEK FORMATION, TAYLOR CREEK AREA,
EGGLESTON, 1987
20) "
21) "
22) "
23) "
24) "

	25	26	27	28	29	30	31
SiO2	56.54	53.22	58.13	59.40	61.36	55.46	59.74
Al2O3	18.18	17.34	15.98	15.94	16.42	16.57	16.76
Fe2O3	8.65	8.20	7.01	5.35	5.05	7.57	5.89
MgO	.90	3.47	3.79	3.56	2.43	5.56	2.79
CaO	5.42	8.20	6.00	5.13	4.97	7.07	4.83
Na2O	3.90	3.05	3.53	4.25	3.69	3.36	3.78
K2O	2.36	1.90	2.61	2.33	2.46	1.51	3.32
TiO2	1.90	2.59	.99	.93	.79	.95	1.24
P2O5	.58	.44	.45	.33	.20	.22	.63
MnO	.49	.11	.10	.07	.08	.11	.06
LOI	1.90	2.59					
SUM	100.17	99.69	100.06	97.29	97.45	98.38	99.04
87Sr/86Sr				.70521		.70518	

25) POVERTY CREEK FORMATION, TAYLOR CREEK AREA, EGGLESTON, 1987
26) "
27) RAZORBACK FORMATION, ELSTON, 1957
28) POVERTY CREEK FORMATION INTRUSIVE, 33-08'-57"N,107-46'-19"W, ABITZ, 1989
29) POVERTY CREEK FORMATION, LAVA, 33-04'-36"N, 107-46'-48"W, ABITZ, 1989
30) POVERTY CREEK FORMATION, LAVA, 33-12'-36"N, 107-45'-07"W, ABITZ, 1989
31) POVERTY CREEK FORMATION, LAVA, 33-11'-26"N, 107-45'-44"W, ABITZ, 1989

	32	33
SiO2	58.00	61.76
Al2O3	16.28	16.78
Fe2O3	5.77	4.44
MgO	3.43	2.20
CaO	5.06	4.83
Na2O	3.86	3.71
K2O	2.97	2.89
TiO2	.97	.72
P2O5	.45	.24
MnO	.08	.05
SUM	96.87	97.62

32) POVERTY CREEK FORMATION, LAVA, 33-11'-35"N, 107-45'-40"W, ABITZ, 1989
33) POVERTY CREEK FORMATION, LAVA, 33-11'-32"N, 107-45'-37"W, ABITZ, 1989

Figure 32. Major-element variation diagrams for the basaltic andesite of Poverty Creek and correlative units in south-central and southwestern New Mexico: (a) SiO_2 vs. K_2O + Na_2O; (b) SiO_2 vs. K_2O, Na_2O, CaO, Fe_2O_3, Al_2O_3.

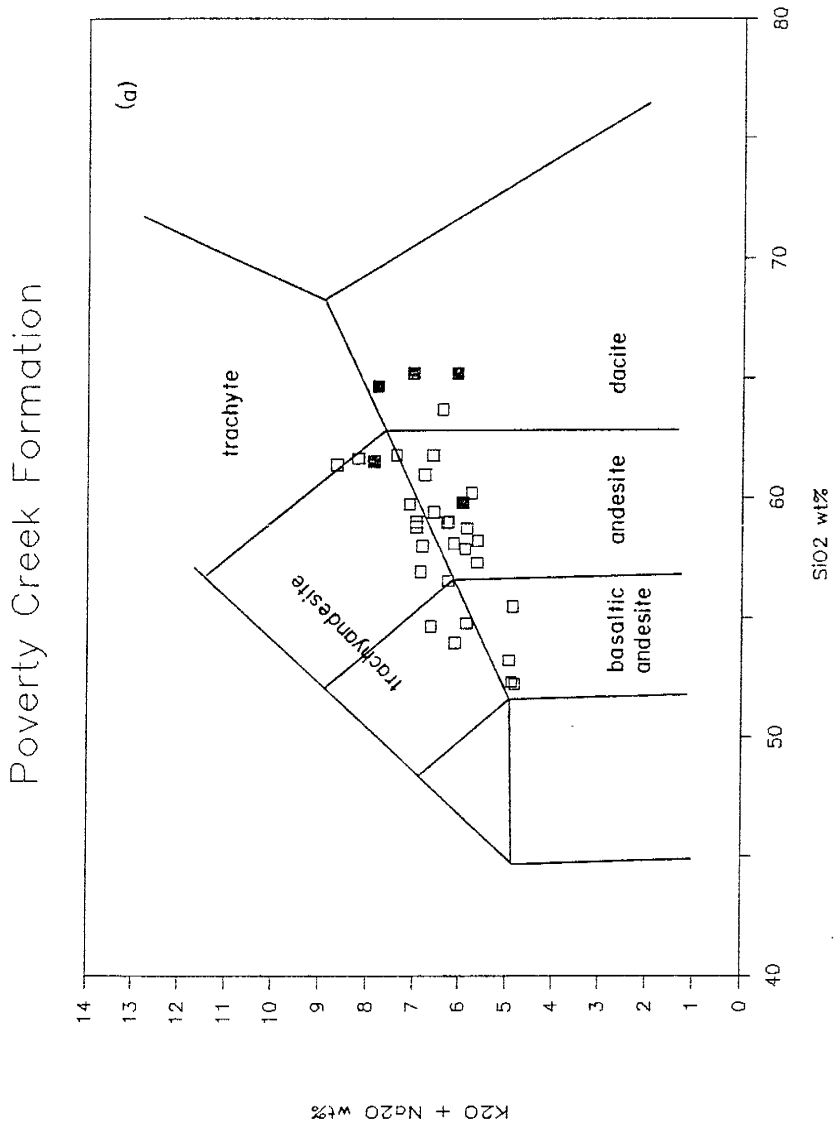
Poverty Creek Formation
(a)
trachyte
dacite
trachyandesite
andesite
basaltic andesite
K2O + Na2O wt%
SiO2 wt%
0
1
2
3
4
5
6
7
8
9
10
11
12
13
14
40
50
60
70
80

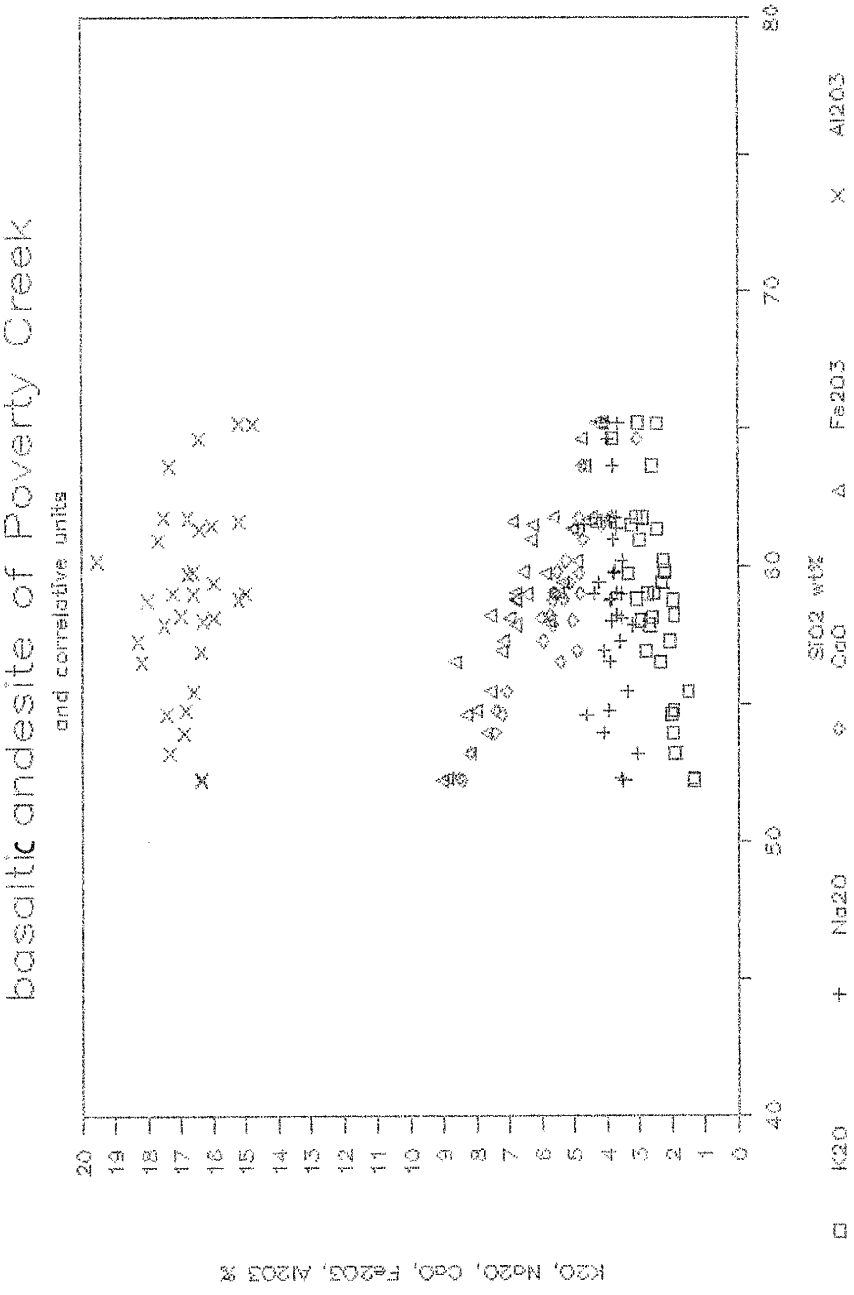
basaltic andesite of Poverty Creek
and correlative units
K2O, Na2O, CaO, Fe2O3, Al2O3 %
SiO2 wt%
K20
Na20
CaO
Fe2O3
Al2O3

Poverty Creek and correlative units are extremely similar in major-element composition to rocks of Rubio Peak Formation (compare Figs. 32 and 13). The only apparent differences are that Poverty Creek group has slightly higher Fe2O3 contents and higher silica end members.

Data from Abitz (1989) indicates that chemical similarities between rocks of Poverty Creek group and Rubio Peak Formation are also true for trace-element compositions, with the possible exception of zirconium; his values for rocks of Rubio Peak Formation are generally lower in Zr content than rocks of Poverty Creek Formation (possibly related to different iron contents ?). Based on this Zr difference and TiO2 vs. Zr variation plot of Pearce and Norry (1979), Abitz (1989) speculated that rocks of Rubio Peak Formation have volcanic arc affinities, but rocks of Poverty Creek section are transitional from volcanic arc to within-plate affinities. However, when geochemical data of Eggleston (1987) for basaltic andesite of Poverty Creek is plotted on TiO2 vs. Zr diagram, all samples fall within volcanic arc field of Pearce and Norry (9179), and all Poverty Creek samples are similar in Zr values to those of Rubio Peak Formation.

Perhaps the only chemical discriminant between rocks of Poverty Creek group and those of Rubio Peak Formation is in their respective strontium isotope compositions, although there is also some overlap in these values. Data from Stinnett and Stueber (1976), Bornhorst (1980), and Abitz

(1989) indicate that initial 87Sr/86Sr values for basaltic andesite of Poverty Creek and correlative units range from .7051 to.7067, while values for Rubio Peak Formation range from .7060 to.7077. Both sets of values are within ranges reported for island-arc volcanics and continental mafic rocks (Faure and Powell, 1972). It seems generally accepted that the slightly higher initial 87Sr/86Sr values determined for rocks of Rubio Peak Formation are indicative of slightly more differentiation or of more crustal involvment in their genesis magmas.

Source areas for basaltic andesite of Poverty Creek and correlative units were numerous and widespread throughout the area delineated in Figure 31. Most vents appear to have had the form of dikes and small flow-dome complexes. In north-central Black Range, there are many dikes and plug-shaped intrusives that are believed to have been feeders for basaltic andesite of Poverty Creek. However, it is difficult to distinguish between Poverty Creek and younger intermediate intrusives of similar appearance (Bearwallow Formation) in the field, especially if the full extent of cross-cutting relationships is no longer preserved due to erosion. The only way to clearly confirm the ages of these intermediate intrusive bodies, without radiometric age dating, lies in the ability to physically connect intrusive and extrusive phases. In most cases, this is not possible.

Two vents, where this is possible, are recognized in north-central Black Range. One is located in sec. 33, T. 10

S., R. 9 W. and sec. 4, T. 11 S. R. 9 W. (Sawmill Peak quadrangle, Plate 3), where a dike (90-120-m wide) that is intrusive into Kneeling Nun Tuff can be traced into outflow lava deposits that overlie sandstone of Monument Park and Kneeling Nun Tuff. This dike has a crescent shape, concave towards the northeast, with arms striking north-south and northwest. A second area where intrusive basaltic andesite of Poverty Creek can be physically traced into outflow lavas occurs in sec. 2, T. 12 S., R. 8 W. (Winston quadrangle, Plate 1). There, a flow-dome complex is well exposed by Chloride Creek drainage, with volcanic rocks extruding onto a paleo-surface of Kneeling Nun Tuff. These are the rocks dated by C.E. Chapin at 28.8 ± 0.6 Ma. Also in this area, an 800-m-long dike of basaltic andesite of Poverty Creek radiates away from the flow-dome complex on a strike of S45W.

Figure 33 is a compass-rose diagram for intermediate dikes believed to be feeders for lava flows of basaltic andesite of Poverty Creek in north-central Black Range. Unfortunately, most of these dikes do not have relative age constraints and, therefore, some of them could be younger than Poverty Creek age.

Eruption of basaltic andesite of Poverty Creek throughout south-central New Mexico marks the end of a 5-6 Ma hiatus in volcanic activity in this area. It also marks the beginning of a relatively brief, but very extensive and voluminous, volcanic episode in early Oligiocene.

Figure 33. Compass-rose diagram for approximately 3.9 km of aphanitic, intermediate dike orientations believed to be feeders for the basaltic andesite of Poverty Creek in north-central Black Range. Due to lack of age restraints, some of these dikes could be feeders for younger volcanic rocks, i.e. Bearwallow Formation.

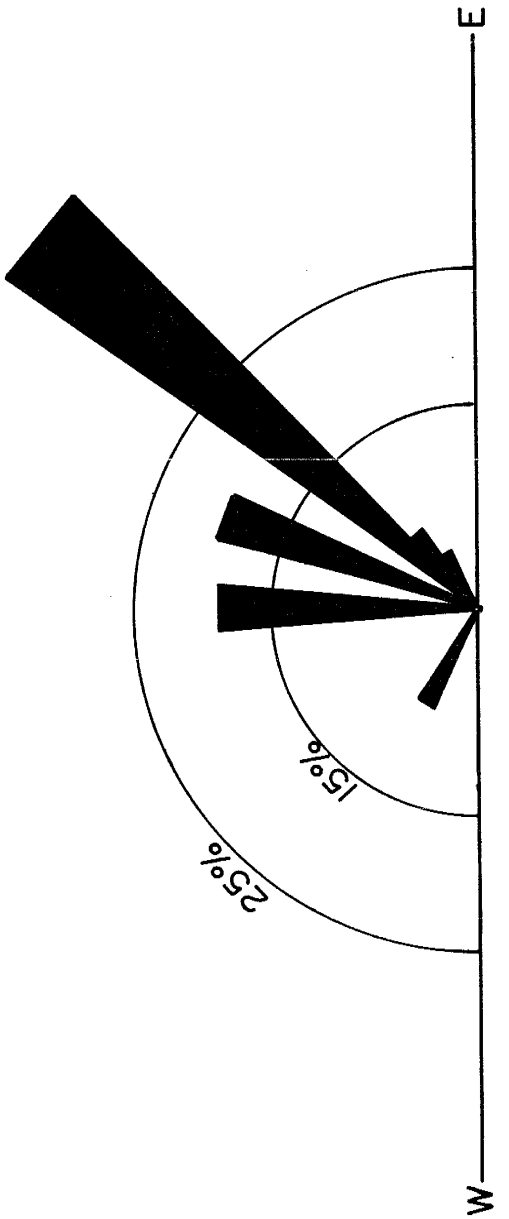
E
W
15%
25%

Intermediate rocks of this period have recently been referred to as the Southern Cordilleran basaltic andesite suite (SCORBA) by Cameron et al. (1989). In southern New Mexico, these rocks generally have been regarded as the product of initial phases of extension related to Rio Grande rifting (Chapin and Seager, 1975; Seager and Morgan, 1979; Elston and Bornhorst, 1979; Seager et al., 1984). The fact that basaltic andesite of Poverty Creek and correlative units are blanket-like in occurrence and are not interfingered with basin-related volcaniclastic rocks (Santa Fe and Gila Groups) in south-central New Mexico indicates that major faulting with formation of significant uplifts and basins postdates eruption of basaltic andesite of Poverty Creek. As discussed in the following chapter on Cenozoic structure of Chloride mining district, it is interpreted that basaltic andesite of Poverty Creek was erupted during a time when horizontal stresses were essentially equal in all directions and subordinate to vertical stress. Under such a regime, emplacement of dikes was controlled primarily by pre-existing structures.

Late Oligocene (29-28 Ma) volcanism

In the roughly one-million-year period following eruption of basaltic andesite of Poverty Creek and correlative units, voluminous and widespread silicic volcanism occurred throughout south-central New Mexico. In contrast to northern and western portions of Mogollon-Datil volcanic field where volcanism during this period took the form of large, caldera-forming volcanic eruptions with extensive, low-aspect-ratio ash-flow tuff sheets, 29-28 Ma volcanism in south-central New Mexico consisted of numerous rhyolitic flow-dome complexes with associated high-aspect-ratio ash-flow tuffs. Figure 34 lists the sequence of rhyolite flow-domes and ash-flow tuffs of this time period recognized in north-central Black Range, and shows their stratigraphic and age relationships. Distal facies of two regional ash-flow tuff sheets, Vicks Peak Tuff of Deal and Rhodes (1976) and La Jencia Tuff of Osburn and Chapin (1983), are intercalated within the sequence of local ignimbrites and lava flows in north-central Black Range.

This sequence of units in the north-central Black Range is part of a major north-south belt of non-caldera-related silicic volcanism that covered more than 5,500 sq km in the center of the Mogollon-Datil volcanic field during late Oligocene (Fig. 35). In the Black Range and Sierra Cuchillo alone, these rocks have an approximate volume of more than

Figure 34. Stratigraphic and age relationships between late Oligiocene rhyolite flow-domes and ash-flow tuffs in north-central Black Range, New Mexico.

Flows & Domes	Ash-flow tuffs	Ages Ma	
	Bloodgood Canyon Tuff	28.1	40Ar/39Ar
	tuff of Garcia Camp	28.1	40Ar/39Ar
Taylor Cr. Rhyolite	Taylor Cr. tuffs	28.1	"
Rhy. of Franks Mt.		28.4 ±1.2	K-Ar
	Vicks Peak Tuff	28.6	40Ar/39Ar
	tuff of Diamond Cr.	28.7	"
	tuff of Lookout Mt.		
	& tuff of Stiver Canyon		
	La Jencia Tuff	28.9	"
Rhy. of Dolan Peak	tuff of Straight Gulch		
	tuff of Kline Mt.		
Rhy. of Sawmill Pk.			
Moccasin John Rhy.	tuff of Little Min. Cr.	29.1	"
	& tuff of Mud Hole	29.11	"

40Ar/39Ar dates from McIntosh (1989); K-Ar date on Rhyolite of Franks Mountain from Eggleston (1987).

Figure 35. Approximate distribution of late Oligocene non-caldera-related silicic volcanism in south-central New Mexico and adjoining areas.

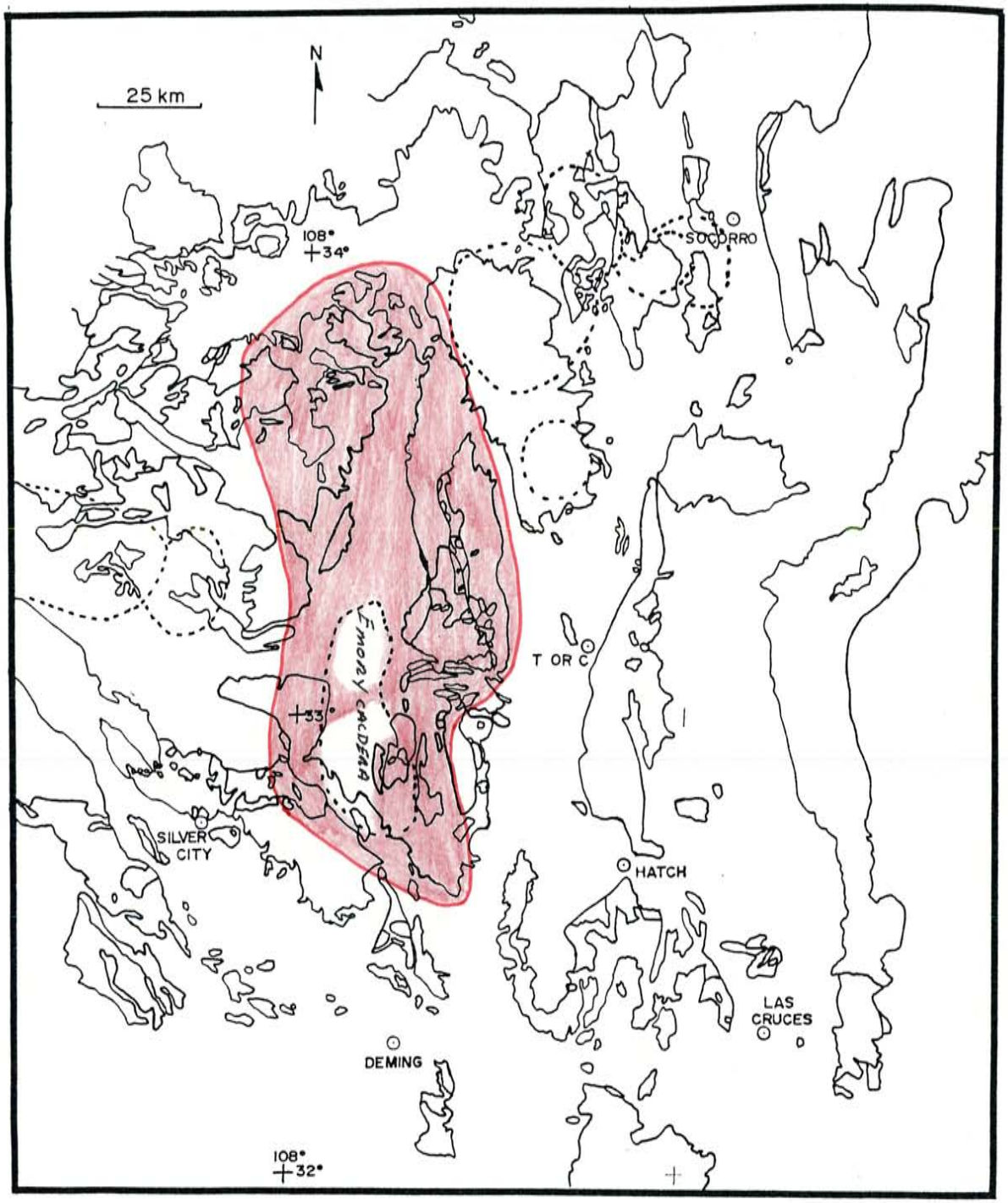
25 km
N
108°
+34°
SOCORRO
T OR C
+33
EMORY CALDERA
SILVER CITY
HATCH
LAS CRUCES
DEMING
108°
+32°

4,000 cubic km.

It was proposed by Harrison (1986, 1988) that a regional hydrothermal event related to emplacement and eruption of rhyolitic magmas during this time period was responsible for epithermal base- and precious-metal mineralization of Chloride mining district. Plate 5 shows distribution of late Oligocene rhyolite intrusives, epithermal vein systems, and hydrothermal alteration in north-central Black Range.

High-precision 40Ar/39Ar age dating by McIntosh (1989) indicates that units in south-central New Mexico were erupted rapidly during a time period that extended from about 29.1 to 28.1 Ma. All units in this area are rhyolite to high-silica rhyolite in composition. In general, there is an overall increase in phenocryst content with time for these units.

tuff of Mud Hole

Tuff of Mud Hole is an informal name given by Eggleston and Harrison (in review) for a minor, poorly welded, crystal-poor ash-flow tuff exposed immediately north of Mud Hole in sec. 11, T. 10 S., R. 10 W., Sawmill Peak quadrangle (Plate 3). At this locality, tuff of Mud Hole directly overlies basaltic andesite of Poverty Creek, is below Rhyolite of Sawmill Peak, and has a thickness of approximately 40 m. This unit contains phenocrysts of sanidine (~2%), quartz (~1%), and trace amounts of plagioclase and biotite in a vitroclastic groundmass. As much as 5 % lithic fragments (1-2 cm in diameter) of aphanitic, flow-banded rhyolite (and andesite ?) lavas occur within tuff of Mud Hole. Mapping by Eggleston (1987) included tuff of Mud Hole with tuff of Stiver Canyon, but he discussed the possibility that these were two different units. It is now recognized that tuff of Mud Hole is probably correlative to tuff of Little Mineral Creek. Locally tuff of Mud Hole contains a basal interval of conglomerate, sandstone, and mudstone (Eggleston & Norman, 1983).

Tuff of Mud Hole is chemically a rhyolite with a K2O content approximately twice Na2O content which, in turn, is approximately two to three times CaO content (Table 8 & Fig. 36). A 40Ar/39Ar age of 29.11 by McIntosh (1989) indicates that tuff of Mud Hole is the oldest ash-flow tuff unit of

Table 8. Major-element analyses for the tuff of Mud Hole.

	1	2	3	4	5	6	7
SiO2	70.87	75.17	75.33	75.40	76.47	77.06	77.12
Al2O3	13.71	11.62	12.07	11.96	11.93	12.07	11.32
Fe2O3	1.84	1.08	1.24	1.10	1.24	1.08	1.29
MgO	.44	.77	.22	.28	.31	.43	.14
CaO	.90	.53	.27	.38	.34	.30	.19
Na2O	3.04	3.57	2.65	2.85	2.35	3.15	.18
K2O	5.83	5.63	6.02	5.58	5.25	5.28	8.09
TiO2	.27	.15	.17	.18	.18	.16	.17
P2O5	.03	.03	.02	.03	.03	.01	.01
MnO	.07	.06	.03	.04	.04	.04	.03
LOI	3.88	2.18	1.32	1.26	2.02	1.10	1.72
Total	100.88	100.79	99.58	99.04	100.19	100.68	100.26

1) Tuff of Mud Hole, sec. 11, T. 10 S., R. 10 W., this report.
2) Tuff of Mud Hole, sec. 2, T. 10 S., R. 10 W., Eggleston (1987).
3) Tuff of Mud Hole, sec. 2, T. 10 S., R. 10 W., Eggleston (1987).
4) Tuff of Mud Hole, sec. 1, T. 10 S., R. 10 W., Eggleston (1987).
5) Tuff of Mud Hole, sec. 2, T. 10 S., R. 10 W., Eggleston (1987).
6) Tuff of Mud Hole, sec. 2, T. 10 S., R. 10 W., Eggleston (1987).
7) Tuff of Mud Hole, from upper Poverty Creek, sec. 10, T. 10 S. R. 10 W., Eggleston (1987).

	8	9	10	11	12	13	14
SiO2	77.28	77.50	77.55	77.68	77.70	77.94	78.14
Al2O3	11.37	10.80	10.97	11.39	9.87	10.72	10.72
Fe2O3	.99	.98	1.03	.97	.92	.98	.87
MgO	.32	.62	.45	.38	.32	.21	.29
CaO	.36	.37	.32	.29	.40	.32	.23
Na2O	2.22	2.06	1.55	2.65	1.69	1.97	2.24
K2O	4.98	5.90	5.54	5.00	4.03	4.60	5.42
TiO2	.15	.12	.13	.13	.15	.13	.12
P2O5	.05	.02	.01	.01	.02	.09	.01
MnO	.02	.02	.13	.03	.03	.03	.03
LOI	1.86	1.52	1.86	1.40	2.53	2.34	1.27
Total	99.60	99.91	99.54	99.93	99.64	99.33	99.59

8) Tuff of Mud Hole, sec. 2, T. 10 S. R. 10 W., Eggleston (1987).
9) Tuff of Mud Hole, sec. 10, T. 10 S., R. 10 W., Eggleston (1987).
10) Tuff of Mud Hole, sec. 11, T. 10 S., R. 10 W., Eggleston (1987).
11) Tuff of Mud Hole, sec. 2, T. 10 S., R. 10 W., Eggleston (1987).
12) Tuff of Mud Hole, sec. 10, T. 10 S., R. 10 W., Eggleston (1987).
13) Tuff Of Mud Hole, sec. 2, T. 10 S., R. 10 W., Eggleston (1987).
14) Tuff of Mud Hole, sec. 11, T. 10 S., R. 10 W., Eggleston (1987).

Figure 36. Major-element variation diagrams for tuff of Mud Hole.

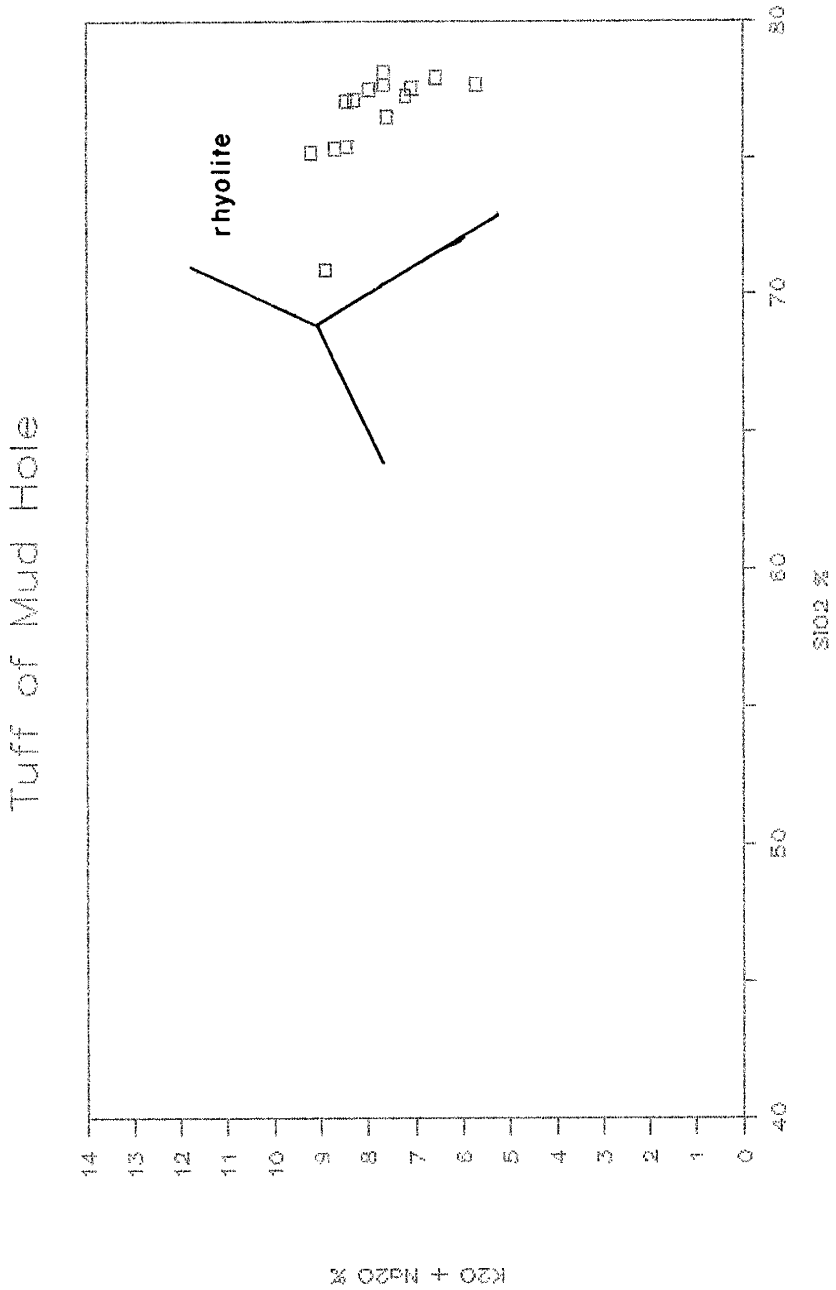
Tuff of Mud Hole
rhyolite
K2O + Na2O %
SiO2 %
0
1
2
3
4
5
6
7
8
9
10
11
12
13
14
40
50
60
70
80

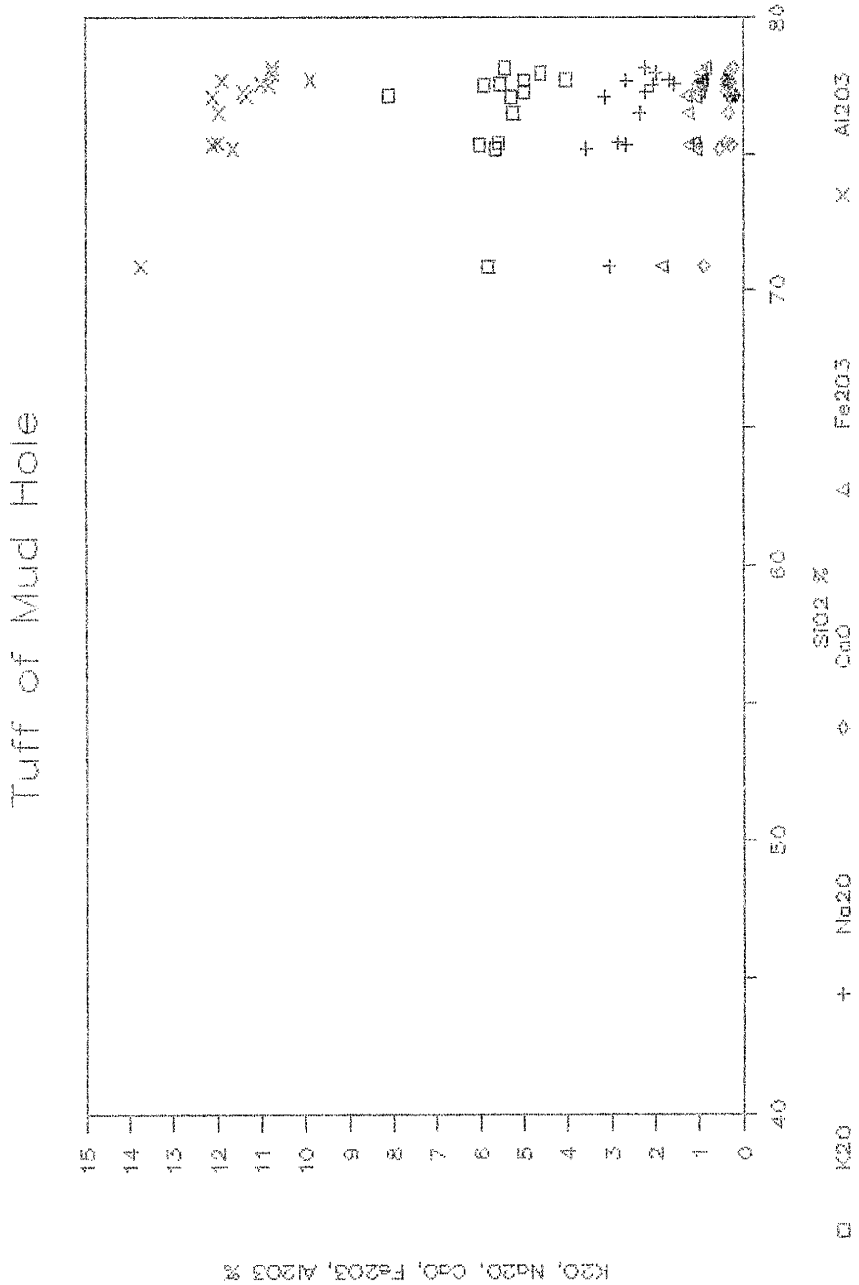
Tuff of Mud Hole
K2O, Na2O, CaO, Fe2O3, Al2O3 %
SiO2 %
K2O
Na2O
CaO
Fe2O3
Al2O3
0
1
2
3
4
5
6
7
8
9
10
11
12
13
14
15
40
50
60
70
80

this time period. This age is very close to that obtained for the tuff of Little Mineral Creek (see next section); and unfortunately, there are no known exposures that reveal the relative relationships between these two tuffs.

Tuff of Little Mineral Creek

The name rhyolite of Little Mineral Creek was proposed by Woodard (1982) for "rhyolite flows, intrusions, and pyroclastic rocks that intrude and overlie basaltic andesite of Poverty Creek and are overlain by tuff of Stiver Canyon" in the Lookout Mountain area, western Chloride mining district. Pyroclastics rocks of this unit were segregated from flows and intrusives by Harrison (1986) and given the names tuff of Little Mineral Creek and Moccasin John Rhyolite, respectively. Type locality for tuff of Little Mineral Creek is in SE1/4 sec. 15, T. 11 S., R. 9 W., along Little Mineral Creek. There, this unit directly overlies basaltic andesite of Poverty Creek and is below Moccasin John Rhyolite. McIntosh (1989) has obtained a 40Ar/39Ar age of 29.10 Ma from a sample of the tuff of Little Mineral Creek collected near its type locality.

Tuff of Little Mineral Creek crops out extensively throughout the southern and western portions of Chloride mining district, southern Winston graben, and southern portions of Sierra Cuchillo. Excellent exposures occur along the Continental Divide, south of Lookout Mountain.

Generally, this tuff forms prominant cliffs and bluffs, and has a maximun thickness of approximately 125 m.

Tuff of Little Mineral Creek is a poorly welded, lithic-rich, pumice-rich, crystal-poor ash-flow tuff. Red and gray, angular, aphanitic flow-banded rhyolite lithics make up 10-50% of the tuff of Little Mineral Creek and range in diameter to several centimeters. Sparse (1-4 %) broken crystals of quartz and sanidine with rare biotite occur in a highly pumiceous matrix. Intervals of fluvial reworking and air-fall deposits are common in this unit. Zeolitic alteration of volcanic glass to clinoptilolite (and other zeolite minerals) is locally pervasive in outcrops of tuff of Little Mineral Creek that occur in the southern portion of the Winston graben (Bowie & Barker, 1986).

Microscopically, tuff of Little Mineral Creek is composed of partly devitrified glass and pumice, with common axiolitic textures. Fragments of angular, aphanitic, flow-banded rhyolite lava are very abundant; broken quartz, sanidine, and biotite phenocrysts, from 1-2 mm in size, are rare.

Chemically, tuff of Little Mineral Creek is classified as a rhyolite (-dacite), with silica contents from 69.70 to 75.52 %, and total alkalis from 5.67 to 9.05 %. Table 9 lists five major-element analyses for this unit; Figure 37 shows variation diagrams. Note that the single dacite analysis has a very low total, probably indicative of alteration.

Table 9. Major-element analyses for tuff of Little Mineral Creek and Moccasin John Rhyolite.

	1	2	3	4	5	6	7	8
SiO2	75.52	69.70	71.90	73.67	72.98	73.16	77.63	73.52
Al2O3	11.70	13.15	13.09	12.65	13.55	13.25	12.10	12.62
Fe2O3	1.03	1.68	1.20	1.34	1.78	1.76	1.09	1.31
MgO	2.17	.79	.10	.57	.53	.56	1.37	.29
CaO	1.77	1.60	.68	.65	.48	.66	.51	.64
Na2O	1.54	2.39	3.56	3.41	3.00	3.23	1.54	3.42
K2O	4.13	4.39	4.85	5.07	6.16	5.91	6.46	6.16
TiO2	.14	.28	.24	.18	.27	.26	.12	.27
P2O5	.02	.05	.01	.01	.03	.03	.02	.03
MnO	.05	.05	.04	.05	.04	.04	.02	.05
LOI	2.76			2.70	.83	1.05	1.30	2.70
Total	100.83	93.98	95.67	100.30	99.65	99.91	102.16	99.84

1) Tuff of Little Mineral Creek, from Coyote Canyon, sec. 23, T. 12 S., R. 8 W., this report, slightly altered.
2) Tuff of Little Mineral Creek, 33-17'-04"N, 107-45'-13"W, Abitz (1984).
3) Tuff of Little Mineral Creek, 33-15'-16"N, 107-46'-17"W, Abitz (1984).
4) Moccasin John Rhyolite, south side of Dine's Mt., 33-15'-42"N, 107-44'-10"W, this report.
5) Moccasin John Rhyolite, Chloride Creek dome, sec. 23, T. 11 S., R. 9 W. (unsurveyed), this report.
6) Moccasin John Rhyolite, Chloride Creek dome, sec. 23, T. 11 S., R. 9 W. (unsurveyed), this report.
7) Moccasin John Rhyolite, Chloride Creek dome, sec. 23, T. 11 S., R. 9 W. (unsurveyed), this report, slightly altered.
8) Moccasin John Rhyolite, vitrophyre from base of lava flow, 33-16'-50"N, 107-45'-05"W, this report.

	9	10	11	12	13	14	15
SiO2	74.21	74.98	67.41	79.31	82.75	74.72	76.08
Al2O3	14.47	13.65	17.40	10.85	9.15	13.37	13.92
Fe2O3	1.86	.72	1.82	.78	.65	.51	.60
MgO	.55	.20	.50	.31	.11	.27	.27
CaO	1.12	.34	1.19	.60	.35	.57	.54
Na2O	.60	3.54	3.76	2.70	1.93	2.67	3.33
K2O	6.68	5.51	5.18	4.05	3.91	5.54	5.28
TiO2	.35	.20	.33	.13	.11	.16	.10
P2O5	.08	.01	.15	.01	.01	.01	.01
MnO	.04	.07	.04	.10	.05	.02	.02
Total	99.96	99.22	97.78	96.84	99.02	97.84	100.23

9) Tuff of Little Mineral Creek, 33-17'-24"N, 107-48'-32"W, Abitz (1984).
10) Tuff of Little Mineral Creek, 33-16'-30"N, 107-50'-21"W, Abitz (1984).
11) Moccasin John Rhyolite, lava, 33-17'-27"N, 107-50'-42"W, Abitz (1984).
12) Moccasin John Rhyolite, carapace breccia, 33-17'-09"N, 107-51'-11"W, Abitz (1984).
13) Moccasin John Rhyolite, carapace breccia, 33-16'-55"N, 107-30'-21"W, Abitz (1984).
14) Moccasin John Rhyolite, lava, 33-13'-18"N, 107-45'-22"W, Abitz (1989).
15) Moccasin John Rhyolite, lava, 33-13'-00"N, 107-50'-49"W, Abitz (1989).

Figure 37. Major-element variation diagrams for the tuff of Little Mineral Creek and Moccasin John Rhyolite; solid boxes are tuff of Little Mineral Creek.

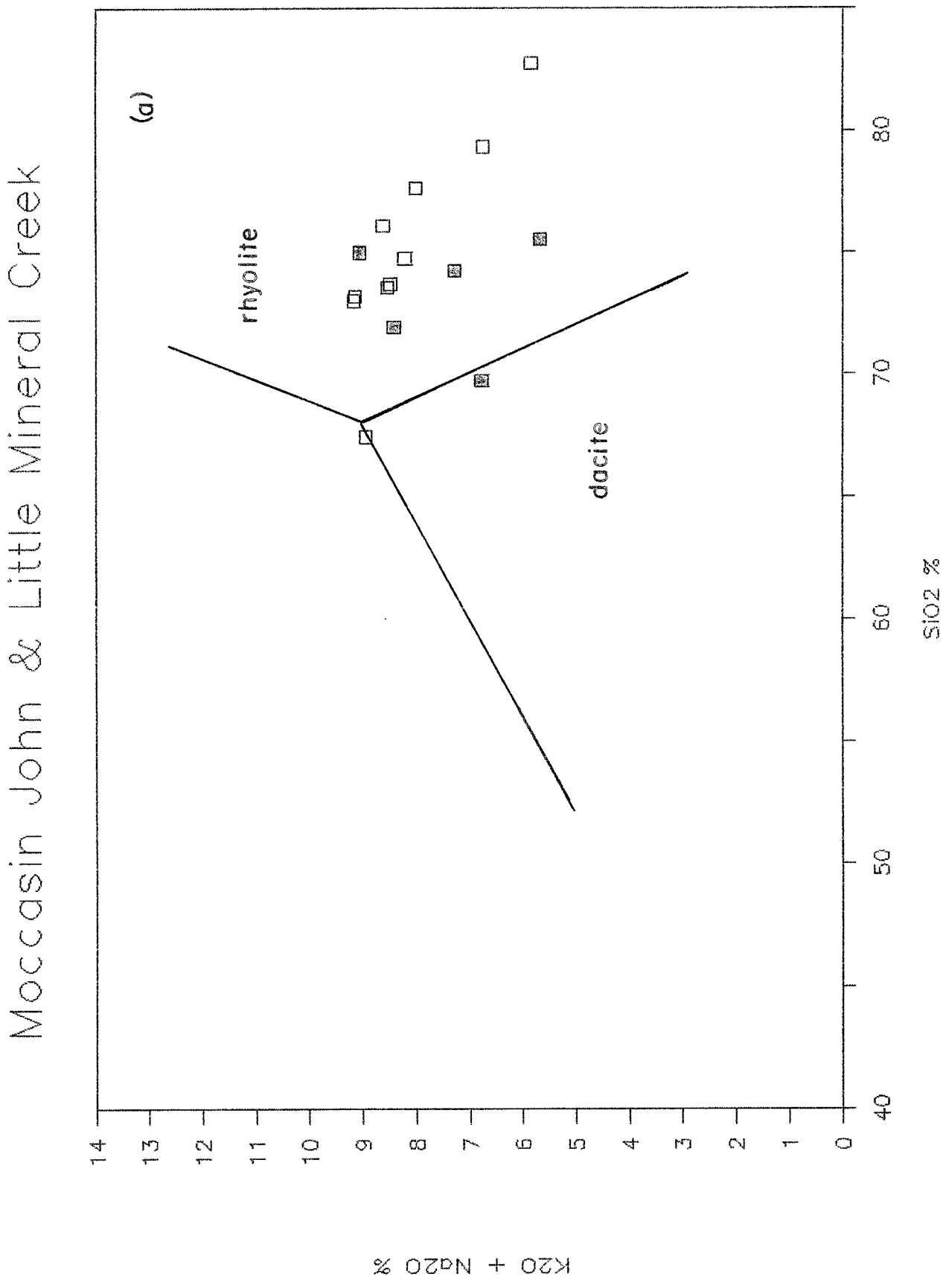
Moccasin John & Little Mineral Creek
(a)
rhyolite
dacite
K2O + Na2O %
SiO2 %
0
1
2
3
4
5
6
7
8
9
10
11
12
13
14
40
50
60
70
80

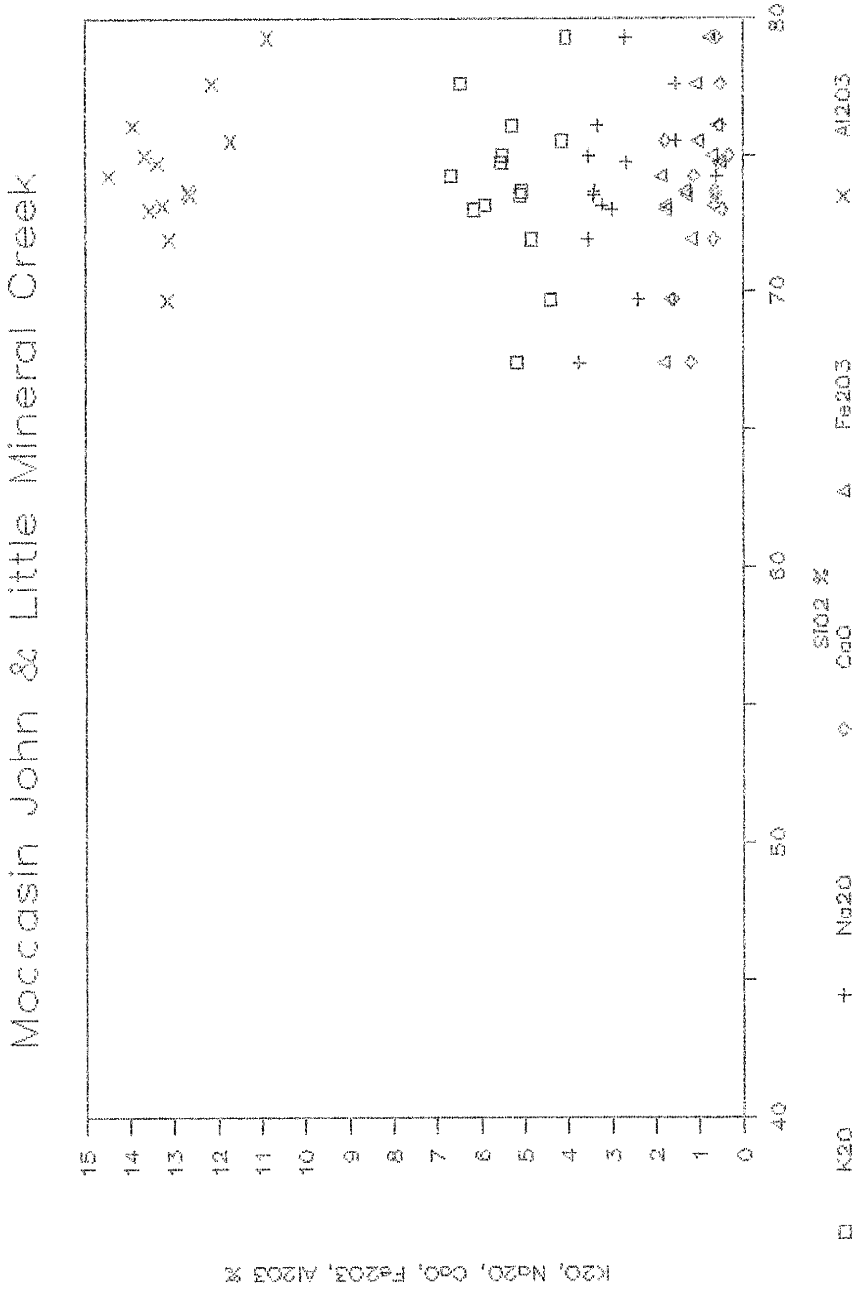
Moccasin John & Little Mineral Creek
K2O, Na2O, CaO, Fe2O3, Al2O3 %
SiO2 %
K2O
Na2O
CaO
Fe2O3
Al2O3

The abundant lithic fragments found in tuff of Little Mineral Creek are identical in all aspects to overlying Moccasin John Rhyolite. It is interpreted that this tuff represents vent-clearing eruptions, possibly influenced by interactions with groundwater, that preceded extrusion of Moccasin John Rhyolite. Eichelberger et al. (1986) suggest that explosive, vent-clearing eruptions (such as represented by tuff of Little Mineral Creek) are necessary events for subsequent non-explosive lava extrusion in silicic volcanism, in that they provide high-permeability environment required for non-explosive degassing.

Major vent areas for tuff of Little Mineral Creek (and Moccasin John Rhyolite) are Moccasin John Mountain-Cobb Mountain area immediately south of Chloride mining district, Chloride Creek dome in south-central Chloride mining district, and several dikes and plugs in southwestern Chloride district. The maximun size of lithic fragments in tuff of Little Mineral Creek is crudely zoned around major vent areas, ranging from several tens of cm in diameter within a few km, to a few cm in diameter at distances of 10-15 km.

Moccasin John Rhyolite

Ericksen et al. (1970) used the name rhyolite of Moccasin John area for "distinctive rhyolite sequence (that) crops out on Moccasin John Mountain and in the area drained by Moccasin John Creek and the North Fork of Palomas Creek." Among other possibilities, they suggested that the Moccasin John area constituted a flow-dome complex, although they were uncertain of its stratigraphic position. Woodard (1982) referred to this unit as flow-banded rhyolite member of rhyolite of Little Mineral Creek. Abitz (1984) mis-identified this unit as the Mimbres Peak Formation in southernmost portion of the north-central Black Range. Harrison (1986) suggested the name Moccasin John Rhyolite in respect to original name from Ericksen et al. (1970). The type locality is in the vicinity of Moccasin John Mountain, sec. 33, T. 12 S., R. 9 W. There, Moccasin John Rhyolite directly overlies basaltic andesite of Poverty Creek, and is overlain by tuff of Diamond Creek (Abitz, 1989).

Moccasin John Rhyolite consists of highly contorted flow-banded domes and lava flows with some interbedded perlitic tuffs and tuffaceous sedimentary rocks. Carapace breccias exist around flanks of intrusives on Moccasin John and Cobb Mountains; basal vitrophyres are common for flows. This unit is generally very crystal-poor, containing from 1 to 3 % quartz, sanidine, plagioclase, and biotite. An abundance of volcanic glass and spherulites is

characteristic of Moccasin John Rhyolite. Hydrothermal alteration (silicification, kaolinization, alunitization) is common in upper portions and/or along margins of all Moccasion John Rhyolite flow-dome complexes.

Microscopically, Moccasin John Rhyolite consists dominantly of devitrified glass, with sparse phenocrysts of quartz, sanidine, plagioclase (An 20-30), and rare biotite. Spherulites, perlitic textures, and flow banding are all common features.

Chemically, this unit has a rhyolite to high-silica rhyolite composition. Table 9 lists major-element chemical analyses for Moccasin John Rhyolite; Figure 37 presents variation diagrams.

As discussed in the previous section, Moccasin John Rhyolite and tuff of Little Mineral Creek are believed to be genetically related. As such, the 29.10 Ma age obtained by McIntosh (1989) for tuff of Little Mineral Creek also applies to Moccasin John Rhyolite. These two units combined represent initial rhyolitic volcanism of this time period in south-central New Mexico. Their main characteristic that separates them from subsequent rhyolitic volcanism is an extreme paucity of phenocrysts.

rhyolite of Sawmill Peak

The name rhyolite of Sawmill Peak was given by Eggleston (1987) to a sequence of dark, red-brown lavas that cap Sawmill Peak in sec. 7, T. 10 S., R. 9 W. At this locality, Rhyolite of Sawmill Peak overlies tuff of Stiver Canyon, and consists of two distinct lava flows with an autobrecciated contact (Eggleston, 1987). Each lava flow is approximately 20-30 m thick. Coney (1976) included these lavas within his Dolan Peak Rhyolite unit. North and west of Sawmill Peak, rhyolite of Sawmill Peak overlies tuff of Mud Hole and is overlain by tuff of Kline Mountain and Dolan Peak Rhyolite. Rhyolite of Sawmill Peak has not been radiometrically dated, but its age is tightly constrained by underlying tuff of Mud Hole at 29.11 Ma and overlying La Jencia Tuff at 28.9 Ma (40Ar/39Ar ages from McIntosh, 1989).

Rhyolite of Sawmill Peak contains approximately 10 % phenocrysts of conspicuously large (0.7-1.5 cm) sanidine, and trace amounts of biotite and quartz. Except for argillically altered areas, a dark, brick-red color is distinctively characteristic of this unit. Locally, thin, discontinuous pyroclastic rocks are intercalated within lavas. Microscopically, the matrix of rhyolite of Sawmill Peak is flowbanded and commonly displays a trachytic texture of subparallel sanidine microlites.

Chemically, rhyolite of Sawmill Peak is unique among other volcanic rocks of south-central New Mexico, in that it

has very high total alkali contents of 9.5 to 11.5 %. The agpaitic coefficient (Na+K/Al) for this unit ranges from 0.7-0.8. Table 10 lists major-element analyses for rhyolite of Sawmill Peak; Figure 38 shows major-element variation diagrams for this unit.

The Sheep Canyon dome of Harrison (1986) in secs. 26 and 35, T. 9 S., R. 9 W. is a major vent area for rhyolite of Sawmill Peak. Margins of this vent area are marked by silicic, argillic, and advanced-argillic alteration of lavas and pyroclastic rocks. Also, Sheep Canyon dome lies at the center of a regional low in Ag/Au ratios for epithermal veins of northern Chloride mining district, interpreted as a upwelling zone for hydrothermal fluids responsible for precious metal mineralization (Harrison, 1989).

Table 10. Major-element analyses for rhyolite of Sawmill Peak.

	1	2	3	4	5	6
SiO2	70.86	71.45	71.81	71.95	72.33	73.12
Al2O3	14.29	14.24	13.23	13.72	13.74	13.00
Fe2O3	3.14	2.03	3.17	2.64	2.25	2.49
MgO	.23	.27	.21	.11	.19	.26
CaO	.30	.33	.26	.29	.31	.27
Na2O	3.81	5.11	4.15	4.01	4.07	3.92
K2O	6.07	6.13	5.69	5.77	5.96	5.69
TiO2	.56	.48	.43	.48	.47	.45
P2O5	.06	.07	.05	.05	.05	.06
MnO	.01	.02	.40	.03	.02	.07
LOI	.56	.45	.80	.75	.64	.69
Total	99.89	100.58	100.20	99.80	100.03	100.02

1) Rhyolite of Sawmill Peak, NE1/4 sec. 2, T. 10 S., R. 9 W., this report.
2) Rhyolite of Sawmill Peak, sec. 1, T. 10 S., R. 10 W., Eggleston (1989).
3) Rhyolite of Sawmill Peak, sec. 2, T. 10 S., R. 10 W., Eggleston (1989), mild alteration.
4) Rhyolite of Sawmill Peak, sec. 2, T. 10 S., R. 10 W., Eggleston (1989).
5) Rhyolite of Sawmill Peak, sec. 2, T. 10 S., R. 10 W., Eggleston (1989), mild alteration.
6) Rhyolite of Sawmill Peak, sec. 1, T. 10 S., R. 10 W., Eggleston (1989).

Figure 38. Major-element variation diagrams for the rhyolite of Sawmill Peak.

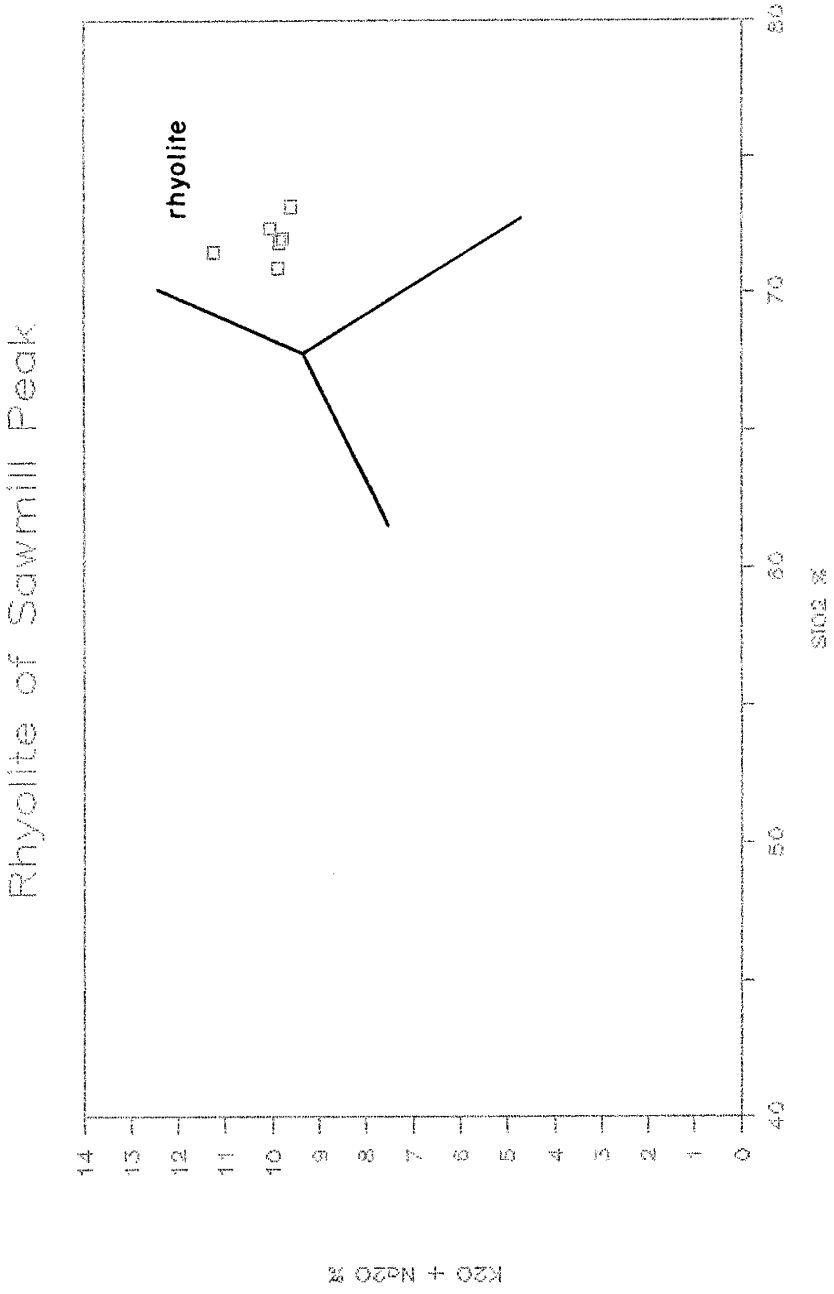
Rhyolite of Sawmill Peak
rhyolite
K2O + Na2O %
SiO2 %
40
50
60
70
80
0
1
2
3
4
5
6
7
8
9
10
11
12
13
14

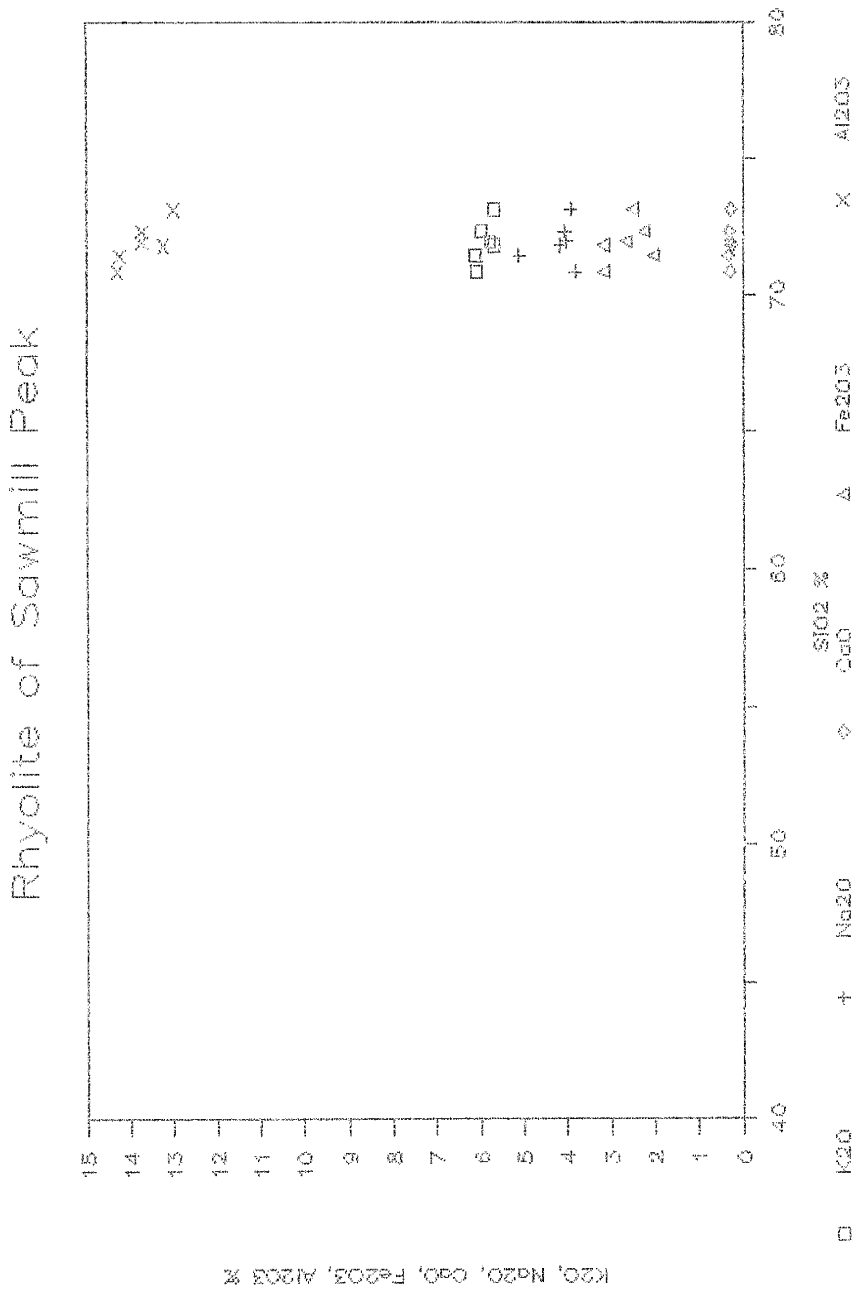
Rhyolite of Sawmill Peak
K2O, Na2O, CaO, Fe2O3, Al2O3 %
15
14
13
12
11
10
9
8
7
6
5
4
3
2
1
0
40
50
60
70
80
SiO2 %
□ K2O
+ Na2O
◇ CaO
△ Fe2O3
× Al2O3

Tuff of Kline Mountain

Tuff of Kline Mountain was named by Eggleston (1987) for the sequence of ash-flow tuffs that crops out on the northern flank of Kline Mountain, principally in sec. 22, T. 10 S., R. 10 W. In this area, tuff of Kline Mountain overlies rhyolite of Sawmill Peak and is overlain by rhyolite of Dolan Peak. Tuff of Kline Mountain is as much as 200 m thick, and consists of multiple, thinly bedded (generally 1-3 m thick), poorly to densely welded, moderately crystal-rich, pumice-rich ash-flow tuffs. Phenocryst content is variable, averaging about 12 %, with sanidine more abundant than quartz, and trace amounts of biotite and plagioclase. Chemical analyses by Eggleston (1987) indicate that this unit is a high-silica rhyolite with total alkali contents of approximately 7 %.

In upper portions of the sequence, lithic fragments of overlying rhyolite of Dolan Peak are found within tuff beds, suggesting a genetic relationship where tuff of Kline Mountain represents vent-clearing eruptions that preceded extrusion of rhyolite of Dolan Peak lava. As such, tuff of Kline Mountain is basically correlative to tuff of Straight Gulch (described in next section), a tuff that is interbedded with lavas of rhyolite of Dolan Peak.

Tuff of Kline Mountain has been pervasively altered to an advanced-argillic assemblage of kaolinite, alunite, and chalcedony along a north-trending zone that parallels the

Continental Divide north of Kline Mountain. This assemblage shows a rough zonation pattern centered on a sub-volcanic intrusion (Rhyolite of Franks Mountain) located on Kline Mountain proper (Eggleston, 1986). This zonation pattern has alunite as the dominant mineral closest to intrusive, grading to kaolinite as dominant mineral away from the intrusive. On the north flank of Kline Mountain, tuff of Kline Mountain has been converted to 70 % alunite, 20 % kaolinite, and 10 % silica; approximately 2 km to the north, tuff of Kline Mountain has been altered to nearly pure kaolinite with minor silica (Eggleston, 1986).

Tuff of Straight Gulch

Tuff of Straight Gulch is an informal name suggested by Eggleston (1986) for ash-flow tuff beds that are intercalated with rhyolite of Dolan Peak in exposures along Straight Gulch, sec. 25, T. 9 S., R. 10 W. This unit consists of as much as 70 m of ash-flow tuffs beds that are moderately to densely welded and moderately crystal-rich. Lower half of this unit consists of numerous 1-5 m thick beds, while upper half is a single, relatively massive interval. Phenocryst contents of 3-5 % quartz and 10-12 % sanidine occur in a vitroclastic groundmass. Much sanidine is of moonstone variety, and quartz is smokey in color. Since this unit is local in extent and is completely enveloped by rhyolite of Dolan Peak, tuff of Straight Gulch

is interpreted as a pyroclastic eruptive-phase of rhyolite of Dolan Peak.

rhyolite of Dolan Peak

The name, rhyolite of Dolan Peak, was given by Elston et al. (1973) and Coney (1976) to a sequence of rhyolite lavas and ash-flow tuffs below Taylor Creek Rhyolite and above basaltic andesite of Poverty Creek in northern Black Range. Eggleston (1986) restricted the unit to high-silica rhyolite lavas that occur above rhyolite of Sawmill Peak and below La Jencia Tuff in northern Black Range. Type locality is at Dolan Peak, sec. 18, T. 9 S., R. 9 W. This unit is as much 500 m thick in Sawmill Peak quadrangle (Plate 3). Two isolated outcrops of rhyolite of Dolan Peak occur along Chloride Creek above JHW Well in south-central Chloride mining district (Plate 2).

Rhyolite of Dolan Peak is typically flowbanded and contains from 10-25 % phenocrysts of sanidine and quartz, with rare biotite. Quartz/sanidine ratios for this unit are usually from 0.1 to 0.3; a characteristic that can be used to distinguish it in hand specimen from Taylor Creek Rhyolite, whose quartz/sanidine ratios are approximately 1 (Eggleston, 1987). Sanidine crystals in rhyolite of Dolan Peak are subhedral and commonly of moonstone variety, quartz is rounded and partially smokey in color. Spherulitic devitrification is very common in rhyolite of Dolan Peak, as is vapor-phase mineralization in gas cavities.

Microscopically, rhyolite of Dolan Peak consists of as much as 25 % total phenocrysts of broken, subhedral sanidine

and rounded and embayed quartz, with minor amounts of biotite, and very rare pyroxene. Granophyric intergrowths of quartz and feldspar are common. Groundmass is devitrified with abundant spherulitic textures.

Chemically, rhyolite of Dolan Peak is a high-silica rhyolite, with total alkali contents from 7.5-9.2 %. Table 11 lists major-element analyses for this unit; Figure 39 presents major-element variation diagrams.

In the southern Taylor Creek tin district, tin mineralization in association with intense vapor-phase crystalization along margins of domes of rhyolite of Dolan Peak was reported by Foord et al. (1985). However, no tin mineralization has been found or reported elsewhere in rhyolite of Dolan Peak.

La Jencia Tuff

La Jencia Tuff (formerly the lower member of A-L Peak Tuff) is a regionally extensive ash-flow tuff found throughout northeastern Mogollon-Datil volcanic field (Osburn and Chapin, 1983). Source area for La Jencia Tuff is interconnected Sawmill Canyon-Magdalena cauldrons in Magdalena Mountains (Osburn and Chapin, 1983). A high-precision 40Ar/39Ar age of 28.9 Ma has been determined for this unit by Kedzie (1984) and McIntosh (1989).

In north-central Black Range, La Jencia Tuff crops out in extreme northwestern corner of the Sawmill Peak

Table 11. Major-element analyses for rhyolite of Dolan Peak.

	1	2	3	4	5	6	7
SiO2	77.80	75.02	75.42	75.44	76.41	76.50	79.27
Al2O3	11.02	11.82	11.89	11.43	12.09	11.94	10.33
Fe2O3	1.98	1.79	1.85	1.88	1.65	1.17	1.17
MgO	.50	.25	.20	.60	.16	.01	.36
CaO	.23	.15	.15	.45	.23	.17	.15
Na2O	3.47	3.34	3.57	3.29	3.64	2.98	2.93
K2O	4.42	4.89	5.17	5.63	5.27	6.09	4.68
TiO2	.18	.16	.16	.16	.18	.10	.16
P2O5	.02	.02	.02	.02	.02	.02	.03
MnO	.03	.06	.04	.04	.03	.06	.03
LOI	.99	.99	.88	1.04	.58	.57	.76
Total	100.64	98.49	99.35	100.26	100.26	99.59	100.29

1) Rhyolite of Dolan Peak, north side of Chloride Creek above JHW Well, 33-20'-20"N, 107-45'-23"W, this report.
2) Rhyolite of Dolan Peak, Seventyfour Draw, sec. 4, T. 11 S., R. 10 W., 33-21'-33"N, 107-53'-26"W, Eggleston (1987).
3) Rhyolite of Dolan Peak, same loction as above, Eggleston (1987).
4) Rhyolite of Dolan Peak, Straight Creek, sec. 36, T. 9 S., R. 10 W., 33-29'-00"N, 107-49'-45"W, Eggleston (1987).
5) Rhyolite of Dolan Peak, Mud Hole area, sec. 2, T. 10 S., R. 10 W., 33-25'-51"N, 107-50'-58"W, Eggleston (1987).
6) Rhyolite of Dolan Peak, near Lookout Mt., sec. 3, T. 11 S., R. 10 W., Eggleston (1987).
7) Rhyolite of Dolan Peak, Mud Hole area, sec. 2, T. 10 W., R. 10 W., Eggleston (1987).

Figure 39. Major-element variation diagrams for rhyolite of Dolan Peak.

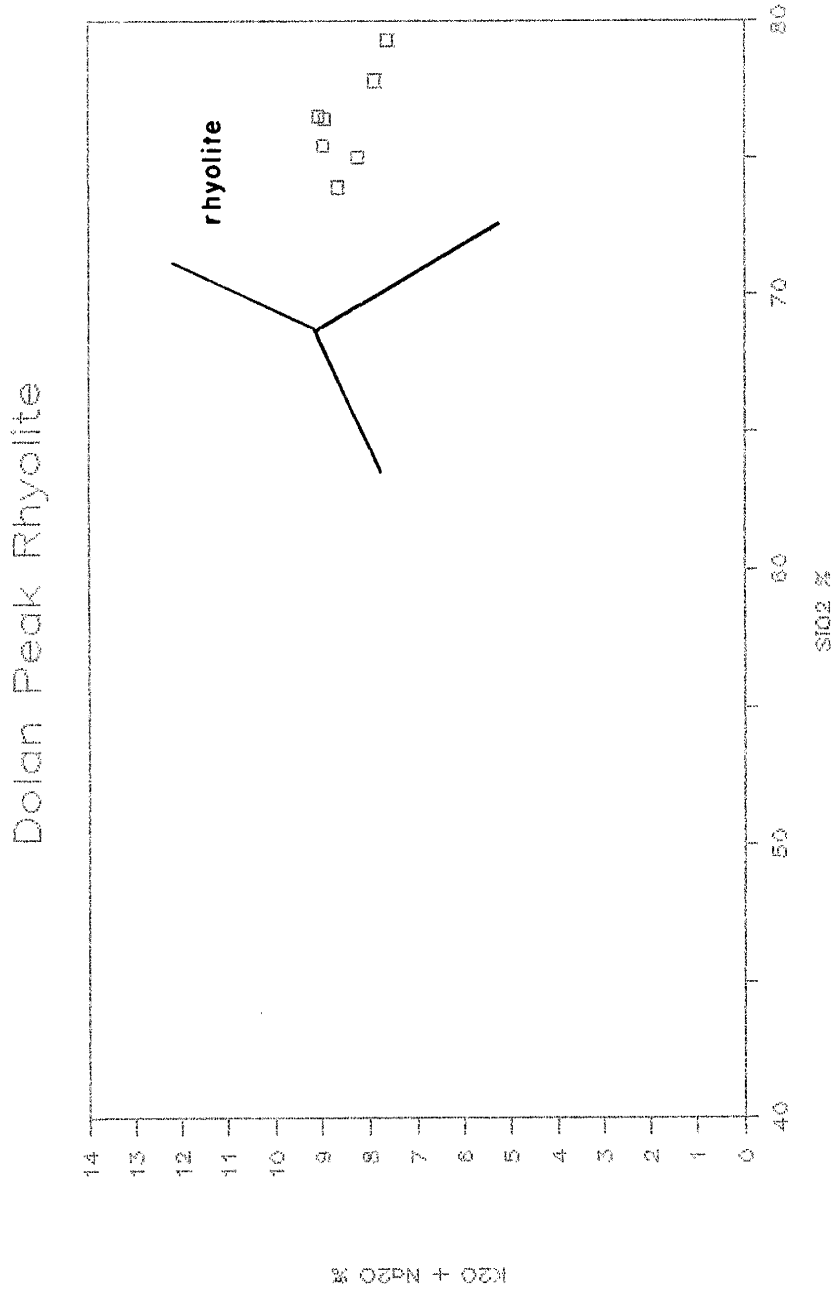
Dolan Peak Rhyolite
rhyolite
K2O + Na2O %
SiO2 %
0
1
2
3
4
5
6
7
8
9
10
11
12
13
14
40
50
60
70
80

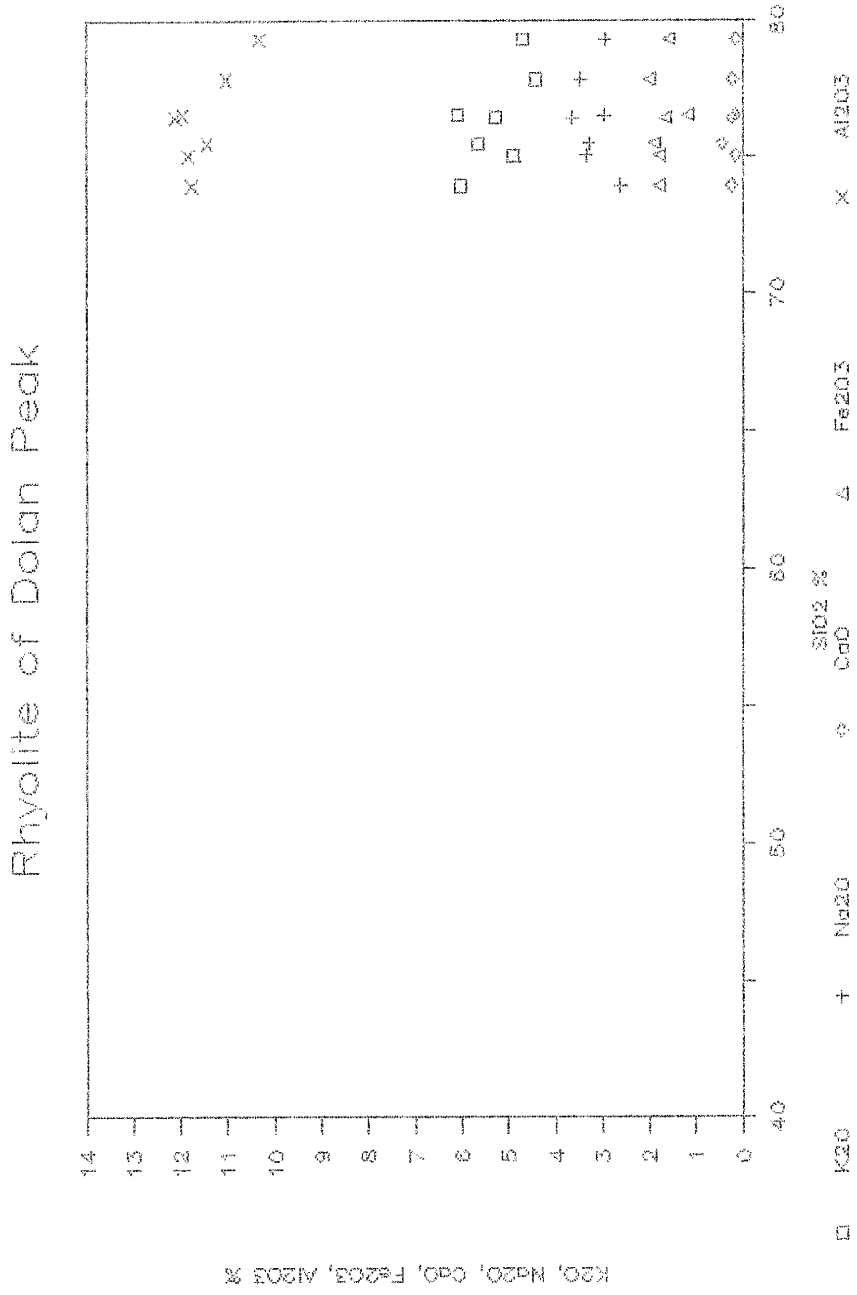
Rhyolite of Dolan Peak
K2O, Na2O, CaO, Fe2O3, Al2O3 %
SiO2 %
K2O
Na2O
CaO
Fe2O3
Al2O3
40
50
60
70
80
0
1
2
3
4
5
6
7
8
9
10
11
12
13
14

quadrangle (Plate 3). There, it occurs in a narrow north-northeast-striking paleovalley, disconformably overlies rhyolite of Dolan Peak and tuff of Kline Mountain, and is overlain by unnamed sedimentary rocks (Tss map unit on Plate 3), Vicks Peak Tuff, and tuff of Garcia Camp. Maximun thickness in this area is approximately 30 m. These exposures are on distal edge of La Jencia ash-flow sheet, approximately 80 km from source cauldron (McIntosh, 1989).

La Jencia Tuff in the Sawmill Peak quadrangle is a multiple-flow, densely welded, very crystal-poor ash-flow tuff. It typically is flowbanded and contains lineated pumice. Phenocrysts consist of 3-5 % sanidine and trace amounts of quartz, set in a vitroclastic matrix. Three zones are recognized in La Jencia Tuff: lower densely welded zone, middle vitric zone, and upper densely welded zone.

tuff of Stiver Canyon

The name tuff of Stiver Canyon was proposed by Woodard (1982) for the ash-flow tuff that overlies Moccasin John Rhyolite and tuff of Little Mineral Creek in Lookout Mountain area. Type locality was given as along Stiver Canyon in SE1/4NW1/4 sec. 2., T. 11 S., R. 10 W. In vicinity of the type locality, tuff of Stiver Canyon is overlain unconformably by tuff of Lookout Mountain and Taylor Creek Rhyolite. Tuff of Mud Hole was incorrectly included with tuff of Stiver Canyon by Eggleston (1987). However, based on differing phenocryst contents and paleomagnetic signatures obtained by McIntosh (1989), tuff of Stiver Canyon and tuff of Mud Hole are recognized as two different units.

Tuff of Stiver Canyon crops out throughout the central portion of north-central Black Range (Plates 2 & 3), principally between Lookout Mountain and Sawmill Peak. Isolated outcrops also occur along Chloride Creek in sec. 24, T. 10 S., R. 8 W. Tuff of Stiver Canyon is a poorly resistant unit, generally forming gentle slopes. Maximum thickness is approximately 170 m.

Tuff of Stiver Canyon is a poorly to moderately welded, moderately crystal-rich ash-flow tuff. Lithics and pumice are both rare; phenocryst content varies from 10 to 20% and includes sanidine, quartz, and minor biotite. Sanidine typically displays 'moonstone' coloring, and is 2-3 times

more abundant than quartz.

Microscopically, tuff of Stiver Canyon consists of as much as 15 % rounded quartz, 5 % subhedral sanidine, and minor biotite and opaque minerals. Intergrowths of quartz and feldspar with granophyric textures locally rim or replace quartz and sanidine in tuff of Stiver Canyon (Woodard, 1982). Groundmass consists of devitrified glass and pumice, with common axiolitic textures. Rare lithic fragments of flow-banded rhyolite and andesite occur in this unit.

Chemically, tuff of Stiver Canyon is of rhyolitic to high-silica rhyolite composition, with K2O content approximately twice Na2O content, and low CaO content. Table 12 lists major-element analyses for this unit; Figure 40 presents variation diagrams.

There is no known source area for tuff of Stiver Canyon. Nor have there been any radiometric ages determined for this unit, although it is tightly bracketed by 40Ar/39Ar ages on underlying tuff of Little Mineral Creek, 29.10 Ma, and overlying La Jencia Tuff, 28.9 Ma (McIntosh, 1989).

Table 12. Major-element analyses for tuff of Stiver Canyon.

	1	2	3	4	5
SiO2	75.70	71.64	76.76	74.89	75.26
Al2O3	12.13	14.57	12.12	13.09	12.07
Fe2O3	1.85	2.42	2.08	2.05	2.22
MgO	.35	.47	.44	.21	.29
CaO	.29	.50	.18	.13	.20
Na2O	3.15	2.71	3.43	2.55	1.92
K2O	5.18	6.96	5.32	5.21	5.83
TiO2	.20	.48	.19	.02	.16
P2O5	.03	.08	.01	.10	.02
MnO	.02	.07	.02	.01	.02
LOI	1.40	1.00	1.66	1.06	1.38
Total	100.30	100.90	102.21	99.56	99.37

1) From Stiver Canyon, near type locality, sec. 2, T. 11 S., R. 10 W., this report.
2) From north side of Chloride Creek, above JHW Well, center sec. 24, T. 11 S., R. 9 W., this report.
3) From Sawmill Peak, sec. 12, T. 10 S., R. 10 W., this report.
4) East side of Lookout Mountain, SE1/4NW1/4 sec. 18, T. 11 S., R. 9 W., Woodard (1984).
5) West side of Lookout Mountain, Whiskey Spring, sec. 34, T. 10 S., R. 10 W., Eggleston (1987).

Figure 40. Major-element variation diagrams for the tuff of Stiver Canyon.

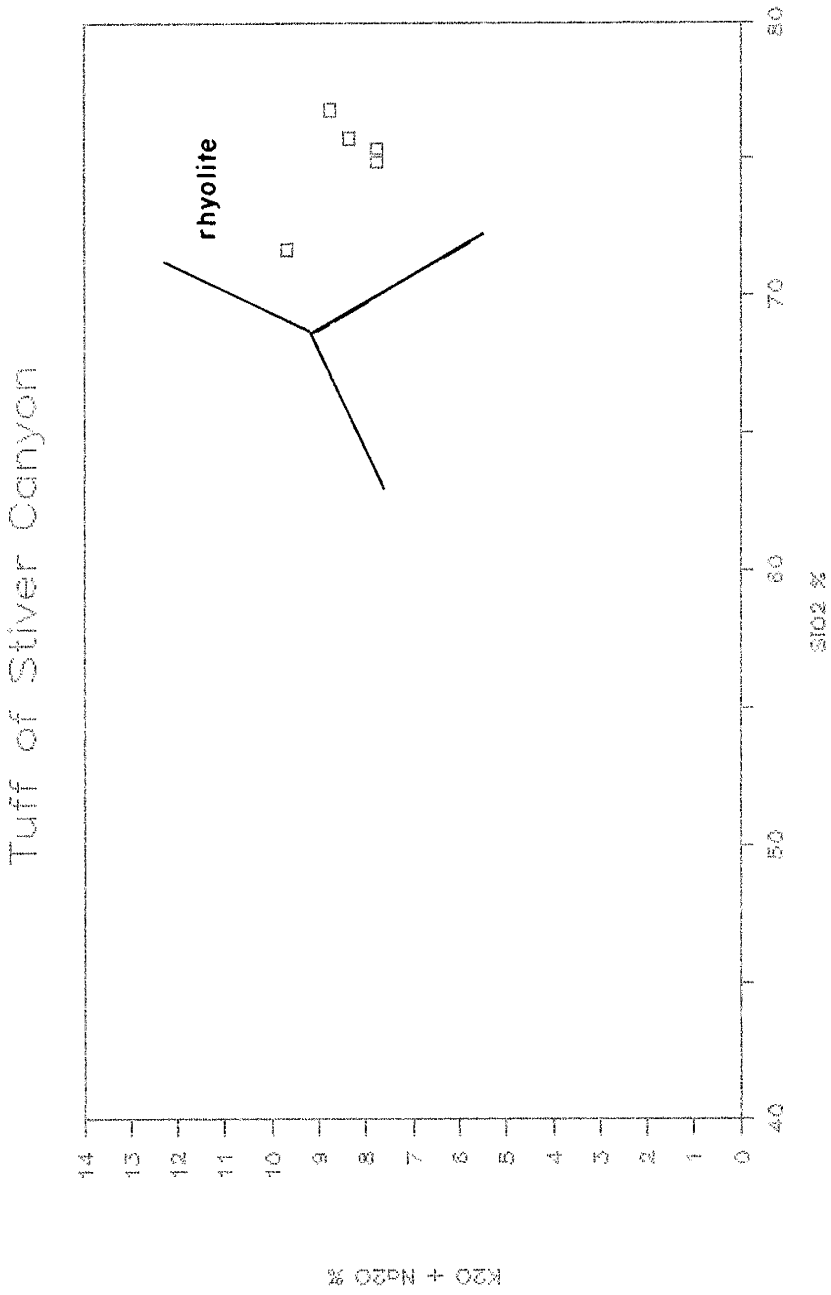
Tuff of Stiver Canyon
rhyolite
K2O + Na2O %
SiO2 %
40
50
60
70
80
0
1
2
3
4
5
6
7
8
9
10
11
12
13
14

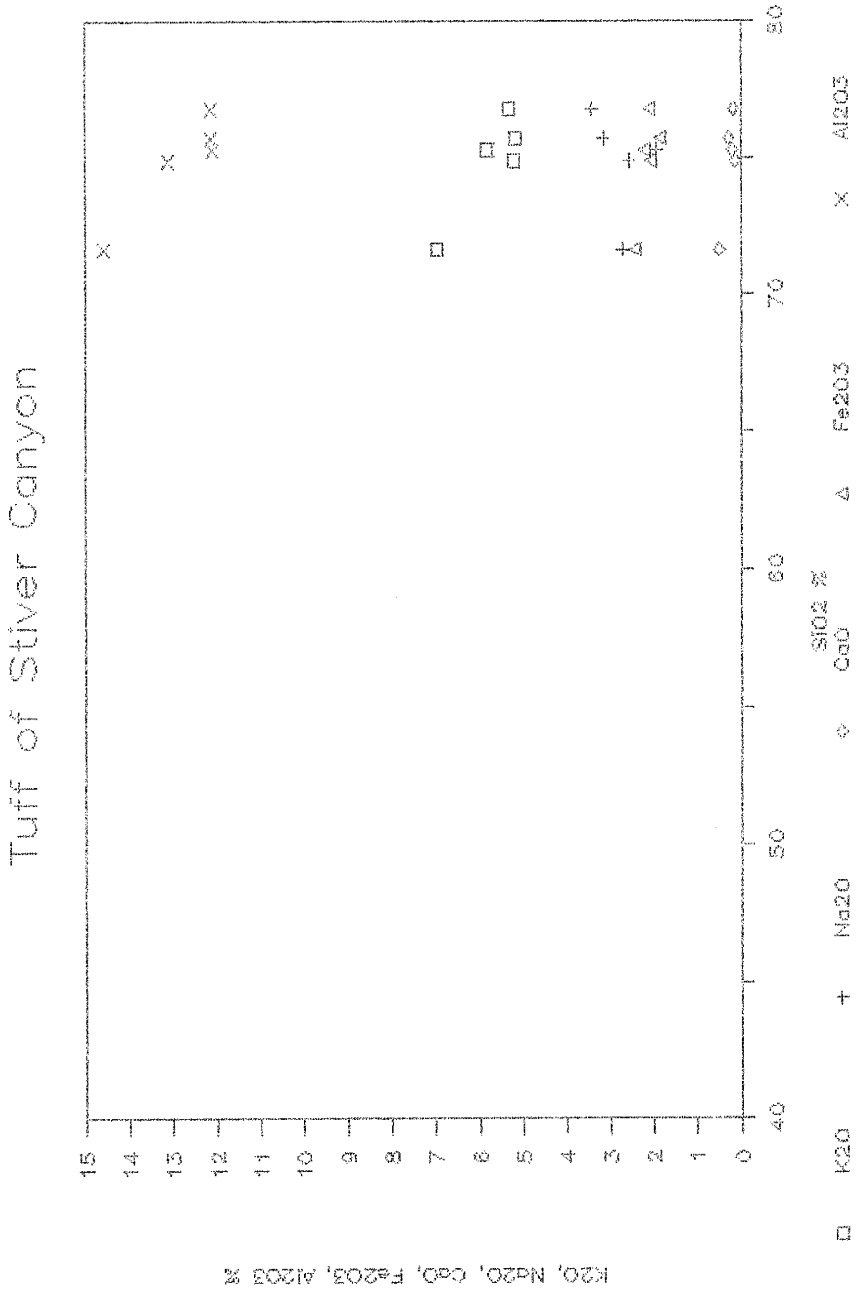
Tuff of Stiver Canyon
K2O, Na2O, CaO, Fe2O3, Al2O3 %
0
1
2
3
4
5
6
7
8
9
10
11
12
13
14
15
40
50
60
70
80
SiO2 %
□ K2O
+ Na2O
◇ CaO
△ Fe2O3
× Al2O3

Tuff of Diamond Creek-tuff of Lookout Mountain

In the southern part of north-central Black Range (Lookout Mountain quadrangle-Plate 2), a thick sequence of seven (or more ?) ash-flow tuffs and intercalated lavas crops out along, and to west of the Continental Divide. This sequence has a thickness in excess of 300 m in Diamond and South Diamond Creeks.

Several names have been applied to this poorly understood sequence. Ericksen et al. (1970) referred to it as rhyolite of Diamond Creek, but also included overlying rhyolite flows. Woodard (1982) first proposed the name tuff of Diamond Creek for the sequence of ash-flow tuffs and gave a type locality along the steep sides of Diamond Creek in SW1/4SE1/4 sec. 28, T. 11 S., R. 10 W. However, he failed to correlate this sequence to the Lookout Mountain area, where he gave a new name, tuff of Lookout Mountain, to the some of these ash-flow tuffs and included others with tuff of Stiver Canyon. He also misinterprepted their stratigraphic position as younger than Taylor Creek Rhyolite.

Abitz (1984) reproposed the name tuff of Diamond Creek for this sequence and suggested a type locality close to that of Woodard (1982), along the northwest-trending ridge that divides Diamond Creek and Fisherman Canyon (33 degrees-15'-50"N, 107 degrees-50'-00"W). In this vicinity, tuff of Diamond Creek unconformably overlies both

Moccasin John Rhyolite and tuff of Little Mineral Creek, and is overlain by rhyolite of Franks Mountain (a.k.a. rhyolite of Turkey Run and rhyolite of Rocky Canyon). This report, Wagener (1987), and Reisinger (1988) refer to this unit as tuff of Diamond Creek.

Tuff of Diamond Creek is an extremely variable and complex sequence with poorly documented internal stratigraphy. Individual beds vary over short distances, both horizontally and vertically, from crystal-rich to crystal-poor, poorly welded to densely welded, and lithic-rich to lithic-poor. Air-fall tuffs and volcaniclastic sediments are locally intercalated within the sequence. Phenocrysts reported for this sequence are dominantly sanidine and quartz, with lesser amounts of plagioclase, biotite, and hornblende. Abitz and Matheney (1987) suggest that most of the sanidine and quartz crystals contained within tuff of Diamond Creek are xenocrystic and derived from Precambrian granitic basement. However, McIntosh (1987) reports a 40Ar/39Ar age of 28.7 Ma derived from sanidine in tuff of Diamond Creek. This age is in good agreement with stratigraphic position.

Wagener (1987), Reisinger (1988), and Reisinger and Wagener (1987) have considered tuff of Diamond Creek as a large, single outflow sheet. However, from reconnaissance traverses and mapping, it is suggested that this sequence is the product of numerous small eruptions rather than a single large eruption. It is interpreted that these deposits are

the result of vent-clearing pyroclastic eruptions from the numerous rhyolite flow-dome complexes that are occur throughout this region. If the dike-like structure (300 X 1500 m) of ash-flow tuff described by Reisinger and Wagener (1987) is indeed a vent for tuff of Diamond Creek, it is unique and anomalous.

Vicks Peak Tuff

Vicks Peak Tuff is a regionally extensive ash-flow tuff sheet that erupted from the Nogal Canyon cauldron in the southern San Mateo Mountains (Deal and Rhodes, 1976). Correlation by McIntosh (1989) of Vicks Peak Tuff with Bell Top 7 tuff of Clemons (1976) and the upper tuff of Tularosa Canyon of Rhodes and Smith (1976) make this unit the most widely distributed ignimbrite in the northern and eastern Mogollon-Datil volcanic field. The distinctive field appearance of Vicks Peak Tuff makes it a most useful stratigraphic marker horizon. A mean 40Ar/39Ar age of 28.56 ± .06 Ma was obtained for Vicks Peak Tuff by McIntosh (1989).

Vicks Peak Tuff is a massive, moderately to densely welded, very crystal-poor ash-flow tuff. Phenocrysts consist of 1-3 % sanidine and sparse quartz, set in vitroclastic groundmass. Large, elongated pumice containing vapor-phase mineralization with granular texture are characteristic of this unit. These pumice generally define well-developed foliation planes. Chemically, Vicks Peak Tuff is a high-silica rhyolite. Table 13 presents one major-element analysis for this unit from north-central Black Range.

Scattered, sparse outcrops of Vicks Peak Tuff occur throughout north-central Black Range. In the extreme northwest corner of Sawmill Peak quadrangle (Plate 3),

Table 13. Major-element analysis for Vicks Peak Tuff from outcrop in Winston graben, Coyote Canyon, sec. 22, T. 12 S., R. 8 W., Winston quadrangle.

SiO2	78.07
Al2O3	10.62
Fe2O3	1.50
MgO	.55
CaO	.15
Na2O	2.78
K2O	5.49
TiO2	.16
P2O5	.03
MnO	.07
LOI	.93
Total	100.35

approximately 30 m of Vicks Peak overlies La Jencia Tuff, and is below unnamed volcaniclastic sediments (Tss map unit) and tuff of Garcia Camp. A small, fault-bounded outcrop of Vicks Peak Tuff occurs in SE1/4SE1/4 sec. 32, T. 9 S., R. 9 W., on the western margin of Winston graben in Iron Mountain quadrangle (Plate 4). Unpublished drill logs of Gulf Minerals indicate that as much as 100 m of Vicks Peak Tuff exists below Santa Fe Group sediments approximately 5 km east of this fault-bounded outcrop in sec. 3, T. 10 S., R. 8 W. (P. Willard, 1987, personal commun.). In the southeastern corner of the Winston quadrangle (Plate 1), within the Winston graben, isolated, thin (15 m or less) outcrops of Vicks Peak Tuff rest with angular unconformity upon basaltic andesite of Poverty Creek and tuff of Little Mineral Creek.

Structurally intriguing exposures of Vicks Peak Tuff occur near the center of Winston graben, approximately 1 km east of the town of Winston, in sec. 13, 14, 23, & 24, T. 11 S., R. 8 W.. There, in an area of about 2 km2, a block-like mass of this tuff crops out with vertical to near-vertical pumice foliations that strike north-south. Chaotic breccia is found around the margins of this block. The base of this block is not exposed. The upper contact is a pronounced angular unconformity with overlying, near-horizontal beds of Santa Fe Group sediments and Miocene Winston Andesite. It is interpreted that these exposures are of a large gravity-slide block that was rotated during emplacement.

Presumedly, the detachment area for this block was along the eastern margin of Winston graben.

Rhyolite of Franks Mountain

The name rhyolite of Franks Mountain is used collectively to identify the numerous rhyolitic flow-dome complexes that occur above tuff of Diamond Creek, are older than Taylor Creek Rhyolite, and crop out principally along the Continental Divide in south-central New Mexico. Included under this nomenclature are: rhyolite of Franks Mountain of Woodard (1982), Abitz (1984), Wagener (1987), and Reisinger (1988); rhyolite of Turkey Run of Woodard (1982) and Wagener (1987); rhyolite of Rocky Canyon of Ericksen et al. (1970), Reisinger (1988), and Abitz (1989); and parts of rhyolite of Diamond Creek of Ericksen et al. (1970), and Woodard (1982). Portions of tuff of Diamond Creek are probably pyroclastic deposits derived from vent-clearing eruptions of these flow-dome complexes. Additional rhyolite flow-dome complexes that are stratigraphically equivalent to above units occur west of the Continental Divide in extreme western Black Range, and several kilometers east of the Continental Divide in eastern Sierra Cuchillo. These rocks are described in following section on other rhyolite flow-dome complexes.

An upper age constraint for these flow-dome complexes is problematic. The only units that clearly overlie these rocks are Bearwallow Formation (~21-18 Ma) and sediments of Gila Group. Straightforward stratigraphic relationships with Taylor Creek Rhyolite are not exposed anywhere.

Ericksen et al. (1970) considered rhyolite of Rocky Canyon to be older than Taylor Creek Rhyolite, however Wagener (1987) believed the opposite. Eggleston (1987) gives a K-Ar age of 28.4 ± 1.2 Ma for alunite alteration that is related to an intrusive body occurring at Kline Mountain, suggesting that this rhyolite of Franks Mountain intrusive is approximately the same age as Taylor Creek Rhyolite. In general, it appears that rhyolite of Franks Mountain flow-dome complexes were erupted from approximately 28.7-28.1 Ma (ages of tuff of Diamond Creek and Taylor Creek Rhyolite, respectively).

Rhyolite of Franks Mountain is characteristically flowbanded and contains from 10-20 % phenocrysts of sanidine and quartz, with minor to trace amounts of biotite, hornblende, and pyroxene. Sanidine is typically 2-3 times more abundant than quartz. Groundmass of these lavas is granophyric to microgranophyric in texture. Spherulites are common, ranging in size from microscopic to 3-4 cm in diameter. Chemically, these rocks are rhyolite to high-silica rhyolite, with total alkali contents of 7-10.5 %, and low CaO contents. Table 14 lists major-element analyses for these rocks; Figure 41 shows variation diagrams.

Virtually all rhyolite of Franks Mountain flow-dome complexes have associated argillic to advanced argillic alteration halos. Alteration dominantly affects surrounding country rock, but locally intrusive rocks are also strongly

Table 14. Major-element analyses for rhyolite of Franks Mountain and related rhyolite intrusives in south-central New Mexico.

	1	2	3	4	5	6	7	8
SiO2	70.55	76.64	76.99	70.58	75.68	75.35	76.96	76.22
Al2O2	15.30	12.72	12.51	15.30	13.03	12.98	13.36	12.87
Fe2O3	2.27	.71	1.63	2.23	1.43	1.21	.99	1.61
MgO	.42	.18	.12	.32	.15	.41	.13	.05
CaO	.55	.59	.12	.91	.54	1.01	1.00	.14
Na2O	3.74	3.76	3.46	4.33	3.74	3.62	4.10	3.72
K2O	5.71	4.19	4.88	5.74	5.05	5.03	3.13	5.13
TiO2	.04	.13	.21	.44	.28	.22	.27	.17
P2O5	.05	.01	.06	.06	.02	.04	.02	.03
MnO	.02	.07	.08	.08	.07	.08	.04	.06
LOI	.76		.58	.37	.61	.46	5.60	.34
Total	99.42	99.00	100.64	100.36	100.60	100.47	105.60	100.34

1) Rhyolite of Turkey Run, north side of Turkey Run, NW1/4NE1/4 sec. 21, T. 11 S., R. 10 W., Woodard (1982).
2) Rhyolite of Franks Mountain, 33-16'-34"N, 107-51'-32"W, Abitz (1984).
3) Sample 15, field # 434, Ericksen et al. (1970).
4) Sample 16, field # 442, Ericksen et al. (1970).
5) Sample 17, field # 466, Ericksen et al. (1970).
6) Sample 18, field # 469, Ericksen et al. (1970).
7) Sample 19, field # 550, Ericksen et al. (1970).
8) Sample 20, field # 581, Ericksen et al. (1970).

	9	10	11	12	13	14	15	16	17
SiO2	75.42	75.80	75.86	75.87	75.95	76.50	76.64	76.75	80.97
Al2O3	11.85	12.48	11.66	12.17	11.92	12.44	11.66	11.59	10.03
Fe2O3	1.78	1.63	1.63	1.50	2.13	1.05	1.79	1.19	.66
MgO	.18	.17	.15	.22	.23	.11	.21	.13	.13
CaO	.09	.16	.13	.23	.12	.05	.26	.05	.04
Na2O	.60	.67	.58	.68	.82	.76	2.00	.96	.48
K2O	7.38	7.25	7.34	6.43	7.35	6.71	5.38	7.08	6.29
TiO2	.16	.16	.15	.15	.16	.16	.15	.14	.12
P2O5	.02	.02	.01	.01	.01	.01	.02	.01	.01
MnO	.02	.01	.01	.01	.02	.01	<.01	<.01	.01
LOI	1.50	2.08	2.02	1.98	1.22	1.71	1.18	1.34	1.29
Tot.	99.00	100.11	99.52	99.25	99.93	99.51	99.28	99.73	100.03

9) Rhyolite porphyry of Kline Mountain, sec. 23, T. 10 S., R. 10 W., altered, feldspar leached, Eggleston (1987).
10) Rhyolite porphyry of Kline Mountain, sec. 23, T. 10 S., R. 10 W., feldspar altered to clays, Eggleston (1987).
11) Rhyolite porphyry of Kline Mountain, sec. 23, T. 10 S., R. 10 W., argillic alteration, Eggleston (1987).
12) Rhyolite porphyry of Kline Mountain, sec. 23, T. 10 S., R. 10 W., feldspars altered to clays, Eggleston (1987).
13) Rhyolite porphyry of Kline Mountain, sec. 23, T. 10 S., R. 10 W., mild argillic alteration, Eggleston (1987).
14) Rhyolite porphyry of Kline Mountain, sec. 35, T. 10 S., R. 10 W., relatively fresh, Eggleston (1987).
15) Rhyolite porphyry of Kline Mountain, sec. 23, T. 10 S., R. 10 W., mildly altered, Eggleston (1987).
16) Rhyolite porphyry of Kline Mountain, sec. 35, T. 10 W., R. 10 W., silicified, Eggleston (1987).
17) Rhyolite porphyry of Kline Mountain, sec. 23, T. 10 S., R. 10 W., silicified with quartz stringers, Eggleston (1987).

Figure 41. Major-element variation diagrams for the rhyolite of Franks Mountain and related intrusives.

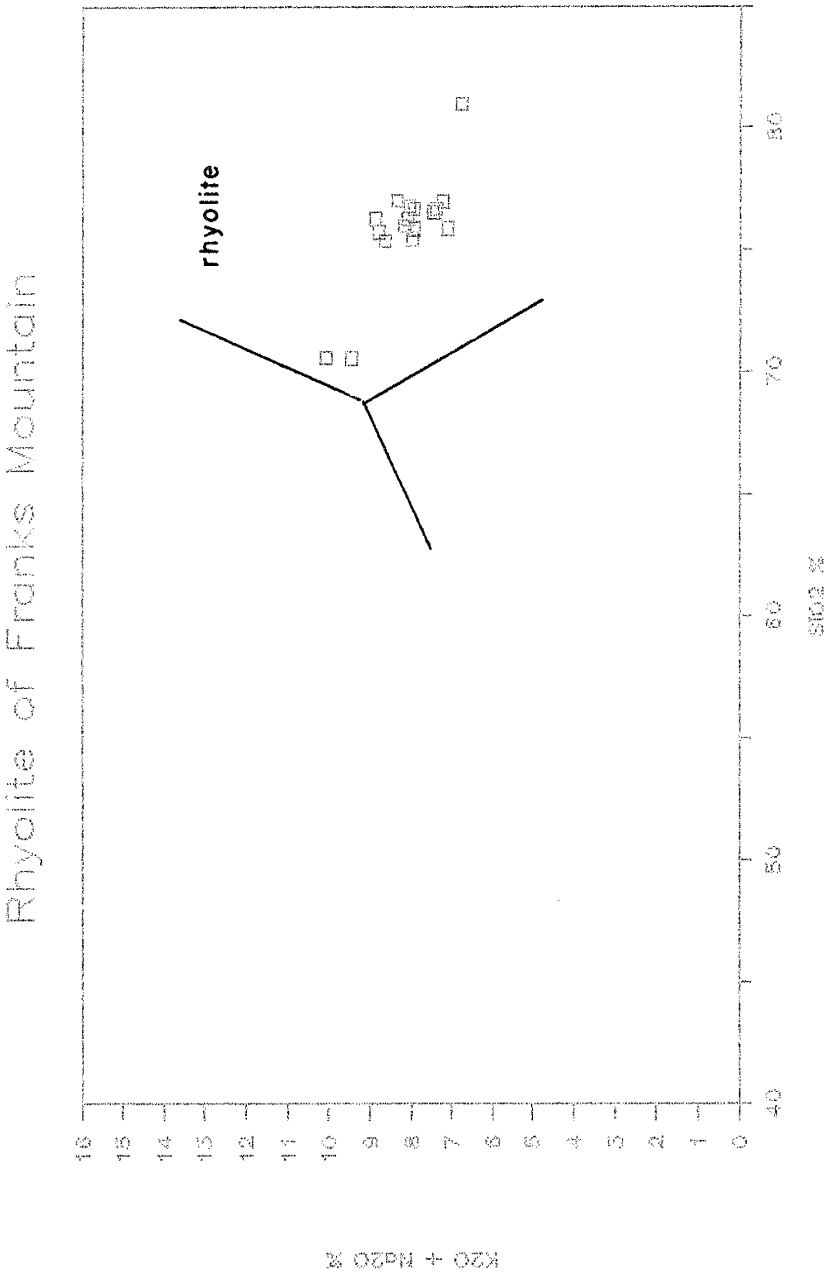
Rhyolite of Franks Mountain
rhyolite
K2O + Na2O %
SiO2 %
16
15
14
13
12
11
10
9
8
7
6
5
4
3
2
1
0
40
50
60
70
80
90

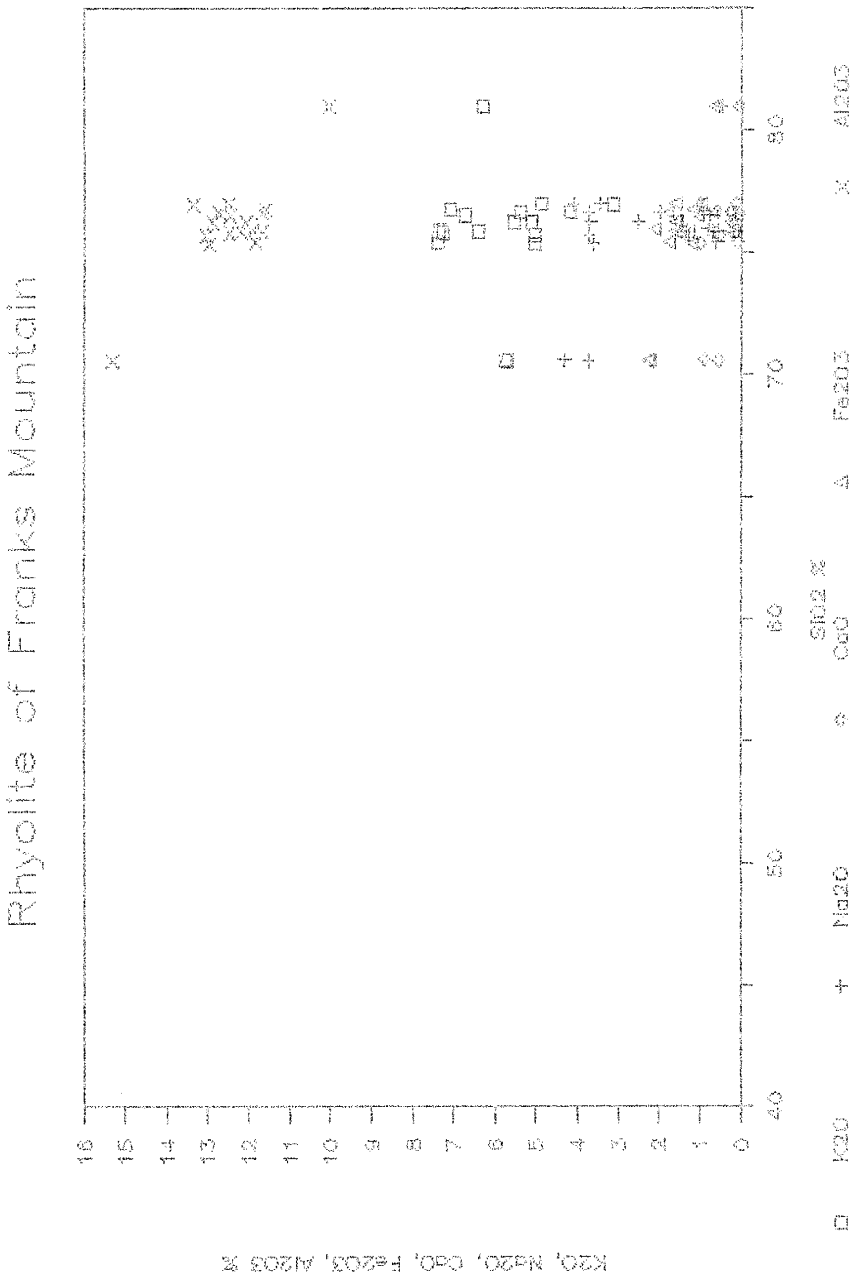
Rhyolite of Franks Mountain
K2O, Na2O, CaO, Fe2O3, Al2O3 %
SiO2 %
K2O
Na2O
CaO
Fe2O3
Al2O3
40
50
60
70
80
0
1
2
3
4
5
6
7
8
9
10
11
12
13
14
15
16

altered. Comparison of major-element compositions for relatively fresh rocks (# 1-8, Table 14) with altered rocks (# 9-17, Table 14) indicates that alkali contents show greatest effect of alteration. Altered rocks consistantly show an increase in K2O content with corresponding decrease in Na2O content, and little change in other elements except in cases of strong silicification. The two most pervasive and extensive alteration areas related to these intrusives occur at White Horse kaolin deposit in secs. 9, 10, 15, 16, 21, 22, & 27, T. 10 S., R. 10 W. and Ramsey kaolin deposit in secs. 8, 9, 10, 15, 16, 20, 21, 22, 27, and 28, T 11 S., R. 10 W. Descriptions of the alteration at White Horse deposit are provided by Patterson and Holmes (1965), and Eggleston (1986, 1987). Description of the Ramsey deposit is given by McKinlay and Clippinger (1947).

other rhyolite flow-dome complexes

In addition to the flow-dome complexes grouped together as rhyolite of Franks Mountain, other rhyolite flow-dome complexes occur in north-central Black Range and in eastern Sierra Cuchillo. These complexes are similar in composition and stratigraphic position to rhyolite of Franks Mountain. They include rhyolite of Whitetail Canyon and rhyolite of Hoyt Creek of Richter et al. (1986), rhyolite of Keith Tank of Eggleston (1987), and rhyolite of HOK Ranch of Osburn et al. (1986).

Rhyolite of Whitetail Canyon and rhyolite of Hoyt Creek of Richter et al. (1986) crop out in the Wall Lake area of extreme western Black Range. These units are closely associated spatially and are both chemically and texturally similar. It is interpreted that rhyolite of Whitetail Canyon is a late effusive phase of rhyolite of Hoyt Creek (Eggleston, 1987). Both of these units are crystal-poor, finely flow-banded rhyolite lavas. Rhyolite of Whitetail Canyon contains approximately 5 % plagioclase, 1 % pyroxene, 0.3 % biotite, and trace amounts of amphibole and opaque oxides set in a microtrachytic groundmass of feldspar microlites. Perlitic cracks are common in this unit, and most phenocrysts exhibit incipient alteration rims. Vapor-phase alteration is mild and ubiquitous, imparting a slightly bleached appearance to rhyolite of Whitetail Canyon. Rhyolite of Hoyt Creek contains trace to 0.5 % phenocrysts of plagioclase and biotite, with rare pyroxene, amphibole, and zircon. Groundmass consists of feldspar microlites displaying a microtrachytic texture. Microlites do not stain for potassium, indicating an albitic composition.

Rhyolite of Keith Tank of Eggleston (1987) crops out at a single locality in sec. 3, T. 11 S., R. 11 W. This unit is a vitric, crystal-poor, moderately lithic-rich, flow-banded rhyolite lava. It contains approximately 1 % quartz, 1 % plagioclase, 0.2 % sanidine, 0.4 % biotite, and traces of green hornblende, pyroxene, zircon, and opaque

minerals. Generally, all phenocrysts are less than 0.5 mm in diameter. Lithic fragments make up approximately 12 % of rock volume, are less than 1 cm in diameter, and consist of flow-banded rhyolite, coarsely crystalline gabbro (?), and basalt. Amphibole and pyroxene crystals contained within rhyolite of Keith Tank may in part be xenocrysts derived from mafic lithic fragments (Eggleston, 1987).

Rhyolite of HOK Ranch was named by Osburn et al. (1986) for exposures near HOK Ranch headquarters in eastern Sierra Cuchillo, sec. 36, T. 11 S., R. 7 W. It is roughly equivalent to lower portion of the coarse-moonstone-porphyritic rhyolite tuff of Heyl et al. (1983). Rhyolite of HOK Ranch is a massive (cliff-forming), moderately crystal-rich rhyolite lava. It has phenocryst contents of approximately 9 % quartz, 3 % plagioclase, 2 % biotite, and trace amounts of zircon and opaque oxides. Groundmass is granophyritic in texture. Quartz phenocrysts are rounded and embayed; sanidine phenocrsts are euhedral to subhedral; vapor-phase crystallization is minimal to absent. In the eastern Sierra Cuchillo, erosion has exposed several dikes and plugs of porphyritic rhyolite that are believed to be feeders for rhyolite of HOK Ranch.

Chemically, rhyolites of Whitetail Canyon, Hoyt Canyon, Keith Tank, and HOK Ranch are rhyolite to high-silica rhyolite in composition. Major-element analyses for these rocks are listed in Table 15, and are very similar to analyses for fresh rhyolite of Franks Mountain (Table 14).

Table 15. Major element analyses for rhyolites of Whitetail Canyon, Hoyt Canyon, Keith Tank, and HOK Ranch.

	1	2	3	4	5	6
SiO2	73.71	73.83	69.20	76.47	76.78	76.84
Al2O3	12.58	12.34	14.23	11.98	11.70	11.68
Fe2O3	1.26	.94	2.00	1.61	1.58	1.53
MgO	.55	.29	.71	.28	.34	.34
CaO	.84	.86	1.62	.41	.60	.75
Na2O	3.28	3.44	4.10	3.11	3.10	3.40
K2O	4.91	4.28	4.32	4.96	5.38	4.74
TiO2	.19	.12	.35	.16	.16	.16
P2O5	.03	.02	.10	.03	.03	.03
MnO	.06	.04	.07	.04	.12	.08
LOI	3.25	4.46	3.74	.87	.59	.84
Total	100.66	100.62	100.44	99.92	100.38	100.39

1) Rhyolite of Keith Tank, Keith Tank, sec. 3, T. 11 S., R. 11 W., 33-22'-30"N, 107-58'-20"W, Eggleston (1987).
2) Rhyolite of Hoyt Creek, Hoyt Creek, sec. 20, T. 11 S., R. 11 W., 33-19'-37"N, 108-00'-54"W, Eggleston (1987).
3) Rhyolite of Whitetail Canyon, Whitetail Canyon, sec. 5, T. 11 S., R. 11 W., 33-21'-47"N, 108-00'-35"W, Eggleston (1987).
4) Rhyolite of HOK Ranch, Willow Springs Draw, sec. 25, T. 11 S., R. 7 W., 33-19'-12"N, 107-31'-12"W, Eggleston (1987).
5) Rhyolite of HOK Ranch, HOK Ranch, sec. 23, T. 11 S., R. 7 W., 33-20'-05"N, 107-31'-35"W, Eggleston (1987).
6) Rhyolite of HOK Ranch, HOK Ranch, sec. 25, T. 11 S., R. 7 W., 33-19'-06"N, 107-30'-45"W, Eggleston (1987).

Table 15a. Major-element analyses for porphyritic dike believed to be feeder for rhyolite of HOK Ranch in eastern Sierra Cuchillo.

	1	2
SiO2	79.77	77.67
Al2O3	12.60	11.72
Fe2O3	.50	1.34
MgO	.41	.74
CaO	.19	.14
Na2O	2.03	1.11
K2O	6.27	6.17
TiO2	.15	.21
P2O5	.04	.03
MnO	<.10	.01
LOI	.45	1.17
Total	100.24	100.31

1) Porphyritic dike, sec. 23, T. 11 S., R. 7 W., 33-20'-29"N, 107-31'-52"W, Eggleston (1987).

2) Porphyritic dike, approximately 30 m north of NM Highway 59, center of sec. 23, T. 11 S., R. 7 W., this report.

Variation diagrams for rhyolites of Whitetail Canyon, Hoyt Canyon, Keith Tank, and HOK Ranch are presented in Figure 42. Although based on only a few analyses, it appears that each flow-dome complex has its own distinct, major-element signature.

In the eastern Sierra Cuchillo, erosion has exposed several porphyritic rhyolite dikes and plugs that are believed to be feeders for rhyolite of HOK Ranch. One very prominent dike that crosses NM Highway 59 in center of sec. 22, T. 11 S., R. 7 W. can be traced eastward into rhyolite of HOK Ranch, where it loses all identity. Two chemical analyses of this dike are given in Table 15a and Figure 43. Comparison of these analyses with those for rhyolite of HOK Ranch indicates that the dike contains slightly more SiO2 and K2O, and distinctly less Na2O and CaO than lavas. If this dike is indeed a feeder for rhyolite of HOK Ranch, chemical differences are ascribed to zonation within the source magma chamber.

Figure 42. Major-element variation diagrams for the rhyolites of Whitetail Canyon, Hoyt Canyon, Keith Tank, and HOK Ranch.

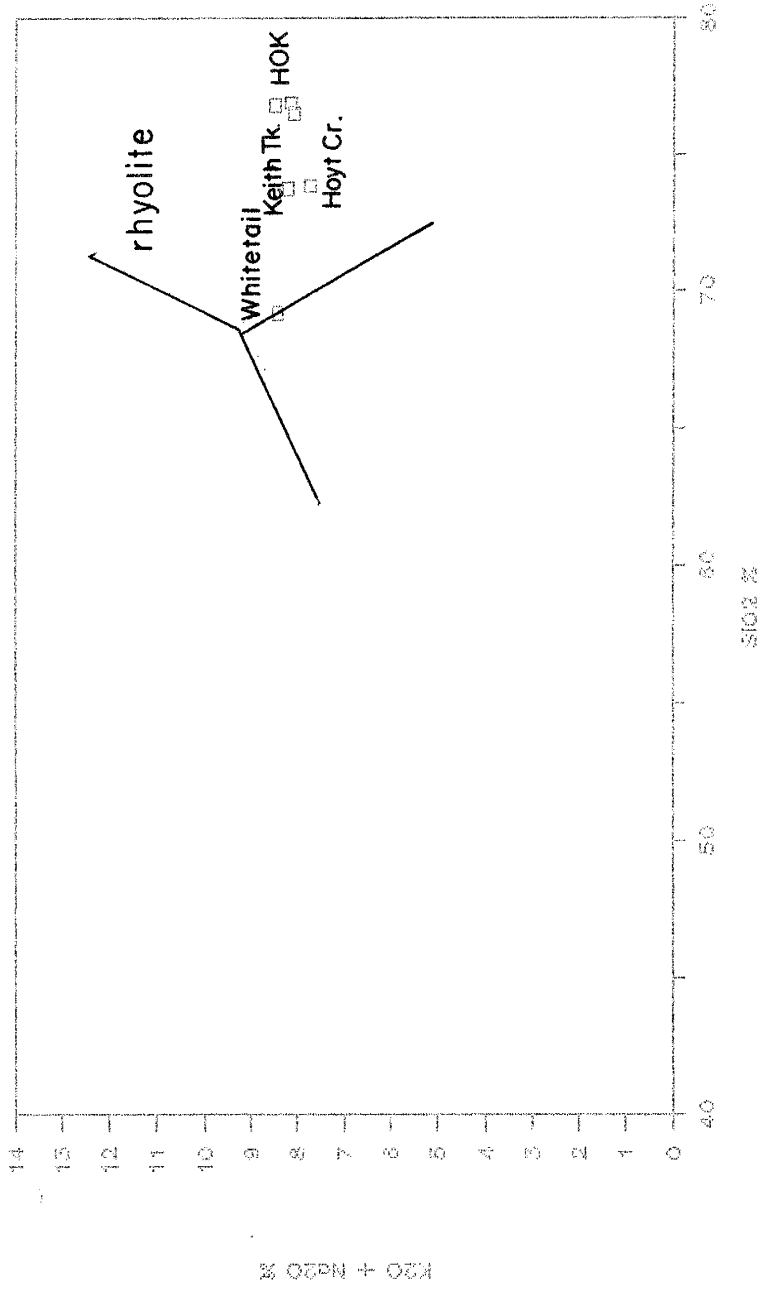
rhyolite
Whitetail
Keith Tk.
HOK
Hoyt Cr.
40
50
60
70
80
SiO2 %
14
13
12
11
10
9
8
7
6
5
4
3
2
1
0
K2O + Na2O %

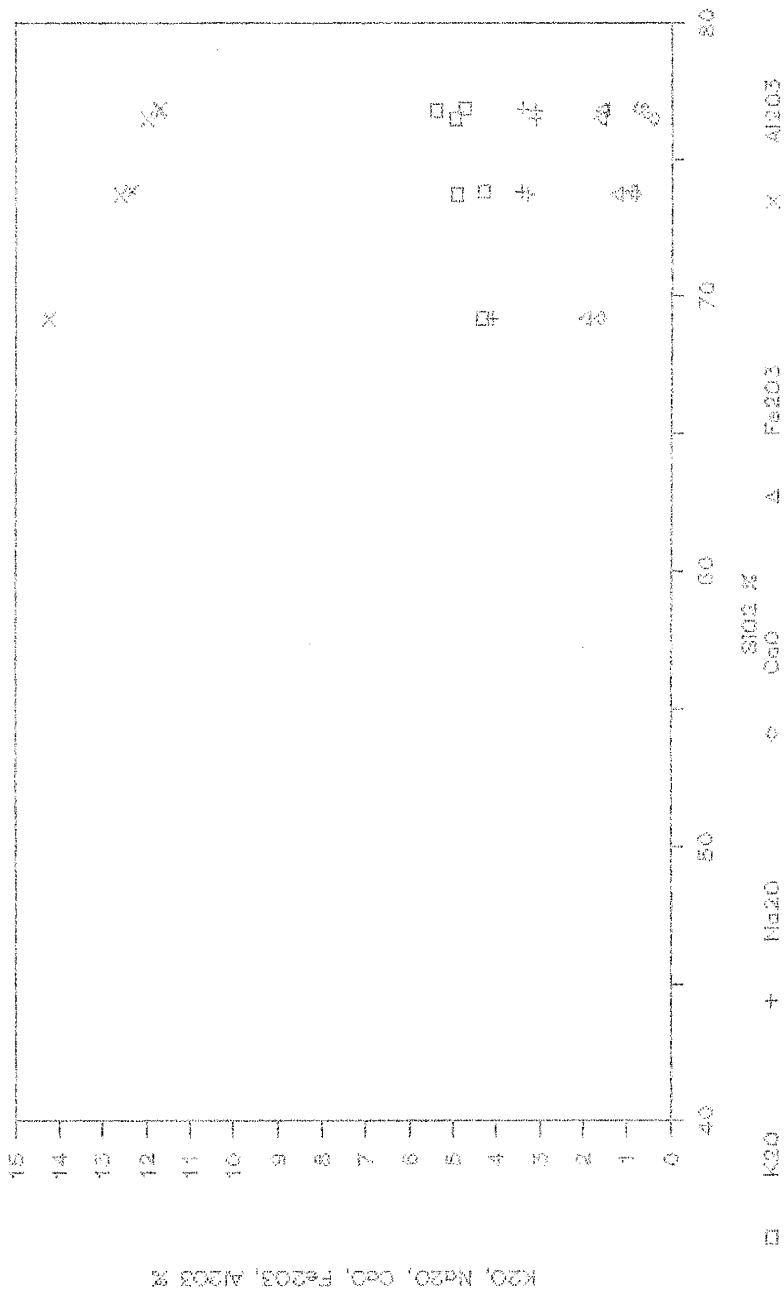
K2O, Na2O, CaO, Fe2O3, Al2O3 %
0
1
2
3
4
5
6
7
8
9
10
11
12
13
14
15
40
50
60
70
80
SiO2 %
□ K2O
+ Na2O
◇ CaO
△ Fe2O3
× Al2O3

Figure 43. Major-element variation diagrams for a porphyritic dike in eastern Sierra Cuchillo believed to be a feeder for the rhyolite of HOK Ranch.

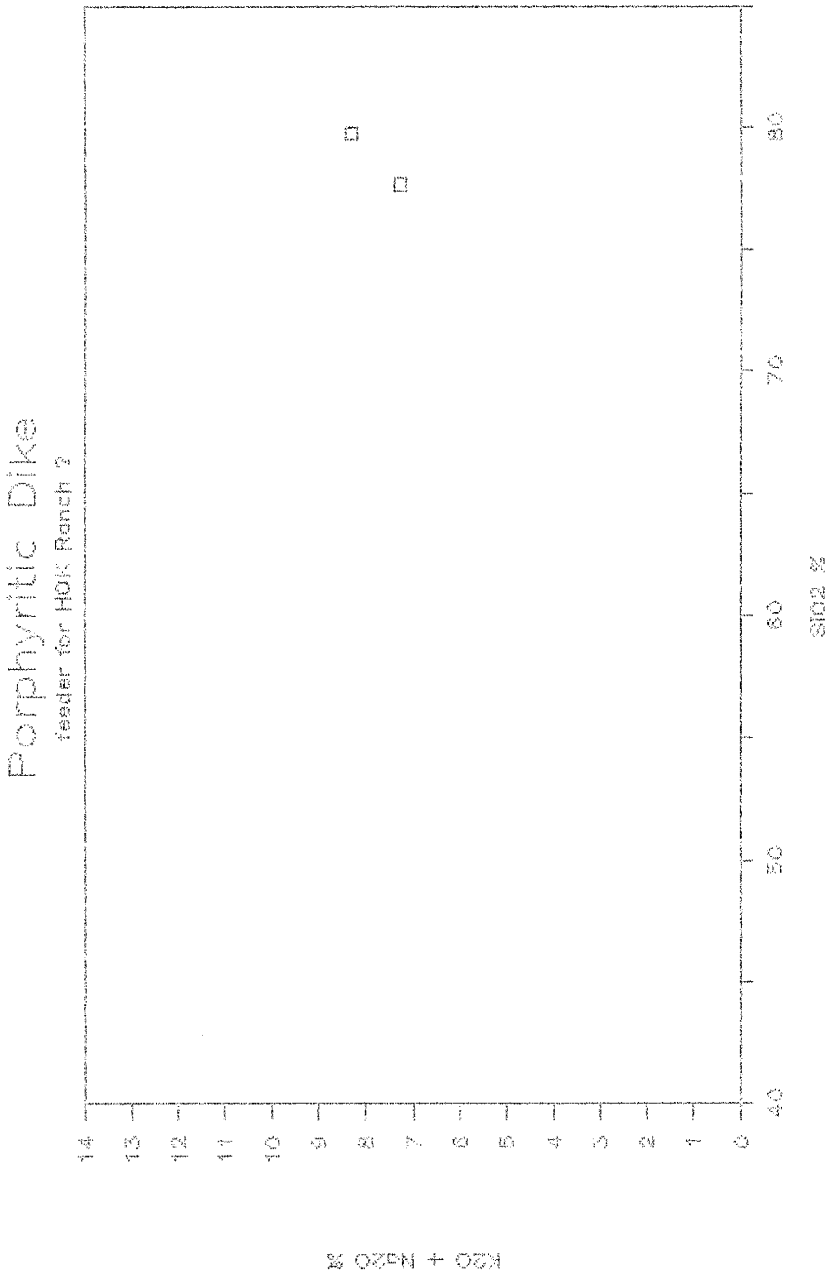
Porphyritic Dike
Feeder for HOK Ranch ?
K2O + Na2O %
SiO2 %
14
13
12
11
10
9
8
7
6
5
4
3
2
1
0
40
50
60
70
80
90

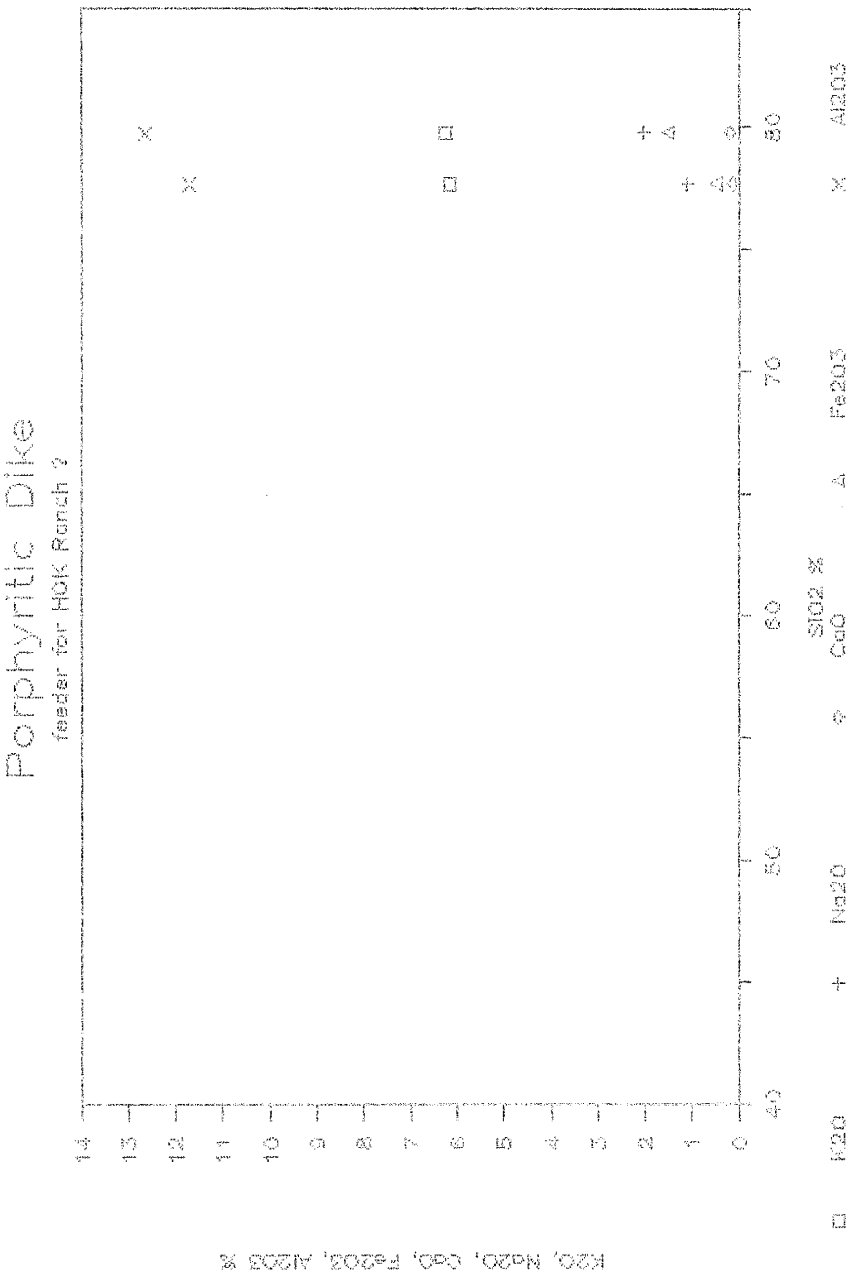
Porphyritic Dike
feeder for Hok Ranch ?
K2O, Na2O, CaO, Fe2O3, Al2O3 %
SiO2 %
40
50
60
70
80
0
1
2
3
4
5
6
7
8
9
10
11
12
13
14
K2O
Na2O
CaO
Fe2O3
Al2O3

unnamed ash-flow tuff

A multiple-flow, crystal-poor, moderately pumice-rich, nonwelded ash-flow tuff crops out directly beneath Taylor Creek in a small tributary to Scales Canyon and along the western edge of Burnt Cabin Flats in sec. 30, T. 10 S., R. 10 W. This tuff is as much as 30 m thick with its base not exposed, and consists of a 10-m-thick, massive pyroclastic-flow unit overlain by numerous, thin pyroclastic-flow units. Phenocryst content consists of approximately 5 % sanidine, and trace amounts of plagioclase. Dark-gray to black pumice contrasts in color with a tan to light-gray groundmass. The only known exposure is restricted to a few hundred square meters, thus precluding correlation with other units.

Taylor Creek Rhyolite

Taylor Creek Rhyolite is the name given by Elston (1968) to group of time-equivalent, chemically similar, high-silica rhyolite lavas that occur along the western flank of north-central Black Range. Type exposure is along Taylor Creek, east of Wall Lake in S1/2 sec. 2, T. 11 S., R. 12 W. This unit encompasses as many as twenty separate flow-dome complexes and associated extrusive lavas that crop out over an area of approximately 800 km2 near the geographic center of Mogollon-Datil volcanic field (Duffield et al., 1987).

In addition to similar age and chemical relationships, all Taylor Creek Rhyolite occurrences are characterized by anomalous tin content and associated high-temperature (>700 deg. C), hydrothermal tin mineralization (Eggleston, 1987; Duffield et al., 1987). It has been interpreted that all Taylor Creek Rhyolite flow-dome complexes were fed from a single reservoir of magma (Eggleston, 1987; Duffield et al., 1987).

Numerous studies have been devoted to geology and geochemistry of Taylor Creek Rhyolite, primarily because of associated tin mineralization. Reference is given to following articles for detailed reports: Duffield (1989), Duffield et al. (1987), Du Bray and Duffield (1987), Eggleston (1987), Eggleston and Norman (1983, 1986), Lawrence and Richter (1986), Richter et al. (1986a & b), Maxwell et al. (1986), Foord et al. (1985), Harvey (1985), Lawrence (1985), Ratte' et al. (1984), Correa (1981), Boerold (1981), Richter (1978), Coney (1976), Fries et al. (1972), Lufkin (1972, 1976, 1977), Volin et al. (1947), Fries and Butler (1943), and Fries (1940).

Stratigraphically, Taylor Creek Rhyolite is the youngest rhyolite lava in north-central Black Range. It overlies unnamed, genetically related, vent-clearing pyroclastic deposits, as well as Vicks Peak Tuff, La Jencia Tuff, and rhyolite of Dolan Peak; it is overlain by tuff of Garcia Camp, sandstone of Inman Ranch, and the regionally extensive Bloodgood Canyon Tuff and Shelley Peak Tuff (Eggleston,

1987; Eggleston and Norman, 1986; Eggleston and Harrison, in review). A mean 40Ar/39Ar age of 28.2 Ma was determined fron seven samples of Taylor Creek Rhyolite by Dalrymple and Duffield (1988). This age is in good agreement with constraints provided by 40Ar/39Ar dating of McIntosh (1989), 28.1 Ma for overlying tuff of Garcia Camp, 28.6 Ma for underlying Vicks Peak Tuff, but it indicates that previously reported conventional K-Ar ages for Taylor Creek Rhyolite by Elston et al. (1973), Ratte' et al. (1984), and Maxwell et al. (1986) are in error and much too young (range fron 24.6-27.3 Ma). The 40Ar/39Ar analyses of Dalrymple and Duffield (1988) indicate that various flow-domes complexes of Taylor Creek Rhyolite erupted over an interval of approximately 0.1 m.y. or less.

Typically, Taylor Creek Rhyolite is a moderately crystal-rich to crystal-rich, flowbanded rhyolite lava. Phenocryst contents vary from 15-35 % and include quartz and sanidine, minor plagioclase, and rare biotite and hornblende. Quartz and sanidine are euhedral to subhedral, commonly embayed, and occur in subequal amounts. Groundmass texture is granophyric with rare spherulitic intervals. Both sanidine and plagioclase are typically glomero-porphyritic. Vapor-phase mineralization is common in Taylor Creek Rhyolite, varying from mild to pervasive in intensity. A detailed study of vapor-phase mineralization and its relationship to tin mineralization in Taylor Creek Rhyolite is provided by Eggleston (1987).

Taylor Creek Rhyolite is chemically a high-silica rhyolite with silica contents generally from 76-78 %, Duffield (1989) reports a mean silica content of 77.82 % from 17 analyses. Major-element compositions are very uniform, with only titanium exhibiting any systematic variation (Eggleston, 1987). Table 16 lists major-element analyses for Taylor Creek Rhyolite from Eggleston (1987), Figure 44 presents major element variation diagrams. Note that analyses are quite similar for all samples, regardless of degree of vapor-phase crystallization. Figure 45 compares the chemical composition of a representative sample of Taylor Creek Rhyolite to the average rhyolite of Le Maitre (1976) and the average low-Ca granite of Turekian and Wedepohl (1963). This diagram shows enrichment of SiO2, Rb, and other lithophile elements, and marked depletion of CaO, Fe2O3, Sr, and Ba. This pattern is characteristic of all Taylor Creek Rhyolite (Eggleston, 1987).

pryoclastic rocks associated with Taylor Creek Rhyolite

Pyroclastic deposits believed to be associated with Taylor Creek Rhyolite appear to be widespread in the Taylor Creek area, but are widely separated and nowhere voluminous. These deposits consist of high-silica rhyolite, pyroclastic flow, fall, and surge deposits. Correlations of these deposits with Taylor Creek Rhyolite are tenuous and are not accepted by all workers in the region (W. Duffield, 1986,

Table 16. Major-element analyses for Taylor Creek Rhyolite.

	1	2	3	4	5	6	7	8	9
SiO2	77.05	76.53	74.54	76.71	76.82	77.22	77.84	76.57	76.58
Al2O3	11.72	11.72	12.33	11.94	11.37	11.84	11.71	12.25	12.23
Fe2O3	1.10	1.10	1.17	1.08	1.03	1.10	1.06	1.14	1.14
MgO	.28	<.01	.13	.24	.34	.22	.20	.18	.22
CaO	.46	.18	.40	.23	.46	.30	.26	.30	.27
Na2O	3.16	3.55	3.74	3.53	3.64	3.64	3.42	3.50	3.41
K2O	4.71	4.82	4.69	5.04	4.80	4.94	5.14	5.19	5.19
TiO2	.12	.11	.09	.11	.16	.16	.14	.17	.15
P2O5	.02	.02	.01	.02	.02	.01	.01	.01	.02
MnO	.05	.05	.06	.05	.06	.05	.05	.07	.06
LOI	0.84	.69	2.36	.56	.48	.31	.15	.34	.40
Total	99.51	99.46	99.20	99.51	99.18	99.79	99.98	99.72	99.59

1) Taylor Creek Rhyolite, Nugget Gulch, sec. 28, T. 9 S., R. 10 W., 33-29'-39"N, 107-52'-35" W, moderate vapor-phase crystalization, Eggleston (1987).
2) Taylor Creek Rhyolite, Paramount Canyon, sec. 12, T. 10 S., R. 11 W, 33-26'-57"N, 107-56'-19"W, intense vapor phase crystalization, Eggleston (1987).
3) Taylor Creek Rhyolite, Paramount Canyon, sec. 27, T. 10 S., R. 11 W., 33-25'-02"N, 107-57'-44"W, vitrophyre from carapace breccia, Eggleston (1987).
4) Taylor Creek Rhyolite, Alexander Cienega dome, sec. 1, T. 11 S., R. 11 W., 33-22'-50"N, 107-55'-54"W, relatively fresh, Eggleston (1987).
5) Taylor Creek Rhyolite, Wall Lake, sec. 2, T. 11 S., R. 12 W., 33-21'-40"N, 108-03'-35"W, moderate vapor phase crystalization, Eggleston (1987).
6) Taylor Creek Rhyolite, Indian Creek, sec. 4, T. 11 S., R. 12 W., 33-22'-57"N, 108-05'-20"W, moderate vapor phase crystalization, Eggleston (1987).
7) Taylor Creek Rhyolite, Kemp Mesa, sec. 6, T. 11 S., R 12 W., 33-22'-08"N, 108-07'-06"W, relatively fresh, Eggleston (1987).
8) Taylor Creek Rhyolite, Wall Lake, sec. 2, T. 11 S., R. 12 W., 33-21'-55"N, 108-03-30"W, moderate vapor phase crystalization, Eggleston (1987).
9) Taylor Creek Rhyolite, Wall Lake, sec. 2, T. 11 S., R. 12 W., 33-21'-52"N, 108-03'-45"W, intense vapor phase crystalization, Eggleston (1987).

	10	11	12	13	14	15	16	17	18
SiO2	77.84	77.89	75.67	75.98	76.04	76.27	76.33	76.33	76.40
Al2O3	11.04	11.66	12.56	12.00	12.07	12.12	11.64	12.71	12.04
Fe2O3	1.02	1.11	1.14	1.04	1.03	1.19	1.10	1.16	1.06
MgO	.24	.16	.32	.23	.21	.17	.17	.32	.23
CaO	.45	.46	.33	.36	.27	.34	.38	.31	.31
Na2O	2.85	3.46	3.29	3.67	3.41	3.43	3.53	3.56	3.40
K2O	4.93	4.74	5.33	5.22	4.84	4.96	4.74	4.97	4.84
TiO2	.15	.03	.13	.15	.13	.12	.12	.12	.13
P2O5	.01	.02	.01	.01	.02	.02	.01	.02	.01
MnO	.07	.06	.05	.06	.06	.06	.06	.07	.06
LOI	1.00	.65	.76	.49	.42	.48	.35	.42	.31
Total	99.60	100.34	99.59	99.21	98.50	99.16	99.43	99.99	98.79

10) Taylor Creek Rhyolite, Wall Lake, sec. 2, T. 11 S., R. 12 W., 33-22'-28"N, 108-03'-29"W, moderate vapor phase crystallization, Eggleston (1987).
11) Taylor Creek Rhyolite, Wall Lake, sec. 2, T. 11 S., R. 12 W., 33-21'-51"N, 108-03'-45"W, intense vapor phase crystallization, Eggleston (1987).
12) Taylor Creek Rhyolite, Wall Lake, sec. 2, T. 11 S., R. 12 W., 33-21'-35"N, 108-03'-57"W, fresh lava from nargin of Kemp Mesa dome, Eggleston (1987).
13) Taylor Creek Rhyolite, Kemp Mesa, sec. 5, T. 11 S., R. 12 W., 33-21'-54"N, 108-06'-40"W, moderate vapor phase crystallization, Eggleston (1987).
14) Taylor Creek Rhyolite, Kemp Mesa, 118' of drill hole by D. Fowler, sec. 5, T. 11 S., R. 12 W., 33-21'-54"N, 108-06'-42"W., Eggleston (1987).
15) Taylor Creek Rhyolite, Kemp Mesa, sec. 5, T. 11 S., R. 12 W., 33-21'-35"N, 108-03'-57"W, intense vapor phase crystallization, Eggleston (1987).
16) Taylor Creek Rhyolite, Kemp Mesa, 302' of drill hole by D. Fowler, sec. 5. T11 S., R. 12 W., 33-21'-54"N, 108-06'-35"W, Eggleston (1987).
17) Taylor Creek Rhyolite, 74' mark of above, Eggleston (1987).
18) Taylor Creek Rhyolite, 191' mark of above, Eggleston (1987).

	19	20	21	22	23	24	25	26
SiO2	76.50	76.72	76.73	76.85	76.97	77.43	77.60	77.64
Al2O3	12.14	12.23	12.01	12.04	12.03	12.22	11.88	12.59
Fe2O3	1.04	1.38	1.11	1.06	1.01	1.15	1.30	1.10
MgO	.18	.26	.22	.20	.34	.28	.32	.07
CaO	.26	.17	.39	.35	.25	.34	.33	.30
Na2O	3.44	3.69	3.43	3.36	3.69	3.13	3.22	3.58
K2O	4.99	5.24	4.96	4.84	5.24	5.45	4.71	5.06
TiO2	.13	.15	.13	.12	.15	.16	.16	.15
P2O5	.02	.02	.01	.02	.03	.02	.03	.01
MnO	.06	.09	.06	.08	.05	.11	.06	.07
LOI	.42	.67	.48	.60	.12	.77	.85	.39
Total	99.18	100.62	99.53	99.52	99.88	101.06	100.46	100.96

19) Taylor Creek Rhyolite, Kemp Mesa, 52' mark of drill hole by D. Fowler, sec. 5, T. 11 S., R. 12 W., 33-21'-54"N, 108-06'-42"W, Eggleston (1987).
20) Taylor Creek Rhyolite, Kemp Mesa, sec. 5, T. 11 S., R. 12 W., 33-21'-53"N, 108-06'-40"W, intense vapor phase crystallization, Eggleston (1987).
21) Taylor Creek Rhyolite, Kemp Mesa, 270' mark of drill hole by D. Fowler, same location as # 19, Eggleston (1987).
22) Taylor Creek Rhyolite, Kemp Mesa, 191' mark of drill hole by D. Fowler, Eggleston (1987).
23) Taylor Creek Rhyolite, Kemp Mesa, sec. 6, T. 11 S., R. 12 W., 33-21'-57"N, 108-07'-06"W, mild vapor phase crystallization, Eggleston (1987).
24) Taylor Creek Rhyolite, Wall Lake, sec. 3, T. 11 S., R. 12 W., 33-21'-33"N, 108-04'-30"W, intense vapor phase crystallization, Eggleston (1987).
25) Taylor Creek Rhyolite, Wall Lake, sec. 10, T. 11 S., R. 12 W., 33-20'-57"N, 108-04'-57"W, intense vapor phase crystallization, Eggleston (1987).
26) Taylor Creek Rhyolite, Indian Creek, sec. 32, T. 10 S., R. 12 W., 33-24'-16"N, 108-05-30"W, moderate vapor phase crystallization, Eggleston (1987).

	27	28	29	30	31
SiO2	76.26	76.39	76.40	76.67	77.10
Al2O3	11.57	11.95	11.87	12.00	11.39
Fe2O3	1.23	1.17	1.07	1.21	1.22
MgO	<.01	.02	.01	<.01	.07
CaO	.55	.23	.25	.17	.17
Na2O	3.39	3.66	3.63	3.82	3.12
K2O	4.90	4.87	4.84	4.90	4.92
TiO2	.14	.11	.11	.10	.14
P2O5	.02	.01	.01	.01	.03
MnO	.06	.05	.04	.05	.04
LOI	.33	.26	.21	.04	.58
Total	98.44	98.72	98.44	98.97	98.78

27) Taylor Creek Rhyolite, Indian Peaks, sec. 19, T. 8 S., R. 11 W., 33-36'-21"N, 108-01'-37"W, moderate vapor phase crystallization, Eggleston (1987).
28) Taylor Creek Rhyolite, Indian Peaks, sec. 33, T. 8 S. R. 11 W., 33-33'-49"N, 108-00'-07"W, relatively fresh, Eggleston (1987).
29) Taylor Creek Rhyolite, Indian Peaks, sec. 6, T. 9 S., R. 11 W., 33-33'-16"N, 108-00'-38"W, relatively fresh, Eggleston (1987).
30) Taylor Creek Rhyolite, Indian Peaks, sec. 33, T. 8 S., R. 11 W., 33-34'-16"N, 107-59'-26"W, fresh, Egglestion (1987).
31) Taylor Creek Rhyolite, Indian Peaks, sec. 31, T. 8 S. R. 11 W., 33-34'-14"N, 108-00'-26"W, moderate vapor phase crystallization, Eggleston (1987).

Figure 44. Major-element variation diagrams for the Taylor Creek Rhyolite.

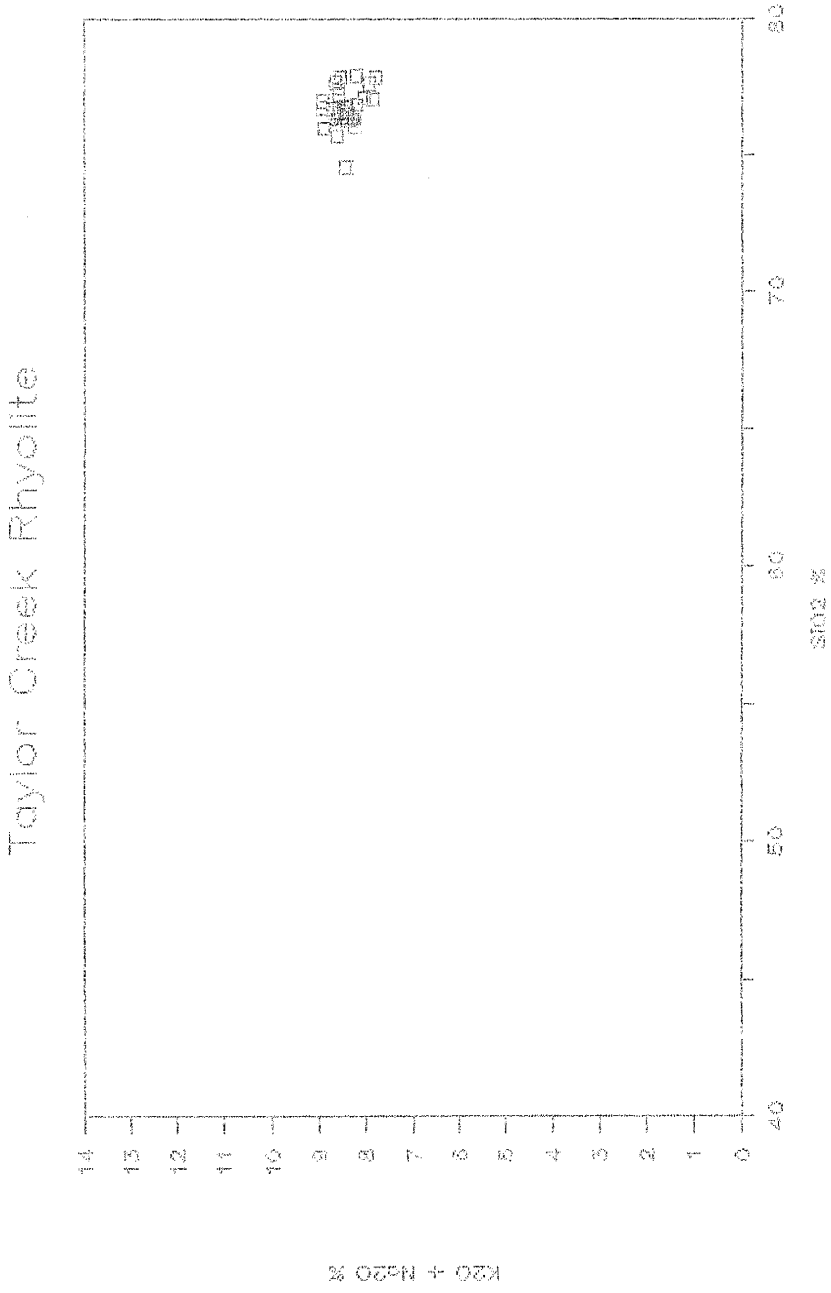
Taylor Creek Rhyolite
K2O + Na2O %
SiO2 %
14
13
12
11
10
9
8
7
6
5
4
3
2
1
0
40
50
60
70
80

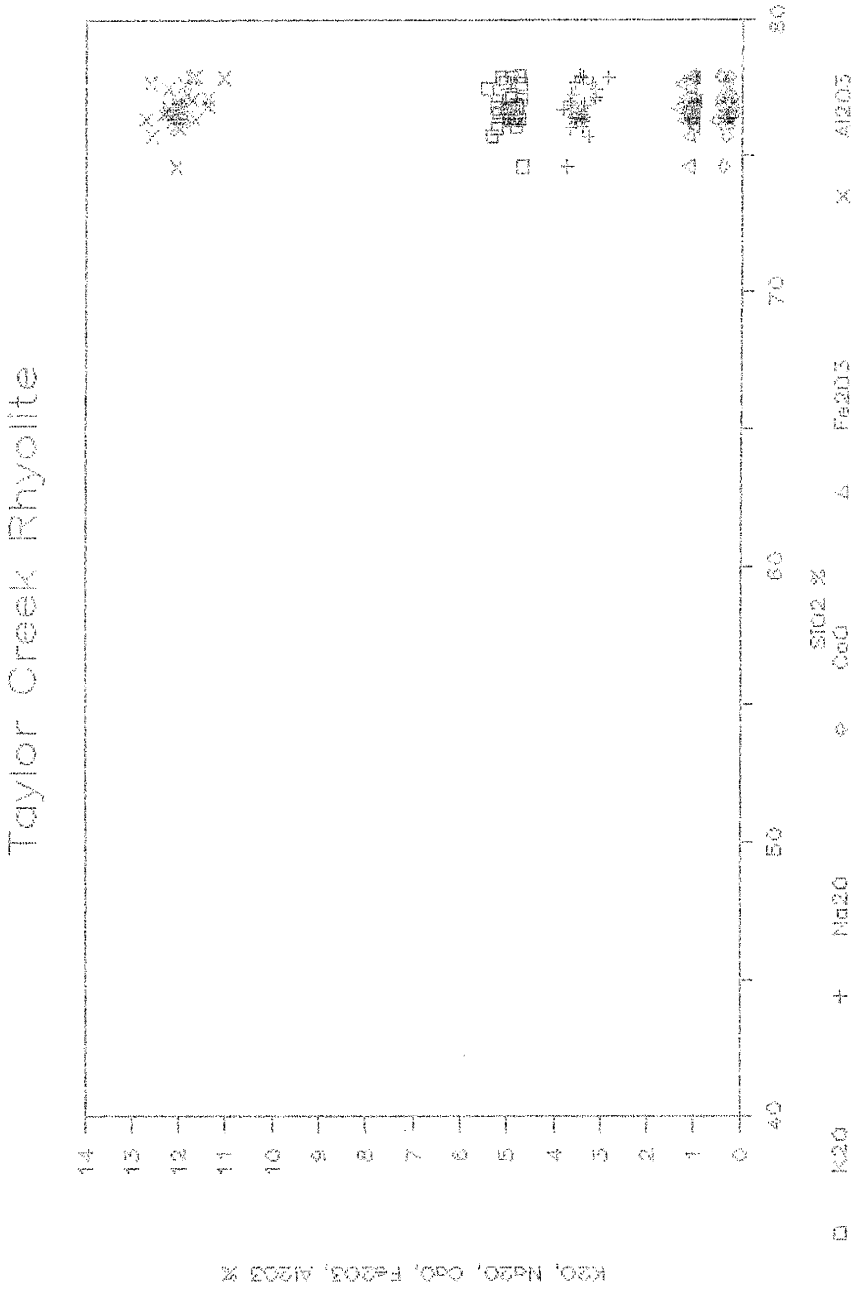
Taylor Creek Rhyolite
K2O, Na2O, CaO, Fe2O3, Al2O3 %
SiO2 %
K2O
Na2O
CaO
Fe2O3
Al2O3
40
50
60
70
80
0
1
2
3
4
5
6
7
8
9
10
11
12
13
14

Figure 45. Enrichment-depletion diagram for typical Taylor Creek Rhyolite. Major elements are compared to average rhyolite of Le Maitre (1976); trace elements are compared to Turekian and Wedepohl's (1961) average low-Ca granite.

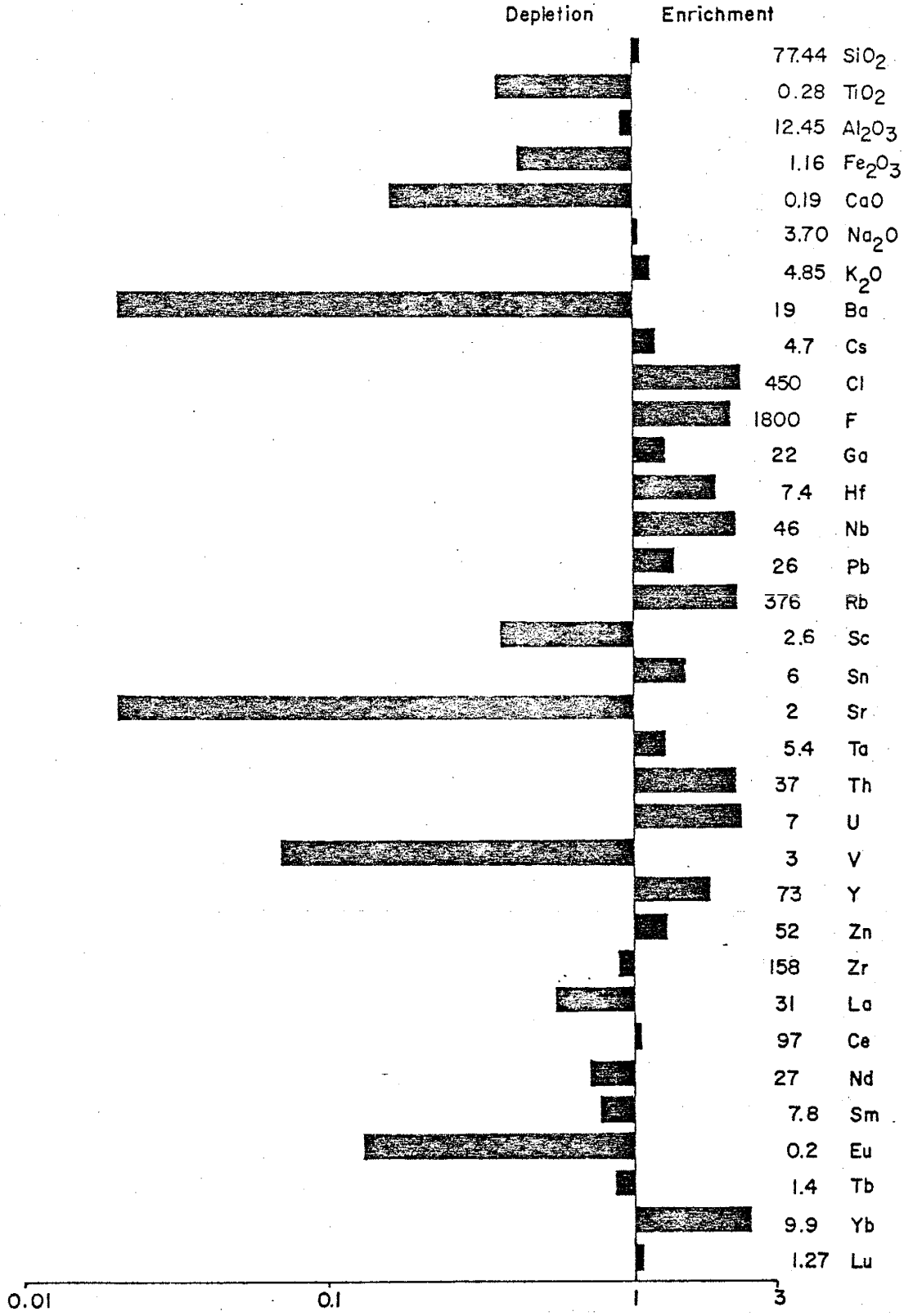
Depletion
Enrichment
77.44 SiO2
0.28 TiO2
12.45 Al2O3
1.16 Fe2O3
0.19 CaO
3.70 Na2O
4.85 K2O
19 Ba
4.7 Cs
450 Cl
1800 F
22 Ga
7.4 Hf
46 Nb
26 Pb
376 Rb
2.6 Sc
6 Sn
2 Sr
5.4 Ta
37 Th
7 U
3 V
73 Y
52 Zn
158 Zr
31 La
97 Ce
27 Nd
7.8 Sm
0.2 Eu
1.4 Tb
9.9 Yb
1.27 Lu
0.01
0.1
1
3

oral commun.).

Ignimbrites are the most common and most voluminous of these pyroclastic deposits. They typically underlie and mantle most of the rhyolite domes in the Taylor Creek region, and consist of individual 0.5-to-2.0-m thick flow units stacked to thicknesses of as much as 80 m. Lithic fragments found within iginimbrites are Taylor-Creek-like lavas. Many of the ignimbrites display vertical zoning similar to that described by Sparks et al. (1973) and Fisher and Schminke (1984).

Kyle et al. (1986) describe five measured sections of such deposits that crop out in Scales Canyon on the eastern flank of Boiler Peak dome. The well-exposed outcrops at this locality were visited by the Fall 1986 New Mexico Geological Society Field Conference (see Stop 4, Osburn et al., 1986). Three eruptive sequences are recognized there: a lower, predominantly pyroclastic-flow and surge sequence, a middle pryoclastic-fall sequence, and an upper, coarse pyroclastic breccia sequence (Kyle et al., 1986).

Agglutinate deposits derived from felsic fire-fountain eruptions have been recognized north of Nugget Gulch and in the northwest wall of Paramount Canyon by Eggleston (1987) and Duffield (1989). These deposits consist of large, flattened vitric and devitrified clasts contained within a matrix of coarse ash. Clasts appear to be nonvesiculated juvenile magma that was emplaced hot enough to flatten, lengths are typically five times greater than thicknesses.

These deposits are thoroughly welded and locally welding is dense enough to impart a rheomorphic aspect to the material. Mode of eruption and emplacement is believed to be similar to that of piperno deposits found in Italy and described by Fisher and Schminke (1984).

rhyolite of Willow Springs Draw

Rhyolite of Willow Springs Draw is an informal name first used by Osburn et al. (1986) for the uppermost rhyolite lava found in the volcanic section of eastern Sierra Cuchillo. Type section is along Willow Springs Draw in sec. 31, T. 11 S., R. 6 W, where as much as 200 m of this unit overlies rhyolite of HOK Ranch and is overlain by basal deposits of Santa Fe Group. Eggleston (1987) describes two trachyte lava flows (domes ?) that occur between rhyolite of HOK Ranch and rhyolite of Willow Springs Draw immediately south of Willow Springs Draw. Rhyolite of Willow Springs is correlative to the upper member of the coarse-moonstone-porphyritic rhyolite tuff unit of Heyl et al. (1983), who report a 27.8 $\pm$ 1.0 Ma age (fission-track method on zircon). In terms of stratigraphic position, age determinations, phenocryst content, whole-rock chemistry, widespread vapor-phase crystallization, and associated tin mineralization, rhyolite of Willow Springs Draw is extremely similar to Taylor Creek Rhyolite (Eggleston, 1987).

Rhyolite of Willow Spring Draw is a crystal-rich, rhyolite lava that characteristically displays mild to intense vapor-phase crystallization. Tin occurrences are similar to those found in Taylor Creek Rhyolite (Eggleston, 1987). Phenocryst contents of rhyolite of Willow Springs Draw are approximately 15 % rounded and embayed quartz, 10 % euhedral to subhedral sanidine, 0.3 % biotite, 0.2 %

plagioclase, and trace amounts of zircon and opaque oxides. The groundmass is granphyric in texture. Locally, intense vapor-phase crystallization has produced bleached, porous rock from a normally dense material.

Rhyolite of Willow Springs Draw is chemically a high-silica rhyolite. Major-element analyses for this unit are listed in Table 17; variation diagrams are presented in Figure 46.

tuff of Garcia Camp

Tuff of Garcia Camp is an informal name used by Lawrence and Richter (1986) for a poorly welded, moderately crystal-rich, multiple-flow ash-flow tuff that crops out in the Indian Peaks area. At Indian Peaks, tuff of Garcia Camp underlies Taylor Creek Rhyolite (Lawrence and Richter, 1986). Based on similar lithology, a multiple-flow ash-flow tuff unit that overlies the Boiler Peak dome of Taylor Creek Rhyolite was tentatively correlated with tuff of Garcia Camp by Eggleston (1987). These rocks in the Boiler Peak area were dated by 40Ar/39Ar at 28.10 Ma (McIntosh, 1989). A mean 40Ar/39Ar laser-fusion age of 28.21 $\pm$ 0.4 Ma for sanidine from tuff of Garcia Camp at Indian Peaks was determined by Dalrymple and Duffield (1988). Paleomagnetic site-mean directions from tuff of Garcia Camp at both localities are tightly grouped, indicating eruption occurred over a brief time interval.

Table 17. Major-element analyses for rhyolite of Willow Springs Draw in eastern Sierra Cuchillo.

	1	2	3	4	5	6	7
SiO2	75.50	76.47	76.66	76.72	76.73	76.81	76.94
Al2O3	12.60	12.28	12.12	11.68	11.85	12.10	12.09
Fe2O3	1.28	1.12	1.21	1.14	1.18	1.21	1.20
MgO	.25	.21	.48	.24	.26	.23	.20
CaO	.34	.31	.47	.66	.26	.41	.42
Na2O	3.30	3.45	2.79	3.24	3.12	3.37	3.20
K2O	5.36	5.16	5.00	5.10	5.22	5.10	5.18
TiO2	.18	.15	.16	.17	.15	.15	.15
P2O5	.02	.02	.02	.06	.02	.02	.03
MnO	.06	.06	.06	.04	.06	.06	.06
LOI	.55	.51	.95	.85	.48	.38	.38
Total	99.44	99.74	99.92	99.90	99.33	99.84	99.85

1) Rhyolite of Willow Springs Draw, Monticello Cutoff Road, sec. 31, T. 11 S, R. 6 W., 33-18'-54"N, 107-30'-13"W, Eggleston (1987).
2) Rhyolite of Willow Springs Draw, Monticello Cutoff Road, sec. 31, T. 11 S., R. 6 W., 33-18'54"N, 107-30'-13"W, Eggleston (1987).
3) Rhyolite of Willow Springs Draw, Monticello Cutoff Road, sec. 31, T. 11 S., R. 6 W., 33-18'-33"N, 107-29'-25"W, Eggleston (1987).
4) Rhyolite of Willow Springs Draw, Monticello Cutoff Road, sec. 31, T. 11 S., R. 6 W., 33-18'-09"N, 107-29'-42"W, Eggleston (1987).
5) Rhyolite of Willow Springs Draw, Monticello Cutoff Road, sec. 31, T. 11 S., R. 6 W., 33-18'-33"N, 107-29'-25"W, Eggleston (1987).
6) Rhyolite of Willow Springs Draw, Monticello Cutoff Road, sec. 31, T. 11 S., R. 6 W., 33-18'-33"N, 107-29'-25"W, Eggleston (1987).
7) Rhyolite of Willow Springs Draw, Monticello Cutoff Road, sec. 31, T. 11 S., R. 6 W., 33-18'-55"N, 107-30'-14"W, Eggleston (1987).

Figure 46. Major-element variation diagrams for rhyolite of Willow Springs Draw.

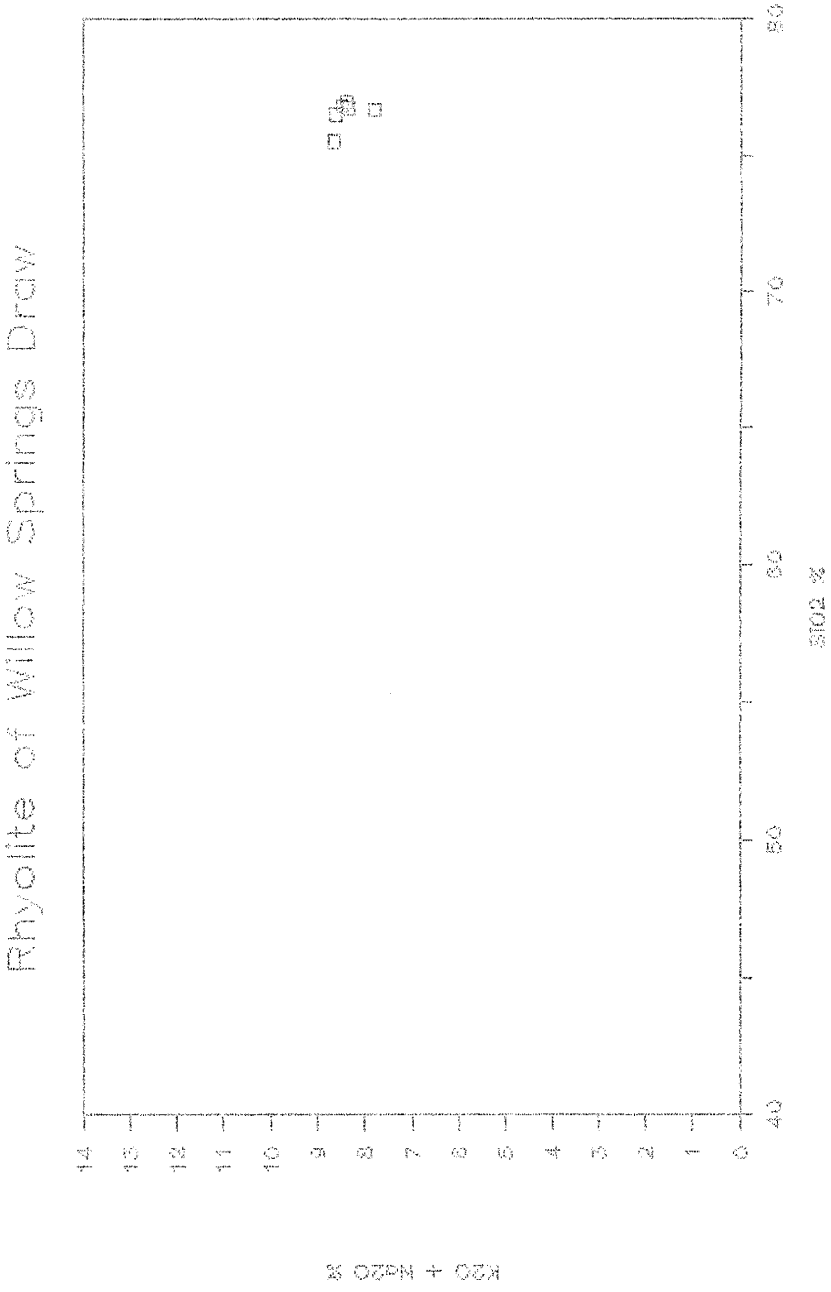
Rhyolite of Willow Springs Draw
K2O + Na2O %
SiO2 %
14
13
12
11
10
9
8
7
6
5
4
3
2
1
0
40
50
60
70
80

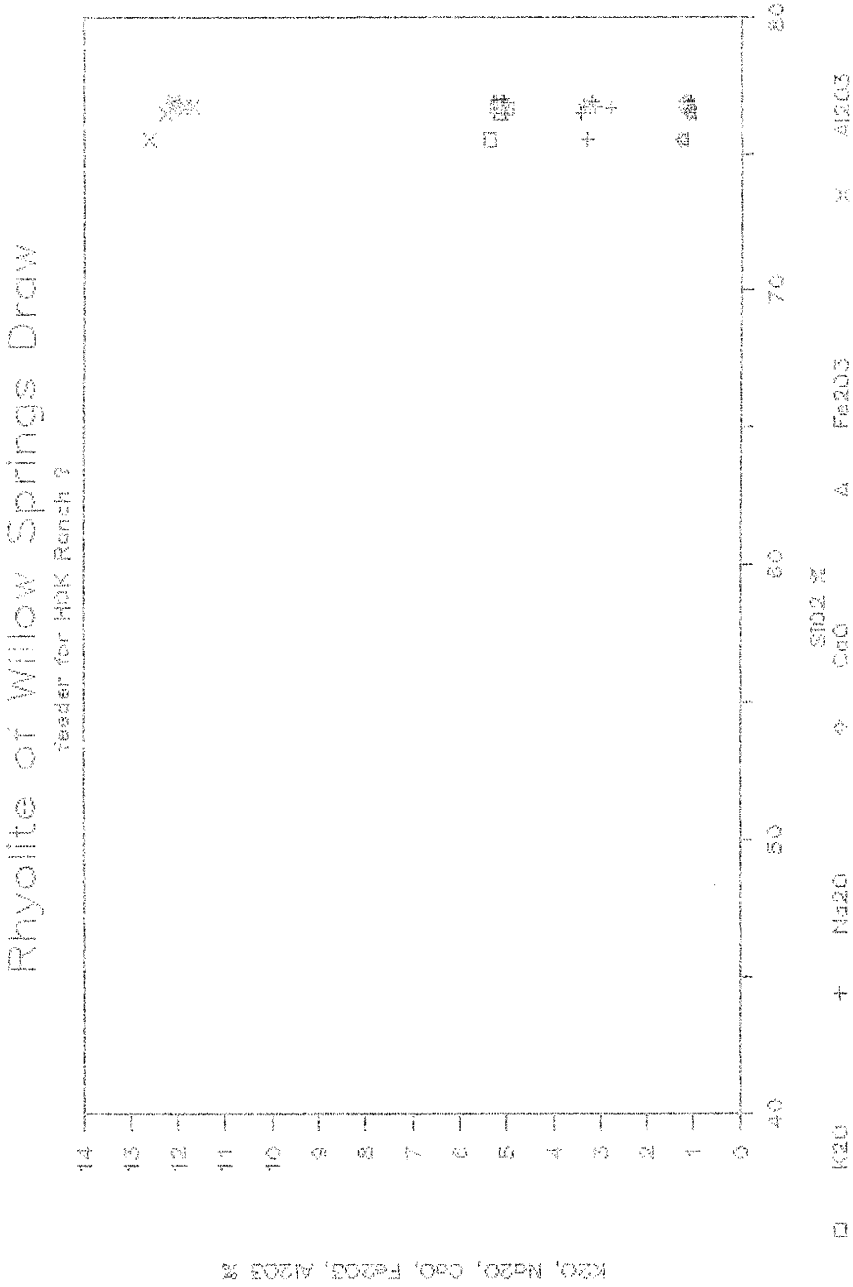
Rhyolite of Willow Springs Draw
feeder for HDK Ranch ?
K2O, Na2O, CaO, Fe2O3, Al2O3 %
SiO2 %
K2O
Na2O
CaO
Fe2O3
Al2O3

Two possible scenarios are envisioned to explain these inconsistencies in stratigraphic position and age determinations. One, rocks at both areas are correlative and separation in age dates reflects inter-laboratory calibration differences (McIntosh, 1989); stratigraphic relationships with Taylor Creek Rhyolite are the result of slight time differences between eruptive centers at Indian Peaks and Boiler Peak. Or two, rocks believed to be tuff of Garcia Camp at Indian Peaks and Boiler Peak are not correlative and represent two similar, yet distinct, units that bracketed eruption of Taylor Creek Rhyolite. This matter remains unresolved.

The unit referred to as tuff of Garcia Camp by Eggleston (1987) and Eggleston and Harrison (in review) in Taylor Creek-Sawmill Peak area consists of about 20 m of poorly welded, cliff-forming, multiple-flow, moderately crystal-rich ash-flow tuff. Phenocryst contents are approximately 10 % quartz, 6 % sanidine, 1 % biotite, and trace amounts of plagioclase, hornblende, zircon, and opaque minerals. Groundmass is typically vitroclastic, except where intense vapor-phase crystallization has produced granophyric texture with overgrowths on quartz and sanidine crystals. Chemically, tuff of Garcia Camp is a high-silica rhyolite with major-element contents very similar to those of Taylor Creek Rhyolite. Table 18 lists major-element analysis for one sample of this unit from Indian Peaks by Eggleston (1987).

Table 18. Major-element analysis for tuff of Garcia Camp.

	1
SiO2	77.20
Al2O3	11.37
Fe2O3	1.27
MgO	.12
CaO	.23
Na2O	3.48
K2O	5.01
TiO2	.16
P2O5	.02
MnO	.06
LOI	.31
Total	99.23

1) Tuff of Garcia Camp, Indian Peaks, sec. 25, T. 8 S., R. 12 W., 33-36'-03"N, 108-00'-26"W, Eggleston (1987).

Bloodgood Canyon Tuff

Bloodgood Canyon Tuff of Elston (1968) occurs in limited outcrops restricted to cusps between coalescing domes of Taylor Creek Rhyolite (Eggleston, 1987). This unit is a regional, high-silica rhyolite ignimbrite that erupted from Bursum cauldron near the town of Mogollon, New Mexico (Ratte' et al., 1984). Outcrops in Taylor Creek area represent the easternmost exposures of this tuff. An average 40Ar/39Ar age of 28.05 $\pm$ .04 Ma is given by McIntosh (1989) for seven samples of Bloodgood Canyon Tuff.

In the Taylor Creek area of north-central Black Range, Bloodgood Canyon Tuff is approximately 50 m thick and contains 3 % quartz, 7 % sanidine, and trace amounts of plagioclase, biotite, sphene, zircon, and opaque oxides. These phenocrysts are set in a vitroclastic groundmass. Lithic fragments are rare to absent.

Chemical analyses by Eggleston (1987) for Bloodgood Canyon Tuff in the Taylor Creek area are listed in Table 19. Major-element variation diagrams are presented in Figure 47.

Table 19. Major-element analyses for Bloodgood Canyon Tuff in Taylor Creek area of north-central Black Range, from Eggleston (1987).

	1	2	3	4	5	6	7
SiO2	75.02	75.18	76.05	76.33	76.92	77.09	77.64
Al2O3	13.20	12.09	11.94	12.13	11.87	12.42	12.42
Fe2O3	1.21	1.15	1.08	1.25	1.10	1.14	1.15
MgO	.29	.21	.49	.15	.23	.19	.39
CaO	.31	.71	.34	.41	.19	.43	.26
Na2O	4.25	3.78	3.31	4.04	3.48	4.07	3.84
K2O	6.05	5.30	5.13	5.16	5.08	4.99	5.06
TiO2	.21	.20	.18	.20	.18	.19	.18
P2O5	.02	.04	.01	.10	.04	.14	.02
MnO	.08	.07	.06	.08	.08	.08	.08
LOI	.55	.90	.96	.28	.59	.47	.55
Total	101.19	99.63	99.55	100.13	99.76	100.90	101.59

1) Bloodgood Canyon Tuff, Wall Lake, sec. 2, T. 11 S., R. 12 W., 33-22'-34"N, 108-03'-38"W, 40 m above base & 10 m below top of unit, Eggleston (1987).
2) Bloodgood Canyon Tuff, Wall Lake, sec. 2, T. 11 S., R. 12 W., 33-22'-34"N, 108-03'-38"W, 20 m above base of unit, Eggleston (1987).
3) Bloodgood Canyon Tuff, Wall Lake, sec. 2, T. 11 S., R. 12 W., 33-22'-34"N, 108-03'-38"W, 7 m above base of unit, Eggleston (1987).
4) Bloodgood Canyon Tuff, Railroad Canyon, sec. 22, T. 8 S., R. 12 W., 33-36'-06"N, 108-03'-14"W, base of unit, Eggleston (1987).
5) Bloodgood Canyon Tuff, Whitetail Canyon, sec. 6, T. 11 S., R. 11 W., 33-21'-43"N, 108-01'-35"W, Eggleston (1987).
6) Bloodgood Canyon Tuff, Railroad Canyon, sec. 22, T. 8 S., R. 12 W., 33-36'-06"N, 108-03'-14"W, Eggleston (1987).
7) Bloodgood Canyon Tuff, Railroad Canyon, sec. 22, T. 8 S., R 12 W., 33-36'-06"N, 108-03'-14"W, Eggleston (1987).

Figure 47. Major element variation diagrams for Bloodgood Canyon Tuff.

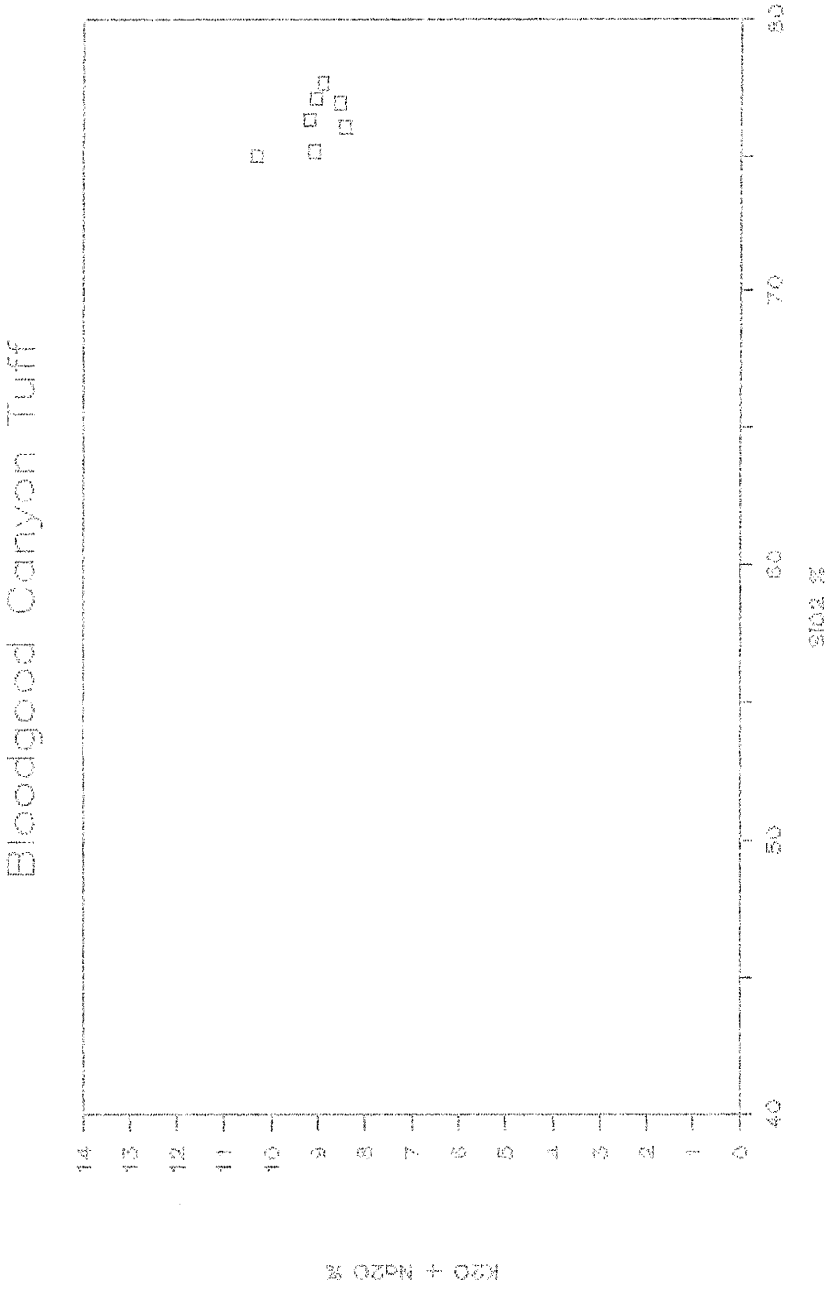
Bloodgood Canyon Tuff
SiO2 %
K2O + Na2O %
40
50
60
70
80
0
1
2
3
4
5
6
7
8
9
10
11
12
13
14

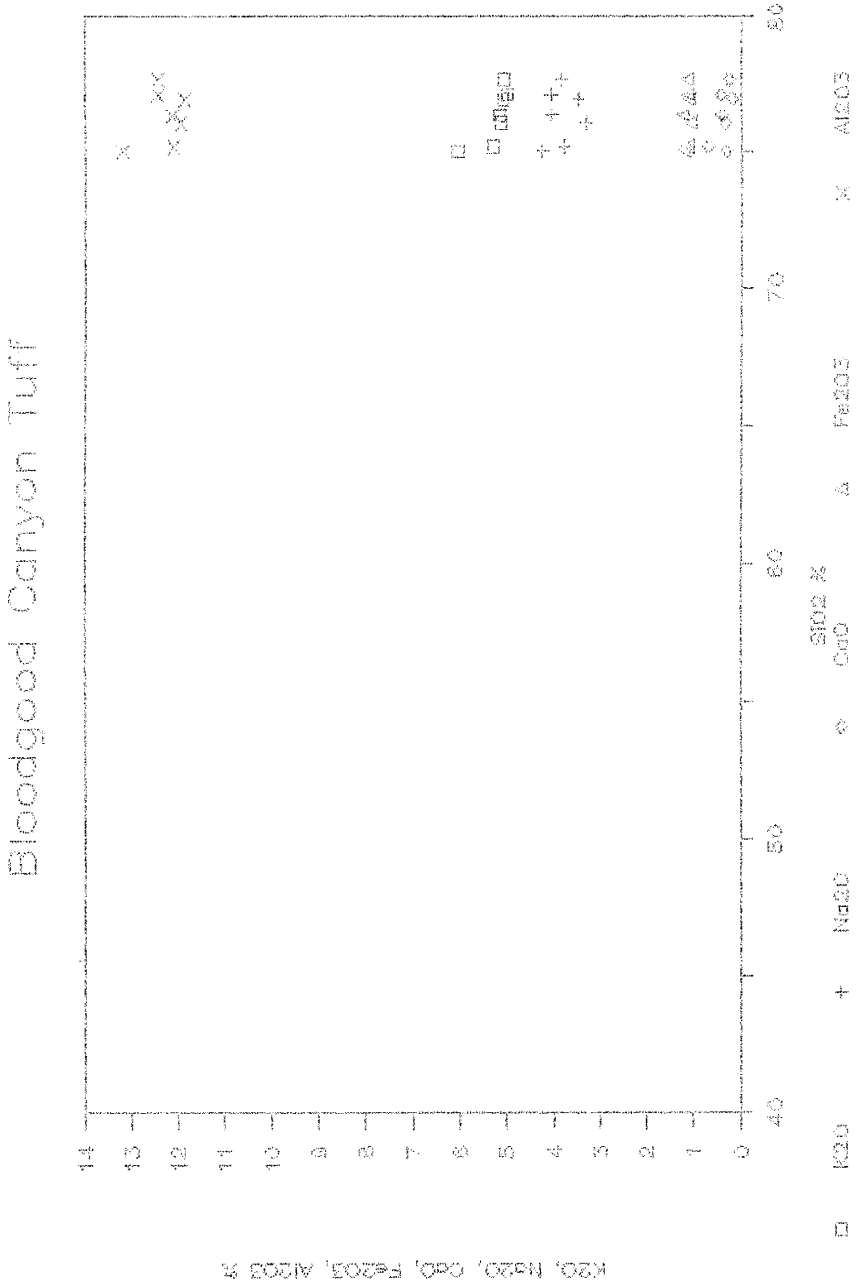
Bloodgood Canyon Tuff
K2O, Na2O, CaO, Fe2O3, Al2O3 %
SiO2 %
K2O
Na2O
CaO
Fe2O3
Al2O3

sandstone of Inman Ranch

Sandstone of Inman Ranch is the informal name proposed by Eggleston (1987) for tuffaceous siltstone, sandstone, and minor conglomerate deposits occurring near Inman Ranch in Stiver Canyon, sec. 31, T. 10 S., R. 10 W. At this locality, sandstone of Inman Ranch unconformably overlies Taylor Creek Rhyolite and is unconformably overlain by conglomerate deposits of Gila Group, of which sandstone of Inman Ranch is technically a basal unit. Vertebrate fossils contained within sandstone of Inman Ranch are of upper Oligocene to lower Miocene age (Tedford, 1981; 1986, written commun.).

Sandstone and siltstone deposits within this unit are poorly sorted, moderately indurated, and thinly bedded. High-angle crossbedding in well-sorted sandstone deposits near the base of this unit suggest aeolian deposition. However, most of sandstone of Inman Ranch is the product of braided stream deposition and consists of numerous, thin, finely crossbedded fluvial beds with basal scour-and-fill features. Individual paleochannels are recognized as having pebble-to-cobble-sized material concentrated along channel bottoms. Clast lithologies reflect local bedrock sources; in the lower portion of this unit, clasts of Taylor Creek Rhyolite are dominant; in its upper beds, clasts of La Jencia Tuff are dominant. Massive, poorly to non-sorted sandstone deposits with no obvious internal structures occur

locally in the upper portions of sandstone of Inman Ranch. These deposits are 0.5 to 2.0 m thick, matrix-supported, and contain abundant exotic clasts of various lithologies from 2 to 5 cm in diameter. They are possibly the product of hyperconcentrated flood flows.

Along Scales and Stiver Canyons, a 1.5- to 8-m thick, nonwelded ash-flow tuff occurs intercalated with upper beds of sandstone of Inman Ranch. This tuff consists of poorly sorted, fine- to coarse-grained ash, pumice, and lithic fragments. Similarities of paleomagnetic orientations and a 40Ar/39Ar age of 27.28 Ma lead McIntosh (1989) to conclude that this tuff is the southern distal end of South Canyon Tuff of Osburn (1978), and Osburn and Chapin (1983). South Canyon Tuff is the youngest major ignimbrite in the northeastern Mogollon-Datil volcanic field. Its source area is Mt. Withington cauldron in the northern San Mateo Mountains (McIntosh, 1989). An additional constraint on the age of the sandstone of Inman Ranch is provided by a 25.8 + 0.6 Ma K/Ar age of a mafic flow interbedded between sandstone of Inman Ranch and conglomerate beds of Gila Group near Alexander Cienega (NE1/4SW1/4, sec. 3, T. 11 S., R. 11 W.) on the west slope of north-central Black Range.

deposits similar to sandstone of Inman Ranch along South Fork of Cuchillo Negro drainage

Along the South Fork of Cuchillo Negro drainage, in

secs. 3, 9, 10, & 11, T. 12 S., R. 8 W., intercalated volcaniclastic and volcanic deposits occur that are similar in stratigraphic position and lithology to sandstone of Inman Ranch. These deposits are 25-30 m thick, rest unconformably upon tuff of Little Mineral Creek, and are overlain with angular unconformity by a thick sequence of Santa Fe Group sediments. Conglomerates and coarse-grained sandstones are the dominant volcaniclastic rock types, and are clast-supported, poorly sorted, and well indurated. Clast lithologies are heterolithic and consist of moderately well-rounded rhyolite lavas and ash-flow tuffs. Transport directions are rather chaotic, locally yielding northerly, westerly, and southwesterly directions.

These volcaniclastic beds are considered to be lower, basal deposits of the Santa Fe Group. They differ from overlying, upper Santa Fe Group deposits in that they are better indurated, coarser grained, show a greater degree of tectonic rotation (dips are generally 25-30 degrees, compared to subhorizontal dips for overlying upper Santa Fe Group deposits), and are intercalated with pyroclastic rocks.

These pyroclastic rocks consist of multiple intervals of water-laid tuffs and poorly to non-welded ash-flow tuffs. All tuffaceous beds are crystal-poor, and consist of coarse to medium ash, with common lithic fragments. The most continuous bed in this interval is an ash-flow tuff that occurs at or near the top of the sequence, and bears strong

resemblance to the South Canyon Tuff occurrence that is interbedded with sandstone of Inman Ranch and described in the previous section. Based on this resemblance, these two ash-flow tuffs are tentatively correlated with each other.

Both volcaniclastic and volcanic deposits occurring along the South Fork of Cuchillo Negro drainage have been altered by zeolitic alteration. This alteration has primarily effected tuffaceous beds within the sequence, as well as the underlying tuff of Little Mineral Creek. Some of overlying, upper Santa Fe Group sediments to north of the South Fork of Cuchillo Negro have also been altered to zeolite. To the south, upper Santa Fe Group sediments contain clasts of zeolitic-altered ash-flow tuff.

The paragenetic sequence of zeolite alteration, from scanning electron microscopy of Bowie and Barker (1986), is unaltered volcanic glass -> early smectite -> cristobalite ? -> clinoptilolite -> late smectite. Clinoptilolite occurrences have been investigated by Leonard Minerals Company, Todilto Exploration and Development Corporation, and most recently by St. Cloud Mining Company as possible economic deposits. No production has occurred to date.

While other mechanisms are considered, Bowie and Barker (1986) favor a percolation of alkaline/saline lake waters from a shallow lake as responsible for zeolitization of most rocks along the South Fork of Cuchillo Negro.
Unfortunately, erosion that is marked by the angular unconformity separating lower and upper Santa Fe Group

sediments in this area has removed an undeterminable amount of the rock record, and no lacustrine deposits are known to exist overlying this zeolitic alteration. Evidence in favor of a paleo-lake having existed in this area occurs in the extraordinarily large number of clastic dikes that are found in the vicinity of zeolitic alteration (Harrison, unpubl. data). Such occurrences are unknown elsewhere in the north-central Black Range.

Santa Fe Group-Gila Conglomerate

The Santa Fe Group generally includes all upper Cenozoic basin-fill deposits related to the Rio Grande rift (Kottlowski, 1953; Hawley et al., 1969; Galusha and Blick, 1971; Lucas and Ingersoll, 1981). Gila Conglomerate (or Gila Group), first used by Gilbert (1875), is correlative to the Santa Fe Group but is restricted geographically to drainages of the Gila and Mimbres Rivers, New Mexico and Arizona (Elston, 1976). The boundary between these two units is arbitrary. In north-central Black Range, this report considers the Continental Divide to be the dividing line, with Gila Conglomerate occurring to the west, Santa Fe Group occurring to the east.

Santa Fe Group deposits in the vicinity of north-central Black Range are restricted to Winston graben, where they have been down-faulted and preserved. Along both margins of Winston graben, sediments of Santa Fe Group are in fault contact with older Tertiary volcanic and Paleozoic rocks. Santa Fe Group sediments within Winston graben have been informally referred to as "Winston beds" by Jahns (1955) and Chapin et al. (1978). Jahns (1955) notes that "Winston beds" can be traced southward into the type section of informal "Palomas gravel" of Gordon and Graton (1907), Gordon (1910), Harley (1934), Kottlowski (1953, 1955). Lozinsky and Hawley (1986) formally defined "Palomas gravel" as Palomas Formation, but did not include "Winston beds"

within this unit. Exploration drilling in the Winston graben just west of Iron Mountain, secs. 3 & 10, T. 10 S., R. 8 W., penetrated as much as 660 m of "Winston beds" (P. Willard, 1986 personal commun.). Geophysical data of Ericksen et al. (1970) suggests that these deposits thicken northward.

Age of the "Winston beds" of the Santa Fe Group range from late Oligocene to Quaternary. As described in the previous section, lower Santa Fe Group sediments are intercalated with late Oligocene ash-flow tuff units along the South Fork of Cuchillo Negro Creek. In the vicinity of Winston townsite, a basaltic andesite flow dated at 18.3 $\pm$ 0.4 Ma by Seager et al. (1984) (Winston andesite member of Bearwallow Mountain Formation, see next section) is intercalated with "Winston beds". Vertebrate and invertebrate fossils of early Pleistocene age have been obtained from two localities in "Winston beds" (Jahns, 1955). An olivine basalt flow that caps Table Top Mountain in eastern Winston graben unconformably overlies "Winston beds" and has a K/Ar age of 4.8 $\pm$ 0.1 Ma (Seager et al., 1984). This basalt flow lies upon a broad and extensive pediment surface that formed upon "Winston beds", as well as older volcanic rocks, in eastern Black Range. "Winston beds" have also yielded fossils of fresh-water mollusks regarded as Quaternary in age (Chapin et al., 1978).

Upper "Winston beds" of the Santa Fe Group consist of poorly consolidated, poorly sorted conglomerate and sandstone deposits with minor mudstone intervals. Clasts

are moderately well rounded and consist of heterolithic, volcanic rock types. There is a conspicuous absence of pre-Cenozoic rock types in all but extreme upper portions of the "Winston beds". Thin, discontinuous ash beds are locally interbedded with sediments.

In the Taylor Creek area, Gila Conglomerate consists of as much as 100 m of nearly flat-lying conglomerate and sandstone deposits that unconformably overlie all other rocks. Clast lithologies are of heterolithic, volcanic rock types with Taylor Creek Rhyolite dominating lower portions. No pre-Cenozoic rock tpyes are found in Gila Conglomerate of the Taylor Creek area. Conglomerate beds are generally clast supported with coarse-grained sand matrix. All deposits are poorly sorted and crudely bedded; locally, large-scale crossbeds and scour-and-fill features have developed. Induration is generally poor to moderate, however, some beds are locally cliff formers.

Much of Gila Conglomerate in the Taylor Creek area may be older than the basin-fill sediments of its type section as defined by Gilbert (1875). Elston (1976) suggests that the Gila Conglomerate spans a time interval from approximately 21 to 0.9 Ma. However, the high-level of preservation of Taylor Creek Rhyolite flow-dome complexes suggests that they were rapidly buried by deposits of the Gila Conglomerate. If the sandstone of Inman Ranch is considered a basal unit of Gila Conglomerate, then a late Oligocene lower age is demonstrated by the 27.20 Ma

40Ar/39Ar age of interbedded distal South Canyon Tuff and the 25.8 + 0.6 K/Ar age of the mafic flow that overlies sandstone of Inman Ranch near Alexander Cienega. There are no upper age constraints on the Gila Conglomerate in the Taylor Creek area.

Bearwallow Mountain Formation

Bearwallow Mountain Formation is a diachronous, complex succession of dark-colored volcanic rocks that erupted from many sources throughout Mogollon-Datil volcanic field. Its type section as given by Elston (1968) is Bearwallow Mountain in the Mogollon Mountains, sec. 11, T. 10 S., R. 18 W. Remnant, dissected stratovolcanoes of Bearwallow Mountain Formation occur at Bearwallow Mountain, West Elk Mountain, O-Bar-O Mountain, Pelona Mountain, Black Mountain, and probably Willow Mountain, Whitewater Baldy, and Mogollon Baldy (Elston, 1976). Andesite of Hodge Canyon of Ericksen et al. (1970) in southern Black Range is correlative to Bearwallow Mountain Formation.

In north-central Black Range, Bearwallow Mountain Formation occurs as numerous, widespread intrusive plugs and dikes and extrusive flows. West of the Continental Divide, flows of Bearwallow Mountain Formation rest with angular unconformity upon tuff of Diamond Creek, rhyolite of Franks Mountain, and sandstone of Inman Ranch, and are overlain by deposits of the Gila Conglomerate. East of the Continental Divide, plugs and dikes of Bearwallow Mountain Formation intrude the entire Eocene-Oligocene volcanic section. In the Winston graben, a large flow-dome complex (Winston andesite of Plate 1) occurs and its outflow is interbedded with Santa Fe Group sediments (Fig. 48). Winston andesite has been dated the by K-Ar method at 18.3 $\pm$ 0.4 Ma by Seager

Figure 48. a) Outcrop of Winston andesite (Bearwallow Mountain Formation) interbedded with sediments of Santa Fe Group in Winston graben, SE1/4 sec. 27, T. 11 S., R. 8 W., approximately 3 km south of Winston, N.M. Seager et al. (1984) report a K/Ar age of 18.3 + 0.4 Ma for a sample of this unit collected just east of Winston, N.M. Extrusive breccia deposits occur along the base of lava flow that are identical to deposits within nearby breccia pipe. b) Exposures of deposits within breccia pipe of the Winston andesite.

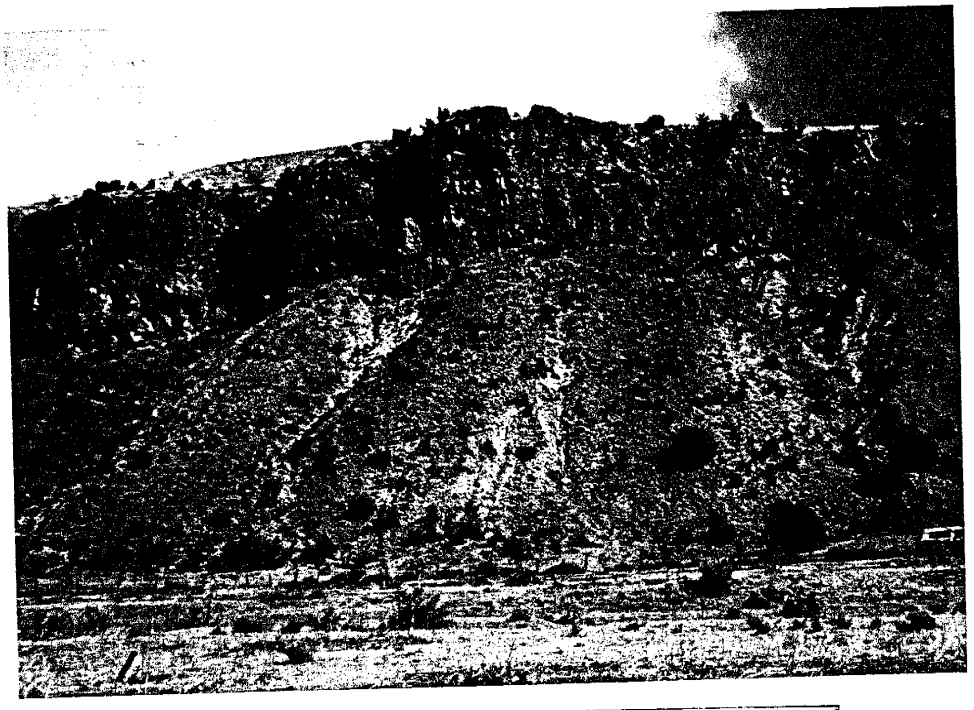

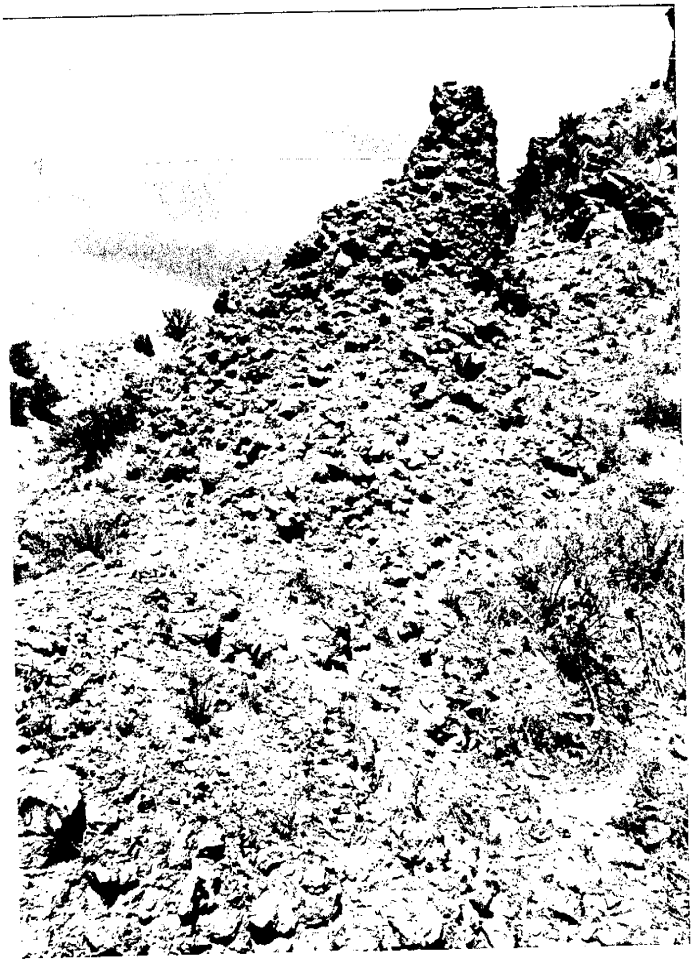

et al. (1984). This is the only known occurrence of Bearwallow Mountain Formation that is interbedded with either Santa Fe Group or Gila Conglomerate in north-central Black Range.

The above age for Winston andesite is the youngest known age determination for the time-transgressive Bearwallow Mountain Formation. Elston (1978) indicates that the lower portion of the Bearwallow Mountain Formation intertongues with the John Kerr Peak Quartz Latite (21.4 ± 1.1 Ma K/Ar age) of Smith (1978) and Smith and Rhodes (1978), and the Jordan Canyon Rhyolite (21.7 ± 0.7 Ma K/Ar age) of Elston et al. (1973). Elston et al. (1973) gives a 20.6 ± 0.5 Ma age for the upper portion of Bearwallow Mountain Formation from the Roberts Lake Dam area in the upper Mimbres Valley. Woodard (1982) reports unpublished K/Ar ages by Stinnett and Damon that range from 21.8 to 23.9 Ma; Abitz (1984) reports an unpublished K/Ar age by Stinnett (1980) of 24.5 ± 0.5 Ma for a flow on Black Mountain, west of Beaverhead, N.M. As mentioned previously, a K/Ar age of 25.8 ± 0.6 Ma was determined for a flow of Bearwallow Mountain Formation near Alexander Cienega in the Taylor Creek area. From these dates, it appears that Bearwallow Mountain Formation in the vicinity of north-central Black Range spans a time period from approximately 26 to 18 Ma. A paleostree study of upper Cenozoic dikes by Aldrich et al. (1986) indicates that magmatism of similar age and composition was extensive in New Mexico, particularily along the Rio Grande rift.

Chemically, Bearwallow Mountain Formation in the vicinity of north-central Black Range is highly varied, ranging from trachybasalt thru andesite-trachyandesite in composition. Table 20 lists major-element analyses for this formation; Figure 49 presents major-element variation diagrams. Comparison of Figure 49 with Figs. 32 & 13 shows that in terms of major-element composition, Bearwallow Mountain Formation closely resembles both basaltic andesite of Poverty Creek and lavas of the Rubio Peak Formation. The only difference appears to be slightly more mafic endmembers for Bearwallow Mountain Formation. However, more-siliceous members of Bearwallow Mountain Formation are reported by Rhodes (1978) from western Mogollon-Datil volcanic field.

In outcrop and hand specimen, Bearwallow Mountain Formation is also very similar in appearance to basaltic andesite of Poverty Creek and Rubio Peak Formation. Bearwallow Mountain Formation is typically dark gray to black in color, fine grained to aphanitic, and vesicular. Flows commonly display autobrecciated tops and bases. Phenocrysts from 1-3 mm in diameter of plagioclase, olivine, pyroxene, and biotite are rare. Microscopically, these phenocrysts are set in a pilotaxitic groundmass of plagioclase (An35-40) microlites. Olivine is generally altered to iddingsite.

Numerous dikes and vent breccias are recognized feeders for flows of Bearwallow Mountain Formation in north-central Black Range. Adjacent to the Continental Divide from Franks

Table 20. Major-element analyses for rocks of Bearwallow Mountain Formation in vicinity of north-central Black Range.

	1	2	3	4	5	6	7
SiO2	56.81	51.55	49.15	53.25	53.94	54.78	48.21
Al2O3	16.35	16.73	16.18	15.33	16.49	17.17	17.74
Fe2O3	8.49	10.04	10.90	9.66	8.78	8.32	10.28
MgO	2.69	4.24	5.49	3.39	3.63	4.05	5.89
CaO	5.90	6.72	7.70	6.53	6.60	6.18	8.12
Na2O	3.83	3.57	3.50	3.44	3.65	3.57	2.42
K2O	2.97	2.18	1.57	2.40	2.51	2.44	3.20
TiO2	1.86	1.95	2.01	1.67	1.60	1.40	1.37
P2O5	1.03	.84	.73	.80	.82	.75	.67
MnO	.16	.15	.16	.18	.12	.12	.16
LOI	2.00	1.11	.95	1.14	.77	1.20	
Total	102.09	99.08	99.63	99.47	99.66	100.59	98.06

1) Bearwallow Mountain Formation from Hodge Canyon, Ericksen et al. (1970) sample # 408.
2) Bearwallow Mountain Formation, Luera Mountains, SE1/4 sec. 10, T. 6 S., R. 10 W., Fodor (1976), analyst, K. Aoki.
3) Bearwallow Mountain Formation, Railroad Canyon, NM Route 78, NE1/4 sec. 28, T. 8 S., R. 12 W., Fodor (1975).
4) Bearwallow Mountain Formation, along NM Route 61, across from old Beaverhead Ranger Station, NE1/4 sec. 7, T. 10 S., R. 12 W., Fodor (1975).
5) Bearwallow Mountain Formation, near NM Route 78, southeast of Pelona Mountain, NW1/4 sec. 34, T. 7 S., R. 11 W., Fodor (1975).
6) Bearwallow Mountain Formation, Sand Canyon, NW1/4 sec. 21, T. 9 S., R. 11 W., Fodor (1975).
7) Bearwallow Mountain Formation, 33-16'-14"N, 107-52'-31"W, Abitz (1984).

	8	9	10	11	12
SiO2	58.49	59.55	59.87	60.17	59.31
Al2O3	14.78	16.10	16.12	16.12	17.09
Fe2O3	7.24	6.61	6.60	6.89	5.90
MgO	2.15	3.44	2.69	2.90	1.05
CaO	4.28	5.57	5.63	5.37	4.28
Na2O	5.77	3.45	3.70	3.73	5.68
K2O	3.86	2.58	3.32	3.13	3.20
TiO2	1.46	1.04	1.09	1.09	1.05
P2O5	.74	.34	.37	.38	.66
MnO	.10	.10	.12	.09	.15
LOI	1.62	2.25	1.20	1.40	1.90
Total	100.49	101.03	100.71	101.47	100.86

8) Bearwallow Mountain Formation, Alexander Cienega, sec. 1, T. 11 S., R. 11 W., 33-22'-30"N, 107-56'-07"W., Eggleston (1987).
9) Bearwallow Mountain Formation, Wall Lake, sec. 10, T. 11 S., R. 12 W., 33-20'-59"N, 108-04'-38"W, Eggleston (1987).
10) Bearwallow Mountain Formation, Kemp Mesa, sec. 3, T. 11 S., R. 12 W., 33-22'-10"N, 108-04'-38"W, Eggleston (1987).
11) Bearwallow Mountain Formation, Kemp Mesa, sec. 3, T. 11 S., R. 12 W., 33-22'-08"N, 108-04'-38"W, Eggleston (1987).
12) Bearwallow Mountain Formation, Winston andesite, SE1/4 sec. 27, T. 11 S., R. 8 W., analysis by P. Kyle and R.B. Hallett.

Figure 49. Major element variation diagrams for Bearwallow Mountain Formation in vicinity of north-central Black Range.

Bearwallow Mountain Formation

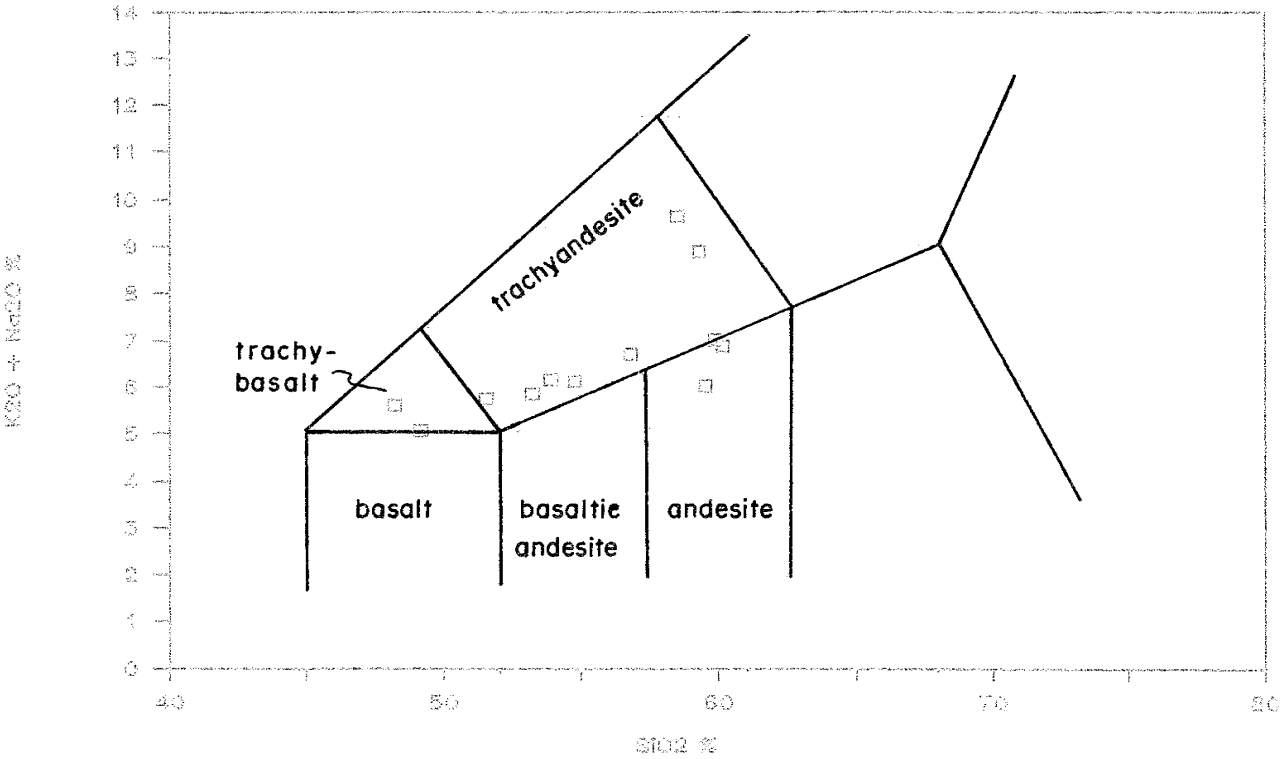

Bearwallow Mountain Formation
K2O, Na2O, CaO, Fe2O3, Al2O3 %
SiO2 %
K2O
Na2O
CaO
Fe2O3
Al2O3

Mountain southward, several dikes (total length in excess of 5.5 km) are observed cutting basaltic andesite of Poverty Creek and younger volcanic rocks. Figure 50 is a compass-rose diagram for these dikes which indicates dominant trends of north-south and northeast-southwest, with lesser northwest-southeast. Richter (1978) has interpreted breccias within Bearwallow Mountain Formation in Indian Creek as vent breccias. A breccia pipe (see Figure 48b) that cross cut basaltic andesite of Poverty Creek in the extreme northeast corner of sec. 34, T. 11 S., R. 8 W. is also believed to be vent area related to eruption of the Winston andesite member of Bearwallow Mountain Formation (rb map unit of Maxwell and Heyl, 1976). Extrusive breccias, similar to those occurring within the breccia pipe, crop out at the base of the Winston andesite adjacent to the pipe (Figure 48a)

Figure 50. Compass-rose diagram for intermediate dikes of the Bearwallow Mountain Formation that cut basaltic andesite of Poverty Creek and younger volcanic rocks along the Continental Divide, north-central Black Range, New Mexico. Sum of lengths is approximately 5.5 km.

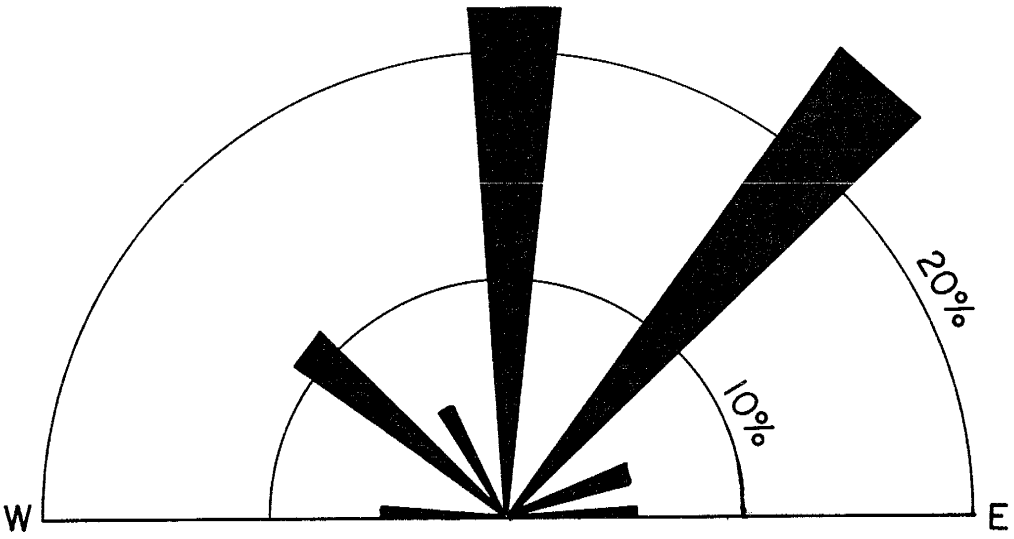
W
E
10%
20%

Pliocene basalts and Pliocene pediment surface

Known occurrences of Pliocene basalt in vicinity of north-central Black Range are restricted to Winston graben and the juncture of Winston graben and Las Animas graben. The map of late Tertiary-Quaternary tectonic and volcanic activity in New Mexico by Callender et al. (1983) shows that these occurrences are but a small part of widespread volcanism active during this time period.

One of the best studied Pliocene volcanic units is a basalt flow on the eastern margin of the Winston graben that caps Tabletop Mountain in sec. 12, T. 11 S., R. 8 W. This flow unconformably overlies sediments of Santa Fe Group, crosses the boundary fault between Winston graben and Sierra Cuchillo uplift (without being offset), and is dated at 4.8 $\pm$ 0.1 Ma (Seager et al., 1984). Major-element chemical analysis of this flow by Fodor (1975) (duplicated in Table 21) indicates that it is alkaline basalt in composition; trace-element analyses are given by Bornhorst (1980). Phenocrysts occurring in this basalt are plagioclase and olivine. Olivine is typically altered partially or entirely to iddingsite. Xenolithic inclusions of spinel lherzolite, clinopyroxenite, and a grabbroic rock type that occurs within this basalt flow are analyzed by Fodor (1978).

The basalt flow on Table Top Mountain was deposited upon an extensive pediment surface (now highly eroded) that developed on top of Santa Fe Group sediments within the

Table 21. Major-element analysis for Pliocene basalt that caps Table Top Mountain along eastern margin of Winston graben, from Fodor (1975).

SiO2	46.38
Al2O3	15.56
Fe2O3	3.49
FeO	8.65
MgO	8.39
CaO	8.73
Na2O	3.18
K2O	1.15
TiO2	2.02
P2O5	.40
MnO	.18
LOI	.41
Total	99.10

Winston graben, and on top of the Eocene-Oligocene volcanic pile along the eastern margin of north-central Black Range. For reference, this surface is herein informally referred to as the Winston surface. The Winston surface crosses both the eastern and western boundary faults of Winston graben and is not offset by these faults (Jahns, 1953; Chapin et al., 1978; Seager et al., 1984). Solutions to three-point problems for the top of Winston surface consistently yield easterly dips, with slopes of approximately 0.5-1.0 degrees. Elevations along the eastern side of Winston surface, adjacent to the Sierra Cuchillo uplift, are from 6800-6900 ft. Only the highest peaks in Sierra Cuchillo rise above eastward projections of the Winston surface. The present-day drainage pattern, which crosscuts the Sierra Cuchillo at right angles and through narrow gorges at several locations, is probably a relict pattern, established initially upon the Winston surface.

Projections of the Winston surface farther eastward suggest that it probably was once continuous with the Cuchillo surface of Lozinsksy and Hawley (1986) in the area of Palomas and Engle basins, a high-level geomorphic surface that dips eastward to southeastward at 1-2 degrees. An eastward slope of approximately 1.6 degrees would connect Winston surface flush with Cuchillo surface.

Quaternary deposits

Quaternary deposits in north-central Black Range consist of alluvium in larger, active stream channels and colluvium on gentle hillslopes and small stream channels. All deposits consist of unconsolidated, fine- to coarse-grained sedimentary material. Alluvial deposits in streams that drain areas with bedrock of Taylor Creek Rhyolite contain wood tin and cassiterite, and are potential tin resources. Minor amounts of gold have been won from streams that crosscut epithermal vein deposits of Chloride mining district.

Chapter 3. CENOZOIC STRUCTURAL GEOLOGY OF NORTH-CENTRAL BLACK RANGE, NEW MEXICO

Introduction

The Cenozoic structural fabric of the Mogollon-Datil volcanic field in southwestern New Mexico, including all of the Black Range, is dominated by three trends: 1) north-south-oriented structures (NNE-NNW conjugate sets) sympathetic to the Rio Grande rift; 2) northwest-southeast structures sympathetic to the Texas lineament; and, 3) northeast-southwest structures sympathetic to the Morenci and Jemez lineaments. The Mogollon-Datil volcanic field is, in effect, structurally outlined by these three geologic features. East-west structures are also common, but are minor and subsidiary.

Regional Cenozoic tectonism that has controlled deformation in southwestern New Mexico includes: 1a) Laramide thrusting and strike-slip faulting along northwest trends (Seager, 1983; Seager et al., 1986; Seager and Mack, 1986); 1b) Laramide thrusting and dextral strike-slip faulting along northerly trends (Kelley and McCleary, 1960; Seager, 1975; Chapin and Cather, 1981; Chapin, 1983); 2) Late Oligocene to Miocene extension associated with the initial development of Rio Grande rift along dominantly north and northwest trends (Chapin and Seager, 1975; Eaton, 1979; Seager et al., 1984; Aldrich et al., 1986); and, 3) Late Miocene and Pliocene extension that formed north-trending basins and uplifts of the Rio Grande rift (Chapin and Seager, 1975; Eaton, 1979; Zoback et al., 1981;

Seager et al., 1984; Smith et al., 1985; Aldrich et al., 1986).

Cenozoic rocks of the north-central Black Range have experienced deformation related to all three periods of tectonism listed above. The Laramide phase of deformation produced a north-northeast-trending zone of dextral wrench faults that cut only rocks of Rubio Peak Formation and pre-Cenozoic units. Late Oligocene deformation occurred as high-angle, normal and oblique-slip faults that were subsequently filled with epithermal vein mineralization (Chloride mining district). The youngest phase of deformation in north-central Black Range formed non-mineralized, normal and oblique-slip faults that in part reactivated vein-filled faults. These non-mineralized faults strike dominantly north-northeast and north-south, with lesser northwest and northeast orientations. A major structural feature related to this youngest phase of Cenozoic faulting is the Winston graben-Las Animas graben system that defines the eastern margin of north-central Black Range.

All phases of Cenozoic tectonism in the north-central Black Range occurred principally along a north-northeast-trending, 20-to-30-km-wide zone of intense faulting adjacent to the Winston and Las Animas grabens. West of this structurally active zone, on the Mogollon Plateau, Cenozoic deformation is relatively minor with an extreme paucity of faulting. The boundary between these structurally active

and quiescenct zones closely follows an extension of the narrow (1.5-3.0-km wide), north-northeast-striking structural high known as the Santa Rita-Hanover axis (Elston et al. 1968, 1970; and Aldrich 1972, 1974, 1976). Figure 51 shows the location of active and quiescenct areas of Cenozoic deformation in north-central Black Range. The Chloride mining district lies within the active zone of intense faulting; the Taylor Creek tin district occurs in the area of tectonic quiescence on the Mogollon Plateau. The northern portion of the Emory caldera is a major volcanic feature that developed within the zone of intense faulting in the north-central Black Range.

Figure 51. Division of Cenozoic tectonic areas in north-central Black Range, New Mexico. The boundary between structurally active and quiescenct areas closely follows an extension of the Santa Rita-Hanover axis of Elston et al. (1968, 1970) and Aldrich (1972, 1974, 1976).

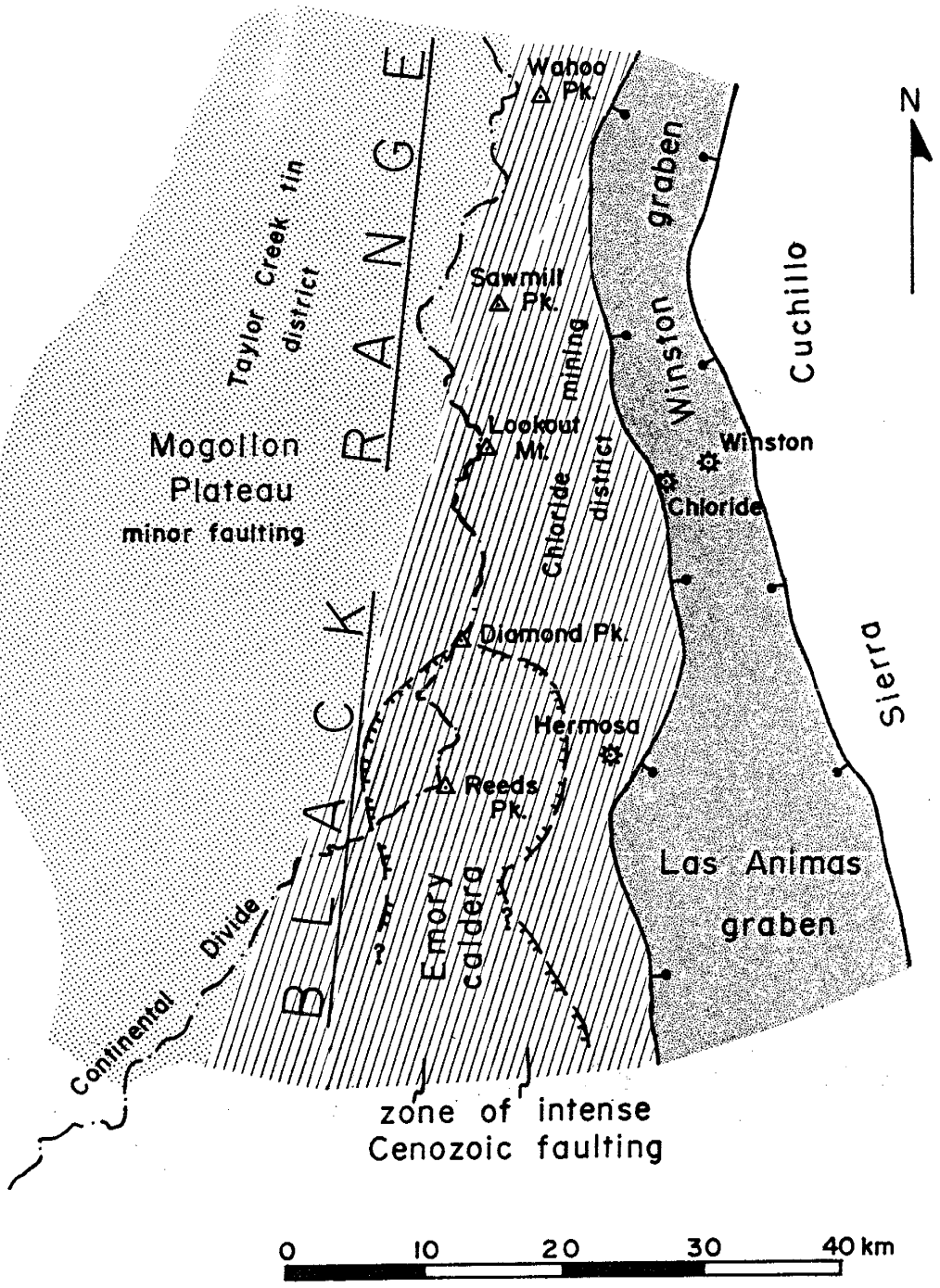
Wahoo Pk.
Sawmill Pk.
Lookout Mt.
Diamond Pk.
Reeds Pk.
Hermosa
Winston
Chloride
Taylor Creek tin district
Mogollon Plateau
minor faulting
BLACK RANGE
Chloride mining district
Winston graben
Cuchillo
Sierra
Las Animas graben
Emory caldera
Continental Divide
zone of intense Cenozoic faulting
N
0 10 20 30 40 km

Eocene wrench faulting

The oldest phase of Cenozoic deformation distinguished in north-central Black Range produced multiple strands of dextral wrench faulting along an overall north-northeast trend. Principal exposures of these structures are along the eastern flank of the Black Range in the central portion of Winston quadrangle (Plate 1). Wrench faults in the Black Range cut only rocks of the Eocene Rubio Peak Formation and pre-Cenozoic units. This deformation is part of a wide zone of dextral-wrench-fault activity recognized by Chapin and Cather (1981) and Chapin (1983) along the eastern margin of the Colorado Plateau during a late stage of the Laramide orogeny.

Structures recognized as belonging to the Black Range wrench-fault system are shown in Figure 52. This system is complex, consisting of numerous strike-slip structures, small thrust and reverse faults, and several syntectonic dikes (dot-dash pattern in Fig. 52) and small plugs (solid pattern in Fig. 52). All wrench-fault structures are cut off by the western boundary fault of the Winston graben, the westernmost structural feature in this region associated with the Rio Grande rift (Chapin and Seager, 1975). Utilizing piercing points defined by exotic limestone blocks that occur within the Rubio Peak Formation, a minimum of 3.14 km of dextral strike slip was estimated for the Black Range system by Harrison (1989), .

Figure 52. Principal structures of the Black Range wrench-fault system. Solid lines are strike-slip faults, barbed lines are reverse or low-angle thrust faults, dot-dash lines are syntectonic dikes, and solid areas are syntectonic plugs. All features of the wrench-fault system are cut off by the western margin of the Winston graben.

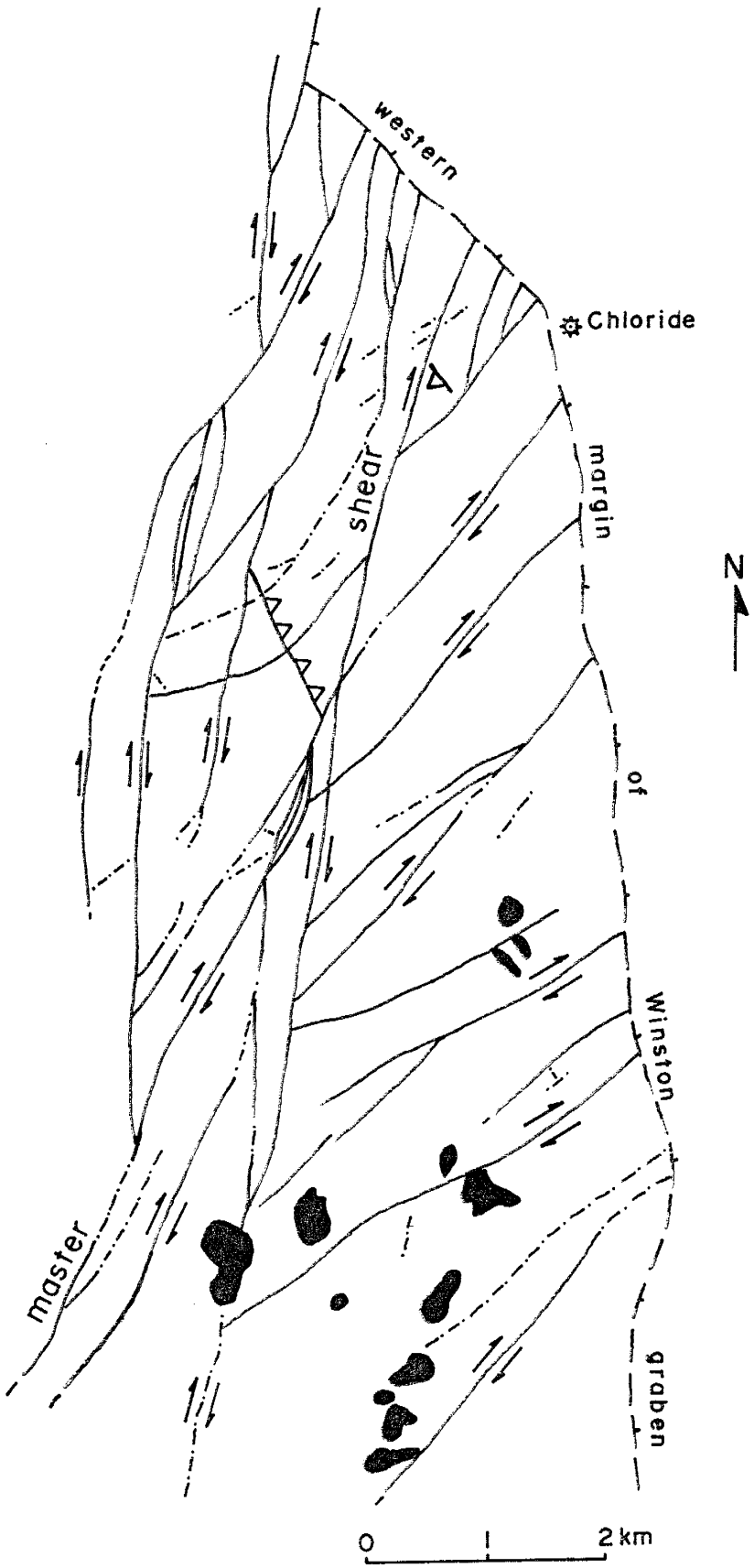
western
Chloride
margin
shear
of
N
Winston
master
graben
0
1
2 km

Figure 53. Photographs of vertical wrench fault with horizontally striated slickenside surfaces: a) exposure along Byers Run in NE1/4 sec. 6, T. 12 S., R. 8 W.; b) exposure along South Fork of Cuchillo Negro Creek in SW1/4 sec. 31, T. 11 S., R. 8 W., approximately 1/2 km NNE along strike from a); c) exposure along Chloride Creek in west-central sec. 20, T. 11 S., R. 8 W., approximately 4.3 km NNE along strike from b). All photographs are of the structure identified as the master shear on Figure 52.

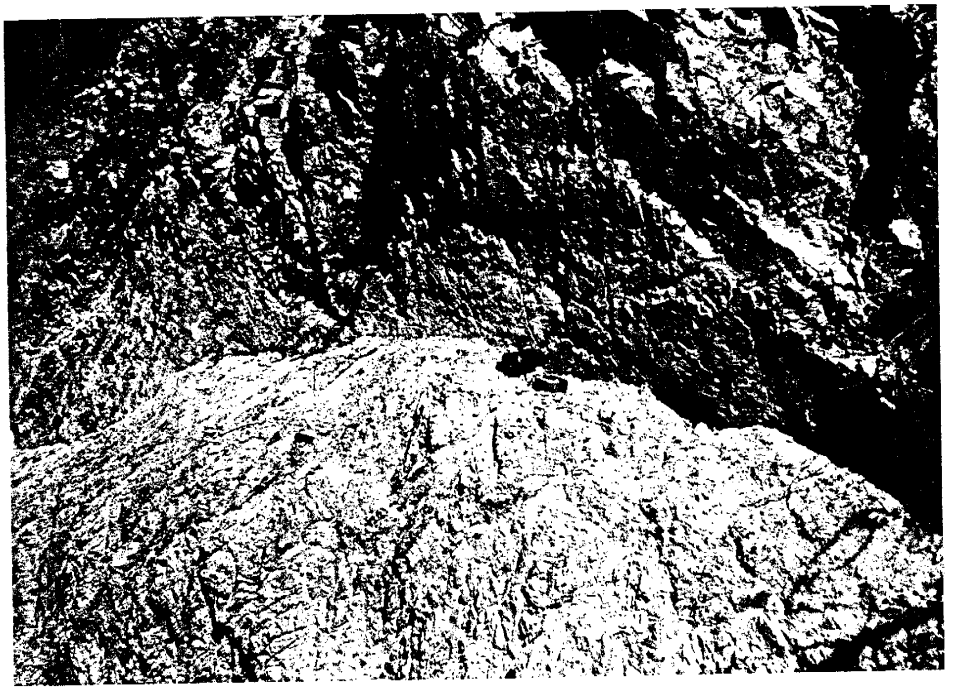

a)

b)

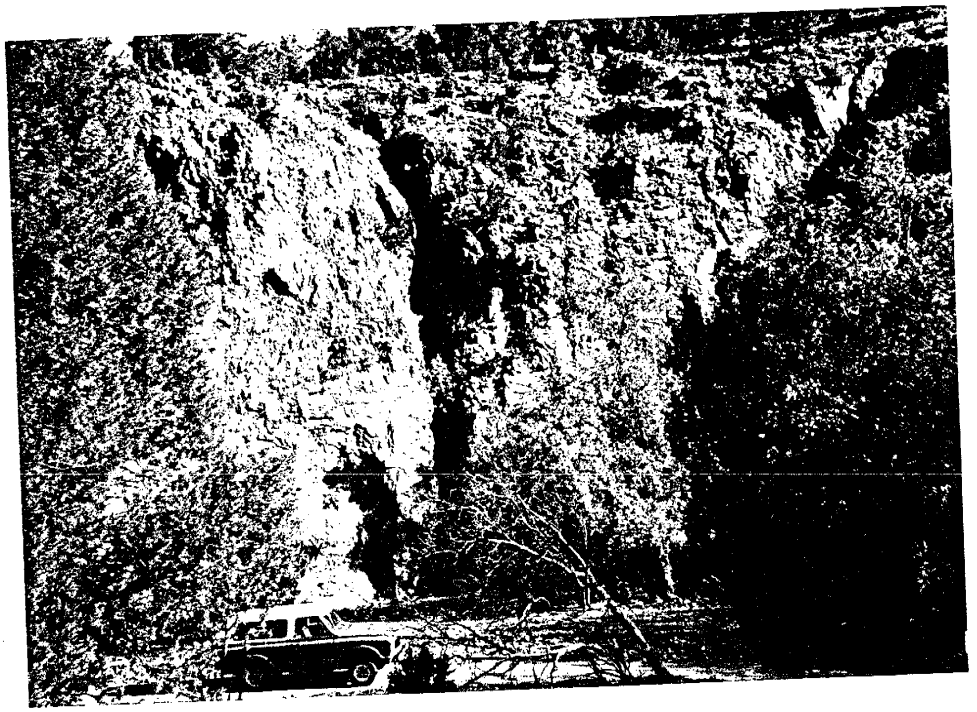

c)

In the field, strike-slip structures vary in occurrence from 30-m-wide cataclastic zones to narrow, vertical faults with well-developed slickenside surfaces that contain horizontal striations and mullions (Fig. 53). Orientations of strike-slip faults are primarily along north-northeast and northeast trends as depicted in Figure 54. From the Riedel model of right simple shear, it is interpreted that P-fracture orientations for this system are approximately N-S, R-fracture orientations are approximately N35E, and the direction of principal displacement zone (PDZ) is approximately N17.5E. From analysis of the strain ellipse adapted from Harding (1974) and Sylvester (1988), shown in Figure 55, the maximum principal stress direction during formation of the Black Range wrench-fault system was approximately N62E. R' shears for this wrench-fault system should be oriented at approximately N77W, but few are recognized in the area of Figure 52. This is due to extensive reactivation of structures along this trend by late Oligocene and Miocene faulting.

Numerous dikes and small plugs interpreted as syntectonic with Eocene strike-slip faulting occur within the area of Figure 52. The syntectonic nature of these intrusives is indicated by three lines of evidence: 1) dikes are offset by late Oligocene quartz veins, indicating that the dikes are related to an older tectonic event; 2) the intrusives are feeders for voluminous and widespread intermediate lavas occurring in the upper Rubio Peak

Figure 54. Compass-rose diagram for approximately 99 km of strike-slip structures in north-central Black Range.

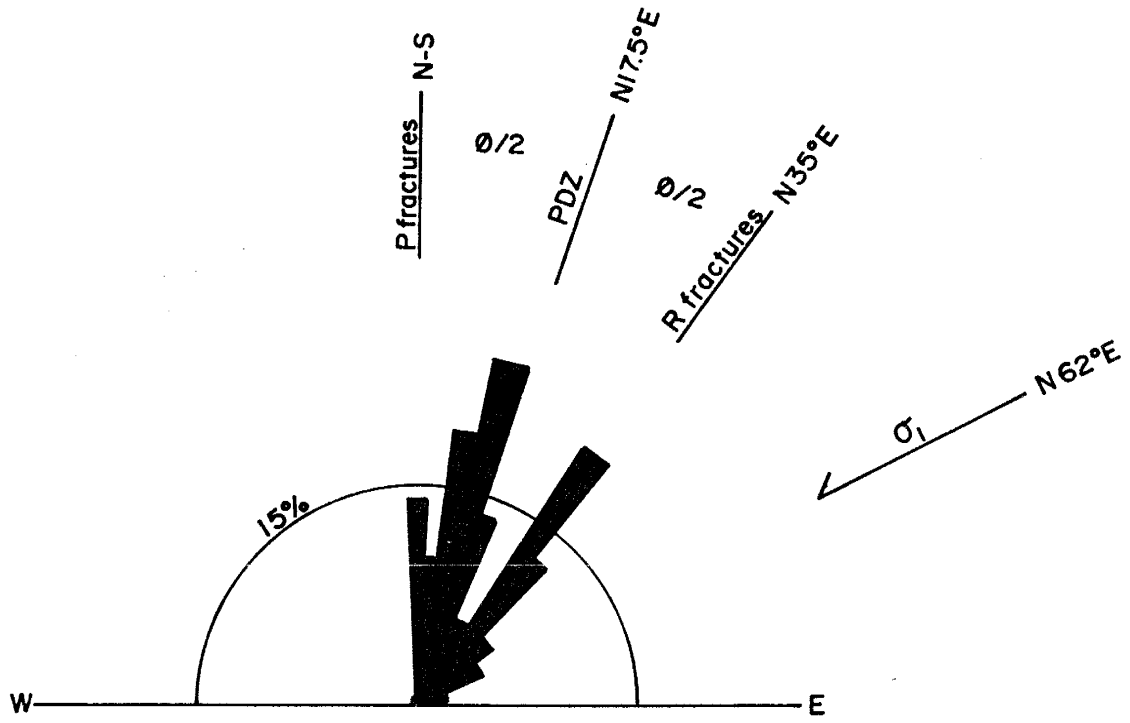
P fractures N-S
Ø/2
PDZ N17.5°E
Ø/2
R fractures N35°E
σ1 N62°E
15%
W
E

Figure 55. Strain ellipse for Riedel model of right simple shear adapted from Harding (1974) and Sylvester (1988).

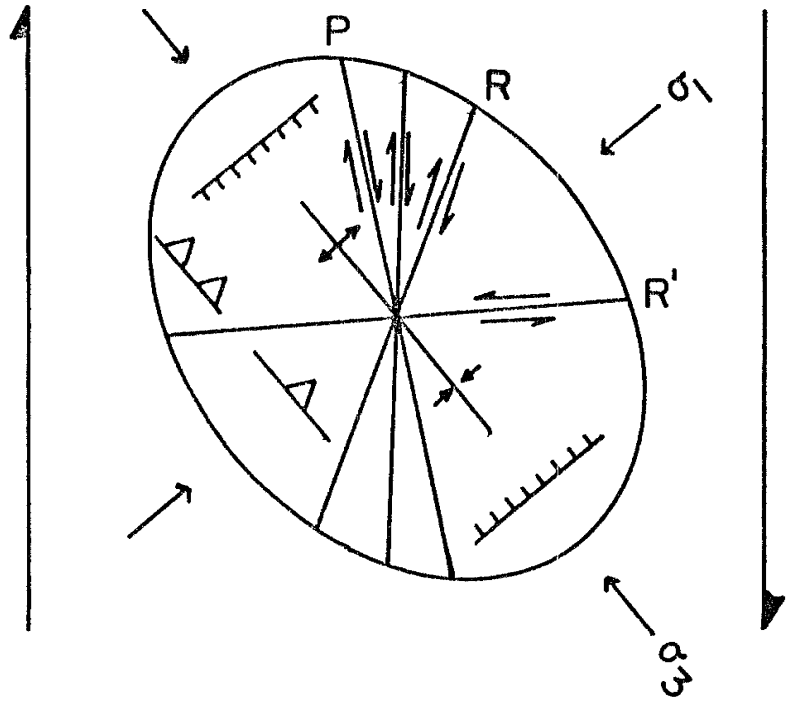

Strain ellipse for horizontally oriented σ_1 & σ_3, simple shear, right lateral (after Harding, 1974; Sylvester, 1988).

Formation that are, in part, cut by wrench faults; and, 3) many dikes occur along wrench-fault structures, and yet their margins locally have developed post-emplacement, horizontally striated slickenside surfaces.

Syntectonic intrusives in a wrench-fault regime are emplaced along the plane of maximum stress (defined by maximum and intermediate principal stress directions) and along shears that locally undergo extension (Fig. 56). A compass-rose diagram for approximately 10.7 km of syntectonic dikes in north-central Black Range is shown in Figure 57. The orientation of these dikes is in good agreement with the stress-strain pattern developed from shear orientations shown in Figure 54. Emplacement of dikes was dominantly along the plane of maximum stress and along R shears, with minor emplacement along shears of the principal displacement zone (PDZ) and P shears. Also, it is important to note the common occurrence of brecciated fragments and remnants of dike-like material that are anomalous to wall-rock compositions in both the St. Cloud and Hoosier mineral deposits (late Oligocene epithermal quartz veins with west-northwest orientations).

An important economic aspect of the Eocene wrench-fault system in the Black Range is its control on the late Oligocene epithermal mineralization of the area. As indicated by Harrison (1988), known occurrences of ore-grade mineralization in the southeastern Chloride mining district are localized primarily along the intersections of wrench

Figure 56. Syntectonic intrusives in a wrench-fault regime are emplaced along the plane of maximum stress and along shears that locally undergo extension.

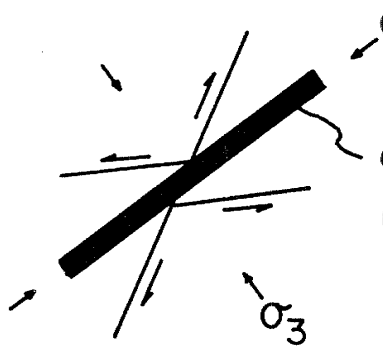

dikes emplaced along the plane of maximum stress

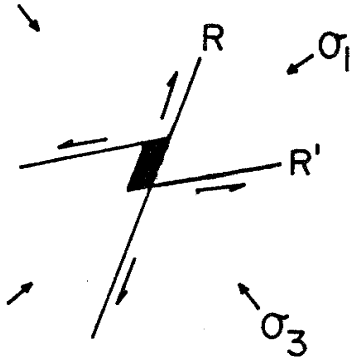

dikes elongated along R shears

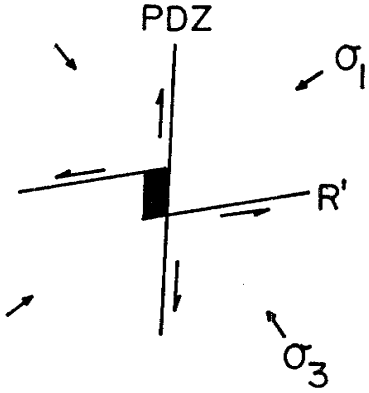

dikes elongated along principal displacement zone

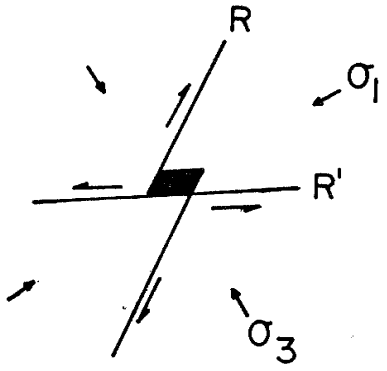

dikes elongated along R' shears

Figure 57. Compass-rose diagram for approximately 10.7 km of syntectonic dikes in north-central Black Range.

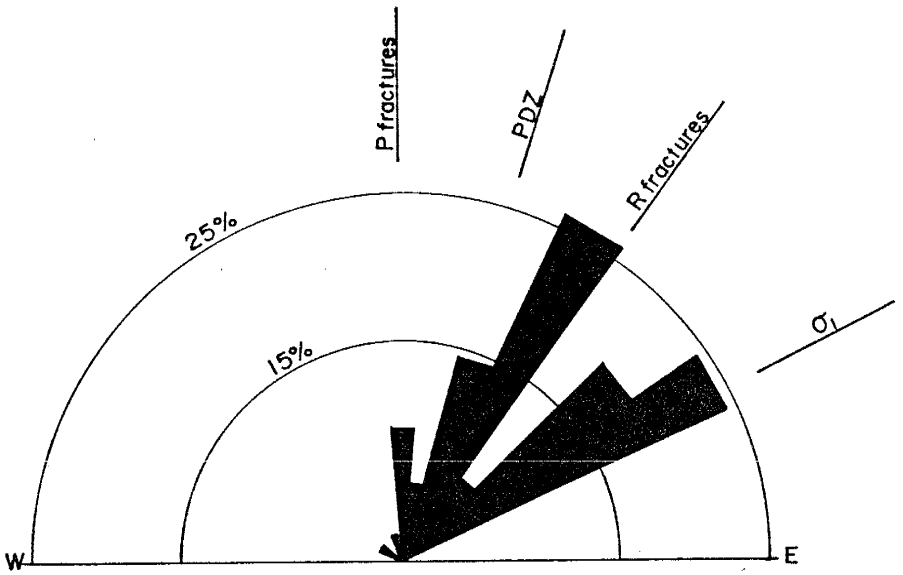
P fractures
PDZ
R fractures
σ_1
25%
15%
W
E

faults with the younger quartz veins. Over 2,500,000 oz of silver, 10,000 oz of gold, 10,000 tons of base metals, and more than 50,000 tons of high-silica smelter flux have been produced from rock in and adjacent to these intersections. The vertical, deeply penetrating wrench-fault structures served as primary conduits for upwelling, metal-bearing hydrothermal fluids.

Late Eocene-early Oligocene, magmatic-related structures

Structural features in the north-central Black Range during late Eocene and early Oligocene were also related to magmatic activity. Early in this time period, regional structure was dominated by evolution of the northern Emory caldera (outflow Kneeling Nun Tuff has a 40Ar/39Ar age of 34.9 Ma, McIntosh, 1989).

Tumescence and erosion prior to eruption of Kneeling Nun Tuff removed much of the upper Rubio Peak Formation and all of tuff of Rocque Ramos Canyon and tuff of Victoria Tank from the northern margin of the Emory caldera. The eruption-related collapse of the Emory caldera formed a complex system of ring-fracture faults elongated in an overall north-south direction (see Abitz, 1989; Ericksen et al., 1970; Harrison et al., in prep., for details). The eastern structural margin of this caldera coincides with the southern extension of the Black Range wrench-fault system shown in Figure 52 (Harrison, 1989). Ring-fracture faults along the northern margin of the caldera strike dominantly west-northwest.

Post-eruption caldera resurgence produced a prominent anticlinal horst-block system through the center of the caldera with a NNE strike and steeply dipping boundary faults (Abitz, 1989; Ericksen et al., 1970). This resurgent block crosscuts northern ring-fracture faults of the Emory caldera (Abitz, 1989) and extends northward from the caldera

margin for several kilometers. Outflow-facies Kneeling Nun Tuff was eroded from most of the northern caldera margin.

The coincidence of the eastern structural margin of the northern Emory caldera with an extension of the Black Range wrench-fault system strongly suggests a structural control on caldera formation. The vertical, deeply penetrative nature of wrench faults should make them ideal structures for influencing the location of upwelling magma. This idea is supported by an alignment of plugs of basaltic andesite of Poverty Creek that occur along the wrench-fault system north of the Emory caldera (Harrison, 1989). Two additional lines of evidence suggest a structural control on the Emory caldera by the older wrench-fault system: 1) the WNW-strike of ring-fracture faults on the northern caldera margin are oriented in the direction of R' shears; and, 2) the post-caldera, resurgent horst-block system parallels the Black Range wrench-fault system.

During the period of magmatic quiescence (~35-30 Ma) that occurred between eruption of Kneeling Nun Tuff and basaltic andesite of Poverty Creek in north-central Black Range, a similar quiescent period occurred in tectonic activity. As discussed in the previous chapter, flows of basaltic andesite of Poverty Creek virtually blanketed all of north-central Black Range and adjacent areas with little indication of any uplift or subsidence of Kneeling Nun Tuff. Figure 26 shows the large area in which basaltic andesite

of Poverty Creek rests directly upon Kneeling Nun Tuff.

Late Oligocene structure

After the 5-my period of quiescence in early Oligocene, regional tectonic activity in southern New Mexico began again during Late Oligocene in association with the initial development of the Rio Grande rift (Chapin and Seager, 1975). Igneous intrusives and hydrothermal mineralization in the north-central Black Range record the progressive development of structures in this area related to this period of deformation.

Basaltic andesite of Poverty Creek was erupted from numerous, widespread fissures during the approximate time period of 30-29 Ma. Figure 33 is a compass-rose diagram for dikes believed to be feeders for basaltic andesite of Poverty Creek in north-central Black Range. [Although there is some uncertainty as to whether all the dikes incorporated into Figure 33 are indeed feeders for basaltic andesite of Poverty Creek (i.e. a few could be Bearwallow Mountain Formation), most dikes are stratigraphically constrained and the overall pattern is believed to be accurate.] It is interpreted that Poverty Creek magma dominantly followed pre-existing structures during this time period . Note that the pattern of dikes in Figure 33 is very similar to Eocene wrench-fault fractures depicted in Figure 54.

The time period from approximately 29-28 Ma saw widespread rhyolitic volcanism throughout north-central Black Range and adjacent areas. Although much of this

volcanism was erupted from flow-dome complexes, there are many rhyolite dikes associated with this volcanic period. Figure 5B is a compass-rose diagram for about 10.7 km of rhyolite dikes that were emplaced during the approximate time period of 29-28 Ma. The strong northwest trend of these dikes is in good agreement with the regional stress patterns for this time period determined by Aldrich et al. (1986), Zoback et al. (1981), and Chapin and Seager (1975).

Open-space portions of faults active during the late Oligocene were filled with quartz-sericite-type, epithermal vein mineralization. Sulfide-mineralized shoots within these vein systems are the substance of the Chloride mining district. Intersections between veins and older wrench faults are the primary structural control on mineralized shoot locations (Harrison, 1988). Mean K-Ar ages for Chloride district vein adularia of 26.2-28.9 Ma are reported by Harrison (1986). See Maxwell and Heyl (1980), Harrison (1986, 1988a, 1988b, 1988c, 1988d), Behr and Norman (1986), and Behr (1988) for descriptions of mineralogy, paragenesis, geochemistry, and other aspects of the Chloride mining district.

Late Oligocene, vein-filled fault structures are typically high-angle (55-90 degrees) normal and oblique-slip types. They cut the entire stratigraphic section including the basaltic andesite of Poverty Creek. Stratigraphic offsets are generally less than a few hundred meters. Vein strikes are highly varied, but reflect three prominant

Figure 58. Compass-rose diagram for approximately 10.7 km of rhyolite dikes (~28-27 Ma) in north-central Black Range.

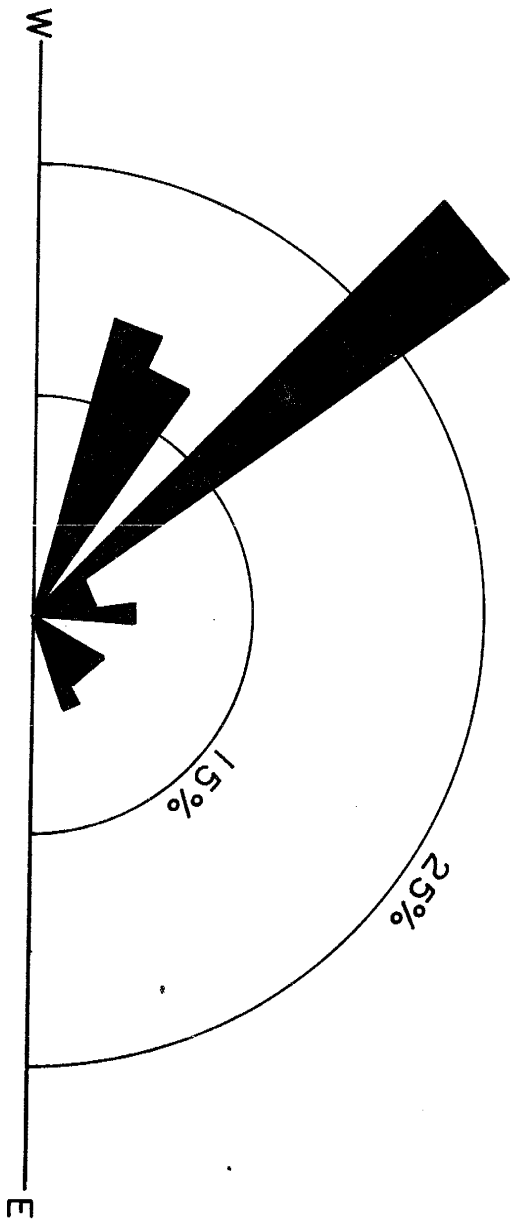
W
15%
25%
E

trends: northeast-southwest, north-south, and northwest-southeast. Figure 59 is a compass-rose diagram for approximately 120 km of epithermal quartz veins in the Chloride mining district. Northwest-southeast and north-south veins commonly show the greatest amount of dilation and contain the widest zones of mineralization. Most vein structures show multiple stages of syn-mineralization faulting, as well as post-mineralization reactivation.

The orientations of late Oligocene dikes and veins in the north-central Black Range show prevalent structural domains (Plate 6b). Structures in the northern half of this area show strong northerly and northeasterly orientations, probably reflecting the reactivation of older structures (see Fig. 54). In contrast, a large domain of dominantly northwest-striking structures occurs in the southeastern Chloride mining district and Moccasin John areas, and extents westward over the Continental Divide. This domain also shows northwest-trending magnetic and gravity anomalies (Plates 6c & 6d), and is interpreted as overlying a relatively shallow pluton of late Oligocene age.

Figure 59. Compass-rose diagram for approximately 120 km of Late Oligocene (~26-29 Ma) epithermal quartz veins in the Chloride mining district of north-central Black Range. Northwest-southeast and north-south veins are the most productive and show the greatest amount of dilation.

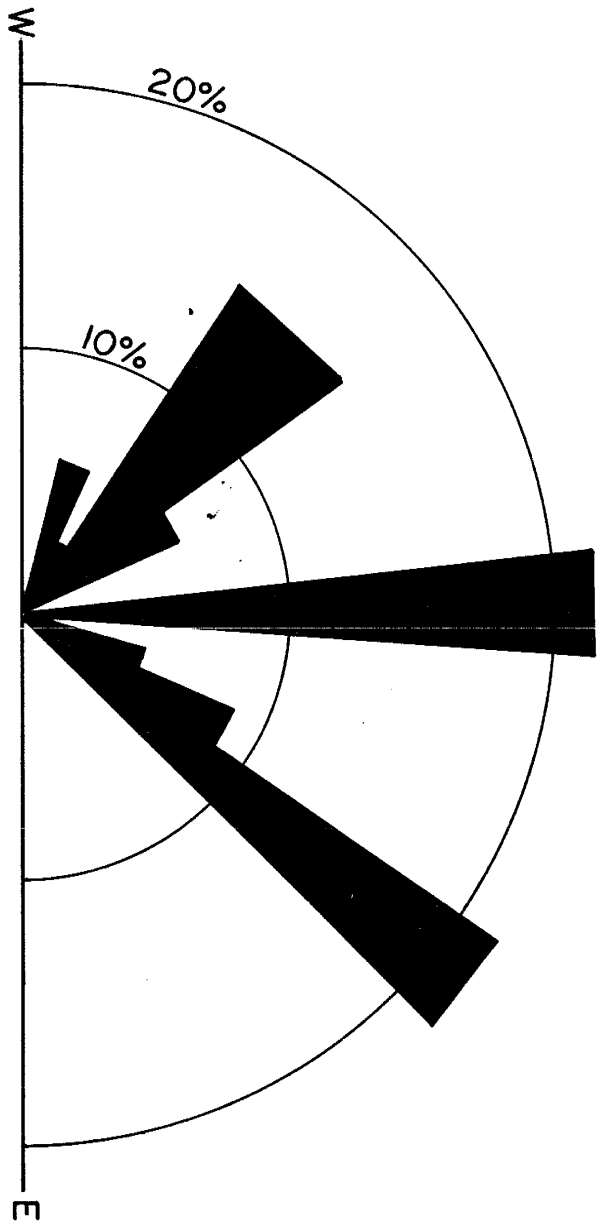
W
20%
10%
E

Neogene structure

Neogene faulting is the dominant stage of structural deformation in the north-central Black Range and adjacent areas. A tectonic sketch map of major Neogene structures in north-central Black Range and vicinity is presented in Figure 60. A generalized east-west cross-section for this area, at the approximate latitude of Winston, New Mexico, is shown in Plate 7. As mentioned earlier, a structural boundary between strongly faulted terrane and virtually non-faulted terrane closely follows an extension of the Santa Rita-Hanover axis (Elston et al., 1968, 1970; Aldrich, 1972, 1974, 1976) northward through the north-central Black Range (Fig. 51). This boundary is considered to be the westernmost edge of graben structures in the Rio Grande rift. West of this boundary, Cenozoic rocks dip gently westward into the Mogollon-Datil plateau. East of this boundary, the Rio Grande rift consists of a complex sequence of north-south elongated grabens and uplifted horst blocks. The largest feature of the Rio Grande rift in this area is an east-dipping, asymmetrical half-graben structure comprised of the Sierra Cuchillo uplift and Palomas basin. Between the Sierra Cuchillo uplift and San Mateo Mountains, an east-dipping, asymmetrical half-graben structure known as the Monticello graben constitutes a western arm of the Palomas basin.

Separating the Sierra Cuchillo uplift from the Black

Figure 60. Sketch map of major Neogene structures in north-central Black Range and vicinity. Shaded areas represent major grabens related to the Rio Grande rift, non-shaded areas are uplifts or horst blocks. Plate 6 is a generalized east-west cross section for this area at the approximate latitude of Winston, New Mexico. Virtually all structural deformation stops at the extension of the Santa Rita-Hanover axis; Cenozoic rocks west of this line dip gently towards the west.

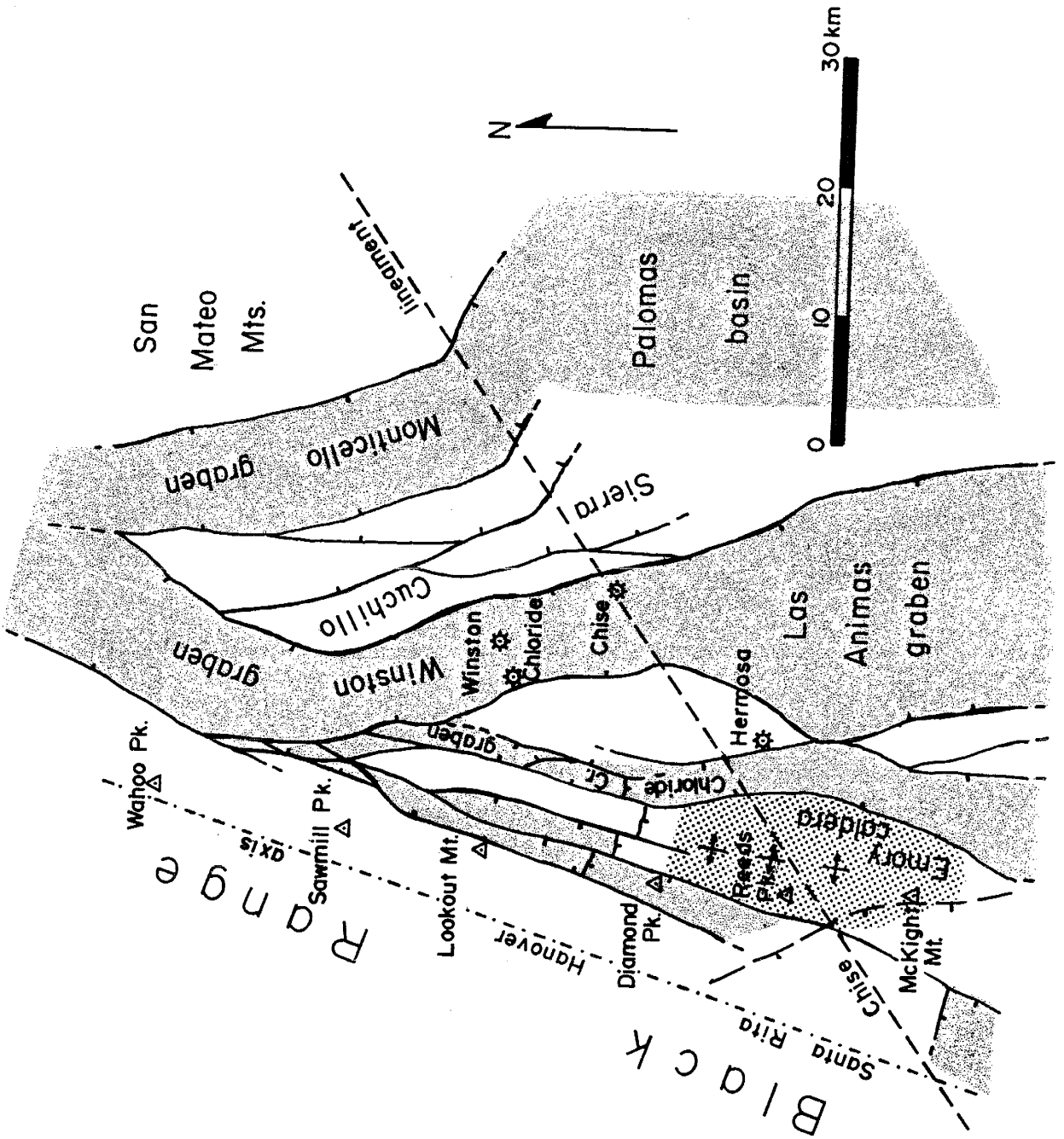
30 km
20
10
0
N
San Mateo Mts.
lineament
Palomas basin
Monticello graben
Sierra
Cuchillo graben
Winston graben
Winston
Chloride
Chise
Hermosa
Las Animas graben
Wahoo Pk.
axis
Sawmill Pk.
Lookout Mt.
Hanover
Diamond Pk.
Chloride Cr.
Reeds Pk.
Emory caldera
McKight Mt.
Chise
Santa Rita
Range
Black

Range is the Winston graben, a major Neogene structure that is approximately 50 km long and 8 km wide. The Winston graben is symmetrical, with a minimum of 2 km of stratigraphic separation along both margins. Geophysical data of Ericksen et al. (1970) suggests that it deepens towards the north. At its southern end, the Winston graben merges with the relatively wide and shallow Las Animas graben across the Chise lineament, a northeast-trending accomodation zone similar to the Socorro accommodation zone described by Chapin et al. (1978) and Chapin (1989). Further descriptions of the Chise lineament will be presented by Harrison (in prep.). The Winston graben follows two prominant trends, NNW and NNE, with a dogleg occurring at the approximate latitude of Sawmill Peak (see Fig. 60). The eastern margin of the north-northeast-trending northern section of the Winston graben is a straight-line projection of the Eocene wrench-fault system described previously.

Age constraints for the Winston graben are poor, but most considerations indicate that it is largely a Miocene structure. Along its western margin, upper Santa Fe Group sediments within the graben are down faulted against various Cenozoic and pre-Cenozoic units. Segments of the western margin, particularly just west of Chloride, New Mexico, are reactivated late Oligocene quartz veins. For the most part, attitudes of the Santa Fe Group sediments and other units within the Winston graben are nearly horizontal. A

local exception is found in the extreme southern portion of the Winston graben, where westerly dips of 22 to 37 degrees occur in basal beds of the Santa Fe Group, tuff of Little Mineral Creek, and basaltic andesite of Poverty Creek which are overlain by nearly horizontal beds of the upper Santa Fe Group (see Plate 1). The occurrence of these tilted beds suggests that a proto-graben of asymmetrical shape probably existed in this area. Along the eastern margin of the Winston graben, outcrops of the andesite of Winston graben (K-Ar age of 18.3 ± 0.4 Ma, Seager et al., 1984) within the graben are downfaulted against rocks of the lower Rubio Peak Formation and pre-Cenozoic units. As described in the section on Vicks Peak Tuff in the chapter on stratigraphy and geochemistry, approximately 1 km east of Winston, New Mexico, a large, vertically tilted block of Vicks Peak Tuff is overlain by horizontal beds of the andesite of Winston graben and Santa Fe Group. This occurrence is interpreted as a gravity-slide block that presumedly detached from the adjacent Sierra Cuchillo upliff and slid into the Winston graben. If this interpretation is correct, then the 18.3 ± 0.4 Ma age of the andesite of Winston graben probably represents a minimum age for formation of the Winston graben. A Pliocene basalt flow (K-Ar age of 4.8 ± 0.1 Ma, Seager et al., 1984) that extends across the eastern margin of the Winston graben without being offset provides an upper age constraint for movement along this boundary. All of the above relationships tend to support the conclusion of Chapin

(1978) that the Winston graben was formed during an early Miocene stage of Rio Grande rifting, and was subsequently abandoned in favor of extension along rift basins to the east.

South of Wahoo Peak in the eastern part of the north-central Black Range (Fig. 60), a NNE-trending belt of graben structures with intervening horst blocks splits away from the Winston graben. This belt closely follows the northerly extension of the axis of resurgence of the Emory caldera and parallels the Eocene wrench-fault system. Faults within this belt are non-mineralized, high-angle normal and oblique-slip structures that cut the entire stratigraphic section and reactivated most older structures. Strikes of major faults within this belt are dominantly northnortheast-southsouthwest to northeast-southwest, with numerous minor faults along north-south, and northeast-southwest trends. Figure 61 presents a compass-rose diagram for more than 400 km of high-angle normal and oblique-slip faults in this area. Slickenside striations and mullions on these structures indicate an E-W to eastsoutheast-westnorthwest horizontal least-principal-stress direction for this stage of deformation (assuming that intermediate principal stress direction was normal to displacement in the fault plane and that maximum-principal-stress direction was approximately 30 degrees to the fault plane). Figure 62 is a compass-rose diagram of least-principal-stress directions obtained for

Figure 61. Compass-rose diagram for more than 400 km of Neogene, high-angle normal faults in north-central Black Range.

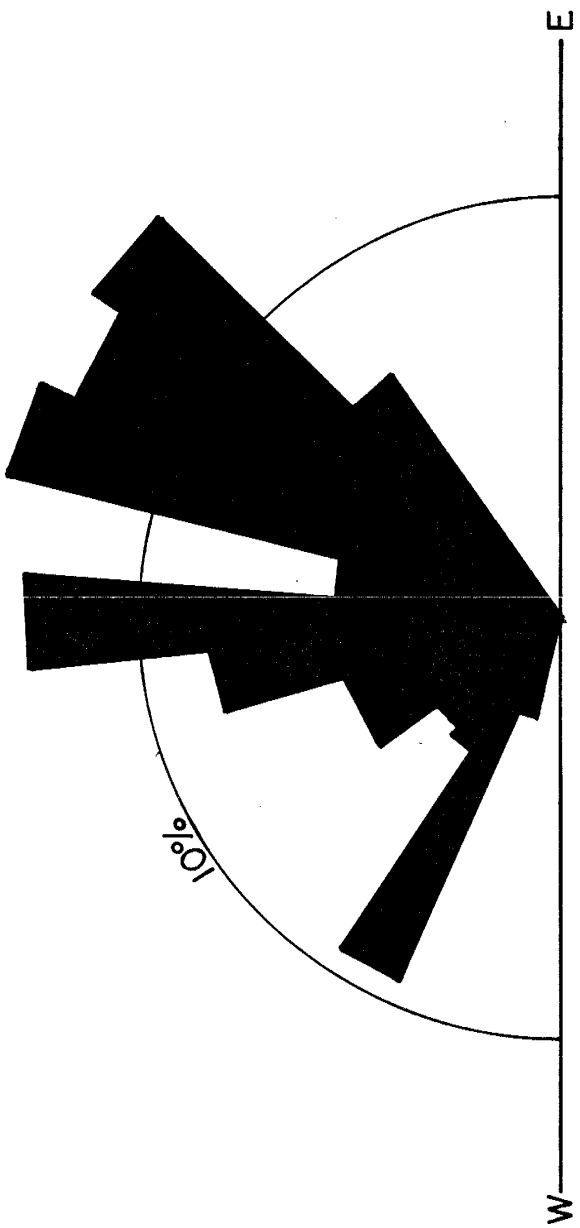
E
W
10%

Figure 62. Compass-rose diagram for horizontal, least principal stress directions determined from slickenside striations and mullions on Neogene faults in north-central Black Range. It is assumed that intermediate principal stress direction is normal to striations in the plane of the fault and that the maximum principal stress direction is oriented at approximately 30 degrees to the plane of the fault.

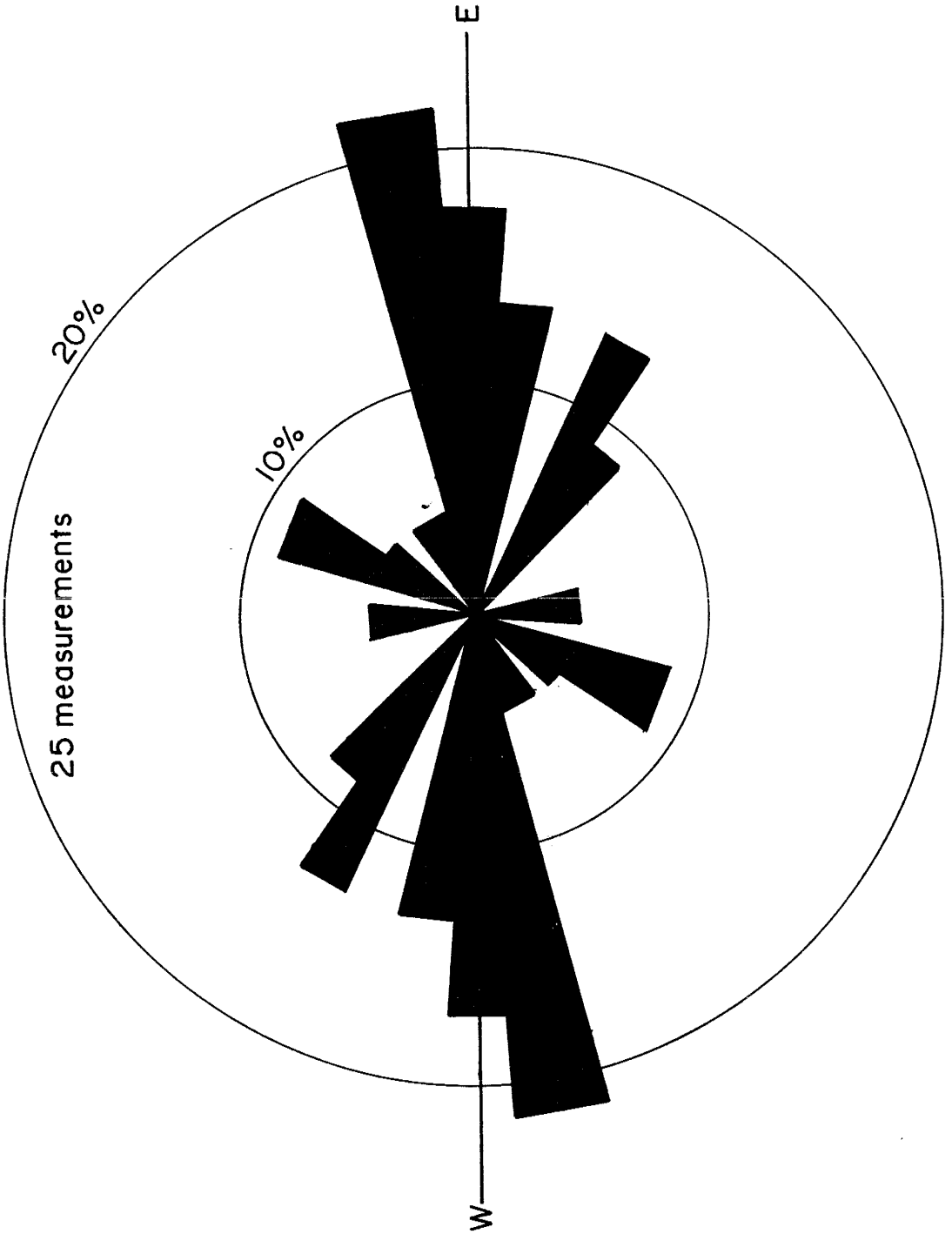
E
W
20%
10%
25 measurements

Neogene faulting in the north-central Black Range.

The NNE-striking boundary faults that define the belt of graben and horst structures in the eastern part of north-central Black Range are continuous for long distances (30 to 70 km), and yet, they typically only show stratigraphic offsets of a few hundred meters. The westernmost boundary fault shown in Figure 60 extensively reactivated a late Oligocene epithermal vein system known as the Blackhawk vein, Ivanhoe-Emporia vein, and Great Master lode. Few of the other boundary faults show this characteristic, but rather, they typically crosscut and offset the older vein-filled faults.

Along the eastern margin of the 33 Ma Emory caldera is a narrow graben that extends northward for more than 25 km before it merges with the larger Winston graben. Woodard (1982) referred to a northern segment of this structure as the Chloride Creek graben and noted that it cut rocks as young as ~28 Ma. The boundary fault between the Emory caldera and Chloride Creek graben shows enigmatic relationships in that it is stratigraphically down to the east, but geometry of fault surfaces dip (67-79 degrees) towards the west (Abitz, 1989). This fault geometry is interpreted by Abitz (1989) as representing either intracaldera resurgence or post-caldera reverse faulting. The Chloride Creek graben has an anomalous magmatic affinity in that the Moccasin John Rhyolite flow-dome complex, Chloride Creek dome, and Sheep Creek dome all occur within

its boundaries.

Between the townsites of Chloride and Hermosa, New Mexico, a horst block occurs between the Winston and Chloride Creek grabens (see Fig. 60). Neogene faulting within this horst block typically resulted in reactivation of the northwest-striking late Oligocene veins, thus sparing most northerly trending structures from reactivation. The Eocene wrench-fault system described earlier and shown in Figure 52 is best preserved and exposed within this horst block.

Chapter 4. SUMMARY: CENOZOIC GEOLOGIC HISTORY OF NORTH-CENTRAL BLACK RANGE, NEW MEXICO

Introduction

Rocks of the north-central Black Range, New Mexico, record a complex and dynamic geologic history for the Cenozoic Era. Located only 300 km from the protruding southwest corner of the North American craton, this area has been strongly influenced by plate-tectonic activity along this margin. On a regional scale, rocks of the north-central Black Range register the growth of the central portion of the Mogollon-Datil volcanic field, development of the Rio Grande rift, and their interrelationships. The geologic history formulated in this chapter represents interpretations based on the data presented in the previous two chapters. Table 21 summarizes the Cenozoic geologic history of the north-central Black Range. The Cenozoic geologic history of this area is divided into time intervals during which similar styles of magmatism, tectonism, and sedimentation occurred.

~66 to ~44 Ma

The geologic history of the north-central Black Range for the time period from approximately 66 to 44 Ma has been largely erased due to uplift and erosion. Removal of the entire Cretaceous section and upper portion of the Permian section probably occurred during this time interval.

Table 22. Summary of Cenozoic geologic history of north-central Black Range, New Mexico, and surrounding areas.

Interval	Magmatism	Sedimentation	Deposits in Black Range
~46 to ~44 Ma	large strato-volcanoes, sills, & laccoliths along NE-trending lineaments	conglomerates & sandstones; Paleozoic & volcanic clasts	basal conglomerate of Rubio Peak Fm.
~44 to ~37 Ma	widespread small stratovolcanoes, dikes & plugs, intermediate comp.	debris flows, sandstones, gravity-slide blocks; volcaniclastics	Rubio Peak Fm.
~37 to ~35 Ma	low-aspect ratio ash-flow tuffs, post-caldera volcanism	fine-grained sandstones & siltstones; volcaniclastics	tuff of Racaue Ramos Canyon, tuff of Victoria Tank, Kneeling Nun Tuff, Cuchillo Negro Complex; sandstone of Cliff Canyon
~35 to ~30 Ma	quiescent	none in eastern Black Range, fine-grained volcaniclastics in western Black Range	minor distal ash-flow tuffs, sandstone of Monument Park
~30 to ~28 Ma	intermediate lavas followed by rhyolitic domes & dikes w/ assoc. high-aspect ratio ash-flow tuffs	very minor, fine-grained volcaniclastics	basaltic andesite of Poverty Creek, numerous rhyolite lavas & tuffs, Taylor Creek Rhyolite
~28 to ~26 Ma	quiescent	conglomerates, sandstone, volcanic clasts	Santa Fe Group
~26 to ~ 5 Ma	intermediate lavas, flow domes, & dikes	conglomerates, sandstones, volcanic clasts in lower section, some Paleozoic clasts in uppermost section	Santa Fe Group, Gila Group, Bearwallow Mt. Fm., and andesite of Winston graben

~5 to Present	alkali basalts	minor, restricted to incised arroyo bottoms & hill slopes	Santa Fe Group, Gila Group, Quaternary alluvium & colluvium

Table 22. (cont.)

Interval	Tectonism
~66 to ~44 Ma	uplift, no data on faulting
~44 to ~37 Ma	dextral strike-slip faulting along overall NNE-trend
~37 to ~35 Ma	tumescence of Emory caldera, NE-SW extension ?, left lateral strike-slip faulting ?, caldera resurgence
~35 to ~30 Ma	quiescent
~30 to ~28 Ma	beginning of extension
~28 to ~26 Ma	NE-SW extension
~26 to ~5 Ma	E-W extension
~5 to Present	epeirogenic uplift

However, there are no real age constraints for the unconformity at the base of the Cenozoic section in the Black Range (i.e. this unconformity could be Late Cretaceous in age).

Similarities in sedimentary style and clast lithologies between the basal conglomerate member of the Rubio Peak Formation in north-central Black Range and the Starvation Draw Member of the Rubio Peak Formation (Clemons, 1982), Lobo Formation (Darton, 1928; Lemley, 1982), and Love Ranch Formation (Kottlowski et al., 1956) in southern New Mexico suggest a common origin for these units. The latter three units are considered to be synorogenic to postorogenic deposits related to late Laramide compressional uplifts (west-northwest- to northwest-trending fault-propagation folds and thrusts) in southern New Mexico (Seager, 1975, 1983; Seager and Mack, 1986; Brown and Clemons, 1983).

Clasts lithologies of Permian Abo Formation, Paleozoic limestone, holocrystaline monzonite, and heterolithic volcanic rock types, plus east-to-west paleoflow directions (Cather, 1986; this report) suggest a probable source area for the basal conglomerate of Rubio Peak Formation somewhere in the vicinity of the Sierra Cuchillo-Animas uplift. Precambrian basement rocks were not exposed in the source area. The occurrence of the tuff of Miranda Homestead interbedded with the basal conglomerate of the Rubio Peak Formation indicates distal volcanic activity during this time period.

~44 to ~37 Ma

The geologic history of the time interval from approximately 44 to 37 Ma in the north-central Black range is recorded in the deposits of the Rubio Peak Formation. The early portion of this interval was dominated by mass-wasting processes such as debris flows, mudflows, rockslides, hyperconcentrated flood flows, and enormous gravity slides. Except for three discrete intervals that contain clasts of Pennsylvanian limestone, these deposits are strictly volcaniclastic. Deposition into an intermontane basin centered in the southern portion of the north-central Black Range is suggested from facies distributions.

Tectonism during this time interval produced dextral strike-slip faulting along an overall north-northeast trend. Syntectonic dikes and plugs fed the extensive lava flows of the upper Rubio Peak Formation that covered most of the north-central Black Range. Analysis of paleostress orientations for this time interval indicates that the maximum principal stress was horizontal and directed northeast-southwest, and that the least principal stress was also horizontal and perpendicularily directed. [It is interesting to note that the only change in principal stresses required to shift from the northwest-southeast-trending compressional features that formed during the 64 to

44 Ma time interval to north-northeast-trending wrench faulting active during the 44 to 37 Ma time interval is an interchange of least- and intermediate-principal-stress directions.]

An idealized model (after Crowell, 1974) for the geologic setting of the north-central Black Range during the time interval of approximately 44 to 37 Ma is that of a pull-apart basin produced by an echelon dextral strike-slip faults (Fig. 63). In cross section, this model is viewed as a negative flower structure. This interpretive model is based largely on exposures from the central portion of the basin characterized by dextral strike-slip structures, slide blocks, and rapid facies changes basinward. The western margin is invisioned as possibly lying along the Santa Rita-Hanover axis and the eastern margin as possibly buried beneath the Winston graben. The southern boundary is possibly along the northeast-trending Chise lineament.

~37 to ~35 Ma

In the north-central Black Range, the time interval from approximately 37 to 35 Ma is dominated by development of the Emory caldera. This development culminated in eruption of the Kneeling Nun Tuff, regionally the most widespread and voluminous Cenozoic volcanic unit. Prior to eruption of the Kneeling Nun Tuff, the tuffs of Rocque Ramos Canyon and Victoria Tank are believed to have erupted from the environs

Figure 63. Idealized model of a pull-apart basin produced by en echelon dextral strike-slip faults for the geologic setting of the north-central Black Range during the time interval from approximately 44 to 37 Ma (modified after Crowell, 1974).

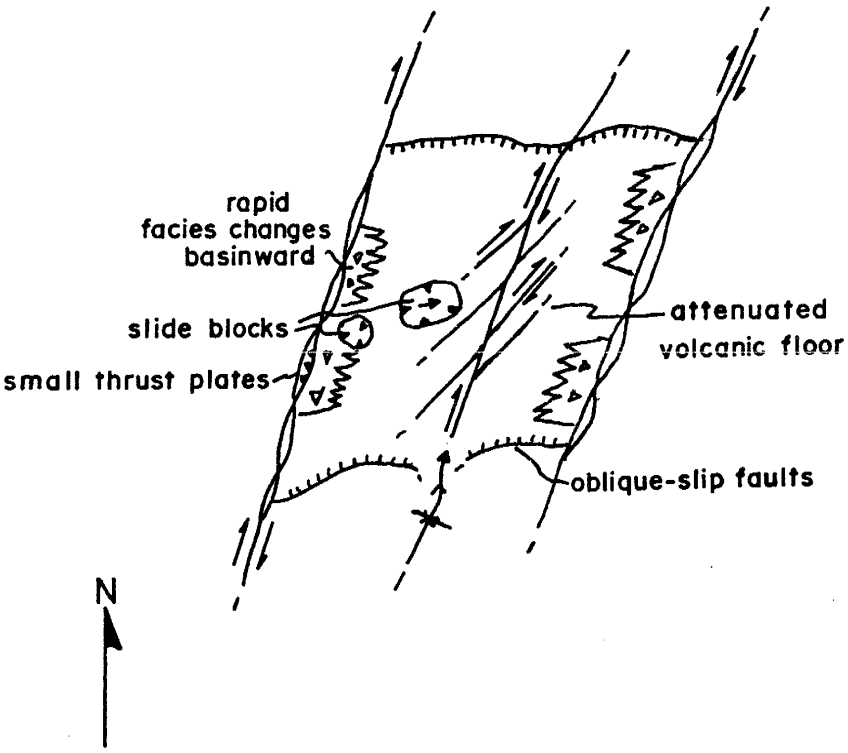
rapid
facies changes
basinward
slide blocks
small thrust plates
attenuated
volcanic floor
oblique-slip faults
N

of the Emory caldera. Also prior to eruption of the Kneeling Nun Tuff, tumescence along a north-northeast axis removed tuff of Rocque Ramos Canyon, tuff of Victoria Tank, and much of upper Rubio Peak Formation from the northern margin of the Emory caldera. Post-caldera volcanism Idacite of Curtis Canyon (Abitz, 1989) and the Cuchillo Negro complexl was localized and relatively minor. Resurgence of the Emory caldera was strong and oriented along a north-northeast-trending axis that persisted northward from the Emory caldera for many tens of kilometers.

The occurrence of the eastern structural margin of the Emory caldera along the southern continuation of the Black Range wrench-fault system is viewed as more than coincidental. Rather, it is interpreted that this caldera margin was structurally controlled by the older wrench-fault system. Unfortunately, regional paleostress orientations for the north-central Black Range are not readily available for this time interval. Paleostress indicators from Aldrich et al. (1986) indicate a regional northeast-southwest least principal horizontal stress for southwestern New Mexico during this time interval. Such a stress field could reactivate the Black Range wrench faults in a left-lateral sense of motion and produce extension in the area of the Emory caldera.

~35 to ~30 Ma

The time interval from approximately 35 to 30 Ma in north-central Black Range is marked by both tectonic and magmatic quiescence. In the eastern portion of the north-central Black Range and in all of the adjacent Sierra Cuchillo, a stable plateau capped by Kneeling Nun Tuff existed throughout this time interval. In the western portion of the north-central Black Range, distal volcanic units (Caballo Blanco Tuff and tuff of Koko Well) intercalated with fine-grained volcaniclastic sediments were deposited on a gentle margin to this plateau. There are no known locally derived volcanic units, nor any known significant structures active during this time period in the north-central Black Range. This hiatus marks the end of a virtually continous progression of magmatism and tectonism active from about 44 to 35 Ma. Chemically, volcanic rocks that originated in the north-central Black Range display an increasing trend in SiO2 content, a decreasing trend in CaO, and a slight increasing trend in K2O with time.

~30 to ~28 Ma

The hiatus in magmatic activity in the north-central Black Range ended at approximately 30 Ma with a widespread 'flareup' in volcanism. Initially, multiple lava flows of the basaltic andesite of Poverty Creek blanketed the entire

area. This volcanism was rapidly followed by eruption of numerous rhyolite and high-silica rhyolite flow-dome complexes and related pyroclastics. Accumulations of several hundreds of meters of these intercalated rhyolitic deposits further blanketed the north-central Black Range. In this area, the Taylor Creek Rhyolite and rhyolite of Franks Mountain (~28 Ma) represent the climax of this brief and dramatic volcanic episode. Chemical trends for this volcanic activity closely approximately those of volcanic rocks erupted prior to the volcanic hiatus, showing an increase in SiO2, a decrease in CaO, and a slight increase in K2O with time. The major difference in the chemistry between the two intervals is the high-silica end member for the 30 to 28 Ma volcanism.

During this time interval, there does not appear to have been any significant fault activity. Both basaltic andesite of Poverty Creek and the rhyolite deposits covered the north-central Black Range with little indication of any uplifts or basins or faulting. From studies elsewhere in southern New Mexico, Chamberlin (1978) and Chapin and Seager (1975) describe the basaltic andesite to high-silica rhyolite assemblage as marking the initial development of the Rio Grande rift, with extensional basins forming shortly after eruptions of high-silica rhyolite.

In the western portion of the north-central Black Range, distal deposits of Bloodgood Canyon Tuff (erupted from the Bursum cauldron in the Mogollon Mountains, Ratte' et al.,

1984) overlie Taylor Creek Rhyolite (Eggleston, 1987). This observation precludes the interpretation of Rhodes (1976) that the Taylor Creek Rhyolite is the product of post-collapse ring-fracture volcanism that followed eruption of the Bloodgood Canyon Tuff.

~28 to ~26 Ma

During the time interval from approximately 28 to 26 Ma, magmatic activity waned and tectonic activity began in the north-central Black Range. Widespread hydrothermal alteration-mineralization of the Chloride mining district and vapor-phase mineralization of Taylor Creek tin district occurred during this time interval. The transition from the previous interval was slightly overlapping and gradational.

Hydrothermal convection cells generated by the numerous rhyolite intrusions from 30 to 28 Ma produced the epithermal vein deposits of the Chloride mining district (Harrison, 1986). Within these veins, 'ore shoots' containing economic and sub-economic concentrations of base and precious metals were formed in structurally controlled areas. District-wide zonations in precious metal mineralization are related to areas of upwelling and boiling, and to regions of lateral flow and fluid mixing (Behr, 1988; Harrison, 1989).

In domes of the Taylor Creek Rhyolite, tin mineralization consisting of fumarolic incrustations were deposited from high temperature (>650 degrees C) magmatic

fluids (Eggleston, 1987). This tin mineralization was followed by very short lived epithermal systems that deposited veinlets of quartz, calcite, and flourite from fluids dominated by meteoric waters at temperatures between 340 and 130 degrees C (Eggleston, 1987). Low-grade disseminated deposits of Be, Ti, Mn, and Fe are also related to domes of the Taylor Creek Rhyolite. This mineralization was the product of vapor-phase crystallization: a post-emplacement process common in certain ignimbrites and high-silica rhyolite lavas with the responsible fluids derived from the host rock during cooling and crystalization (Smith, 1960).

From the geologic setting and known mineral deposits of this time interval, additional mineral deposits can be inferred to possibly exist at depth in the north-central Black Range. Figure 64 is an idealized model [modified and adapted from Burt and Sheridan (1981), and Sillitoe and Bonham (1984)] showing the setting of mineral deposits in the Taylor Creek and Chloride districts and possible buried mineral deposits.

Vein deposits of the Chloride mining district occupy normal and oblique-slip fault structures that developed during this time interval. In most cases, mineralization and faulting were contemporaneous. Mineralized faults were the result of northeast-southwest extension related to initial development of the Rio Grande rift. Location of ore-grade mineralization in the Chloride mining district was

Figure 64. Idealized model showing the geologic setting of mineral deposits in the Taylor Creek tin district and Chloride mining district and possible buried mineral deposits in north-central Black Range [modified and adapted from Burt and Sheridan (1981) and Silliitoe and Bonham (1984)].

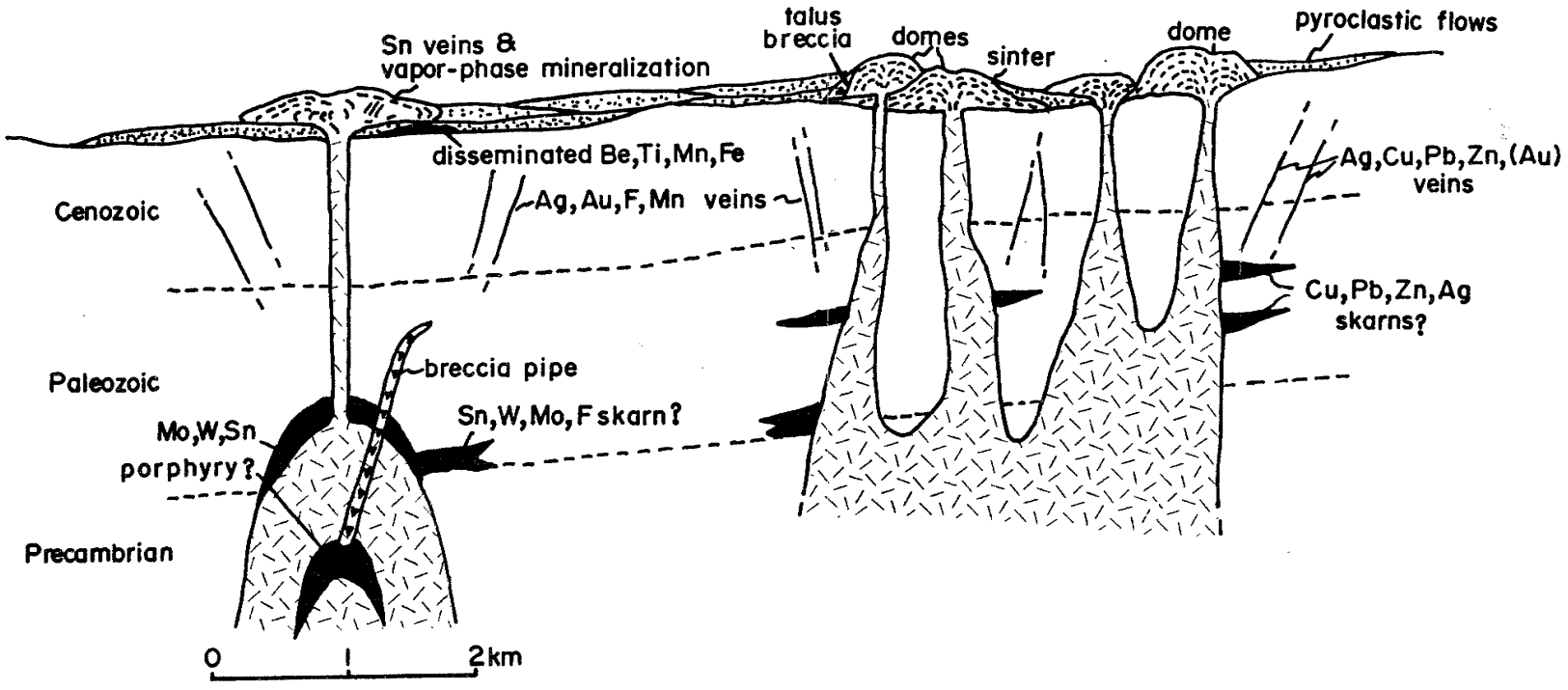
Taylor Creek tin district
Chloride mining district
Sn veins &
vapor-phase mineralization
talus
breccia
domes
sinter
dome
pyroclastic flows
disseminated Be,Ti,Mn,Fe
Ag,Au,F,Mn veins
Ag,Cu,Pb,Zn,(Au)
veins
Cenozoic
Cu,Pb,Zn,Ag
skarns?
breccia pipe
Paleozoic
Sn,W,Mo,F skarn?
Mo,W,Sn
porphyry?
Precambrian
0
1
2km

largely controlled by vein intersections with strands of the older wrench-fault system (Harrison, 1987).

~26 to ~5 Ma

During the time interval from approximately 26 to 5 Ma, extensive normal faulting related to the Rio Grande rift occurred throughout the eastern portion of the north-central Black Range. Most previously existing structures were reactivated and numerous new structures developed. The eastern margin of the present-day Black Range was defined by the formation of the Winston graben, largely during the Miocene epoch. Strain analysis for faulting in the Black Range during this time interval indicates a general east-west extension. The western portion of the north-central Black Range was relatively quiescent with a boundary between tectonically active and inactive areas closely following an extension of the Santa Rita-Hanover axis.

Volcanism (Bearwallow Mountain Formation, andesite of Winston graben) during this time interval was intermittent and widespread, and persisted until approximately 18 Ma. This volcanism represents the third phase of Cenozoic intermediate to mafic magmatic activity in the north-central Black Range. However, unlike the two preceding phases, this phase of magmatic activity never progressed to a rhyolite end member. Unpublished dating by J. Ratte' (1986, oral

communication) suggests that much of the Bearwallow Mountain Formation in the central and western portion of the Mogollon-Datil volcanic field is approximately 20 to 24 Ma, and may thus be a continuation of the bimodal sequence that began with eruption of the basaltic andesite of Poverty Creek. Such bimodal assemblages are known to be typical of extensional environments in the western United States (Christiansen and Lipman, 1972).

Deposits of the Santa Fe Group and Gila Group dominate the stratigraphic section for this time interval in the north-central Black Range. These deposits are typically fanglomerates and coarse conglomerates and sandstones derived largely from uplifts surrounding the Mogollon Plateau. Lower beds are intercalated with distal volcanic units and locally show moderate tilting. The andesite of Winston graben (dated by K/Ar at 18.3 $\pm$ 0.4 Ma, Seager et al., 1984) is intercalated with middle beds of Santa Fe Group sediments in the Winston graben. After a long period of erosion and sedimentation, the entire north-central Black Range was graded to an extensive pediment surface. Concordant surfaces can be found throughout the north-central Black Range on both sides of the Continental Divide. An alkali basalt flow dated by K/Ar at 4.9 $\pm$ 0.1 Ma (Seager et al., 1984) rests on this surface.

~5 Ma to Present

During the past 5 million years, north-central Black Range has experienced epeirogenic uplift. Incised streams on both sides of the Continental Divide have produced canyons as much as 400 m deep with very steep sides. The 4.8 Ma alkali basalt flow in the Winston graben provides a maximum age for initiation of this uplift. This uplift is thus largely contemporaneous with epeirogenic uplift seen elsewhere along the Rio Grande rift in New Mexico (7 to 4 Ma, Chapin, 1979; 8 to 3 Ma, Seager and Morgan, 1979) and Colorado (Scott, 1975). There are no newly formed faults for this time period in the north-central Black Range.

References for Chapters 2, 3, & 4

Abitz, R.J., 1984, Volcanic geology and geochemistry of the northeastern Black Range Primitive Area and vicinity, Sierra County, New Mexico: Unpublished M.S. thesis; University of New Mexico, Albuquerque, 121 pp.

Abitz, R.J., 1989, Geology and petrogenesis of the northern Emory caldera, Sierra County, New Mexico: Unpublished Ph.D. dissertation; University of New Mexico, Albuquerque, 174 pp.

Abitz, R.J., and Matheney, R.K., 1987, Sr and O isotope disequilibrium in a welded high-silica rhyolite tuff: Geological Society of America, Abstracts with Programs, v. 19, no. 7, p. 566.

Aldrich, M.J. Jr., 1972, Tracing a subsurface structure by joint analysis: Santa Rita-Hanover axis, southwestern New Mexico: Unpublished Ph.D. dissertation; University of New Mexico, Albuquerque, 106 pp.

Aldrich, M.J. Jr., 1974, Structural development of the Hanover-Fierro pluton, southwestern New Mexico: Geological Society of America Bulletin, v. 85, p. 963-968.

Aldrich, M.J. Jr., 1976, Geology and flow directions of volcanic rocks of the North Star Mesa quadrangle, Grant County, New Mexico; in Elston, W.E. and Northrop, S.A. (eds.), Cenozoic volcanism in southwestern New Mexico: New Mexico Geological Society, Special Publication Number 5, p. 79-81.

Aldrich, M.J. Jr., Chapin, C.E., and Laughlin, A.W., 1986, Stress history and tectonic development of the Rio Grande rift, New Mexico: Journal of Geophysical Research, v. 91, no. B6, p. 6199-6211.

Axelrod, D.I., 1975, Tertiary floras from the Rio Grande rift: New Mexico Geological Society, Guidebook 26, p. 85-88.

Axelrod, D.I., and Bailey, H.P., 1976, Tertiary vegetation, climate, and altitude of the Rio Grande depression, New Mexico-Colorado: Paleobiology, v. 2, p. 235-254.

Behr, C., 1988, Geochemical analyses of ore fluids from the St. Cloud - U.S. Treasury vein system, Chloride mining district, New Mexico: Unpublished M.S. thesis; New Mexico Institute of Mining and Technology, Socorro, 125 pp.

Behr, C., and Norman, D.I., 1986, Geochemical analyses of

epithermal ore fluids: St. Cloud - U.S. Treasury vein system, Chloride mining district (abstract): U. S. Geological Society, Abstracts with Programs, v. 18, no. 6, p. 538.

Bornhorst, T.J., 1980, Major- and trace-element geochemistry and mineralogy of upper Eocene to Quaternary volcanic rocks of the Mogollon-Datil volcanic field, southwestern New Mexico: Unpublished Ph.D. dissertation; University of New Mexico, Albuquerque, 1100 pp.

Bowie, M.R., and Barker, J.M., 1986, Clinoptilolite west of Cuchillo Negro Creek, New Mexico-zeolite authigenesis of the tuff of Little Mineral Creek: New Mexico Geological Society, Guidebook 37, p. 283-286.

Brown, G.A., and Clemons, R.E., 1983, Florida Mountains section of southwest New Mexico overthrust belt-a reevaluation: New Mexico Geology, v. 5, p. 26-29.

Burt, D.M., and Sheridan, M.F., 1981, Model for the formation of uranium/lithophile element deposits of fluorine-rich volcanic rocks: American Association of Petroleum Geologists, Studies in Geology, v. 13, p. 99-109.

Bushnell, H.P., 1953, Geology of the McRae Canyon area, Sierra County, New Mexico: Unpublished M.S. thesis; University of New Mexico, Albuquerque, 106 pp.

Bushnell, H.P., 1955, Stratigraphy of the McRae Formation: Compass, v. 33, p. 9-17.

Callender, J.F., Seager, W.R., and Swanberg, C.A., 1983, Late Tertiary and Quaternary tectonics and volcanism: Geothermal Resources of New Mexico: New Mexico State University Energy Institute, Scientific Map Series scale 1:500,000 , 1 sheet.

Cameron, K.L., Nimz, G.J., Kuentz, D., Niemeyer, S., and Gunn, S., 1989, Southern Cordilleran basaltic andesite suite, southern Chihuahua, Mexico: A link between Tertiary continental arc and flood basalt magmatism in North America: Journal of Geophysical Research, v. 94, no. B6, p. 7817-7840.

Cather, S.M., 1896, Volcano-sedimentary evolution and tectonic implications of the Datil Group (latest Eocene-early Oligocene), west-central New Mexico: Unpublished Ph.D. dissertation; University of Texas at Austin, 482 pp.

Chamberlain, R.M., 1978, Structural development of the Lemitar Mountains, an intrarift tilted fault-block

uplift, central New Mexico: Los Alamos Scientific Laboratory, University of California, p. 22-24.

Chapin, C.E., 1978, Overview of Cenozoic features, San Marcial basin; in Hawley, J.W., compiler, Guidebook to Rio Grande rift in New Mexico and Colorado: New Mexico Bureau of Mines and Mineral Resources, Circular 163, p. 96-97.

Chapin, C.E., 1979, Evolution of the Rio Grande rift-a summary; in Reiker, R.E., (ed.), Rio Grande rift: tectonics and magmatism: American Geophysical Union, Washington, D.C., p. 1-15.

Chapin, C.E., 1983, An overview of Laramide wrench faulting in southern Rocky Mountains with an emphasis on petroleum exploration: Rocky Mountain Association of Geologists, Guidebook to 1983 Field Conference, p. 169-179.

Chapin, C.E., 1989, Volcanism along the Socorro accommodation zone, Rio Grande rift, New Mexico, in Chapin, C.E., and Zirdek, J., (eds.), Field excursions to volcanic terranes in the western United States, Volume I: Southern Rocky Mountain Region: New Mexico Bureau of Mines and Mineral Resources Memoir 46, p. 46-57.

Chapin, C.E., and Cather, S.M., 1981, Eocene tectonics and sedimentation in the Colorado Plateau-Rocky Mountain area: Arizona Geological Society Digest, v. 14, p. 173-198.

Chapin, C.E., and Seager, W.R., 1975, Evolution of Rio Grande rift in the Socorro and Las Cruces areas: New Mexico Geological Society, Guidebook 26, p. 297-322.

Chapin, C.e., Chamberlain, R.M., Osburn, G,R., Sanford, A.R., and White, D.W., 1978, Exploration framework of the Socorro geothermal area, New Mexico; in Chapin, C.E., and Elston, W.E., (eds.), Field guide to selected cauldrons and mining districts of the Datil-Mogollon volcanic field, New Mexico: New Mexico Geological Society, Special Publication No. 7, p. 115-129.

Chapin, C.E., Jahns, R.H., Chamberlain, R.M., and Osburn, G.R., 1978, First day road log: Truth or Consequences via Magdalena and Winston; in Chapin, C.E., Elston, W.E., and James, H.L. (eds.), Field guide to selected cauldrons and mining districts of the Datil-Mogollon volcanic field, New Mexico: New Mexico Geological Society, Special Publication No. 7, p. 1-31.

Chapin, C.E., Siemers, W.T., and Osburn, G.R., 1975, Summary

of radiometric ages of New Mexico rocks: New Mexico Bureau of Mines and Mineral Resources, Open-file Report 60.

Christiansen, R.L., and Lipman, P.W., 1972, Cenozoic volcanism and plate tectonic evolution of the United States, II, late Cenozoic: Royal Society of London, Philosophical Transactions (A), v. 272, p. 249-284.

Clemons, R.E., 1975, Petrology of the Bell Top Formation: New Mexico Geological Society, Guidebook 26, p. 123-130.

Clemons, R.E., 1976, Sierra de las Uvas ash-flow field, south-central New Mexico; in Woodward, L.A., and Northrop, S.A. (eds.), Tectonics and Mineral Resources of southwestern New Mexico: New Mexico Geological Society, Special Publication Number 6, p. 115-121.

Clemons, R.E., 1978, Cross section of Good Sight - Cedar Hills depression; in Chapin, C.E., Elston, W.E., and James, H.L. (eds.), Field guide to selected cauldrons and mining districts of the Datil-Mogollon volcanic field, New Mexico: New Mexico Geological Society, Special Publication No. 7, Plate 3.

Clemons, R.E., 1979, Geology of Good Sight Mountains and Uvas Valley, southwest New Mexico: New Mexico Bureau of Mines and Mineral Resources, Circular 169, 32 pp..

Clemons, R.E., 1982, Geology of the Massacre Peak quadrangle, Luna County, New Mexico: New Mexico Bureau of Mines and Mineral Resources, Geologic Map 51, scale 1:24,000.

Clemons, R.E., and Mack, G.H., 1988, Geology of southwestern New Mexico: New Mexico Geological Society, Guidebook 39, p. 45-57.

Clemons, R.E., and Seager, W.R., 1973, Geology of the Souse Springs quadrangle, New Mexico: New Mexico Bureau of Mines and Mineral Resources, Bulletin 100, 31 pp.

Coney, P.J., 1976, Structure, volcanic stratigraphy, and gravity across the Mogollon Plateau, New Mexico; in Elston, W.E., and Northrop, S.A. (eds.), Cenozoic volcanism in southwestern New Mexico: New Mexico Geological Society, Special Publication Number 5, p. 29-41.

Correa, B.P., 1981, The Taylor Creek Rhyolite and associated tin deposits, southwestern New Mexico: Unpublished M.S. thesis; Arizona State University, Tempe, 105 pp.

Crowell, J.C., 1974, Orgin of Late Cenozoic basins in

southern California; in Dickinson, W.R., (ed.), Tectonics and sedimentation: Society of Economic Paleontologists and Mineralogists, Special Publication No. 22, p. 190-204.

Dalrymple, G.B., and Duffield, W.A., 1988, High precision 40Ar/39Ar dating of Oligocene rhyolites from the Mogollon-Datil volcanic field using a continuous laser system: Geophysical Research Letters, v. 15, no. 5, p. 463-466.

Darton, N.H., 1928, "red beds" and associated formations in New Mexico, with an outline of the geology of the state: U.S. Geological Survey Bulletin, v. 794, p. 1-356.

Dane, C.H., and Bachman, G.O., 1965, Geological Map of New Mexico: U.S. Geological Survey, State Geologic Map, scale 1:500,000, 2 sheets.

Deal, E.G., and Rhodes, R.C., 1976, Volcano-tectonic structures in the San Mateo Mountains, Socorro County, New Mexico; in Elston, W.E., and Northrop, S.A. (eds.), Cenozoic volcanism in southwestern New Mexico; New Mexico Geological Society, Special Publication No. 5, p. 51-56.

Du Bray, E.A., and Duffield, W.A., 1987, Compositions of feldspar phenocrysts and petrogenetic implications, Taylor Creek Rhyolite, New Mexico: Geological Society of America, Abstracts with Programs, v. 19, no. 5, p. 272.

Duffield, W.A., 1989, Field guide to the Taylor Creek Rhyolite, Black Range, New Mexico; in Chapin, C.E., and Zidek, J. (eds.), Field excursions to volcanic terranes in the western United States, Volume 1: Southern Rocky Mountain region: New Mexico Bureau of Mines and Mineral Resources, Memoir 46, p. 107-110.

Duffield, W.A., Richter, D.H., and Priest, S.S., 1987, Preliminary geologic map of the Taylor Creek Rhyolite, Catron and Sierra Counties, New Mexico: U. S. Geological Survey, Open-file Report 87-515, 1 sheet.

Dunham, K.C., 1935, The geology of the Organ Mountains, with an account of the geology and mineral resources of Dona Ana County: New Mexico Bureau of Mines and Mineral Resources, Bulletin 11, 272 pp.

Eaton, G.P., 1979, A plate-tectonic model for late Cenozoic crustal spreading in the western United States; in Riecker, R.E. (ed.), Rio Grande rift: tectonics and magmatism: American Geophysical Union, Washington, D.C., p. 7-32.

Eggleston, T.L., 1986, Alteration associated with the rhyolite porphyry of Kline Mountain, Black Range, New Mexico: New Mexico Geological Society, Guidebook 37, p. 16-17.

Eggleston, T.L., 1987, The Taylor Creek district, New Mexico: Geology, petrology, and tin deposits: Unpublished Ph.D. dissertation; New Mexico Institute of Mining and Technology, Socorro, 473 pp.

Eggleston, T.L., and Norman, D.I., 1983, Taylor Creek tin district-stratigraphy, structure, and timing of mineralization: New Mexico Geology, v. 5, no. 1, p. 1-4.

Eggleston, T.L., and Norman, D.I., 1986, A summary of the geology, geochemistry, and tin occurrences in the Black Range, New Mexico: New Mexico Geological Society, Guidebook 37, p. 173-177.

Eggleston, T.L., and Harrison, R.W., in review, Geology of Sawmill Peak Quadrangle, Sierra and Catron Counties: New Mexico Bureau of Mines and Mineral Resources, Geologic Map, scale 1:24,000.

Eichelberger, J.C., Carrigan, C.R., Westrich, H.R., and Price, R.H., 1986, Non-explosive silicic volcanism: Nature, v. 323, p. 598-602.

Elston, W.E., 1957, Geology and mineral resources of Dwyer quadrangle, Grant, Luna, and Sierra Counties, New Mexico: New Mexico Bureau of Mines and Mineral Resources, Bulletin 38, 86 pp.

Elston, W.E., 1968, Terminology and distribution of ash flows of the Mogollon-Silver City-Lordsburg region, New Mexico: Arizona Geological Society, Guidebook III to southern Arizona, p. 231-240.

Elston, W.E., 1976, Glossary of stratigraphic terms of the Mogollon-Datil volcanic province, New Mexico; in Elston, E.E., and Northrop, S.A. (eds.), Cenozoic volcanism in southwestern New Mexico: New Mexico Geological Society, Special Publication 5, 131-144.

Elston, W.E., Coney, P.J., and Rhodes, R.C., 1968, A progress report on the Mogollon Plateau volcanic province, southwestern New Mexico; in Epis, R.C. (ed.), Cenozoic volcanism in the Southern Rocky Mountains: Colorado School of Mines Quarterly, v. 63, p. 261-287.

Elston, W.E., Coney, P.J., and Rhodes, R.C., 1970, Progress report on the Mogollon Plateau volcanic province, southwestern New Mexico, No. 2: New Mexico Geological Society, Guidebook 21, p. 75-86.

Elston, W.E., Damon, P.E., Coney, P.J., Rhodes, R.C., Smith, E.I., and Bikerman, M., 1973, Tertiary volcanic rocks, Mogollon-Datil province, New Mexico, and surrounding region: K-Ar dates, patterns of eruption, and periods of mineralization: Geological Society of America Bulletin, v. 84, p. 2259-2273.

Elston, W.E., Seager, W.R., and Clemons, R.E., 1975, Emory cauldron, Black Range, New Mexico: source of Kneeling Nun Tuff: New Mexico Geological Society, Guidebook 26, p. 283-292.

Elston, W.E., and Bornhorst, T.J., 1979, The Rio Grande rift in context of regional post-40 m.y. volcanic and tectonic events, in Riecker, R.E. (ed.), **Rio Grande Rift: Tectonics and Magmatism**: American Geophysical Union, Washington, D.C., p. 416-438.

Ericksen, G.E., Wedow, H., Jr., Eaton, G.P., and Leland, G.R., 1970, Mineral resources of the Black Range Primitive Area, Grant, Sierra, and Catron Counties, New Mexico: U.S. Geological Survey, Bulletin 1319-E, 162 pp.

Farkas, S.E., 1969, Geology of the southern San Mateo Mountains, Socorro and Sierra Counties, New Mexico: Unpublished Ph.D. Dissertation; University of New Mexico, Albuquerque, 137 pp.

Faure, G., and Powell, J.L., 1972, **Strontium Isotope Geology**: Springer-Verlag, Berlin, 188 pp.

Ferguson, H.G., 1927, Geology and ore deposits of the Mogollon mining district, New Mexico: U.S. Geological Survey, Bulletin 787, 100 pp.

Fisher, R.V., and Schminke, H.V., 1984, Pyroclastic Rocks: Berlin, Springer-Verlag, 472 p.

Fodor, R.V., 1975, Petrology of basalt and andesite of the Black Range, New Mexico: Geological Society of America Bulletin, v. 86, p. 295-304.

Fodor, R.V., 1976, Volcanic geology of the northern Black Range, New Mexico; in Elston, W.E., and Northrpo, S.A. (eds.), Cenozoic volcanism in southwestern New Mexico: New Mexico Geological Society, Special Publication Number 5, p. 68-70.

Fodor, R.V., 1978, Ultramafic and mafic inclusions and megacryts in Pliocene basalt, Black Range, New Mexico: Geological Society of America Bulletin, v. 89, p. 451-459.

Foord, E.E., Oakman, M.R., and Maxwell, C.H., 1983, Durangite from the Black Range, New Mexico, and new data on durangite from Durango and Cornwall: Canadian Mineralogist, v. 23, p. 241-246.

Fries, C. Jr., 1940, Tin deposits of the Black Range, Catron and Sierra Counties, New Mexico: U. S. Geological Survey, Bulletin 922-M, p. 355-379.

Fries, C. Jr., and Butler, A.P., 1943, Geologic Map of the Black Range tin district, New Mexico: U. S. Geological Survey, Open-file Map, scale 1:62,500, 1 sheet.

Fries, C. Jr., Schaller, W.T., and Glass, J.J., 1942, Bixbyite and pseudobrookite from the tin-bearing rhyolite of the Black Range, New Mexico: American Mineralogist, v. 27, p. 305-323.

Galusha, T., and Blick, J.C., 1971, Stratigraphy of the Santa Fe Group, New Mexico: American Museum of Natural History Bulletin, v. 144, art.1, 127 pp.

Gilbert, G.K., 1875, Report on the geology of portions of New Mexico and Arizona examined in 1873: U.S. Geographic and Geological Surveys West 100th Meridian (Wheeler), v. 3, pt. D, p. 503-567.

Glover, T.J., 1975, Geology and ore deposits of the northwestern Organ Mountains, Dona Ana County, New Mexico: Unpublished M.S. thesis; University of Texas at El Paso, El Paso, 93 pp.

Goerold, W.T., 1981, Geology and geochemistry of tin occurrences in southwestern New Mexico: Unpublished M.S. thesis; The Pennsylvanian State University, 131 pp.

Gordon, C.H., 1910, Sierra and central Socorro Counties, in Lindgren, W., Graton, L.C., and Gordon, C.H. (eds.), The Ore Deposits of New Mexico: U.S. Geological Survey, Professional Paper 68, p. 213-225.

Gordon, C.H., and Graton, L.C., 1907, Lower Paleozoic formations in New Mexico: Journal of Geology, v. 15, p. 91-92.

Griswold, G.B., 1961, Mineral deposits of Luna County, New Mexico: New Mexico Bureau of Mines and Mineral Resources, Bulletin 72, 157 pp.

Harley, G.T., 1934, The geology and ore deposits of Sierra County, New Mexico: New Mexico Bureau of Mines and Mineral Resources, Bulletin 10, 220 pp.

Harrison, R.W., 1984, General geology of Chloride mining

district, Sierra and Catron Counties, New Mexico: New Mexico Geological Society, Guidebook 37, p. 265-272.

Harrison, R.W., 1988a, Mineral paragenesis, structure, and "ore shoot" geometry at the U.S. Treasury mine, Chloride mining district, New Mexico: New Mexico Geology, v. 10, no. 1, p. 10-11, 15-16.

Harrison, R.W., 1988b, Primary structural control of epithermal mineralized shoots in southeastern Chloride mining district, New Mexico: New Mexico Geology, v. 10, no. 4, p. 80-81.

Harrison, R.W., 1989a, Exotic blocks within the early Tertiary Rubio Peak Formation in the north-central Black Range, New Mexico: occurrence, insights into post-emplacement tectonic activity, economic implications, and emplacement hypotheses: New Mexico Geological Society, Guidebook 40, p. 99-104.

Harrison, R.W., 1989b, Geology of Winston quadrangle, Sierra County, New Mexico: New Mexico Bureau of Mines and Mineral Resources, Open-file Report 358, 17 pp, scale 1:24,000, 2 sheets.

Harrison, R.W., 1990c, A regional study of precious metal mineralization: Chloride mining district, New Mexico; in Torma, A.E., and Gundiler, I.H. (eds.), Precious and Rare Metal Technologies: Elsevier Science Publishers B.V., Amsterdam, The Netherlands, p. 51-67.

Harrison, R.W., in prep., Chise lineament of southwestern New Mexico and observations relative to the influence of northeast-trending magnetic lineaments on Cenozoic tectonism and mineralization in New Mexico and Colorado.

Harrison, R.W., Eggleston, T.L., Lozinsky, R.P., in prep., Geologic map of the Truth or Consequences, New Mexico 30 X 60 minute quadrangle: New Mexico Bureau of Mines and Mineral Resources, Geologic Map, scale 1:100,000.

Harvey, D.B., 1985, Cassiterite mineralization in the Black Range tin district, Sierra and Catron Counties, New Mexico: Unpublished M.S. thesis, University of Texas at El Paso, El Paso, 147 pp.

Hawley, J.W., Kottlowski, F.E., Seager, W.R., King, W.E., Strain, W.S., and LeMone, D.V., 1969, The Santa Fe Group in the south-central New Mexico border region; in Kottlowski, F.E., and Lemone, D.V. (eds.), Border stratigraphy symposium: New Mexico Bureau of Mines and Mineral Resources, Circular 104, p. 52-76.

Headlund, D.C., 1977, Geology of the Hillsboro and San

Lemenez quadrangles, Sierra and Grant Counties, New Mexico: U.S. Geological Survey, Map MF-900-A, scale 1:48,000 2 sheets.

Hermann, M.L., 1986, Geology of the southwestern San Mateo Mountains, Socorro County, New Mexico; Unpublished M.S. thesis; New Mexico Institute of Mining and Technology, Socorro, 192 pp.

Heyl, A.V., Maxwell, C.H., and Davis, L.L., 1983, Geology and mineral deposits of the Priest Tank quadrangle, Sierra County, New Mexico: U.S. Geological Survey, Miscellaneous Field Studies Map MF-1665, scale 1:24,000, 1 sheet.

Hilland, P.D., 1969, Geology and beryllium mineralization near Apache Warm Springs, Socorro County, New Mexico: New Mexico Bureau of Mines and Mineral Resources, Circular 103, 14 pp.

Irvine, T.N., and Baragar, W.R., 1971, A guide to the chemical classification of the common volcanic rocks: Canadian Journal of Earth Sciences, v. 8, p. 523-548.

Johns, R.H., 1955, Geology of Sierra Cuchillo, New Mexico: New Mexico Geological Society Guidebook 6, p. 150-174.

Johns, R.M., McMillan, D.K., O'Brient, J.D., and Fisher, D.L., 1979, Geologic section in the Sierra Cuchillo and flanking areas, Sierra and Socorro Counties, New Mexico; in Chapin, C.E., Elston, W.E., and James, H.L. (eds.), Field guide to selected cauldrons and mining districts of the Datil-Mogollon volcanic field, New Mexico: New Mexico Geological Society Special Publication 7, p. 130-138.

Jicha, H.L., Jr., 1954, Geology and mineral deposits of Lake Valley quadrangle, Grant, Luna, and Sierra Counties, New Mexico: New Mexico Bureau of Mines and Mineral Resources, Bulletin 37, 93 pp.

Jones, W.R., Hernon, R.M., and Moore, S.L., 1967, General geology of Santa Rita quadrangle, Grant County, New Mexico: U.S. Geological Survey, Professional Paper 555, 144 pp.

Keddie, L.L., 1984, High-precision 40Ar/39Ar dating of major ash-flow tuff sheets, Socorro, New Mexico: Unpublished M.S. thesis; New Mexico Institute of Mining and Technology, Socorro, 197 pp.

Kelley, V.C., and McCleary, J.T., 1960, Laramide orogeny in south-central New Mexico: American Association of Petroleum Geologists Bulletin, v. 44, p. 1419-1420.

Kelley, V.C., and Silver, C., 1952, Geology of the Caballo Mountains: University of New Mexico, Publications in Geology, no. 4, 286 pp.

Kottlowski, F.E., 1953, Tertiary-Quaternary sediments of the Rio Grande Valley in southern New Mexico: New Mexico Geological Society, Guidebook 4, p. 144-148.

Kottlowski, F.E., 1955, Cenozoic sedimentary rocks of south-central New Mexico: New Mexico Geological Society, Guidebook 6, p. 88-91.

Kottlowski, F.E., Flower, R.H., Thompson, M.L., and Foster, R.W., 1956, Stratigraphic studies of the San Andres Mountains, New Mexico: New Mexico Bureau of Mines and Mineral Resources, Memoir 1, 132 pp.

Kuellmer, F.J., 1954, Geologic section of the Black Range at Kingston, New Mexico: New Mexico Bureau of Mines and Mineral Resources, Bulletin 33, 100 pp.

Kyle, P.R., Eggleston, T.L., McIntosh, W.C., Dunbar, N., Hammond, C.M., Johnson, W.D., Knoper, M., and Moore, J., 1986, Pyroclastic rocks associated with the Taylor Creek Rhyolite, Scales Canyon, New Mexico: New Mexico Geological Society, Guidebook 37, p. 197-201.

LaMarre, A.L., 1974, Fluorite in jasperoid of the Salado Mountains-significance to metallogeny of the western United States: Unpublished M.S. thesis, University of Western Ontario, London, 134 pp.

Lawrence, V.A., 1983, A study of the Indian Peaks tin-bearing rhyolite dome-flow complex, northern Black Range, New Mexico: Unpublished M.S. thesis, University of Colorado, Boulder, 112 pp.

Lawrence, V.A., and Richter, D.H., 1986, Geologic map of the Indians Peak West quadrangle, Catron County, New Mexico: U. S. Geological Survey, Map MF-1949, scale 1:24,000, 1 sheet.

Le Maitre, R.W., 1976, The chemical variability of some common igneous rocks: Journal of Petrology, v. 17, p. 589-637.

Le Maitre, R.W., 1984, A proposal by the IUGS Subcommission on the Systematics of Igneous Rocks for a chemical classification of volcanic rocks based on the total alkali silica (TAS) system: Australian Journal of Earth Sciences, v. 31, p. 243-255.

Lemley, I.S., 1982, The Lobo Formation and lithologically

similar units in Luna and southwestern Dona Ana Counties, New Mexico: Unpublished M.S. thesis, New Mexico State University, Las Cruces, 95 pp.

Loring, A.K., and Loring, R.B., 1980, K-Ar ages of middle Tertiary igneous rocks from southern New Mexico: Isochron/West, no. 28, p. 17-19.

Lozinski, R.P., and Hawley, J.W., 1986, Upper Cenozoic Palomas Formation of south-central New Mexico: New Mexico Geological Society, Guidebook 37, p. 239-247.

Lucas, S.G., 1986, Oligocene mammals from the Black Range, southwestern New Mexico: New Mexico Geological Society, Guidebook 37, p. 261-263.

Lucas, S.G., and Ingersoll, R.V., 1981, Cenozoic continental deposits of New Mexico: An overview: Geological Society of America Bulletin, pt. 1, v. 92, no. 12, p. 917-932.

Lufkin, J.L., 1972, Tin mineralization within rhyolite flow-domes, Black Range, New Mexico: Unpublished Ph.D. dissertation, Stanford University, Stanford, California, 149 pp. (also available as New Mexico Bureau of Mines and Mineral Resources Open-file Report 57).

Lufkin, J.L., 1976, Oxide minerals in mineralized rhyolite, Black Range, New Mexico: American Mineralogist, v. 61, p. 425-436.

Lufkin, J.L. 1977, Chemistry and mineralogy of woodtin, Black Range, New Mexico: American Mineralogist, v. 61, p. 100-104.

Maldonado, F., 1974, Geology of the northern part of the Sierra Cuchillo, Socorro and Sierra Counties, New Mexico: Unpublished M.S. thesis, University of New Mexico, Albuquerque, 59 pp.

Marvin, R.F., and Dole, J.C., 1978, Radiometric ages: Compilation A: Isochron/West, no. 22, p. 3-14.

Maxwell, C.H., and Heyl, A.V., 1976, Preliminary geologic map of the Winston quadrangle, Sierra County, New Mexico: U.S. Geological Survey, Open-file Report 76-853, scale 1:24,000, 1 sheet.

Maxwell, C.H., Foord, E.E., Oakman, M.R., and Harvey, D.D., 1986, Tin deposits in the Black Range tin district: New Mexico Geological Society, Guidebook 37, p. 273-281.

Mayer, A.B., 1987, Structural and volcanic geology of the Salado Mountains-Garcia Peaks area, Sierra County, New Mexico: Unpublished M.S. thesis, New Mexico State University, Las Cruces, 61 pp.

McDowell, F.W., 1971, K-Ar ages of igneous rocks from the western United States: Isochron/West, no. 2, p. 1-16.

McIntosh, W.C., 1989, Ages and distribution of ignimbrites in the Mogollon-Datil volcanic field, southwestern New Mexico: a stratigraphic framework using 40Ar/39Ar dating and paleomagnetism: Unpublished Ph.D. Dissertation; New Mexico Institute of Mining and Technology, Socorro, 351 pp.

McKinlay, P.F., and Clippinger, D.M., 1947, A report of the Ramsey and Bunnell-Schneider claims, Black Range, Sierra County, New Mexico: New Mexico Bureau of Mines and Mineral Resources, 6 pp.

McMillan, D.K., 1979, Crystallization metasomatism of the Cuchillo Mountain laccolith, Sierra County, New Mexico: Unpublished Ph.D. dissertation; Stanford University, Stanford, California, 217 pp.

Osburn, G.R., and Chapin, C.E., 1983, Nomenclature for Cenozoic rocks of northeast Mogollon-Datil volcanic field, New Mexico: New Mexico Bureau of Mines and Mineral Resources, Stratigraphic Chart 1, 1 sheet, 7 pp.

Osburn, G.R., 1978, Geology of eastern Magdalena Mountains, Water Canyon to Pound Ranch, Socorro County, New Mexico: Unpublished M.S. thesis; New Mexico Institute of Mining and Technology, Socorro, 150 pp.; also available as New Mexico Bureau of Mines and Mineral Resources, Open-file Report 113, 160 pp.

Osburn, G.R., Harrison, R.W., Eggleston, T.L., Lasinsky, R.P., and Maxwell, C.H., 1986, First-day roadlog, from Truth or Consequences to Sierra Cuchillo, Winston graben, Winston, South Fork of Cuchillo Negro Creek, Fluorine, and central Black Range: New Mexico Geological Society, Guidebook 37, p. 1-19.

Patterson, G.W., and Holmes, R.W., 1965, Clays; in report prepared by the United States Geological Survey for the U.S. Senate Committee on Interior and Insular Affairs, Mineral and water resources of New Mexico: New Mexico Bureau of Mines and Mineral Resources, Bulletin 87, p. 312-320.

Pearce, J.A., and Norry, M.J., 1979, Petrogenetic implications of Ti, Zr, Y, and Nb variation in volcanic rocks: Contributions to Mineralogy and Petrology, v. 69, p. 33-47.

Pierson, T.C., and Scott, K.M., 1985, Downstream dilution of a lahar: transition from debris flow to

hyperconcentrated streamflow: Water Res. Res., v. 21, p. 1511-1524.

Ratte', J.C., Landis, E.R., Gaskill, D.L., and Raabe, R.G., 1969, Mineral resources of the Blue Range Primitive Area, Greenlee County, Arizona, and Catron County, New Mexico, with a section on Aeromagnetic interpretation by E.P. Eaton: U.S. Geological Survey, Bulletin 1261-E, 91 pp.

Ratte', J.C., Gaskill, D.L., Stotelmeyer, R.B., and Meeves, H.C., 1972, Mineral resources of the Gila Primitive Area and Gila Wilderness, Catron and Grant Counties, New Mexico: U.S. Geological Survey, Open-file Report 72-306, 440 pp.

Ratte', J.C., Marvin, R.F., and Naeser, C.W., 1984, Calderas and ash-flow tuffs of the Mogollon Mountains, southwestern New Mexico: Journal of Geophysical Research, v. 89, p. 8713-8732.

Ratte', J.C., McIntosh, W.C., and Howser, B.B., 1989, Geologic map of Horse Mountain West quadrangle, Catron County, New Mexico: U.S. Geological Survey, Open-file Report 89-310, scale 1:24,000, 1 sheet, 22 pp.

Reisinger, H.R., 1988, Geologisch-petrologische untersuchungen der vulkanite der sudwestlichen Alde Leopold Wilderness, Black Range, New Mexico, USA: Unpublished Geologische Diplomarbeit, Institut fur Mineralogie und Lagerstattenkunde der Rheinisch-Westfalischer Technischen Hochschule Aachen, West Germany, 153 pp.

Reisinger, H.R., and Wagener, J., 1987, An Oligocene ash-flow tuff vent correlated to a regional high-silica rhyolite tuff sheet: Geological Society of America, Abstracts with Programs, v. 19, no. 7, p. 815

Rhodes, R.C., 1976, Volcanic geology of the Mogollon Range and adjacent areas, Catron and Grant Counties, New Mexico; in Elston, W.E., and Northrop, S.A. (eds.), Cenozoic volcanism in southwestern New Mexico: New Mexico Geological Society, Special Publication Number 5, p. 42-50.

Rhodes, R.C., and Smith, E.I., 1976, Stratigraphy and structure of the northwestern part of Mogollon Plateau volcanic province, Catron County, New Mexico; in Elston, W.E., and Northrop, S.A. (eds.), Cenozoic volcanism in southwestern New Mexico: New Mexico Geological Society, Special Publication No. 5, p. 57-62.

Richter, D.H., 1975, Geologic map of the Spring Canyon

quadrangle, Catron County, New Mexico: U. S. Geological Survey, Map MF-944, scale 1:24,000 , 1 sheet.

Richter, D.H., Eggleston, T.L., and Duffield, W.A., 1986a, Geologic map of the Wall Lake quadrangle, Catron County, New Mexico: U. S. Geological Survey, Miscellaneous Field Studies Map Mf-1909, scale 1:24,000, 1 sheet.

Richter, D.H., Lawrence, V.A., and Duffield, W.A., 1986b, Geologic map of the Indian Peaks East quadrangle, Catron County, New Mexico: U.S. Geological Survey, Map MF-1850, scale 1:24,000, 1 sheet.

Scott, G.R., 1975, Cenozoic surfaces and deposits in the southern Rocky Mountains: Geological Society of America, Memoir 144, p. 227-248.

Scott, K.M., 1980, Lahars and lahar-runout flows in the Toutle-Cowlitz river system, Mount St. Helens, Washington-- Origins, behavior, and sedimentology: U.S. Geological Survey, Professional Paper 1447-A, 74 pp.

Seager, W.R., 1975, Cenozoic tectonic evolution of Las Cruces area, New Mexico: New Mexico Geological Society, Guidebook 26, p. 241-250.

Seager, W.R., 1983, Laramide wrench faults, basement-cored uplifts, and complementary basins in southern New Mexico: New Mexico Geology, v. 5, p. 69-76.

Seager, W.R., Hawley, J.W., and Clemons, R.E., 1971, Geology of San Diego Mountain area, Dona Ana County, New Mexico: New Mexico Bureau of Mines and Mineral Resources, Bulletin 97, 38 pp.

Seager, W.R., and Clemons, R.E., 1975, Middle to late Tertiary geology of Cedar Hills-Selden Hills area[Dona Ana County], New Mexico: New Mexico Bureau of Mines and Mineral Resources, Circular 133, 23 pp.

Seager, W.R., and Morgan, P., 1979, The Rio Grande rift in southern New Mexico, west Texas, and northern Chihuahua, in Riecker, R.E. (ed.), Rio Grande Rift: Tectonics and Magmatism: American Geophysical Union, Washington, D.C., p. 87-106.

Seager, W.R., Clemons, R.E., Hawley, J.W., and Kelley, R.E., 1982, Geology of northwest part of Las Cruces 1X2 degree sheet, New Mexico: New Mexico Bureau of Mines and Mineral Resources, Geologic Map 53, scale 1:125,000, 3 sheets.

Seager, W.R., Shafiqullah, M., Hawley, J.W., and Marvin, R.F., 1984, New K-Ar dates from basalts and the

evolution of the southern Rio Grande rift: Geological Society of America Bulletin, v. 95, p. 87-99.

Seager, W.R., Mack, G.H., Raimonde, M.G., and Ryan, R.B., 1984, Laramide basement-cored uplift and basins in south-central New Mexico: New Mexico Geological Society, Guidebook 37, p. 123-130.

Seager, W.R., and Mack, G.H., 1986, Laramide paleotectonics of southern New Mexico; in Peterson, J.A. (ed.), Paleotectonics and sedimentation in the Rocky Mountain region, United States: American Association of Petroleum Geologists, Memoir 41, p. 669-685.

Seager, W.R., Hawley, T.E., Kottlowski, F.E., and Kelley, S.A., 1987, Geology of east half of Las Cruces and northeast El Paso 1 x 2 degree sheets, New Mexico: New Mexico Bureau of Mines and Mineral Resources, Geologic Map 57, scale 1:125,000, 5 sheets.

Seager, W.R., and Mayer, A.B., 1988, Uplift, erosion, and burial of Laramide fault blocks, Caballo Mountains, Sierra County, New Mexico: New Mexico Geology, v. 10, no.3, p. 49-53, 60.

Shepard, M.D., 1984, Geology and ore deposits of the Hermosa mining district, Sierra County, New Mexico: Unpublished M.S. thesis, University of Texas at El Paso, 215 pp.

Sillitoe, R.H., and Bonham, H.F., Jr., 1984, Volcanic landforms and ore deposits: Economic Geology, v. 79, p. 1286-1298.

Smith, E.I., 1970, Structure and petrology of the John Kerr Peak dome complex, southwestern New Mexico; in Elston, W.E., and Northrop, S.A. (eds.), Cenozoic volcanism in southwestern New Mexico: New Mexico Geological Society, Special Publication Number 5, p. 71-78.

Smith, G.A., 1986, Coarse-grained nonmarine volcaniclastic sediment: terminology and depositional processes: Geological Society of America, Bulletin, v. 97, p. 1-10.

Smith, G.A., 1987, The influence of explosive volcanism on fluvial sedimentation: The Deschutes Formation (Neogene) in central Oregon: Journal of Sedimentary Petrology, v. 57, p. 613-629.

Smith, G.A., 1988, Sedimentology of proximal to distal volcaniclastics dispersed across an active foldbelt: Ellensburg Formation (late Miocene), central Washington: Sedimentology, v. 35, p. 953-977.

Smith, L.N., Lucas, S.G., and Elston, W.E., 1985, Paleogene

stratigraphy, sedimentation and volcanism of New Mexico: Society of Economic Paleontologists and Mineralogists, Rocky Mountain Section, Denver, p. 293-315.

Smith, R.L., 1960, Ash flows: Geological Society of America Bulletin, v. 71, p. 795-842.

Sparks, R.S.J., Self, S., and Walker, G.P.L., 1973, Products of ignimbrite eruptions: Geology, v. 1, p. 115-118.

Stearns, C.E., 1962, Geology of the north half of the Pelona quadrangle, Catron County, New Mexico: New Mexico Bureau of Mines and Mineral Resources, Bulletin 78, 46 p.

Stinnett, J.W., 1980, A geochemical study of the calc-alkaline andesites and associated volcanic rocks from the Mogollon-Datil volcanic field, southwestern New Mexico: Unpublished Ph.D. dissertation, Miami University, Ohio, 271 pp.

Stinnett, J.W., Jr., and Steuber, A.M., 1976, A strontium isotopic and geochemical study of volcanic rocks from the Datil-Mogollon field, southwestern New Mexico: Geological Society of America, Abstracts with Programs, v. 8, p. 636-637.

Tedford, R.H., 1981, Mammalian biochronology of the late Cenozoic basins of New Mexico: Geological Society of America Bulletin, v. 92, p. 1008-1022.

Turekian, K.K., and Wedepohl, K.H., 1961, Distribution of the elements in some major units of the Earth's crust: Geological Society of America Bulletin, v. 72, p. 175-192.

Volin, M.E., Russell, P.L.C., and Mullen, D.H., 1947, Catron and Sierra Counties tin deposits, New Mexico: U.S. Bureau of Mines, RI 4068, 60 pp.

Wagener, J., 1987, Zur geologie, geochemie und petrologie des tuff of Diamond Creek, Black Range (sudwest - New Mexico, USA): Unpublished Geologische Diplomarbeit, Institut fur Mineralogie und Lagerstattenkunde der Rheinisch-Westfalischer Technischen Hochschule, Aachen, West Germany, 96 pp.

Walker, G.P.L., 1985, Origin of coarse lithic breccias near ignimbrite source vents: Journal of Volcanology and Geothermal Research, v. 25, p. 157-171.

Woodard, T.W., 1982, Geology of the Lookout Mountain area, northern Black Range, Sierra County, New Mexico: Unpublished M.S. thesis, University of New Mexico, Albuquerque, 93 pp.

Zoback, M.L., Anderson, R.E., and Thompson, G.A., 1981, Cainozoic evolution of the state of stress and style of tectonism of the Basin and Range province of the western United States: Royal Society of London, Philosophical Translations (A), v. 300, p. 407-434.

Legend for Winston, Lookout Mountain, Sawmill Peak, and Iron Mountain 7 1/2' quadrangles (Plates 1, 2, 3, & 4), see text for unit descriptions.

Qal	Quaternary alluvium
Qc	Quaternary colluvium
Qca	Quaternary alluvium and colluvium, undivided
Qpg	Quaternary piedmont slope deposits
Tsf	Santa Fe Group
Tg	Gila Conglomerate
Twa	andesite of Winston graben [previously referred to as Winston andesite]
Tbw	Bearwallow Mountain Formation
Tsft	ash-flow tuff, air-fall tuff, and water-laid tuff beds intercalated with lower Santa Fe Group in Winston quadrangle
Tgc	tuff of Garcia Camp
Tss	unnamed sandstone and conglomerate beds in Sawmill Peak quadrangle, probably correlative to sandstone of Inman Ranch
Tirs	sandstone of Inman Ranch
Tfm	rhyolite of Franks Mountain and other similar units
Ttc	Taylor Creek Rhyolite
Ttct	pyroclastic rocks associated with Taylor Creek Rhyolite
Tvp	Vicks Peak Tuff

Tlj	La Jencia Tuff
Tdp	rhyolite of Dolan Peak
Tsg	tuff of Straight Gulch
Tsp	rhyolite of Sawmill Peak
Tdc	tuff of Diamond Creek
Tkm	tuff of Kline Mountain
Tlm	tuff of Lookout Mountain
Tsc	tuff of Stiver Canyon
Tmj	Moccasin John Rhyolite
Tlmc	tuff of Little Mineral Creek
Tmh	tuff of Mud Hole
Tpc	basaltic andesite of Poverty Creek
Tms	sandstone of Monument Park
Tcb	Caballo Blanco Tuff
Tkwu	upper tuff of Koko Well
Tkwl	lower tuff of Koko Well
Tcnl,cns	Cuchillo Negro Complex, cnl-lavas & vent, cns-sediments & ash-flow tuffs
Tkn	Kneeling Nun Tuff
Tcc	sandstone of Cliff Canyon
Ts,Tdc	tuff of Rocque Ramos Canyon [previously referred to as tuff of Dry Creek & tuff of Bear Creek]
Twh	dacite of Wildhorse Canyon
Trabu	upper aphanitic andesite in Rubio Peak Formation, Sawmill Peak quadrangle
Trpau	upper porphyritic andesite in Rubio Peak Formation, Sawmill Peak quadrangle

Trabm	middle aphanitic andesite in Rubio Peak Formation, Sawmill Peak quadrangle
Trapl	lower porphyritic andesite in Rubio Peak Formation, Sawmill Peak quadrangle
Trlt,Tlt	tuff of Victoria Tank [previously unnamed lithic-rich tuff]
Trbal	lower aphanitic andesite in Rubio Peak Formation, Sawmill Peak quadrangle
Trpa	porphyritic andesite in Rubio Peak Formation
Trpba	aphanitic basaltic andesite in Rubio Peak Formation
Trp	volcaniclastic deposits in Rubio Peak Formation, sandstones, debris-flow deposits, mudflow deposits
Tg	fine-grained granite and aplite, Iron Mountain intrusive, Iron Mountain quadrangle
Tm	white monzonite, Reilly Peak intrusive, Iron Mountain quadrangle
Pme	exotic blocks of Pennsylvanian limestone, gravity slide deposits
Trph	hornblende-pyroxene andesite in lower Rubio Peak Formation
Trpm	tuff of Miranda Homestead
Trpc	basal conglomerate of Rubio Peak Formation
Pys	Permian San Andres and Yeso Formations, undivided
Pa	Permian Abo Formation
Pb	Permian Bursum Formation
P	Permian, undivided
Pm	Pennsylvanian Madera Limestone

Tia	intermediate (aphanitic) dikes of various ages
Tir	rhyolite dikes, both aphanitic & porphyritic

Plate 6A

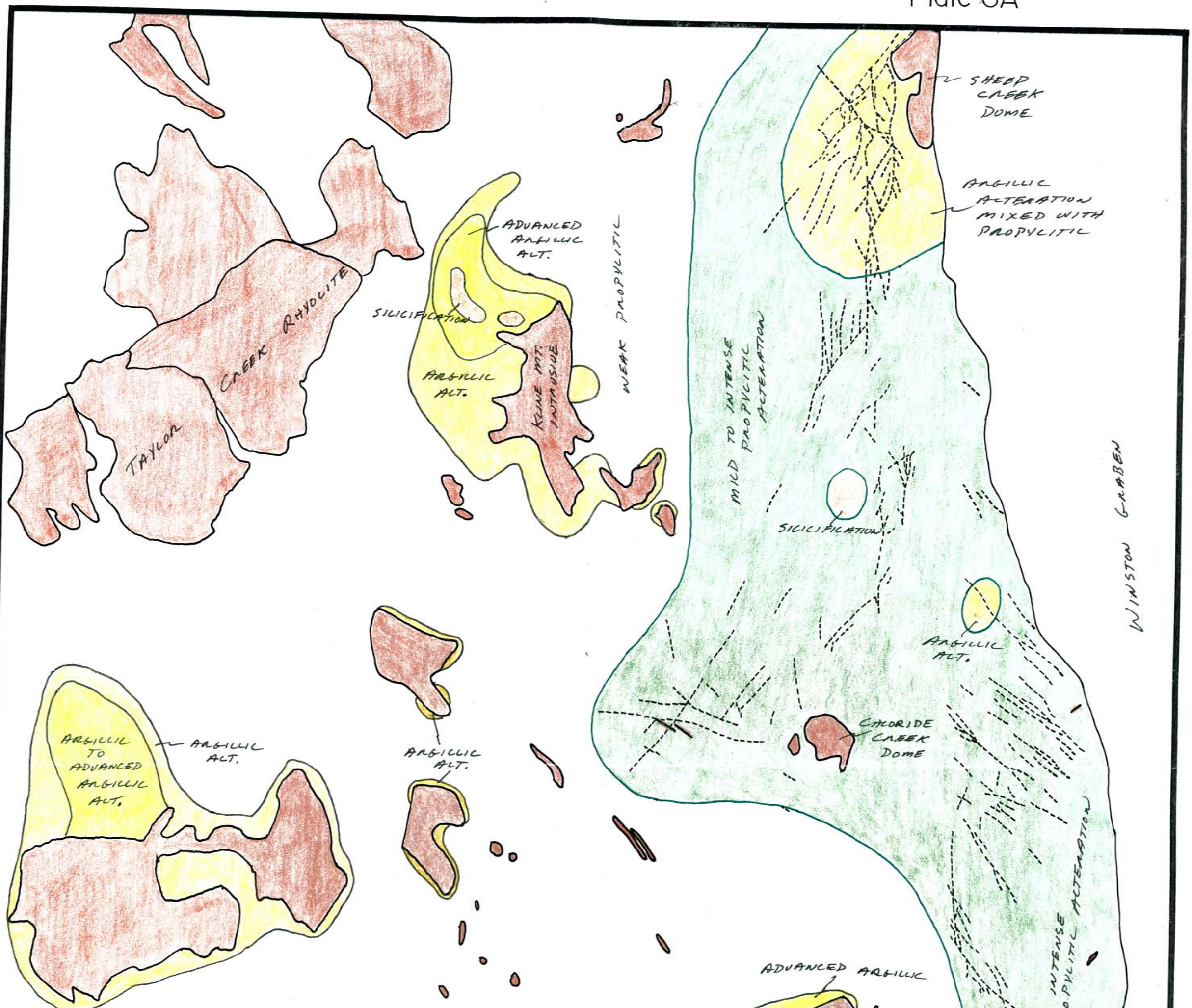
SHEEP CREEK DOME
ARGILLIC ALTERATION MIXED WITH PROPYLITIC
ADVANCED ARGILLIC ALT.
SILICIFICATION
ARGILLIC ALT.
KLINE INT. INTRUSIVE
WEAK PROPYLITIC
MOD TO INTENSE PROPYLITIC ALTERATION
SILICIFICATION
ARGILLIC ALT.
CHLORIDE CREEK DOME
TAYLOR CREEK RHYOLITE
ARGILLIC TO ADVANCED ARGILLIC ALT.
ARGILLIC ALT.
ARGILLIC ALT.
ADVANCED ARGILLIC
WINSTON GRABEN
INTENSE PROPYLITIC ALTERATION

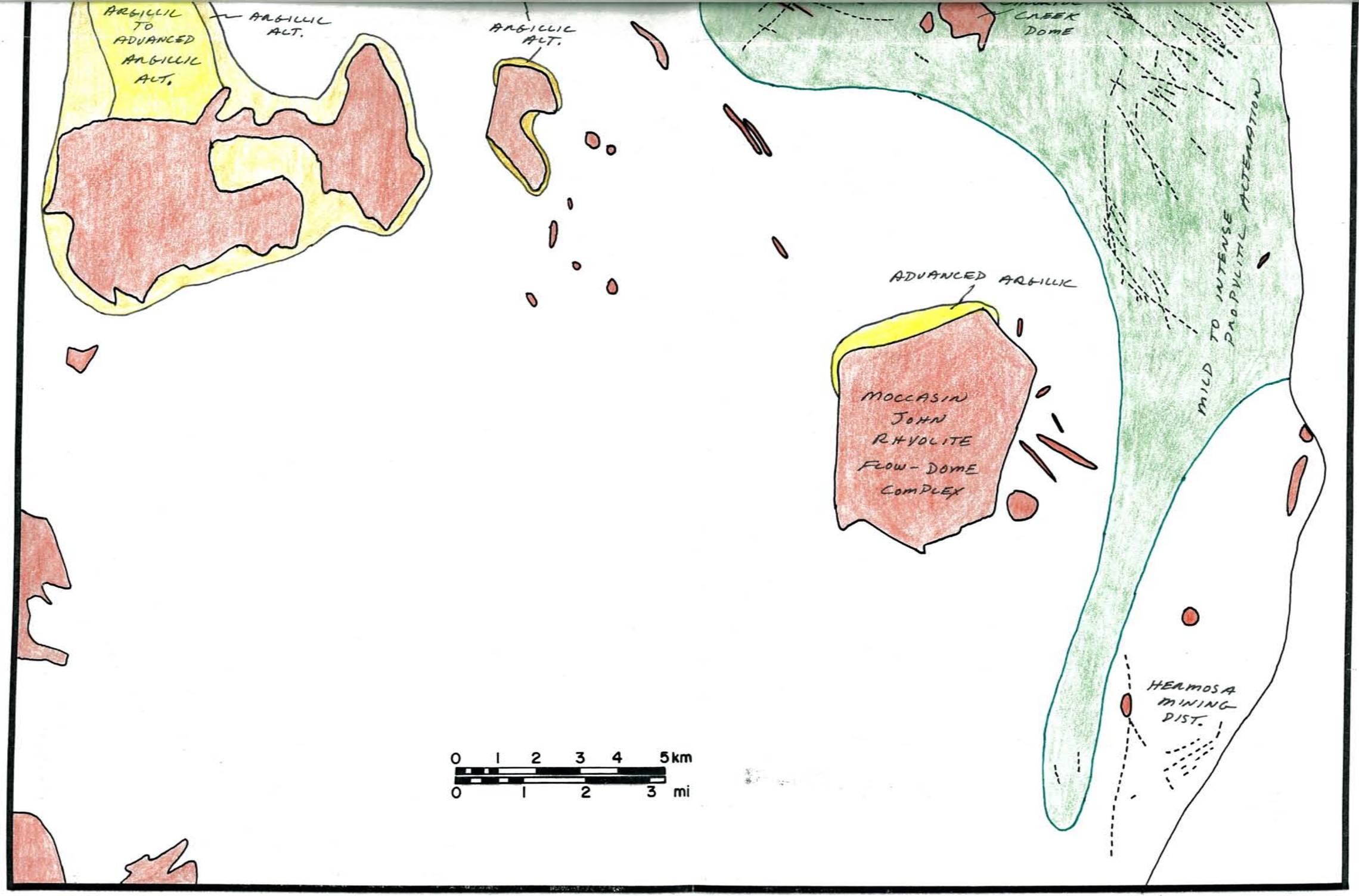
ARGILLIC TO ADVANCED ARGILLIC ALT.
ARGILLIC ALT.
ARGILLIC ALT.
CREEK DOME
ADVANCED ARGILLIC
MOCCASIN JOHN RHYOLITE FLOW-DOME COMPLEX
MILD TO INTENSE PROPYLITIC ALTERATION
HERMOSA MINING DIST.
0 1 2 3 4 5km
0 1 2 3 mi

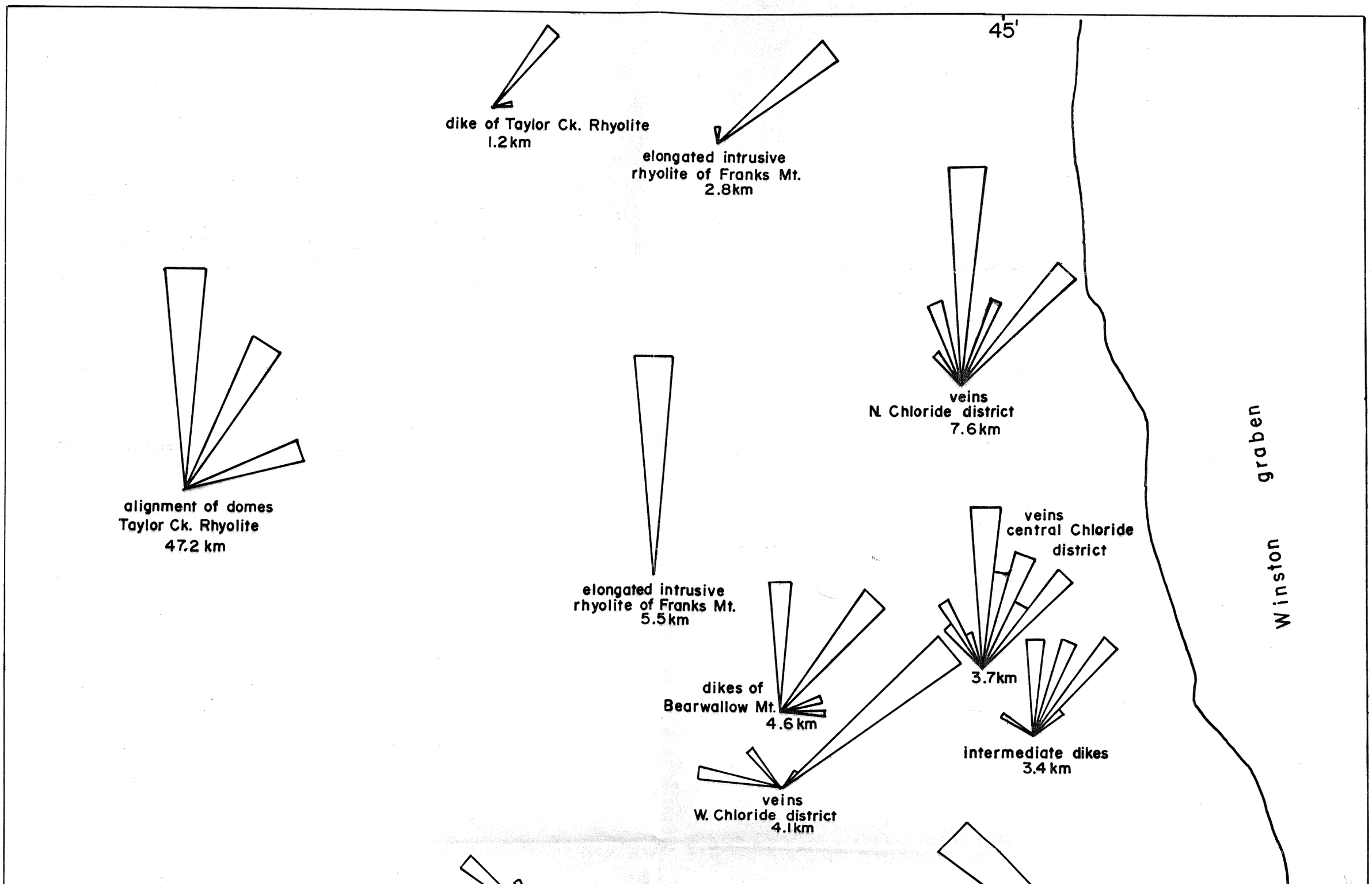
45'
dike of Taylor Ck. Rhyolite
1.2km
elongated intrusive
rhyolite of Franks Mt.
2.8km
veins
N. Chloride district
7.6km
graben
Winston
alignment of domes
Taylor Ck. Rhyolite
47.2 km
elongated intrusive
rhyolite of Franks Mt.
5.5km
veins
central Chloride
district
3.7km
dikes of
Bearwallow Mt.
4.6 km
intermediate dikes
3.4 km
veins
W. Chloride district
4.1km

W. Chloride district
4.1km

dikes
Bearwallow Mt.
.9km

veins
SE. Chloride district
10.7km

rhyolite dikes
Moccasin John Rhyolite
11.3 km

15'

0 1 2 3 4 5 km

Plate ~~6C~~ 5D.

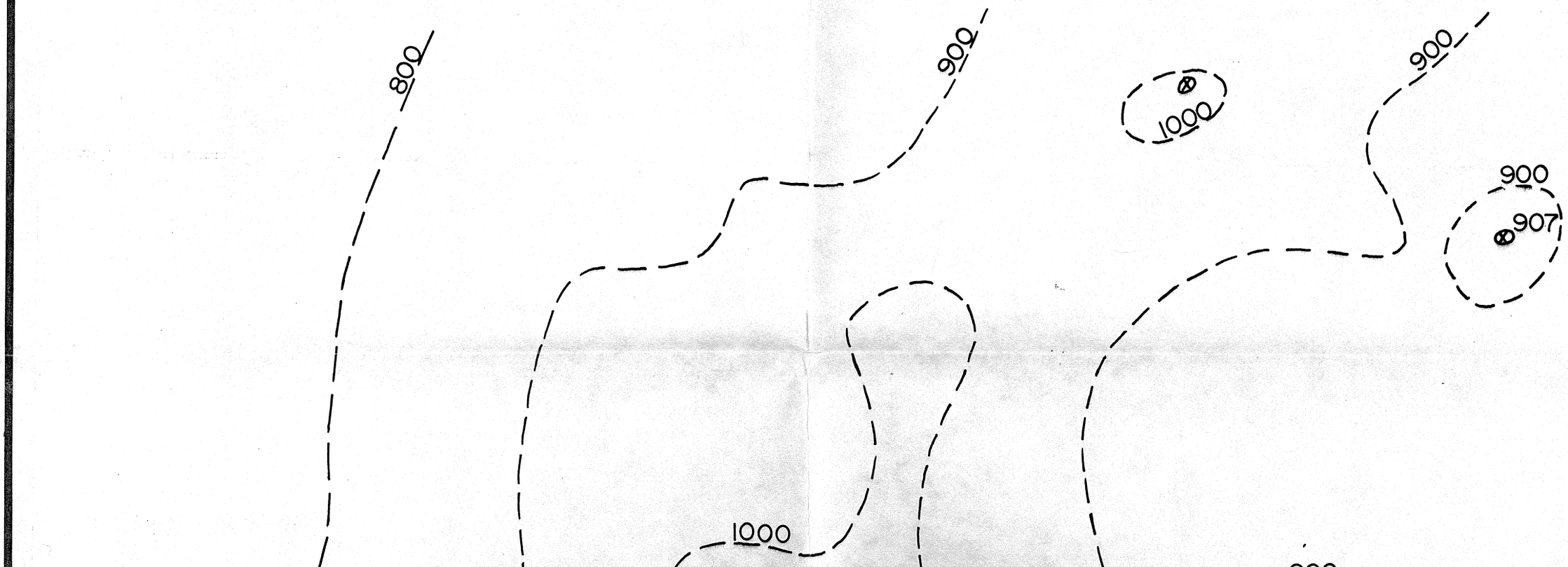

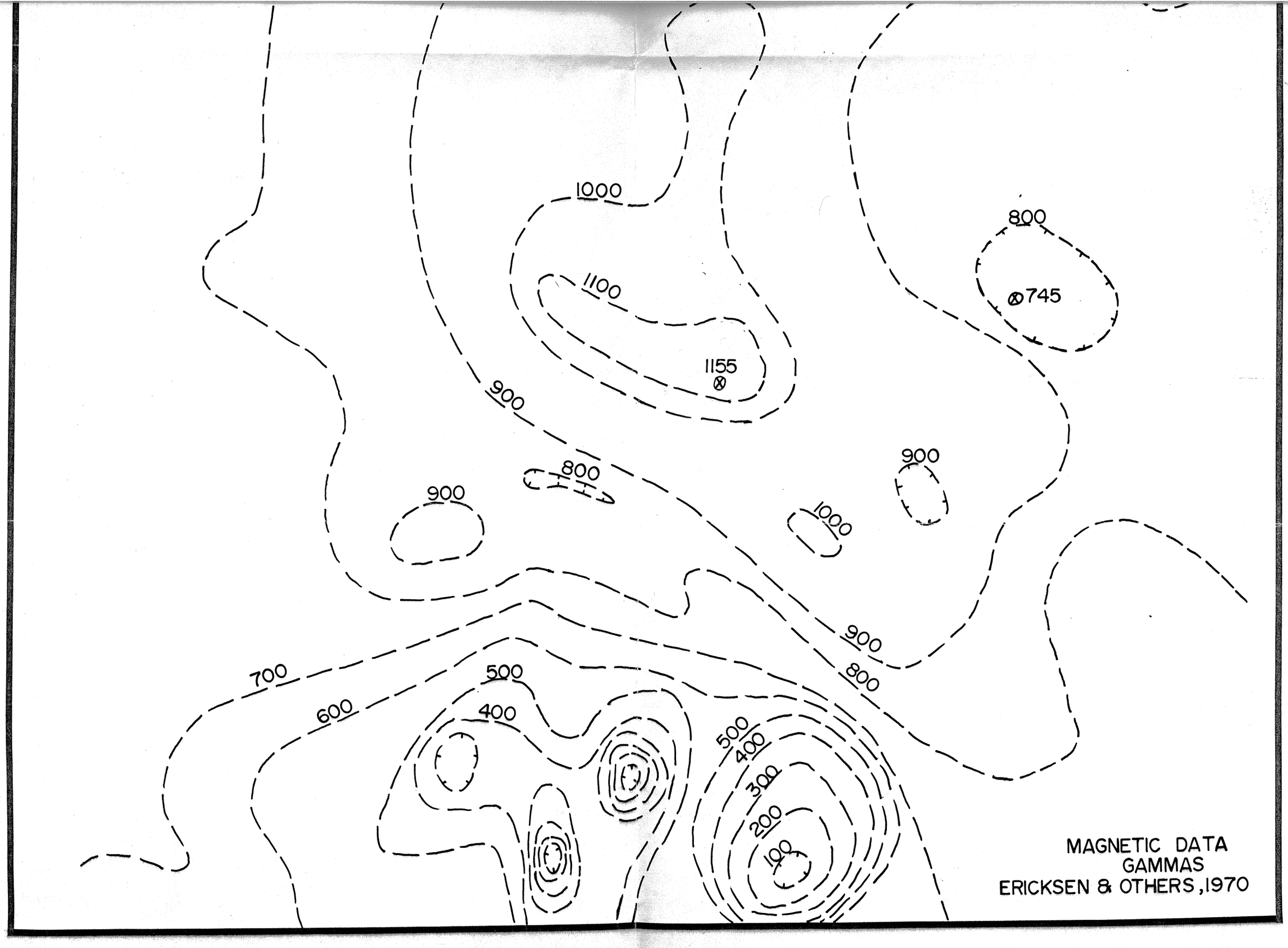
1000
1100
1155
900
800
900
800
745
900
900
1000
900
800
700
600
500
400
500
400
300
200
100
MAGNETIC DATA
GAMMAS
ERICKSEN & OTHERS, 1970

Plate 6D. ~~6D~~ 5C

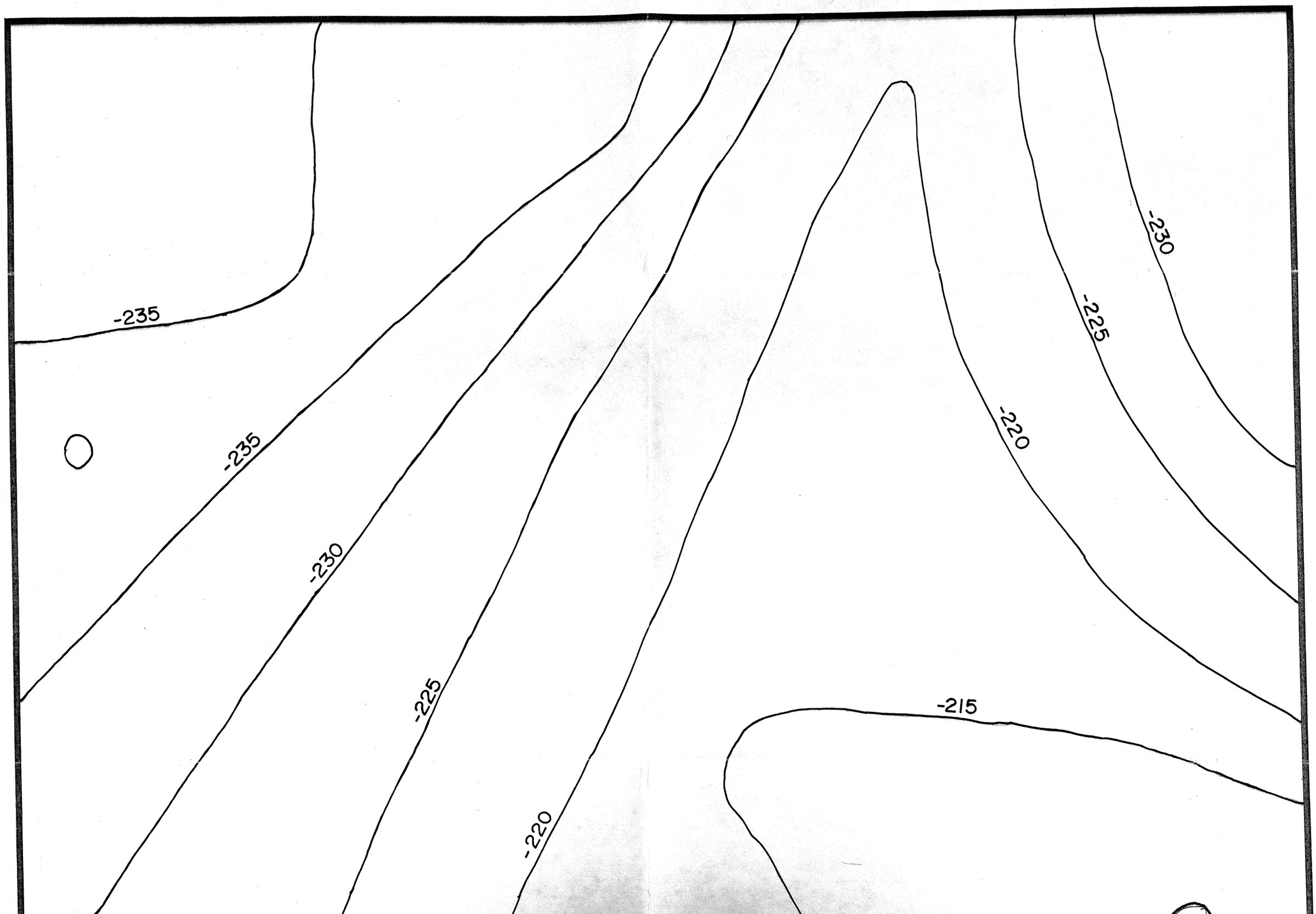

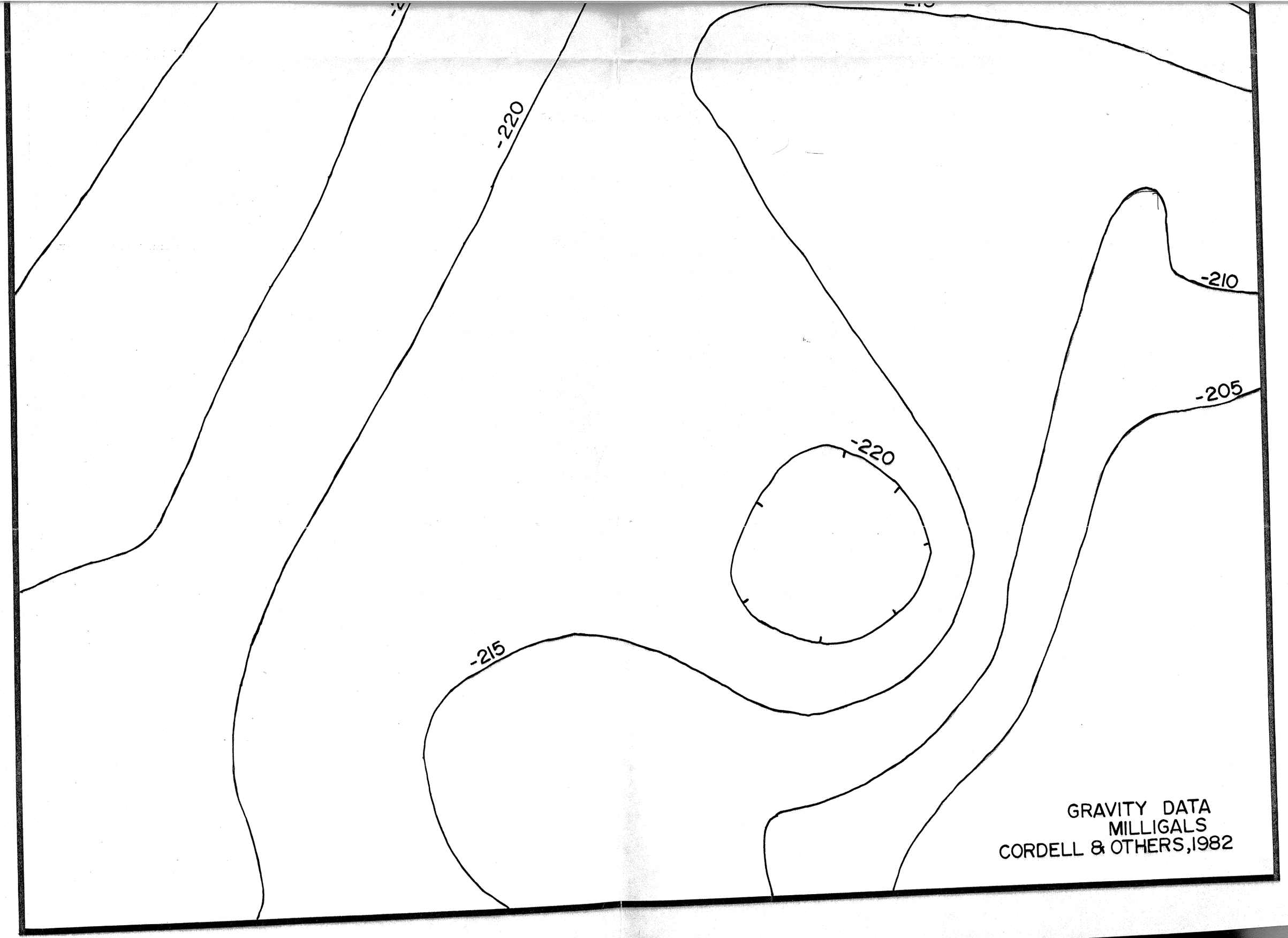
-220
-210
-205
-220
-215
GRAVITY DATA
MILLIGALS
CORDELL & OTHERS, 1982

IRON MOUNTAIN QUADRANGLE
NEW MEXICO
7.5 MINUTE SERIES (TOPOGRAPHIC)

4451 II SE (MONTOYA BUTTE)

560 000 FEET (WEST) 107°37'30" 33°30'

R. 9 W. R. 8 W. 42'30" 40'

4451 II SW (WAHOO RANCH)

DUSTY 13 MI.

CATRON CO SOCORRO CO

NATIONAL FOREST BOUNDARY

BM 7024

CC Tank

Canyon

Creek

T. 9 S.

T. 10 S.

900 000 FEET (WEST)

27'30"

UNITED STATES
DEPARTMENT OF THE INTERIOR
GEOLOGICAL SURVEY

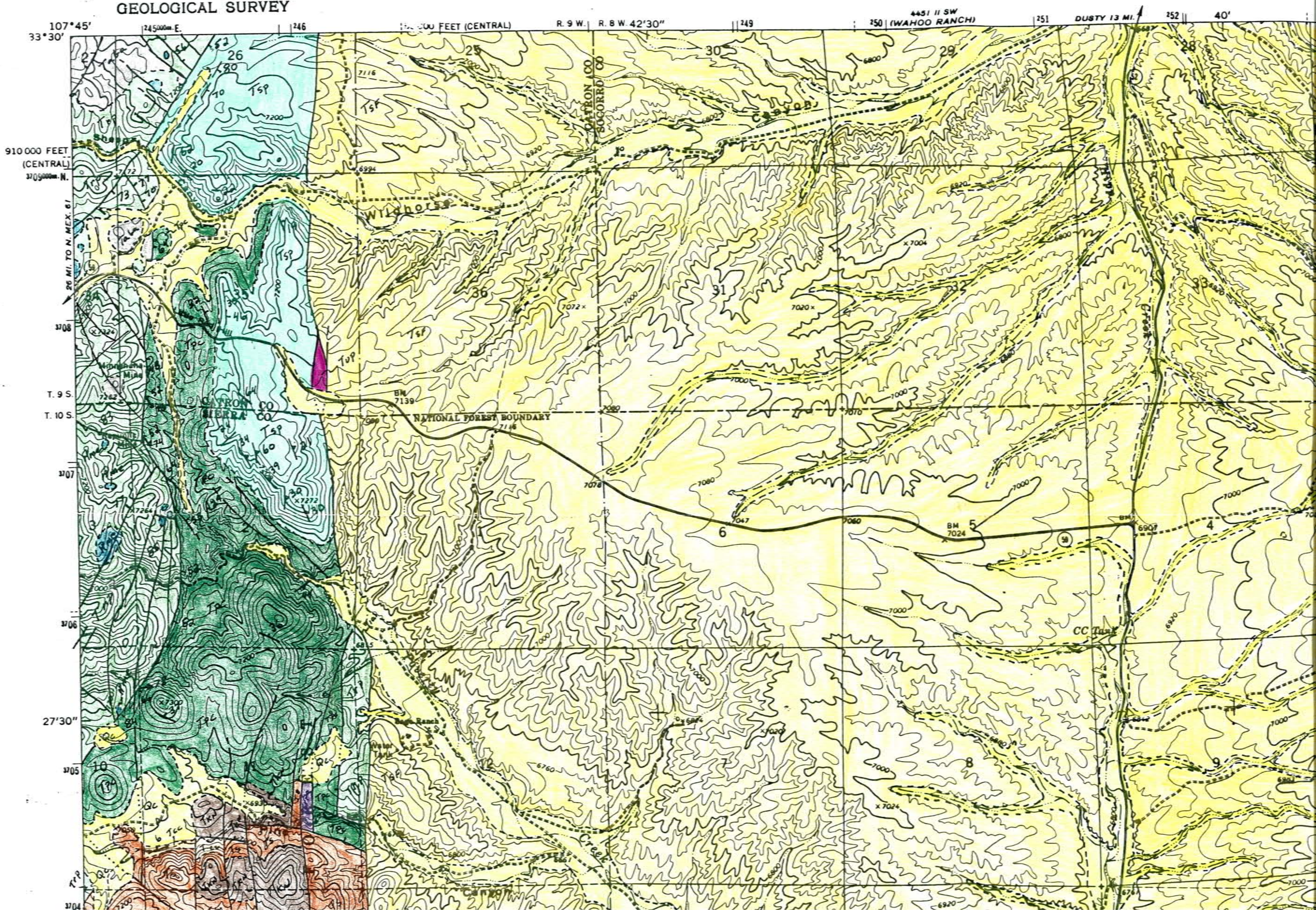

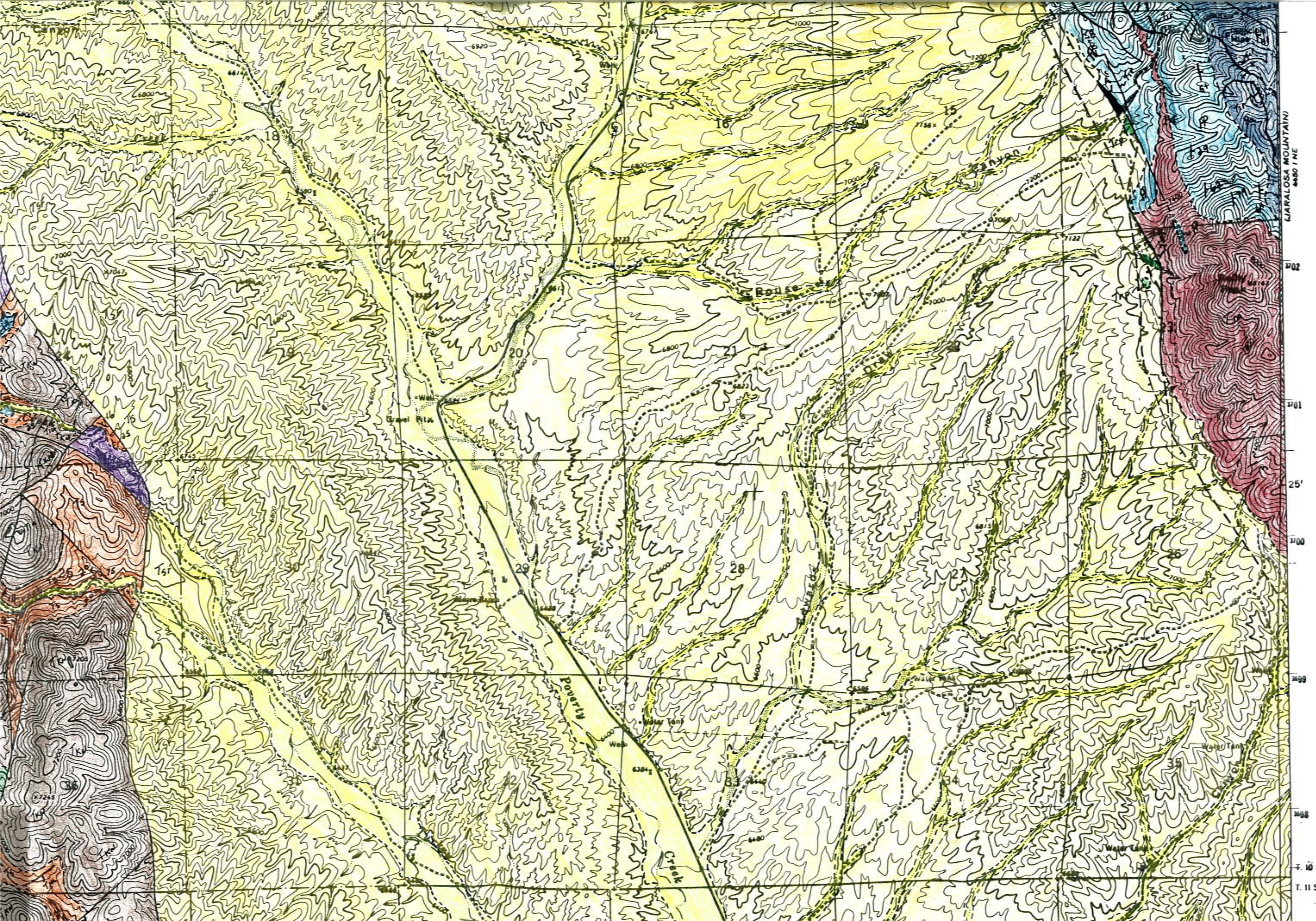
(JARALOSA MOUNTAIN)
4030 I NE
Canyon
Creek
Rouse
Draw
Gravel Pits
Well
Poverty
Creek
Water Tank
25'
T. 10 S.
T. 11 S.
16
15
18
20
21
29
28
27
26
30
33
34
35

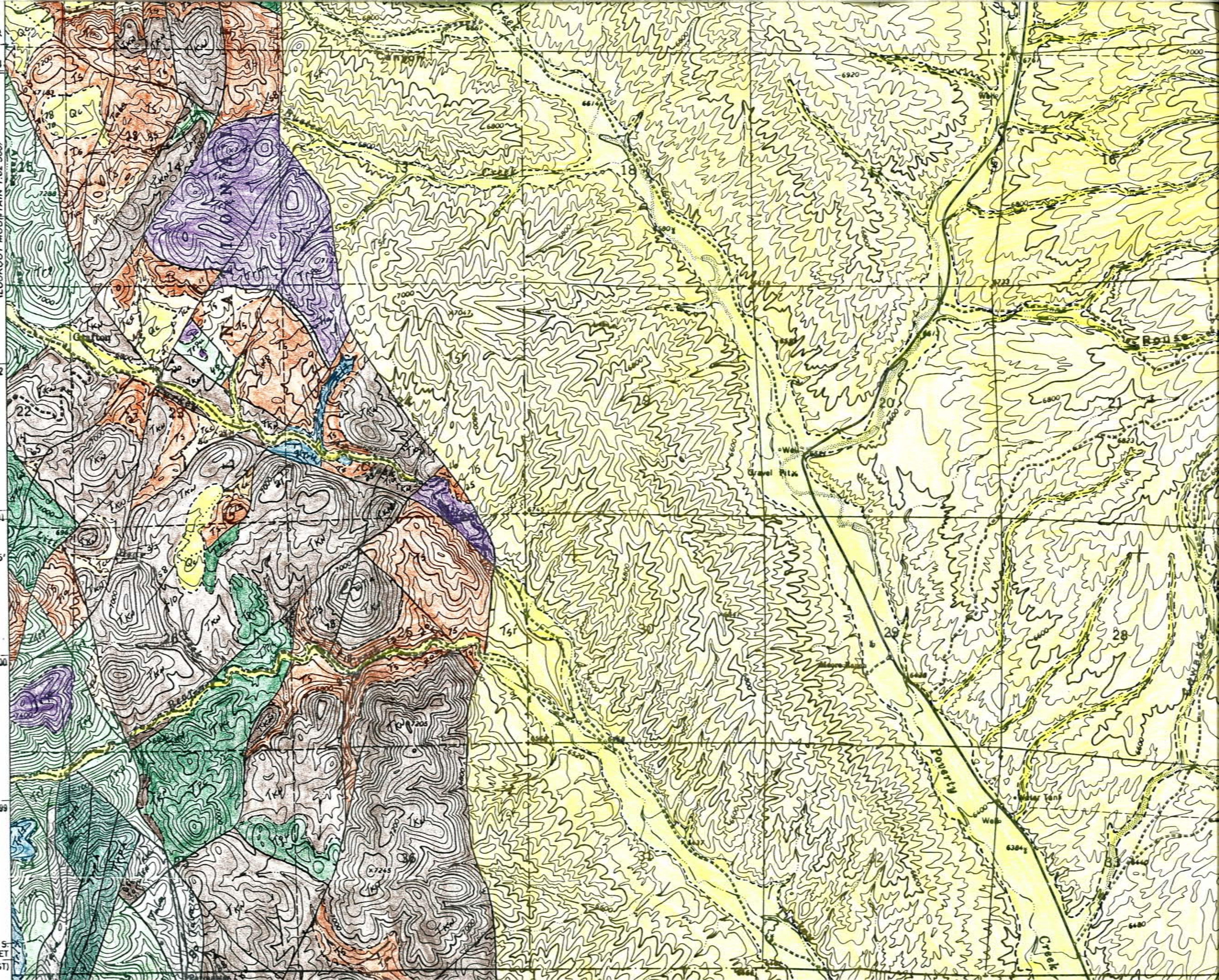

4450 IV
(LOOKOUT MOUNTAIN 1:62 500)
T. 10 S.
870 000 FEET
(WEST)
Canyon
Creek
Gravel Pits
Poverty
Creek
Rouse
Water Tank
Well

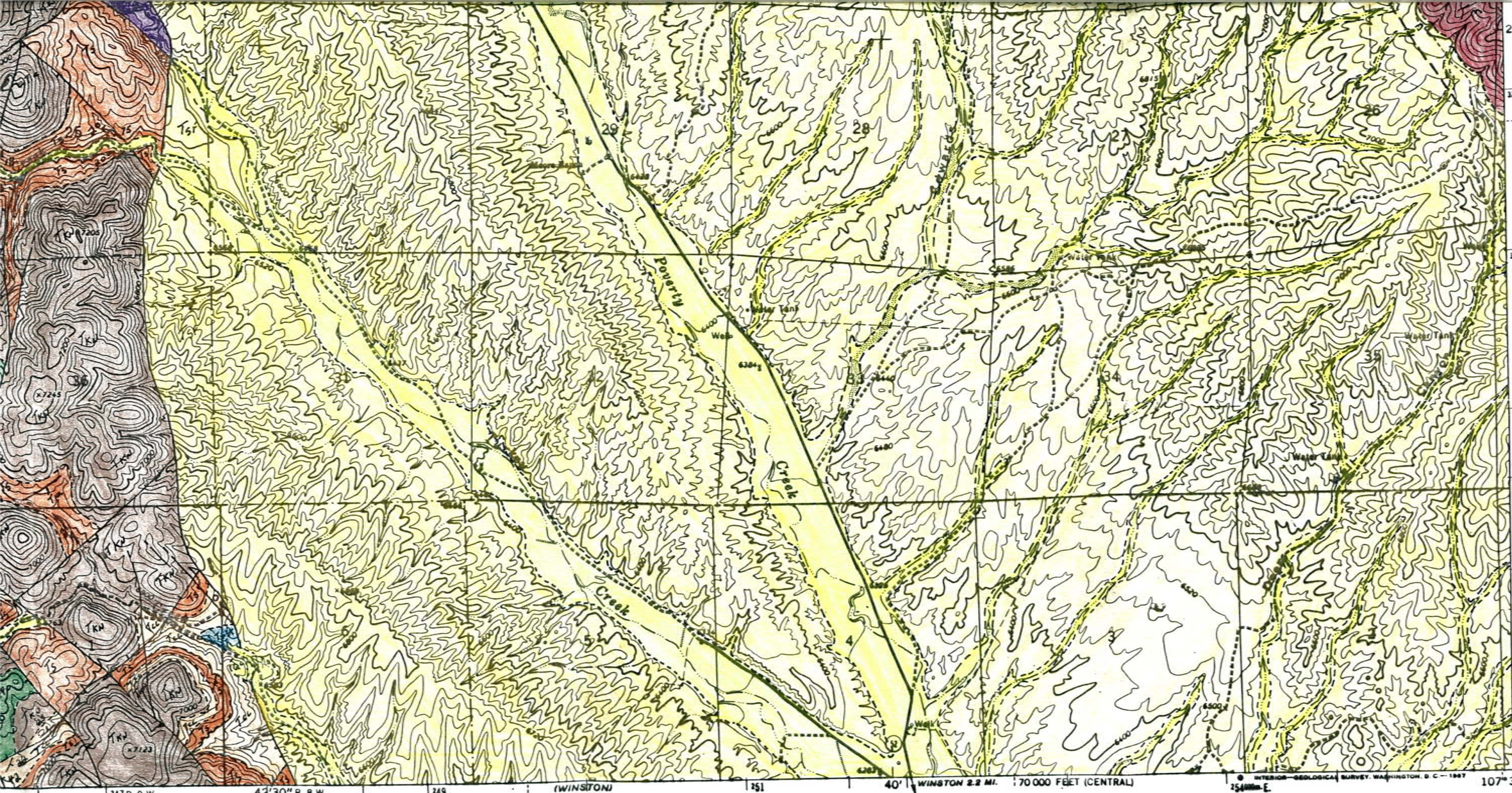

SCALE 1:24000

1 MILE
1000 0 1000 2000 3000 4000 5000 6000 7000 FEET
1 KILOMETER

CONTOUR INTERVAL 40 FEET
DATUM IS MEAN SEA LEVEL

GN MN
1°29' 26 MILS
13° 231 MILS

UTM GRID AND 1965 MAGNETIC NORTH DECLINATION AT CENTER OF SHEET

NEW MEXICO

QUADRANGLE LOCATION

ROAD CLASSIFICATION

Medium-duty ——— Light-duty ———

Unimproved dirt - - - - - -

State Route

PLATE 4.

IRON MOUNTAIN, N. MEX.

N3322.5—W10737.5/7.5

1965

AMS 4450 I NW—SERIES V881

T. 10 S.
870 000 FEET
(WEST)

T. 11 S.

33°22'30"
107°45'

530 000 FEET (WEST)

R. 9 W.

42'30" R. 8 W.

(WINSTON)
4450 I SW

Mapped, edited, and published by the Geological Survey

Control by USGS and USC&GS

Topography by photogrammetric methods from aerial photographs taken 1964. Field checked 1965

Polyconic projection. 1927 North American datum
10,000-foot grids based on New Mexico coordinate system, west and central zones
1000-meter Universal Transverse Mercator grid ticks, zone 13, shown in blue

Fine red dashed lines indicate selected fence lines

1:62 500
KOUT MOUNTAIN)
4450 IV

GN MN
1°29'
26 MILS
13°
231 MILS

UTM GRID AND 1965 MAGNETIC NORTH DECLINATION AT CENTER OF SHEET

SCALE 1:24 000

1 0 1 MILE
1000 0 1000 2000 3000 4000 5000 6000 7000 FEET
1 5 0 1 KILOMETER

CONTOUR INTERVAL 40 FEET
DATUM IS MEAN SEA LEVEL

Plate 3.

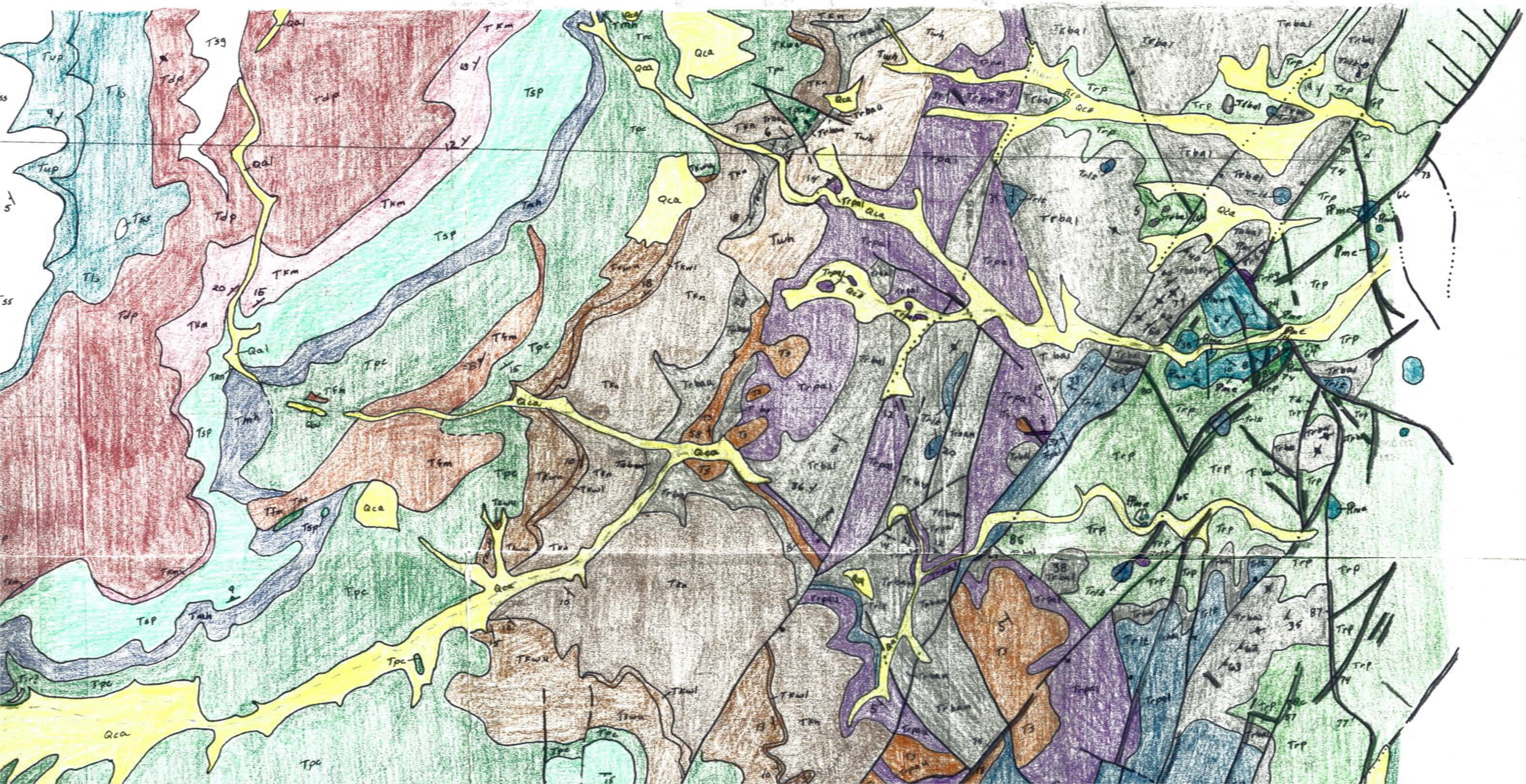
Tup
Tsg
Tdp
Tkm
Tsp
Tpc
Tmh
Tkwu
Tkwl
Tkn
Trbal
Trp
Trpal
Trle
Pmc
Qal
Qca
12 y
36 y

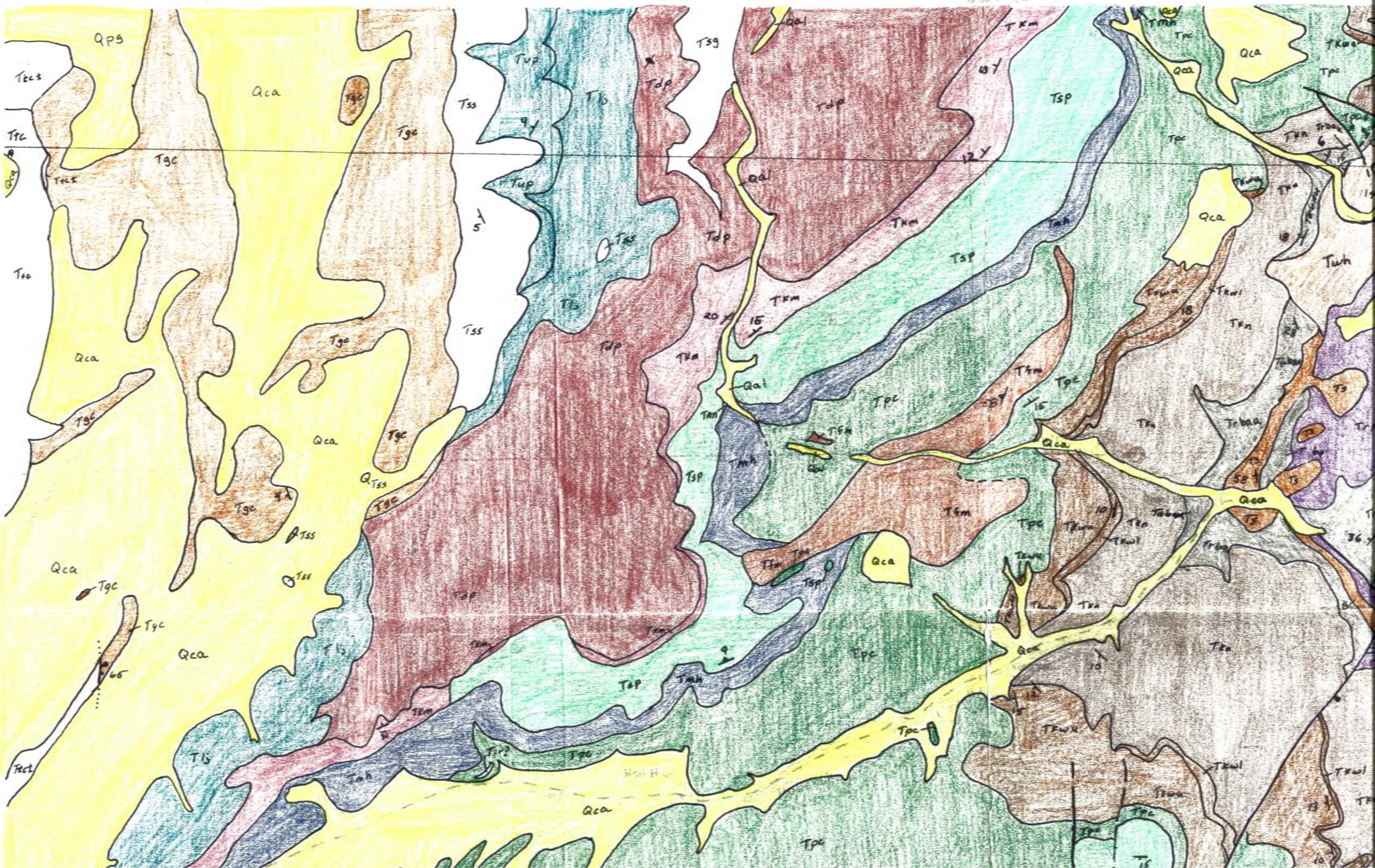

Qps
Qca
Tgc
Tss
Tup
Tls
Tdp
Tsg
Qal
Tkm
Tsp
Tmh
Tpc
Tkn
Tkwl
Tkwu
Twh

Tpc
Tsp
Tsc
Tkm
Ttm
Tdp
Qca
Tkn
Tkwu
Tkwl
Ts
Trpau
Trlk
Trbal
Trp
Tcc
Tms
Tcb
Qal

Qca
Tpc
TKm
Tsc
Tsp
Tfm
Tdp
Qal
QPg
TKn
TKwu
TKwl

Geology mapped by Ted L. Eggleston 1982-85, 1997
Richard Harrison 1984-1997

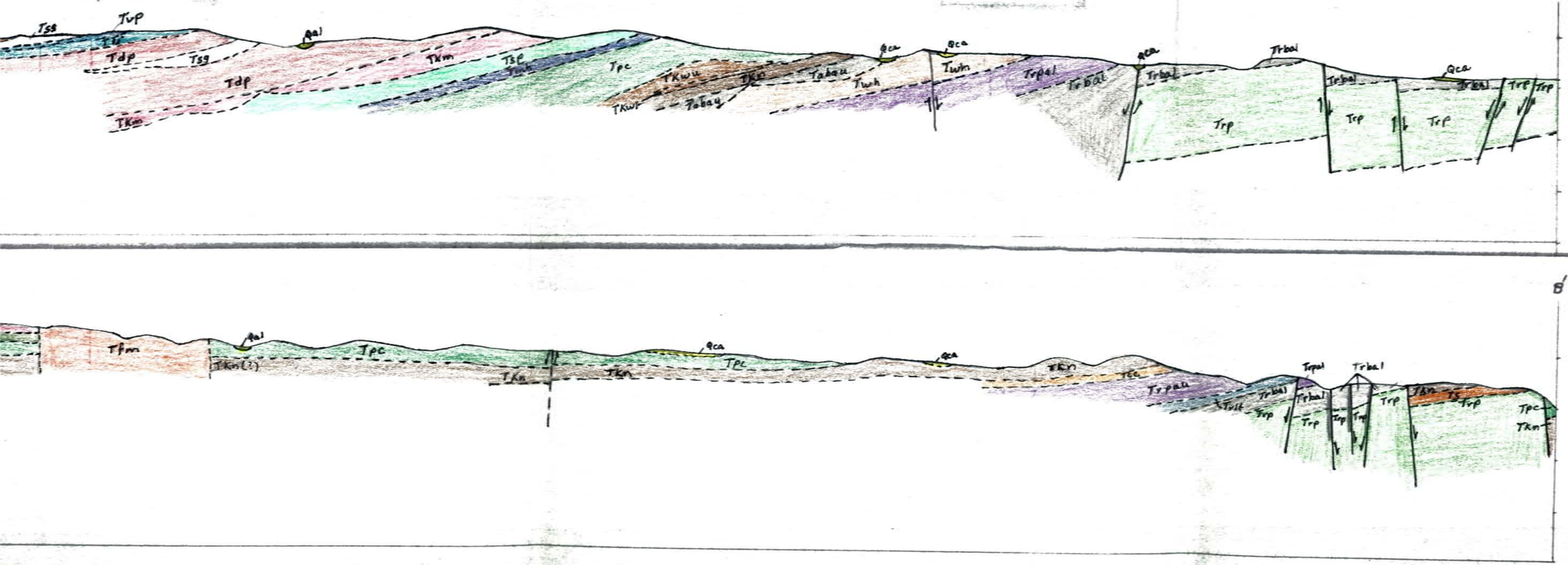

Geologic MAP of the SAWMILL Peak Quadrangle, Sierra and Catron Counties New Mexico

By

Ted L. Eggleston and Richard W. Harrison

New Mexico Bureau of Mines and Mineral Resources
Socorro, NM

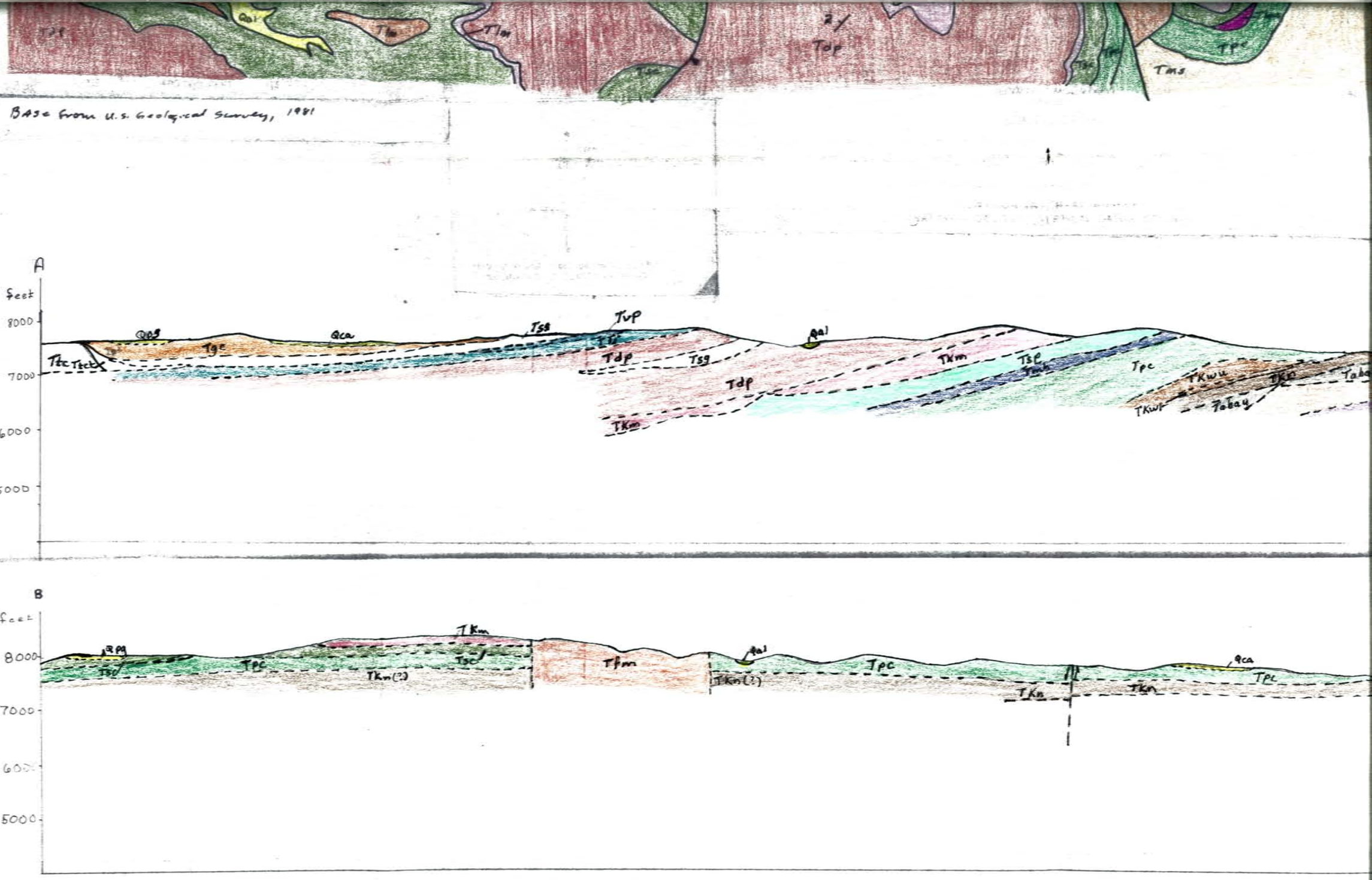

Geologic MAP of the SAWMILL Peak Q
Sierra and Catron Counties New Mex

By

Ted L. Eggleston and Richard W. Harrison

New Mexico Bureau of Mines and Mineral Resources
Socorro, NM

Platel.

NMBM&MR OFR 358

WINSTON QUADRANGLE
NEW MEXICO—SIERRA CO.
7.5 MINUTE SERIES (TOPOGRAPHIC)

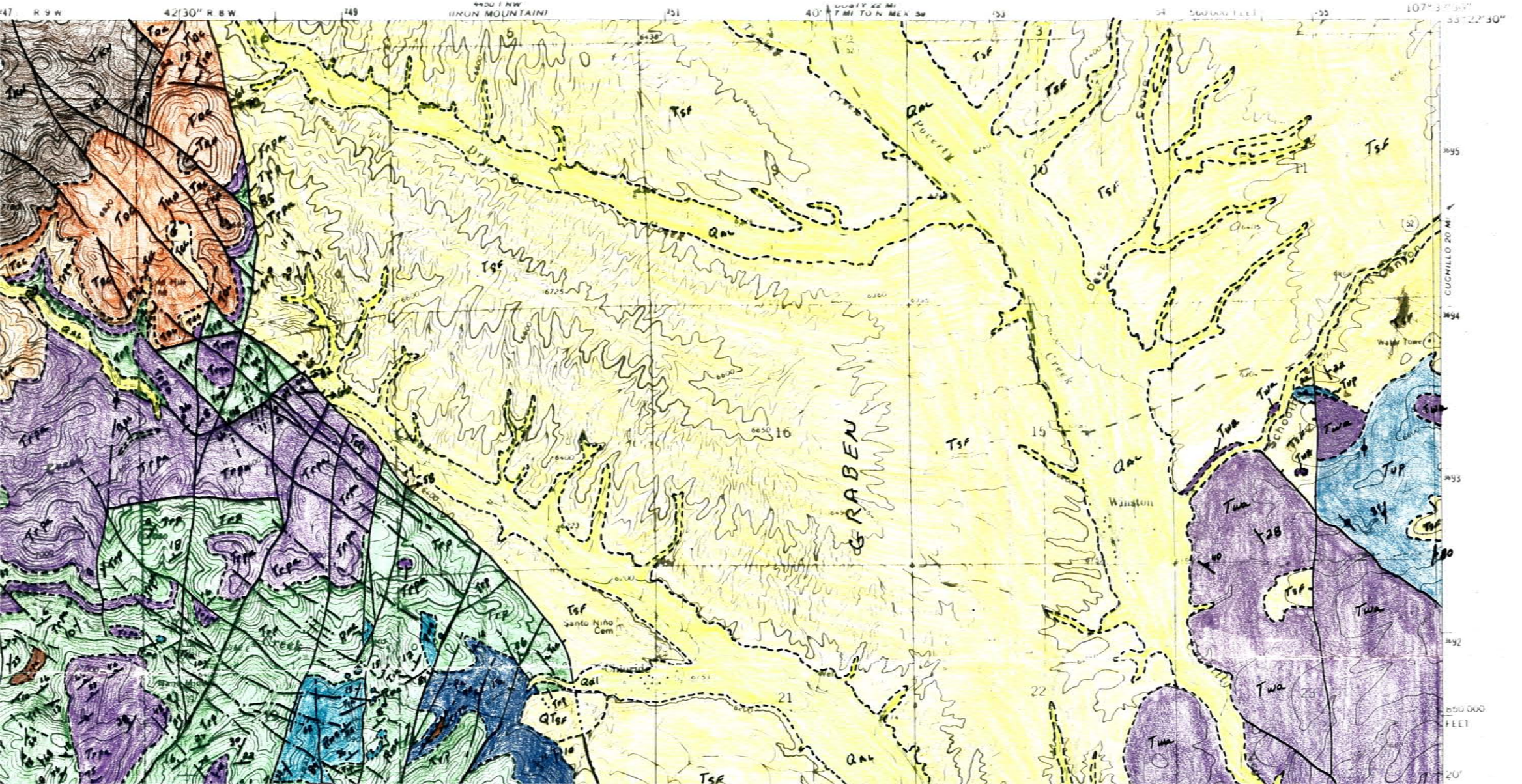

UNITED STATES
DEPARTMENT OF THE INTERIOR
GEOLOGICAL SURVEY

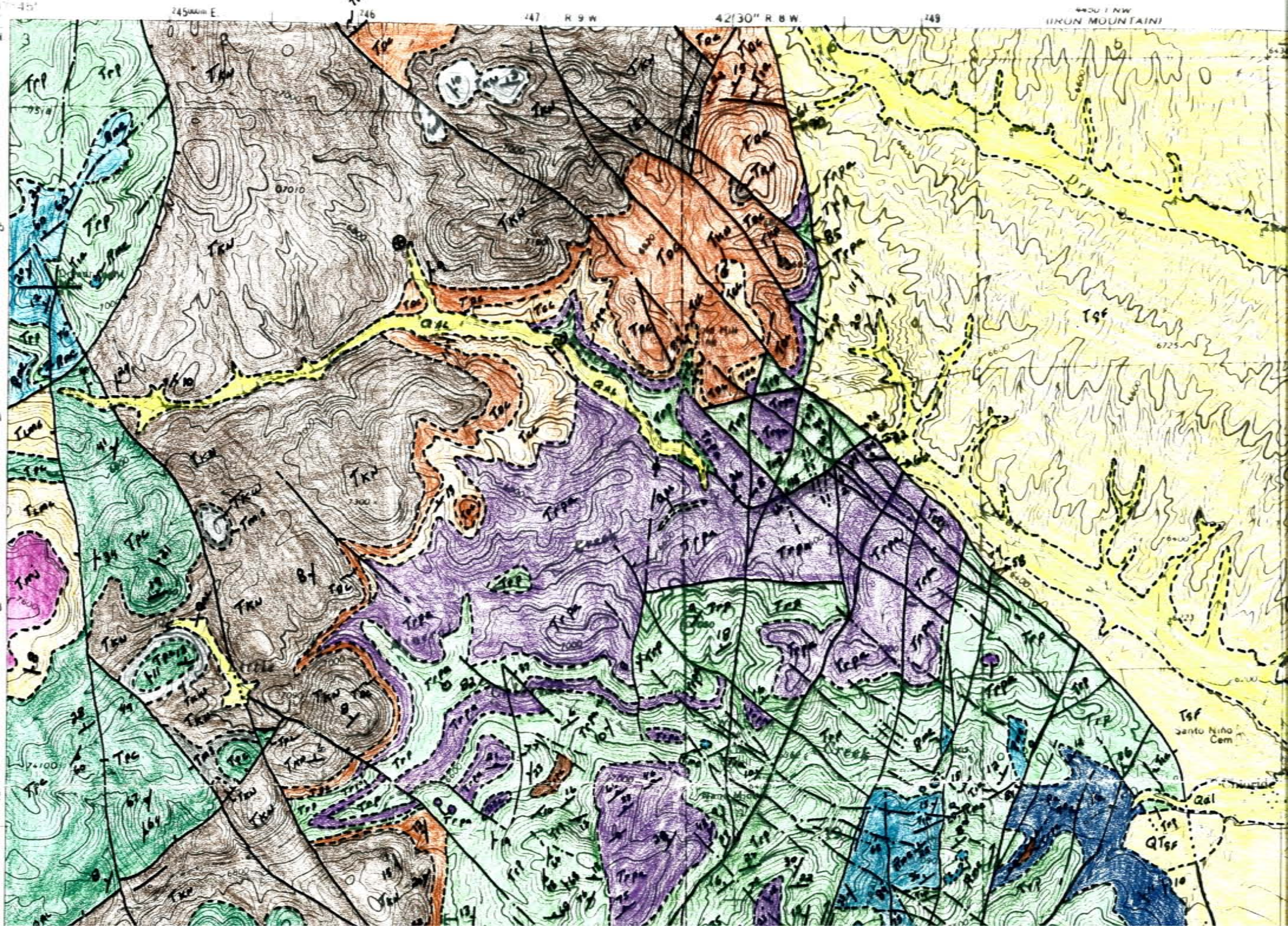

Tlmc

Tpc

TMG

Tkw

Tcwl cng

Tkp

RUBIO PEAK FORM.

Tpc

Tcc

Trpa

Trp

Rme

Trpba

Trph

Trpc

Trpm

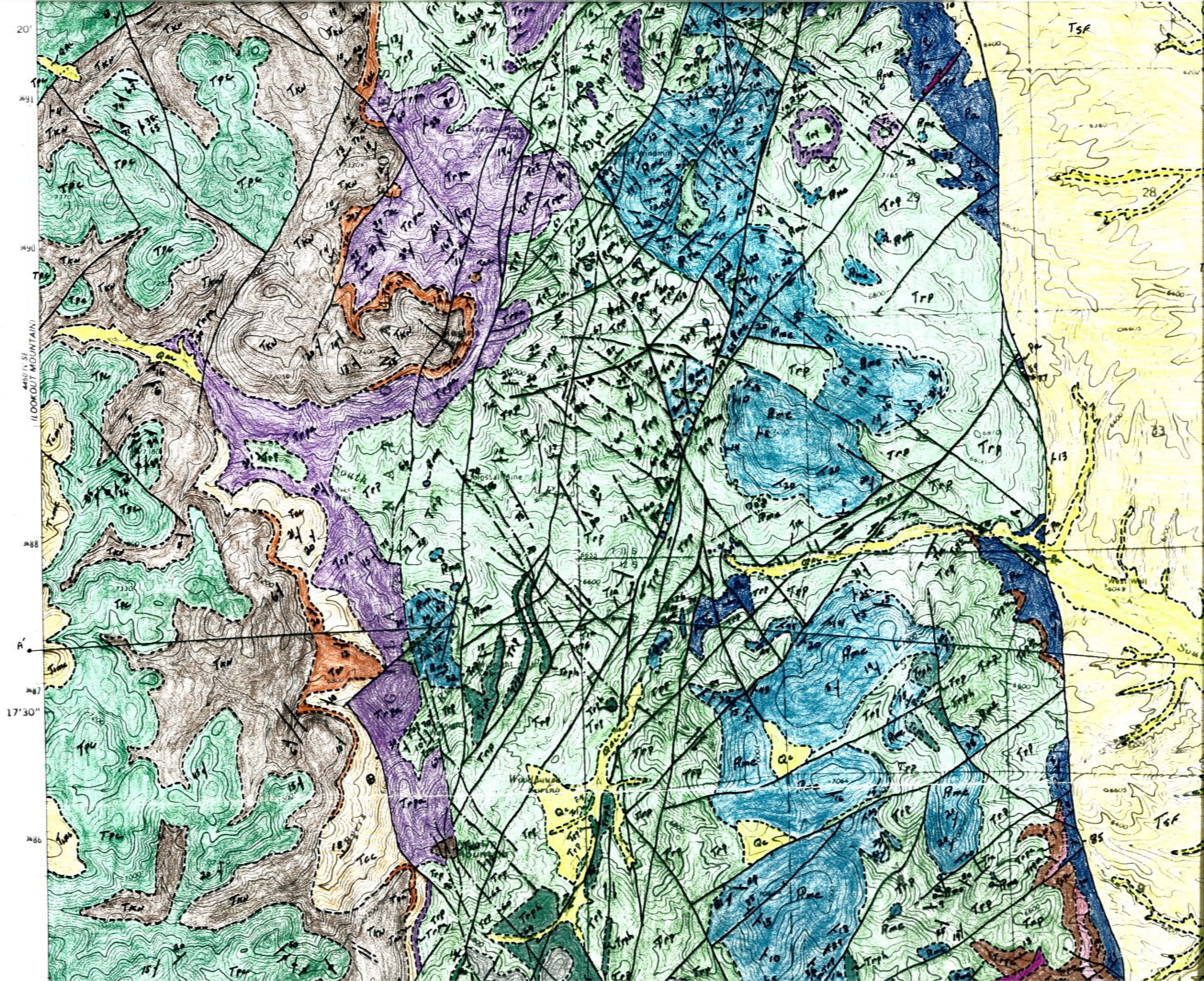
20'
17'30"
A'
(LOOKOUT MOUNTAIN)
Tsf
Trp
Rmc
Tpc
Qc
Qal
28
29
33
West Well

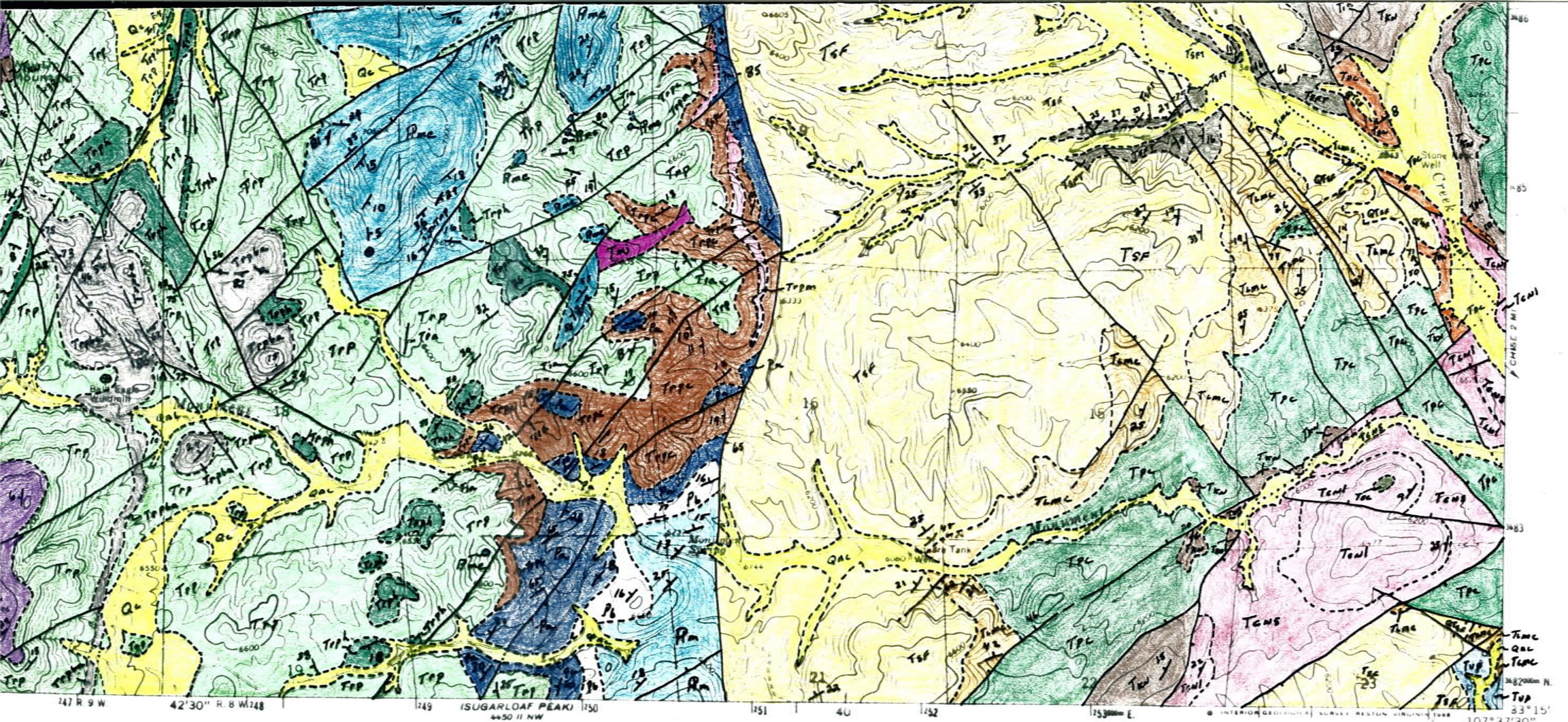

SCALE 1:24000

1 MILE
1000 0 1000 2000 3000 4000 5000 6000 7000 FEET
1 5 0 1 KILOMETER

CONTOUR INTERVAL 40 FEET
NATIONAL GEODETIC VERTICAL DATUM OF 1929

GN MN
1°29' 13°
26 MILS 231 MILS

ROAD CLASSIFICATION

Medium-duty — — — Light duty

Unimproved dirt

Mapped, edited, and published by the Geological Survey

Control by USGS and USC&GS

Topography by photogrammetric methods from aerial photographs taken 1964. Field checked 1965

Polyconic projection. 1927 North American Datum
10,000-foot grid based on New Mexico coordinate system, west zone
1000 meter Universal Transverse Mercator grid ticks,
zone 13, shown in blue

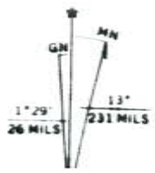

SCALE 1:24000

1 MILE
1000 0 1000 2000 3000 4000 5000 6000 7000 FEET
1 0 1 KILOMETER

CONTOUR INTERVAL 40 FEET
NATIONAL GEODETIC VERTICAL DATUM OF 1929

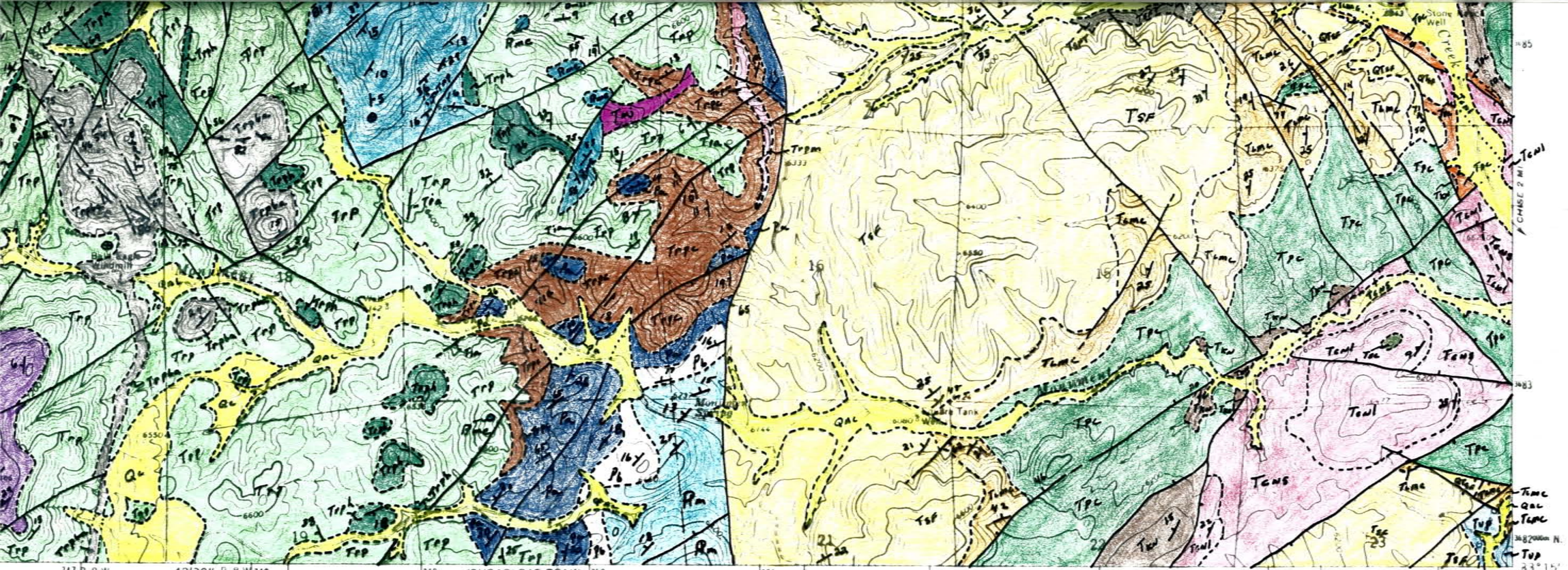

SCALE 1:24000

1 MILE

1000 0 1000 2000 3000 4000 5000 6000 7000 FEET

1 5 0 1 KILOMETER

CONTOUR INTERVAL 40 FEET
NATIONAL GEODETIC VERTICAL DATUM OF 1929

ROAD CLASSIFICATION

Medium-duty — — — Light duty

Unimproved dirt

State Route

GN MN

1°29' 26 MILS 13° 231 MILS

RID AND 1965 MAGNETIC NORTH
LINATION AT CENTER OF SHEET

NEW MEXICO

QUADRANGLE LOCATION

THIS MAP COMPLIES WITH NATIONAL MAP ACCURACY STANDARDS
FOR SALE BY U. S. GEOLOGICAL SURVEY, DENVER, COLORADO 80225, OR RESTON, VIRGINIA 22092
A FOLDER DESCRIBING TOPOGRAPHIC MAPS AND SYMBOLS IS AVAILABLE ON REQUEST

Geology of the Winston 7.5' Quadrangle Sierra County, New Mexico

by Richard W. Harrison, 1989

WINSTON, N. MEX.
33107-C6 TF-024
1965
DMA 4450 I SW-SERIES V881

R. HARRISON
12/11/88

3686
3685
3684
3683
820 000
FEET
33°15'
107°45'
244
245
530 000 FEET
246
247 R 9 W
42'30"
R. 8 W.
248
249
250
251
(SUGARLOAF PEAK)
4450 II NW
(REEDS PEAK)
4450 III NE

Mapped, edited, and published by the Geological Survey

Control by USGS and USC&GS

Topography by photogrammetric methods from aerial photographs taken 1964. Field checked 1965

Polyconic projection. 1927 North American Datum
10,000-foot grid based on New Mexico coordinate system, west zone
1000 meter Universal Transverse Mercator grid ticks, zone 13, shown in blue

Fine red dashed lines indicate selected fence lines

Certain land lines omitted because of insufficient data

To place on the predicted North American Datum 1983 move the projection lines 5 meters south and 54 meters east as shown by dashed corner ticks

There may be private inholdings within the boundaries of the National or State reservations shown on this map

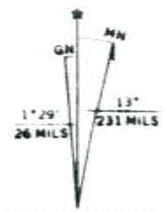

UTM GRID AND 1965 MAGNETIC NORTH DECLINATION AT CENTER OF SHEET

SCALE 1:24 000

1 MILE
1000 FEET
1 KILOMETER

CONTOUR INTERVAL 40 FEET
NATIONAL GEODETIC VERTICAL DATUM OF 1929

THIS MAP COMPLIES WITH NATIONAL MAP ACCURACY STANDARDS
FOR SALE BY U. S. GEOLOGICAL SURVEY, DENVER, COLORADO 80225, OR RESTON, VIRGINIA 22092
A FOLDER DESCRIBING TOPOGRAPHIC MAPS AND SYMBOLS IS AVAILABLE ON REQUEST

Geology of the Winston 7.5' Quadrangle Sierra County, New Mexico

by Richard W. Harrison, 1989

Plate 2

LOOKOUT MOUNTAIN QUADRANGLE

NEW MEXICO—SIERRA CO.

7.5 MINUTE SERIES (TOPOGRAPHIC)

SE/4 LOOKOUT MOUNTAIN 15' QUADRANGLE

4450 I NW (IRON MOUNTAIN)

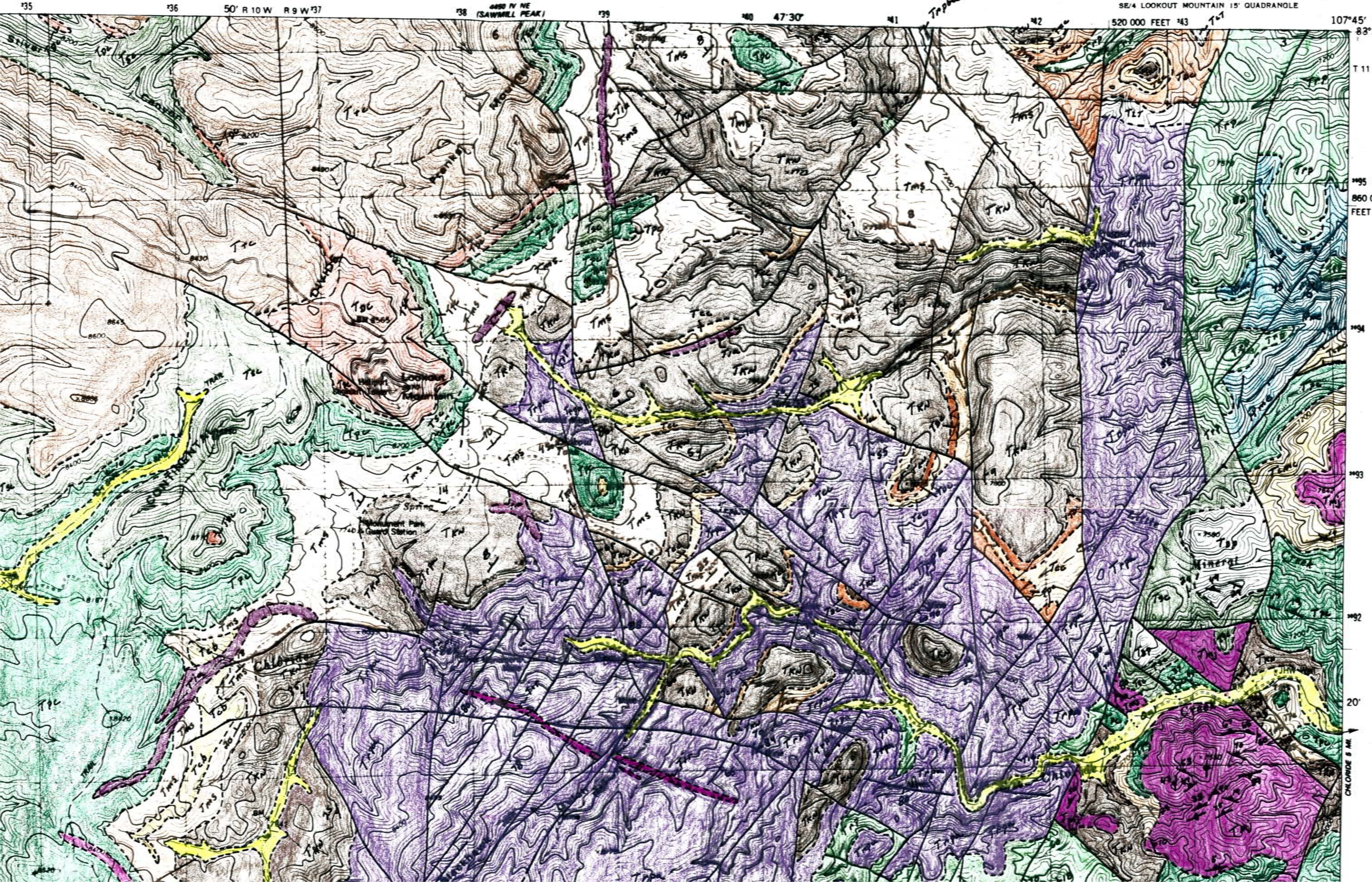

UNITED STATES
DEPARTMENT OF THE INTERIOR
GEOLOGICAL SURVEY

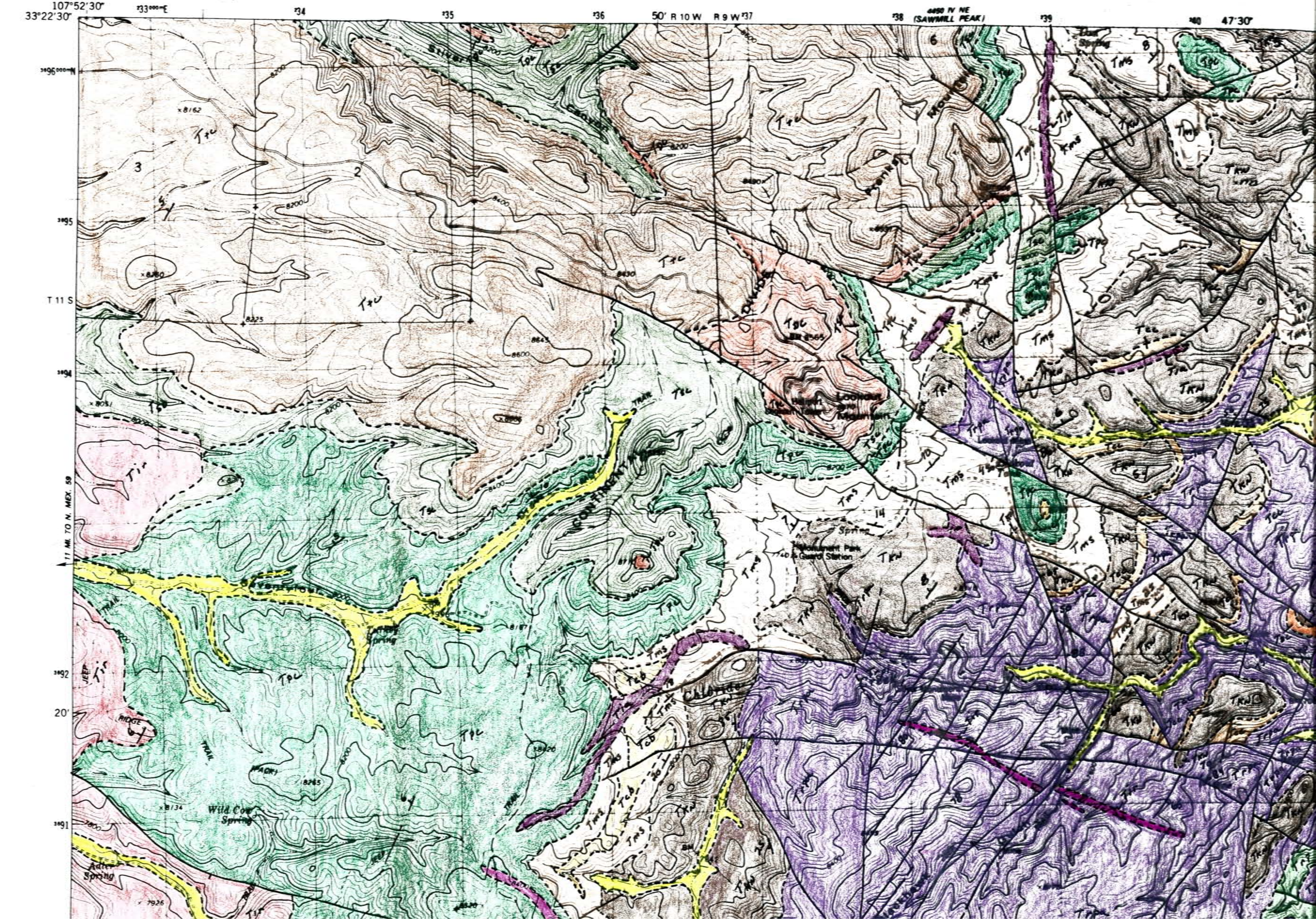

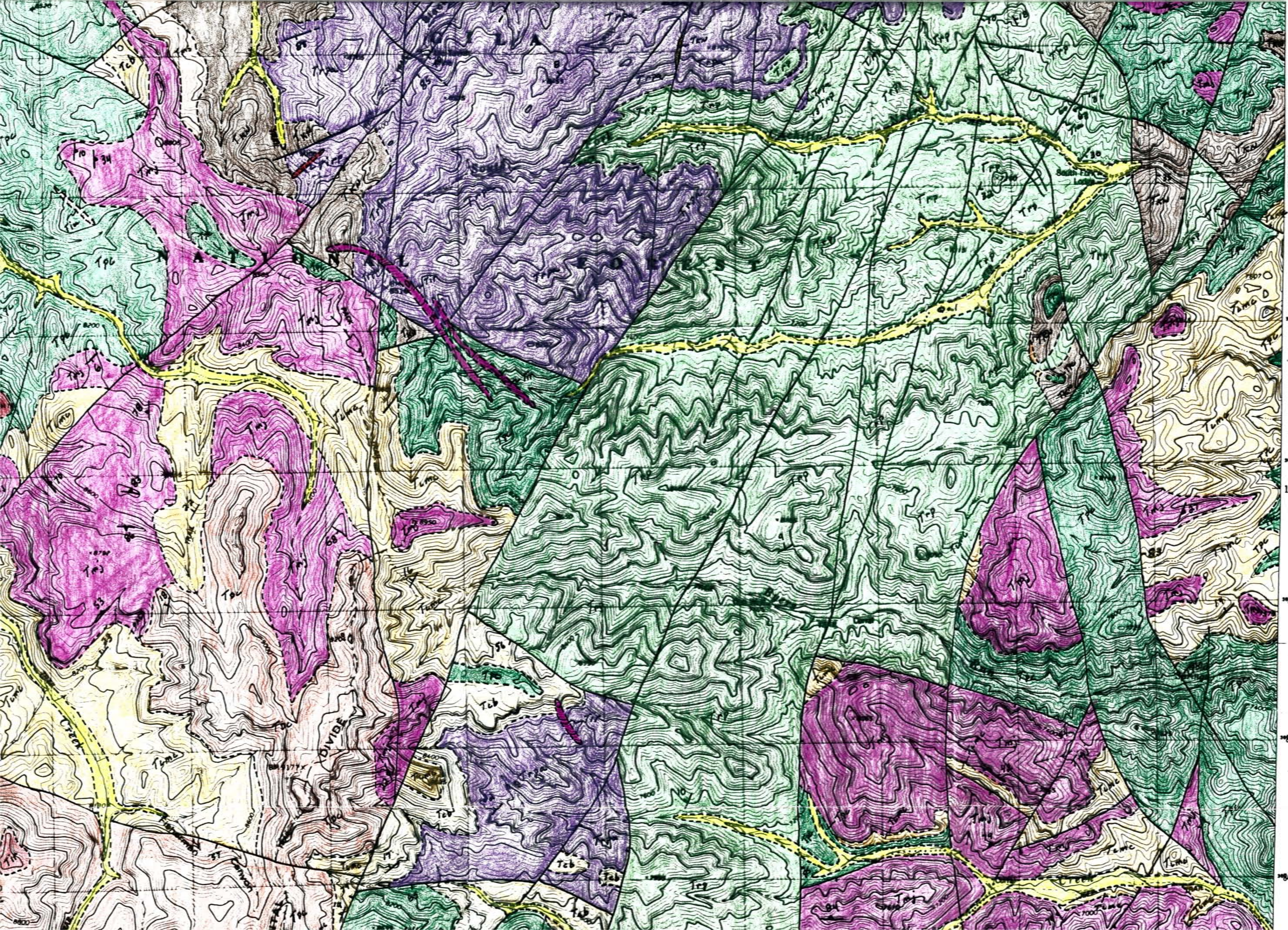
NATIONAL
FOREST
DIVIDE
Creek
(WINSTON)
17'30"

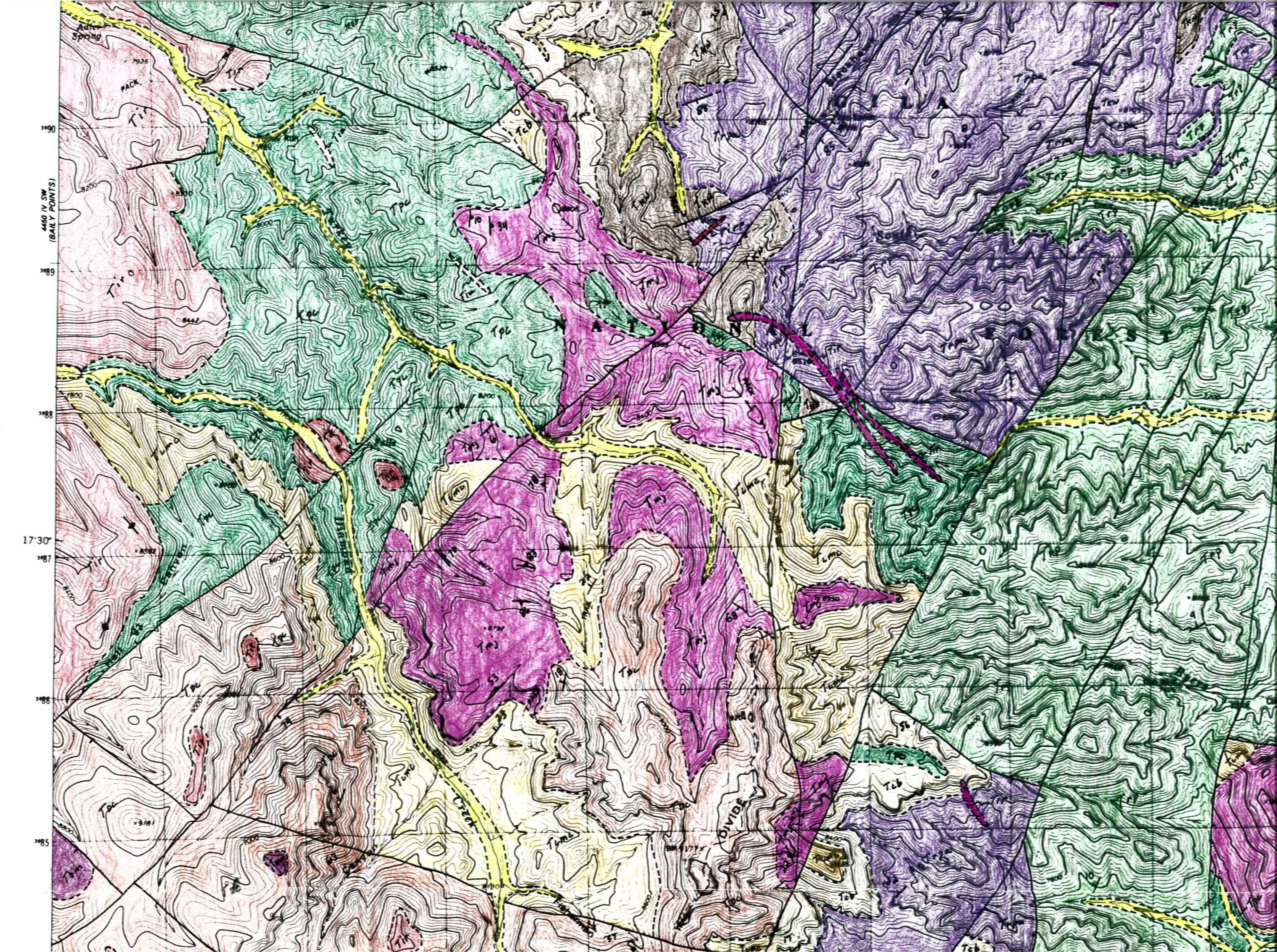
Spring
4460 IV SW
(BAILY POINTS)
3890
3889
3888
17'30"
3887
3886
3885
7926
PACK
8200
8442
7800
8582
8600
9181
8800
9000
8950
BM 9177X
GILA
NATIONAL
FOREST
DIVIDE
Creek
Canyon
Diamond
Tir
Tpc
Kpu
Tmd
Tmc
Tdc
Tcb
Trp
Tdi
Tca
Tpa

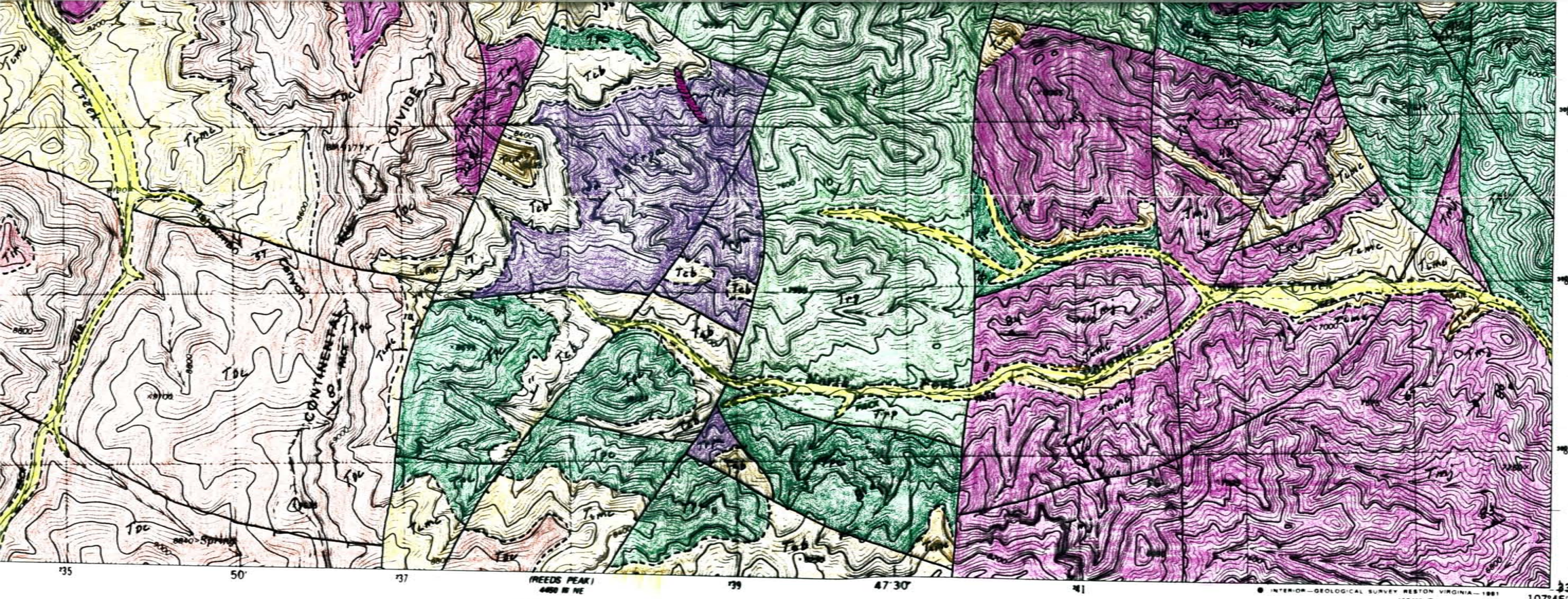

SCALE 1:24 000

1 0 1 MILE

1000 0 1000 2000 3000 4000 5000 6000 7000 FEET

1 5 0 1 KILOMETER

CONTOUR INTERVAL 40 FEET
NATIONAL GEODETIC VERTICAL DATUM OF 1929

GN MN

1°33' (28 MILS) 12° (213 MILS)

UTM GRID AND 1981 MAGNETIC NORTH DECLINATION AT CENTER OF SHEET

THIS MAP COMPLIES WITH NATIONAL MAP ACCURACY STANDARDS

FOR SALE BY U.S. GEOLOGICAL SURVEY, DENVER, COLORADO 80225, OR RESTON, VIRGINIA 22092

A FOLDER DESCRIBING TOPOGRAPHIC MAPS AND SYMBOLS IS AVAILABLE ON REQUEST

QUADRANGLE LOCATION

ROAD CLASSIFICATION

Primary highway, hard surface

Secondary highway, hard surface

Light-duty road, hard or improved surface

Unimproved road

Interstate Route U.S. Route State Route

LOOKOUT MOUNTAIN, N. MEX.

SE 4 LOOKOUT MOUNTAIN 15' QUADRANGLE

N3315—W10745/7.5

1981

DMA 4450 IV SE—SERIES V881

• INTERIOR—GEOLOGICAL SURVEY, RESTON, VIRGINIA—1981

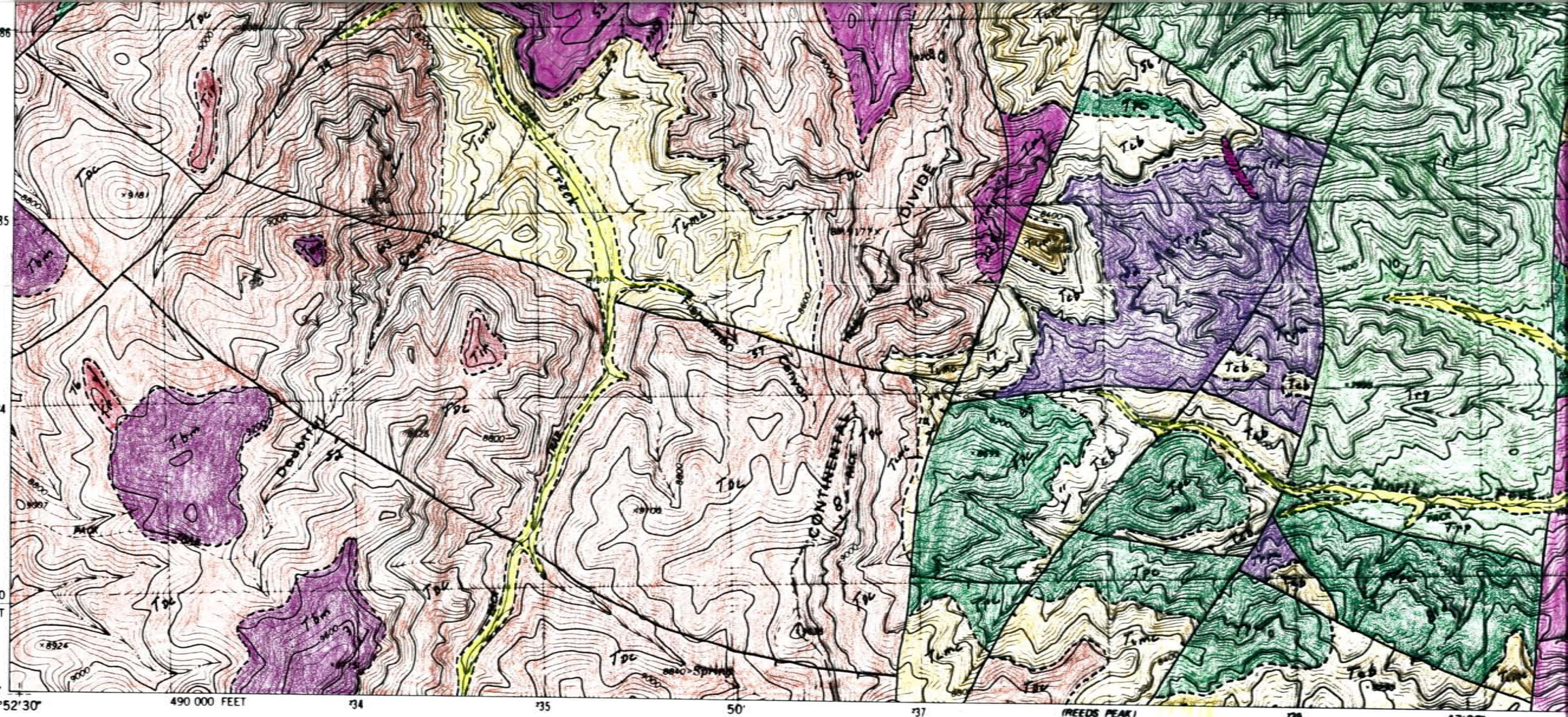

Mapped, edited, and published by the Geological Survey

Control by USGS, NOS/NOAA, and USFS

Topography by photogrammetric methods from aerial photographs taken 1967. Field checked 1975. Map edited 1981

Projection and 10,000-foot grid ticks: New Mexico coordinate system, west zone (transverse Mercator)
1000-meter Universal Transverse Mercator grid, zone 13
1927 North American datum
To place on the predicted North American Datum 1983 move the projection lines 5 meters south and 55 meters east as shown by dashed corner ticks

Certain land lines are omitted because of insufficient data

There may be private inholdings within the boundaries of the National or State reservations shown on this map

GN MN
1°33' 28 MILS | 12° 213 MILS

UTM GRID AND 1981 MAGNETIC NORTH DECLINATION AT CENTER OF SHEET

SCALE 1:24 000

1 0 1 MILE
1000 0 1000 2000 3000 4000 5000 6000 7000 FEET
1 5 0 1 KILOMETER

CONTOUR INTERVAL 40 FEET
NATIONAL GEODETIC VERTICAL DATUM OF 1929

THIS MAP COMPLIES WITH NATIONAL MAP ACCURACY STANDARDS
FOR SALE BY U.S. GEOLOGICAL SURVEY, DENVER, COLORADO 80225, OR RESTON, VIRGINIA 22092
A FOLDER DESCRIBING TOPOGRAPHIC MAPS AND SYMBOLS IS AVAILABLE ON REQUEST